

### Repurposing ubiquitination for innovative antibody conjugation

Hebieshy, A.F. el

#### Citation

Hebieshy, A. F. el. (2025, October 16). *Repurposing ubiquitination for innovative antibody conjugation*. Retrieved from https://hdl.handle.net/1887/4273517

Version: Publisher's Version

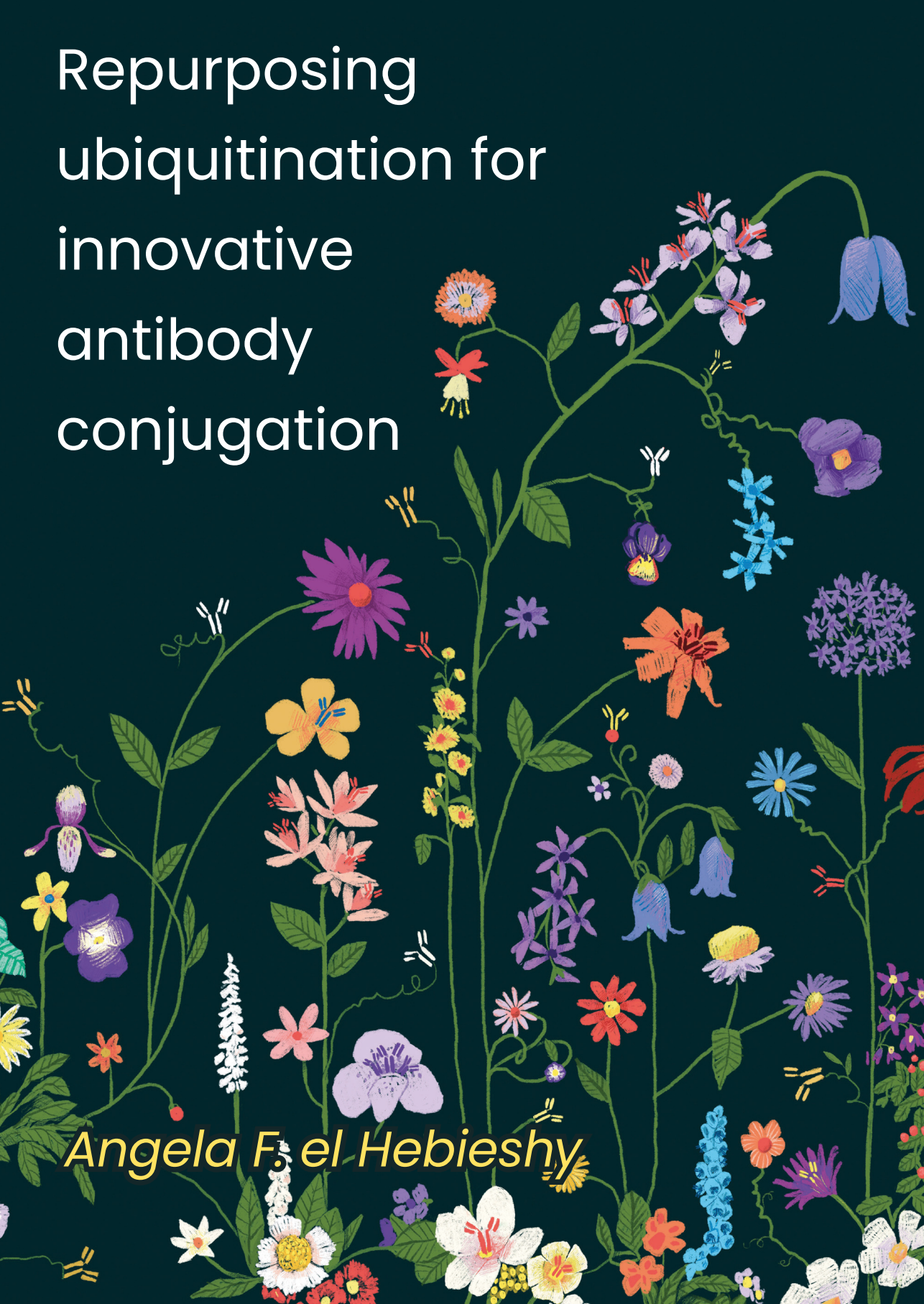
Licence agreement concerning inclusion of doctoral

License: thesis in the Institutional Repository of the University

of Leiden

Downloaded from: <a href="https://hdl.handle.net/1887/4273517">https://hdl.handle.net/1887/4273517</a>

**Note:** To cite this publication please use the final published version (if applicable).



# Repurposing ubiquitination for innovative antibody conjugation

Angela F. el Hebieshy

The research described in this thesis was performed at the Leiden University Medical Center (Department of Cell and Chemical Biology, Leiden, the Netherlands) and at the Netherlands Cancer Institute (Department of Cell Biology II, Amsterdam, the Netherlands). The work was financially supported by the Institute for Chemical Immunology, Oncode Institute, NWO and the strategic fund of the LUMC.

ISBN: 978-94-6473-758-5

Cover: Sieben Medical Art Printed by: Ipskamp Printing

Financial support: Leiden University

Copyright © 2025 by Angela F. el Hebieshy. All rights reserved. No part of this publication may be reproduced or transmitted in any form or by any means without prior written permission of the author, or where appropriate, of the publisher of the articles.

## Repurposing ubiquitination for innovative antibody conjugation

#### Proefschrift

ter verkrijging van

de graad van doctor aan de Universiteit Leiden, op gezag van rector magnificus prof.dr.ir. H. Bijl, volgens besluit van het college voor promoties te verdedigen op donderdag 16 oktober 2025 klokke 13.00 uur

door

Angela Fouad el Hebieshy

geboren te Hulst in 1989

## Repurposing ubiquitination for innovative antibody conjugation

#### Proefschrift

ter verkrijging van

de graad van doctor aan de Universiteit Leiden,
op gezag van rector magnificus prof.dr.ir. H. Bijl,
volgens besluit van het college voor promoties
te verdedigen op woensdag 9 april 2025
klokke 13.00 uur

door

Angela Fouad el Hebieshy

geboren te Hulst in 1989

#### Promotoren:

prof. dr. H. Ovaa prof. dr. J.J.C. Neefjes

#### Co-promotoren:

dr. F.A. Scheeren dr. G.J. van der Heden van Noort

#### Promotiecommissie:

prof. dr. P.W.H.I. Parren prof. dr. P. ten Dijke prof. dr. S.I. van Kasteren – Leiden Institute of Chemistry, Leiden dr. K.M. Bonger – Leiden Institute of Chemistry, Leiden



#### **Table of Contents**

Chapter 1	Introduction and Scope of the Thesis	14
Chapter 2	Ubiquitin as a Conjugation Tag for Labeling and Multimerization of Antibodies	30
Chapter 3	Targeted Dendritic Cell Vaccination through Ubi-tag- based Peptide Delivery	74
Chapter 4	Nanobody Ubi-tag Conjugates for Translation to Human Dendritic Cell Targeted Antigen Delivery	100
Chapter 5	Total Chemical Synthesis of a Functionalized GFP Nanobody	118
Chapter 6	Summary and Future Prospects	156
Appendix	Nederlandse Samenvatting Curriculum Vitae Publications Portfolio Acknowledgments	164 166 167 168 170
	=	

#### **Abbreviations**

Acm Acetamidomethyl

ADCs Antibody-drug conjugates
BITES Bispecific T-cell engagers
BLI Bio-layer interferometry

BMDCs Bone marrow-derived dendritic cells

Boc *tert*-Butyloxycarbonyl CD Circular dichroism

CDR Complementarity-determining region

CRISPR Clustered Regularly Interspaced Short Palindromic Repeats

CTV Cell trace violet

CuAAC Copper(I)-catalyzed azide-alkyne cycloaddition

Cy5 Cyanine dye 5
DCM Dichloromethane
DCs Dendritic cells

DIC N,N'-Diisopropylcarbodiimide
DIPEA N,N-diisopropylethylamine

DMEM Dulbecco's Modified Eagle Medium

DMF Dimethylformamide

DOTA-GA 1,4,7,10-tetraazacyclododecane-1,4,7,10-tetraacetic acid-glutamic acid

DTP 2,2'-Dithio-dipyridin

DTT Dithiothreitol

DUBs Deubiquitinating enzymes

DVD-Ig Dual variable domain immunoglobulin

E1 Ubiquitin-activating enzyme
E2 Ubiquitin-conjugating enzyme
E3 Ubiquitin-ligating enzyme

EDT Ethanedithiol

EDTA Ethylenediaminetetraacetic acid

ELISA Enzyme-linked immunosorbent assay
ESI-TOF Electrospray ionization-time of flight

Fab Fragment antigen-binding
Fc Fragment crystallizable region

FCS Fetal calf serum

FGE Formylglycine generating enzyme

FITC Fluorescein isothiocyanate
Fmoc Fluorenylmethyloxycarbonyl

FPLC Fast protein liquid chromatography

FR Framework region

GFP Green fluorescent protein

GM-CSF Granulocyte-macrophage colony-stimulating factor

HDR Homology Directed Repair

IMDM Iscove's Modified Dulbecco's Medium

*i*Pr₃SiH Triisopropylsilane

IPTG Isopropyl β-D-1-thiogalactopyranoside

K48 Lysine 48

LC-MS Liquid chromatography-mass spectrometry

LDH Lactate dehydrogenase
LPS Lipopolysaccharide
mAb Monoclonal antibody

MeCN Acetonitrile

MES 2-(N-morpholino)ethanesulfonic acid
MESNa Sodium 2-mercaptoethanesulfonate
MHC Major histocompatibility complex
moDCs Monocyte-derived dendritic cells

MOPS 3-(N-morpholino)propanesulfonic acid

MPAA 4-Mercaptophenylacetic acid mTG Microbial transglutaminase

Nbs Nanobodies

NCL Native chemical ligation
NHS N-hydroxysuccinimide

NIeL Non-LEE-encoded effector ligase

NMP N-Methyl-2-pyrrolidone
OTUB1 OTU deubiquitinase 1
OVAP Ovalbumin peptide

PBS Phosphate-buffered saline

PEG Polyethylene glycol PG Protective group

PyBOP Benzotriazol-1-yl-oxytripyrrolidinophosphonium hexafluorophosphate

Rho Rhodamine

RP-HPLC Reverse phase high performance liquid chromatography

RT Room temperature

ScFv Single-chain variable fragment

SD Standard deviation

sdAb Single-domain antibody

SPPS Solid-phase peptide synthesis

Srt Sortase

TCEP Tris(2-carboxyethyl)phosphine

TCR T-cell receptor

TFA Trifluoroacetic acid

THPTA Tris(hydroxypropyltriazolylmethyl)amine

TIPS Triisopropylsilane

 $\begin{array}{ll} \mbox{Ub} & \mbox{Ubiquitin} \\ \mbox{Ub}_2 & \mbox{Di-ubiquitin} \end{array}$ 

Ub<sup>acc</sup> Acceptor Ubi-tag

UbcH7 Ubiquitin-conjugating enzyme H7

Ub<sup>don</sup> Donor Ubi-tag

UBE1 Ubiquitin-activating enzyme E1
Ube2g2 Ubiquitin-conjugating enzyme E2G 2

Ub-PA Ubiquitin-propargylamide

Ub<sup>WT</sup> Wild-type ubiquitin

UCHL3 Ubiquitin carboxyl-terminal hydrolase L3
UPLC Ultra performance liquid chromatography
VHH Variable heavy domain of heavy chain

WT Wild type

β-ME Beta-mercaptoethanol







### Introduction and scope of the thesis

1

Part of this chapter is published in:
G.B.A. van Tilburg, A.F. Elhebieshy, and H. Ovaa. Synthetic and semi-synthetic strategies to study ubiquitin signaling. Curr Opin Struct Biol 38, 92–101 (2016).





#### Monoclonal antibodies and antibody fragments

The concept of using monoclonal antibodies as therapies can be tracked back to the late 19<sup>th</sup> century, when Ehrlich and Behring discovered that injecting animals with foreign material resulted in the production of natural antitoxins, now known as antibodies. These antibodies were proposed to serve as highly specific "magic bullets" against disease. However, it was more than 80 years later that antibody-based therapy truly started to unravel to its potential as a "magic bullet". Particularly, following the revolutionary discovery of both the hybridoma technology¹, enabling larger scale clonal production of antibodies, and the development of humanization approaches²-⁴ to minimize antibody immunogenicity.

Antibodies have a Y-shaped symmetric structure consisting of two identical heavy chains (~50 kDa) and two identical light chains (~25 kDa), connected by interchain disulfide and non-covalent bonds<sup>5</sup>. The structure is divided into two main regions: the variable region (Fab) and the constant region (Fc) (Fig. 1a)<sup>6</sup>. The Fab region, located at the tips of the "Y," contains antigen-binding sites and is responsible for the antibody's specificity. The Fc region, forming the stem, mediates effector functions, such as binding to immune cells and complement activation. Antibody fragments are engineered derivatives of full-length antibodies that retain functional properties while being smaller and more versatile. Common fragments include Fab (fragment antigen-binding)<sup>6</sup>, ScFv (single-chain variable fragment)<sup>7</sup>, and VHHs<sup>8,9</sup>, which consist of the variable heavy-chain domain derived from the unique heavy-chain-only antibodies found in camelids (Fig. 1b). These fragments are valuable for therapeutic and diagnostic applications due to their smaller size, improved tissue penetration, and ease of production in recombinant systems<sup>6-9</sup>.

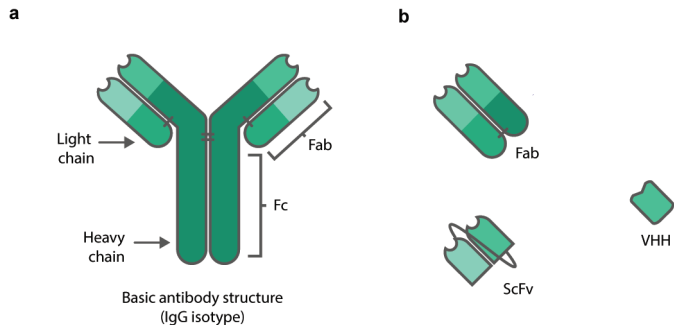


**Figure 1** | **Antibodies and antibody fragments**. (a) Schematic illustration of the basic antibody (IgG) structure. (b) Schematic illustration of commonly used antibody fragments.

#### Antibody engineering and approaches to multispecificity

Antibody engineering is a rapidly advancing field that leverages the specificity and adaptability of antibodies for various therapeutic, diagnostic, and research applications. This field involves the modification and optimization of antibodies to enhance their performance, improve their stability, and tailor their functionality to meet specific needs. The development of multi-specific antibodies represents a significant advancement in

antibody engineering, with many different formats of bi- and multi-specific antibodies developed in the last two decades<sup>10</sup>. While antibodies are naturally monospecific, recognizing one epitope, bi- and multi-specific antibodies are designed to recognize two or more different epitopes<sup>11</sup>. This offers several therapeutic advantages including enhanced targeting, improved efficacy, and synergistic effects. Their ability to integrate diverse functions, such as targeting cancer cells while activating immune responses, has made them valuable in therapeutic applications<sup>11</sup>. Various methods have been developed to generate these innovative molecules, each with distinct advantages and challenges.

One of the earliest approaches for the generation of a bispecific antibody, is using hybrid hybridomas<sup>12</sup>. This classical approach involves the fusion of two hybridoma cell lines producing distinct monoclonal antibodies. The resulting hybrid produces bispecific antibodies naturally but often suffers from low yield and instability, making it less practical for large-scale applications. Similarly, chemical crosslinking of antibody fragments such as Fab or ScFv from different monoclonal antibodies, offers a straightforward method for creating bispecific antibodies<sup>13,14</sup>. However, the lack of precision in chemical crosslinking often results in a heterogeneous product.

Sophisticated designs of multi-specific antibodies can be generated by genetic engineering and expression in various host systems such as CHO cells and *E. coli*<sup>15–17</sup>. Examples include single-chain formats like diabodies, triabodies, and tetrabodies<sup>18</sup>, or dual-variable-domain immunoglobulins (DVD-Ig)<sup>19</sup>, which utilize two sets of variable regions. Another widely used approach involves single-chain variable fragments (ScFvs), where the variable regions of heavy and light chains are linked to form small, functional antibody fragments<sup>7</sup>. These can be used to create bispecific T-cell engagers (BiTEs), which enhance immune-mediated killing by linking T cells to target cells<sup>20</sup>.

Technologies such as knobs-into-holes engineering and CrossMAbs provide additional solutions for bispecific antibody production. Knobs-into-holes engineering introduces complementary mutations in the Fc region of antibodies, promoting heterodimerization and ensuring proper assembly<sup>21–23</sup>. CrossMAbs achieve stability by swapping domains of heavy and light chains, allowing precise pairing of bispecific components<sup>24,25</sup>. These methods represent significant advancements in antibody engineering, enabling the development of tailored therapies for complex diseases like cancer, autoimmune disorders, and infectious diseases.

#### Approaches for the generation of antibody conjugates

Another rapidly expanding area in the field of antibody engineering is that of antibody conjugates, where continuous efforts are made for the attachment of one or multiple payloads, such as toxins, fluorophores or radioisotopes, to antibodies in a controlled and homogeneous manner <sup>26</sup>. These conjugates combine the specificity of antibodies for targeting specific epitopes on cells with the potency of the attached agents, making them highly effective in therapeutics and diagnostics. The generation of antibody conjugates involves various strategies aimed at achieving stable, efficient, and site-specific attachment while preserving the biological activity of the antibody.

Chemical conjugation is one of the earliest and most commonly used approaches. It

involves modifying specific amino acid residues, such as lysines or cysteines, to attach payloads<sup>27–29</sup>. Lysine-based conjugation is widely used due to the high abundance of lysines on antibody surfaces, while cysteine-based conjugation is slightly more specific, targeting the sulfhydryl groups of reduced cysteines. These approaches often produce heterogeneous products because of the limited control over the site and number of lysines or cysteines that are modified. This also often results in compromised stability, functionality and pharmacokinetics<sup>30–33</sup>.

In recent years, site-specific conjugation methods have gained prominence due to their ability to produce homogeneous conjugates with well-defined stoichiometry. Techniques such as engineered glycosylation sites<sup>34–36</sup> or the incorporation of unnatural amino acids<sup>37–41</sup> to introduce unique reactive sites enable precise attachment of payloads to antibodies at designated sites, minimizing off-target effects and enhancing therapeutic efficacy.

Enzyme-mediated conjugation methods have emerged as highly specific approaches for generating antibody conjugates. These methods use enzymes such as sortase, transglutaminase, or glycosyltransferases to catalyze the covalent attachment of payloads to specific amino acid sequences on antibodies. Sortase recognizes a unique pentapeptide sequence (LPXTG) engineered into the antibody, cleaving at the threonine residue and attaching the payload via a covalent bond to an incoming substrate with a glycine residue<sup>42–45</sup>. Transglutaminase targets glutamine residues, forming stable amide bonds with primary amines in the payload, offering flexibility in conjugate design<sup>31,46</sup>. Glycosyltransferases modify antibody glycosylation sites to attach payloads selectively, ensuring stability and functionality<sup>47</sup>. These enzyme-mediated approaches introduce site-specific modifications while preserving antibody integrity and functionality however, the yields are often low, and these approaches often require extensive optimization. As technology evolves, enzyme-mediated strategies continue to expand the possibilities for designing next-generation antibody conjugates with enhanced safety and efficacy profiles.

#### Antibody-antigen conjugates for DC-targeting vaccines

Antibody-antigen conjugates have emerged as an effective strategy for targeting dendritic cells (DCs) in vaccine development<sup>48</sup>. By leveraging the specificity of monoclonal antibodies for DC surface receptors, these conjugates enable the direct and efficient delivery of antigens to DCs, the primary antigen-presenting cells responsible for orchestrating adaptive immune responses<sup>49–52</sup>. Given the pivotal role of DCs in antigen uptake, processing, and subsequent T cell activation, targeted delivery strategies using antibody-antigen conjugates have the potential to significantly enhance the immunogenicity and therapeutic efficacy of vaccines, particularly in cancer immunotherapy and infectious disease control<sup>48,52</sup>.

The underlying mechanism of antibody-antigen conjugates centres on their ability to bind selectively to well-characterized DC surface molecules, such as DEC-205<sup>53–55</sup>, DC-SIGN<sup>56</sup>, or CLEC9A<sup>57,58</sup>. This receptor-mediated targeting facilitates enhanced antigen internalization, processing, and presentation via major histocompatibility complex (MHC) molecules, leading to efficient T cell priming and activation<sup>50,51</sup>. By concentrating

antigen delivery specifically to DCs, antibody-antigen conjugates reduce off-target effects and optimize immune modulation, which is critical for achieving potent and sustained immunological responses with minimal toxicity.

#### Ubiquitin (Ub)

As key player in the process of proteasome-mediated protein degradation and antigenic peptide presentation in the context of immune response initiation, the role of the small protein ubiquitin (Ub) has gained lots of attention. As such, as well as the interesting potential of Ub to be incorporated into poly-Ub chains we explored the potential of employing Ub as means of generating a diverse portfolio of Ab-conjugates. Ubiquitin is a 76-amino acid post-translational modifier fundamental to cellular homeostasis. Cellular processes regulated by ubiquitin modification range from classically known Ub-mediated proteasomal degradation to DNA repair, cell division, endoplasmic reticulum-associated degradation (ERAD), mRNA stability and even regulation of the innate immune system<sup>59</sup>. The post-translational modifier can be covalently attached to substrate proteins at the ε-amino group of lysine residues or at the protein's N-terminal residue<sup>60,61</sup>. Since ubiquitin harbors seven intrinsic lysine residues, it can also be conjugated to another Ub moiety. In this manner, homotypical ubiquitin chains of a single linkage type consisting of M1, K6, K11, K27, K29, K33, K48 or K63 can be formed, all of which are known to

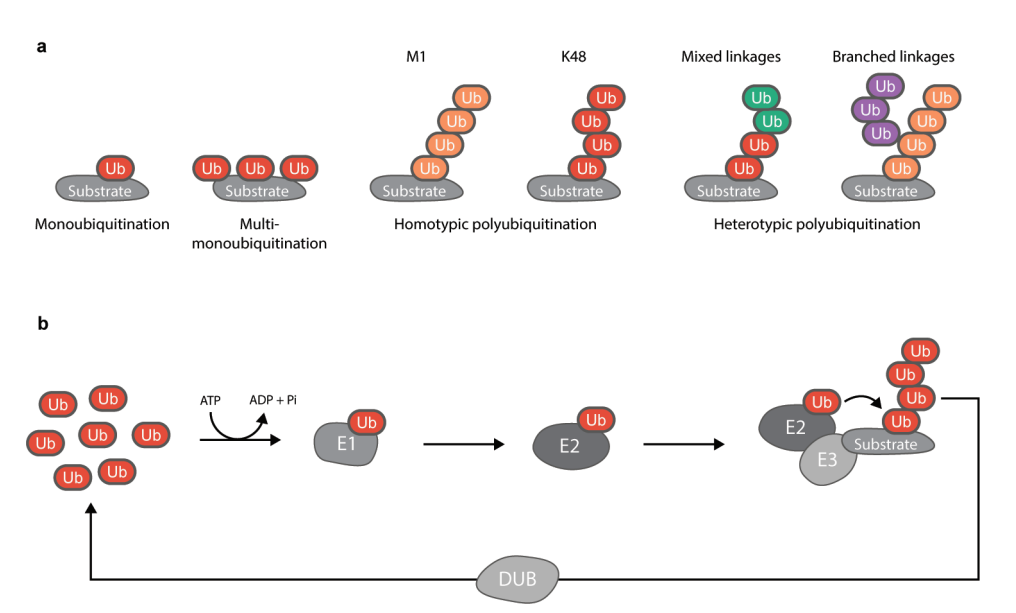


**Figure 2** The ubiquitin system. (a) Types of ubiquitin conjugation: ubiquitin (Ub) can be conjugated as a monomer on one site, or on multiple sites of the substrate protein (multi-monoubiquitination). It can also form homotypical ubiquitin polymers through its N-terminus (M1-linked) or either one of its seven lysine residues (e.g. K48-linked). Mixing of different linkage types gives rise to heterotypic polyubiquitin chains. (b) General overview of ubiquitin conjugation and deubiquitination by E1, E2, E3 enzymes and deubiquitinating enzymes (DUBs). Ubiquitin is activated by an E1 enzyme, transferred to a specific E2 enzyme and conjugated to a substrate protein with the help of an E3 ligase.

exist in vivo<sup>62</sup>. In addition, heterotypical chains of multiple ubiquitin linkage types can be formed, opening up an even more complex layer of post-translational modification (Fig. 2a). Conjugation of Ub to a substrate protein is carried out by a cascade of three enzymatic activities: E1 ubiquitin-activating, E2 ubiquitin-conjugating and E3 ubiquitinligating activities (Fig. 2b). To date, 2 human E1s, about 40 E2s and over 600 E3 enzymes are known. The combination of E2 and E3 enzymes dictates what type of ubiquitin chain is formed and which substrate protein becomes ubiquitinated. In addition, the ubiquitination status of a protein can be regulated by removal or editing of ubiquitin chains, which is carried out by a family of approximately 100 deubiquitinating enzymes (DUBs)<sup>63</sup>. For some of these DUBs, linkage specificity has also been observed. To study ubiquitin signals, much effort has been put into making differentially linked ubiquitin derivatives through synthetic and semi-synthetic methods, since these methods allow site specific incorporation of a specific chemoselective ligation handle. In addition, ubiquitin-based DUB probes and fluorescent ubiquitin-based enzyme substrates have seen an enormous boost, producing ubiquitin-based tools in all sorts of different flavors<sup>64</sup>.

#### **Chemical synthesis of Ubiquitin-based tools**

Native chemical ligation (NCL) has been an extremely useful tool to make ubiquitin, ubiquitin-peptide conjugates, ubiquitin dimers and ubiquitin tetramers, as reviewed by Pham et al.65. Chemical synthesis of ubiquitinated peptides was first established by Muir and co-workers and utilizes a ligation auxiliary where the auxiliary group is removed under photolytic conditions, yielding a natively linked Ub-peptide conjugate<sup>66</sup>. Today, most reported methods rely on the incorporation of a  $\gamma$ -thiolysine or  $\delta$ -thiolysine moiety at a designated lysine residue to allow NCL with a thioester moiety. The thiol containing ubiquitin module can be synthesized with total, linear synthesis<sup>67</sup>, or from two fragments<sup>68</sup>. During the total, linear fluorenylmethyloxycarbonyl (Fmoc)-based solid phase peptide synthesis (SPPS) approach, the growing peptide chain is stabilized by the incorporation of special building blocks that prevent the formation of aggregates as the ubiquitin chain grows. In the two segment approach, an N-terminal Ub(1-45)-SR fragment is synthesized and ligated to a synthetic C-terminal Ub[(46-76)-A46C] fragment. In the latter fragment, alanine 46 is replaced by N-methylcysteine to allow NCL with the first fragment and is afterwards converted into the native alanine residue through a desulphurization step. To make ubiquitin dimers and other conjugates, a thioester needs to be introduced at the ubiquitin C-terminus for NCL with the Ub thiolysine-containing module. The thioester functionality can be incorporated by E1mediated enzymatic conversion with sodium 2-mercaptoethane sulfonate (MESNa) 67 or during Fmoc-based SPPS<sup>69</sup>. Next, NCL can be performed and a subsequent desulphurization step results in a ubiquitin conjugate that bears the native isopeptide linkage. In addition, other strategies yielding a non-native isopeptide linkage have been reported and include oxime-based ligation for non-hydrolysable ubiquitin-conjugate synthesis<sup>70</sup> and thioether based ligation to prepare diubiquitin<sup>71</sup>, branched tri-ubiquitin<sup>72</sup> and polyubiquitin<sup>73</sup> modules that retain a sulfur atom in the forged isopeptide bond. It is clear that synthetic protein chemistry has much to offer to the biological community, but one must keep in mind that the chemistry is not always straightforward. In addition, protein folding must always be checked, although this is less of an issue with the very stable ubiquitin protein.

#### Scope and outline of this thesis

Conjugated antibodies are critical tools across research, diagnostics, and therapeutic applications. These conjugates range from fluorescently labelled antibodies used in imaging, to bispecific antibodies for dual antigen targeting, and antibody-drug conjugates (ADCs) for the targeted delivery of cytotoxic agents. However, current antibody conjugation strategies face several key challenges, notably the efficiency of the conjugation process and the heterogeneity of the resulting conjugates. These factors can significantly influence the stability, pharmacokinetics, toxicity profiles, and batch-to-batch consistency of the conjugated products. Together with the growing interest in multispecific antibodies and antibody complexes for dual or higher-order targeting, this presses for advances in conjugation techniques.

This thesis aims to develop and optimize covalent, site-specific conjugation technologies to enhance the efficiency, reproducibility, and functional performance of antibody conjugates. Additionally, it explores the application of synthetic peptide chemistry to overcome current limitations, offering better control over conjugation sites, improved reproducibility, and enhanced functional performance. By addressing these challenges, the work sets out to contribute to the development of next-generation antibody-based tools with broad implications for diagnostics, research, and therapeutic interventions.

In **chapter 2**, we introduce a novel modular antibody conjugation platform, based on the highly regulated yet versatile ubiquitin biochemistry. We exploit the site-specificity and efficiency of the enzymatic process of ubiquitination, by using ubiquitin as a conjugation tag fused to antibodies or antibody fragments, and hence provide a site-specific conjugation tag for the attachment of fluorescent labels to antibodies or for antibody multimerization. We establish the feasibility and efficiency of this method for the generation of fluorescently labelled Fabs, Fab di-, tri- and multimers, fluorescently labelled mAbs, and for the generation of bivalent, tetrameric antibody complexes.

The versatility of this platform, together with the involvement of ubiquitin in the cellular signalling for proteasomal degradation led us to explore the possible benefit of using ubi-tagging for the generation of antibody-based DC targeting vaccines presented in **chapter 3**. Here, we use our ubi-tagging technology for the conjugation of chemically synthesized Ub-OTI peptides to the DC targeting anti-DEC205 Fab-Ub. We then compare the ubi-tag based anti-DEC205 Fab-OTI conjugates to the state of the art anti-DEC205 Fab-OTI conjugates generated through sortagging. We demonstrate the superiority of ubi-tag-based Fab-OTI conjugates over the sortag-based conjugates *in vitro* and *in vivo*. Results obtained in this chapter provide a foundation for follow-up studies exploring the mechanism underlying the superiority of the ubi-tagged conjugates and further expanding the use of ubi-tagging for the targeted delivery of antigens to DCs.

Ubiquitin is known for its solubility and stability even when exposed to extreme

conditions<sup>74,75</sup>. It is often used as a solubility-tag to enhance the solubility of proteins during their expression in bacterial expression systems<sup>76,77</sup>. This led us to hypothesise that ubi-tagging could enhance the solubility of antigenic-epitopes known for their hydrophobicity such as NY-ESO-1 and 2W1S. In **Chapter 4**, we test the solubility of chemically synthesized Ub-peptides known to be highly hydrophobic and conjugate them to VHH-Ub. In this chapter we also establish the feasibility of using ubi-tagging for smaller antibody fragments as VHHs and demonstrate their functionality in the context of targeted vaccination to human DCs in vitro. We hereby provide a proof-of-concept of using ubi-tag conjugates for targeted antigen delivery in a human setting.

In **Chapter 5**, we present the total chemical synthesis of a 123 amino acid nanobody targeting GFP. We synthesized this nanobody modified with a propargyl functionality at its C-terminus for on-demand functionalization. We demonstrate that the nanobody is properly folded ad functionalize it with either a Biotin or a sulfo-Cyanine 5 dye and demonstrate the functionality of the resulting probes in a pull-down assay and using confocal microscopy. The total chemical synthesis of a nanobody shown here allows the generation of homogenous batches of nanobodies of defined quality and could potentially be applied for the streamlined preparation of nanobody-drug conjugates and multimers. In our opinion, this work underscores the importance of chemical synthesis in expanding the utility of nanobody-based tools across diverse scientific and medical fields.

In **Chapter 6**, we summarise the findings described in this thesis, discuss them in the context of existing literature and contemplate on the future prospects of the work presented in this thesis.

#### References

- 1. Köhler, G. & Milstein, C. Continuous cultures of fused cells secreting antibody of predefined specificity. *Nature* **256**, 495–497 (1975).
- 2. Brüggemann, M. *et al.* Comparison of the effector functions of human immunoglobulins using a matched set of chimeric antibodies. *Journal of Experimental Medicine* **166**, 1351–1361 (1987).
- 3. Brüggemann, M., Winter, G., Waldmann, H. & Neuberger, M. S. The immunogenicity of chimeric antibodies. *Journal of Experimental Medicine* **170**, 2153–2157 (1989).
- 4. Riechmann, L., Clark, M., Waldmann, H. & Winter, G. Reshaping human antibodies for therapy. *Nature 1988 332:6162* **332**, 323–327 (1988).
- 5. Huber, R., Deisenhofer, J., Colman, P. M., Matsushima, M. & Palm, W. Crystallographic structure studies of an IgG molecule and an Fc fragment. *Nature 1976* 264:5585 **264**, 415–420 (1976).
- 6. Schroeder, H. W. & Cavacini, L. Structure and function of immunoglobulins. *J Allergy Clin Immunol* **125**, (2010).
- 7. Ahmad, Z. A. *et al.* scFv Antibody: Principles and Clinical Application. *J Immunol Res* **2012**, 980250 (2012).
- 8. Harmsen, M. M. & De Haard, H. J. Properties, production, and applications of camelid single-domain antibody fragments. *Appl Microbiol Biotechnol* **77**, 13–22 (2007).
- 9. Bever, C. S. *et al.* VHH antibodies: emerging reagents for the analysis of environmental chemicals. *Anal Bioanal Chem* **408**, 5985–6002 (2016).
- 10. Goebeler, M. E., Stuhler, G. & Bargou, R. Bispecific and multispecific antibodies in oncology: opportunities and challenges. *Nature Reviews Clinical Oncology 2024 21:7* **21**, 539–560 (2024).
- 11. Brinkmann, U. & Kontermann, R. E. The making of bispecific antibodies. *MAbs* **9**, 182–212 (2017).
- 12. Milstein, C. & Cuello, A. C. Hybrid hybridomas and their use in immunohistochemistry. *Nature 1983 305:5934* **305**, 537–540 (1983).
- 13. Brennan, M., Davison, P. F. & Paulus, H. Preparation of bispecific antibodies by chemical recombination of monoclonal immunoglobulin G1 fragments. *Science* **229**, 81–83 (1985).
- 14. Segal, D. M. & Bast, B. J. E. G. Production of Bispecific Antibodies. *Curr Protoc Immunol* **14**, (1995).
- 15. Spiess, C. *et al.* Bispecific antibodies with natural architecture produced by coculture of bacteria expressing two distinct half-antibodies. *Nat Biotechnol* **31**, 753–758 (2013).

- 16. Wang, Q. et al. Design and Production of Bispecific Antibodies. *Antibodies* 2019, Vol. 8, Page 43 **8**, 43 (2019).
- 17. Chon, J. H. & Zarbis-Papastoitsis, G. Advances in the production and downstream processing of antibodies. *N Biotechnol* **28**, 458–463 (2011).
- 18. Todorovska, A. *et al.* Design and application of diabodies, triabodies and tetrabodies for cancer targeting. *J Immunol Methods* **248**, 47–66 (2001).
- 19. Wu, C. *et al.* Simultaneous targeting of multiple disease mediators by a dual-variable-domain immunoglobulin. *Nature Biotechnology 2007 25:11* **25**, 1290–1297 (2007).
- 20. Generation of a Half-Life Extended Anti-CD19 BiTE® Antibody Construct Compatible with Once-Weekly Dosing for Treatment of CD19-Positive Malignancies. *Blood* **130**, 2815 (2017).
- 21. Ridgway, J. B. B., Presta, L. G. & Carter, P. 'Knobs-into-holes' engineering of antibody CH3 domains for heavy chain heterodimerization. *Protein Engineering, Design and Selection* **9**, 617–621 (1996).
- 22. Atwell, S., Ridgway, J. B. B., Wells, J. A. & Carter, P. Stable heterodimers from remodeling the domain interface of a homodimer using a phage display library. *J Mol Biol* **270**, 26–35 (1997).
- 23. Kuglstatter, A. *et al.* Structural differences between glycosylated, disulfide-linked heterodimeric Knob-into-Hole Fc fragment and its homodimeric Knob-Knob and Hole-Hole side products. *Protein Engineering, Design and Selection* **30**, 649–656 (2017).
- 24. Klein, C. *et al.* Engineering therapeutic bispecific antibodies using CrossMab technology. *Methods* **154**, 21–31 (2019).
- 25. Fenn, S. *et al.* Crystal Structure of an Anti-Ang2 CrossFab Demonstrates Complete Structural and Functional Integrity of the Variable Domain. *PLoS One* **8**, e61953 (2013).
- 26. Journeaux, T. & Bernardes, G. J. L. Homogeneous multi-payload antibody–drug conjugates. *Nature Chemistry 2024 16:6* **16**, 854–870 (2024).
- 27. Sun, M. M. C. *et al.* Reduction-alkylation strategies for the modification of specific monoclonal antibody bisulfides. *Bioconjug Chem* **16**, 1282–1290 (2005).
- 28. Junutula, J. R. *et al.* Site-specific conjugation of a cytotoxic drug to an antibody improves the therapeutic index. *Nature Biotechnology 2008 26:8* **26**, 925–932 (2008).
- 29. Yamada, K. & Ito, Y. Recent Chemical Approaches for Site-Specific Conjugation of Native Antibodies:T echnologies toward Next-Generation Antibody-Drug Conjugates. doi:10.1002/cbic.201900178.
- 30. Wang, L., Amphlett, G., Blättler, W. A., Lambert, J. M. & Zhang, W. Structural characterization of the maytansinoid-monoclonal antibody immunoconjugate, huN901-

- DM1, by mass spectrometry. Protein Sci 14, 2436–2446 (2005).
- 31. Strop, P. *et al.* Location Matters: Site of Conjugation Modulates Stability and Pharmacokinetics of Antibody Drug Conjugates. *Chem Biol* **20**, 161–167 (2013).
- 32. Shen, B. Q. *et al.* Conjugation site modulates the in vivo stability and therapeutic activity of antibody-drug conjugates. *Nature Biotechnology 2012 30:2* **30**, 184–189 (2012).
- 33. Agarwal, P. & Bertozzi, C. R. Site-specific antibody-drug conjugates: The nexus of bioorthogonal chemistry, protein engineering, and drug development. *Bioconjug Chem* **26**, 176–192 (2015).
- 34. Van Geel, R. *et al.* Chemoenzymatic Conjugation of Toxic Payloads to the Globally Conserved N-Glycan of Native mAbs Provides Homogeneous and Highly Efficacious Antibody-Drug Conjugates. *Bioconjug Chem* **26**, 2233–2242 (2015).
- 35. Ruhe, L., Ickert, S., Beck, S. & Linscheid, M. W. A new strategy for metal labeling of glycan structures in antibodies. *Anal Bioanal Chem* **410**, 21–25 (2018).
- 36. Toftevall, H., Nyhlén, H., Olsson, F. & Sjögren, J. Antibody Conjugations via Glycosyl Remodeling. *Methods in Molecular Biology* **2078**, 131–145 (2020).
- 37. Axup, J. Y. *et al.* Synthesis of site-specific antibody-drug conjugates using unnatural amino acids. *Proc Natl Acad Sci U S A* **109**, 16101–16106 (2012).
- 38. Oller-Salvia, B., Kym, G. & Chin, J. W. Rapid and Efficient Generation of Stable Antibody–Drug Conjugates via an Encoded Cyclopropene and an Inverse-Electron-Demand Diels–Alder Reaction. *Angewandte Chemie International Edition* **57**, 2831–2834 (2018).
- 39. Kim, C. H. *et al.* Synthesis of bispecific antibodies using genetically encoded unnatural amino acids. *J Am Chem Soc* **134**, 9918–9921 (2012).
- 40. Hofer, T., Skeffington, L. R., Chapman, C. M. & Rader, C. Molecularly defined antibody conjugation through a selenocysteine interface. *Biochemistry* **48**, 12047–12057 (2009).
- 41. Zimmerman, E. S. *et al.* Production of site-specific antibody-drug conjugates using optimized non-natural amino acids in a cell-free expression system. *Bioconjug Chem* **25**, 351–361 (2014).
- 42. Beerli, R. R., Hell, T., Merkel, A. S. & Grawunder, U. Sortase Enzyme-Mediated Generation of Site-Specifically Conjugated Antibody Drug Conjugates with High In Vitro and In Vivo Potency. *PLoS One* **10**, e0131177 (2015).
- 43. Swee, L. K. *et al.* Sortase-mediated modification of aDEC205 affords optimization of antigen presentation and immunization against a set of viral epitopes. *Proc Natl Acad Sci U S A* **110**, 1428–1433 (2013).
- 44. Bridoux, J. et al. Anti-Human PD-L1 Nanobody for Immuno-PET Imaging:

- Validation of a Conjugation Strategy for Clinical Translation. *Biomolecules 2020, Vol. 10, Page 1388* **10**, 1388 (2020).
- 45. Morgan, H. E., Turnbull, W. B. & Webb, M. E. Challenges in the use of sortase and other peptide ligases for site-specific protein modification. *Chem Soc Rev* **51**, 4121–4145 (2022).
- 46. Strop, P. Versatility of microbial transglutaminase. *Bioconjug Chem* **25**, 855–862 (2014).
- 47. Boeggeman, E. *et al.* Site specific conjugation of fluoroprobes to the remodeled Fc N-glycans of monoclonal antibodies using mutant glycosyltransferases: Application for cell surface antigen detection. *Bioconjug Chem* **20**, 1228 (2009).
- 48. Lee, K. W., Yam, J. W. P. & Mao, X. Dendritic Cell Vaccines: A Shift from Conventional Approach to New Generations. *Cells* **12**, (2023).
- 49. Banchereau, J. & Steinman, R. M. Dendritic cells and the control of immunity. *Nature* **392**, 245–252 (1998).
- 50. Oliveira, M. M. S. *et al.* Increased cross-presentation by dendritic cells and enhanced anti-tumour therapy using the Arp2/3 inhibitor CK666. *Br J Cancer* **128**, 982–991 (2023).
- 51. Joffre, O. P., Segura, E., Savina, A. & Amigorena, S. Cross-presentation by dendritic cells. *Nat Rev Immunol* **12**, 557–569 (2012).
- 52. Mastelic-Gavillet, B., Balint, K., Boudousquie, C., Gannon, P. O. & Kandalaft, L. E. Personalized Dendritic Cell Vaccines-Recent Breakthroughs and Encouraging Clinical Results. *Front Immunol* **10**, (2019).
- 53. Jiang, W. *et al.* The receptor DEC-205 expressed by dendritic cells and thymic epithelial cells is involved in antigen processing. *Nature* **375**, 151–155 (1995).
- 54. Lehmann, C. H. K. *et al.* Direct Delivery of Antigens to Dendritic Cells via Antibodies Specific for Endocytic Receptors as a Promising Strategy for Future Therapies. *Vaccines 2016, Vol. 4, Page 8* **4**, 8 (2016).
- 55. Bonifaz, L. C. *et al.* In Vivo Targeting of Antigens to Maturing Dendritic Cells via the DEC-205 Receptor Improves T Cell Vaccination. *J Exp Med* **199**, 815 (2004).
- 56. Geijtenbeek, T. B. H. *et al.* Identification of DC-SIGN, a novel dendritic cell-specific ICAM-3 receptor that supports primary immune responses. *Cell* **100**, 575–585 (2000).
- 57. Cauwels, A. *et al.* Delivering type i interferon to dendritic cells empowers tumor eradication and immune combination treatments. *Cancer Res* **78**, 463–474 (2018).
- 58. Cauwels, A. *et al.* Targeting interferon activity to dendritic cells enables in vivo tolerization and protection against EAE in mice. *J Autoimmun* **97**, 70–76 (2019).

- 59. Akutsu, M., Dikic, I. & Bremm, A. Ubiquitin chain diversity at a glance. *J Cell Sci* **129**, 875–880 (2016).
- 60. Ciechanover, A. & Ben-Saadon, R. N-terminal ubiquitination: more protein substrates join in. *Trends Cell Biol* **14**, 103–106 (2004).
- 61. Hershko, A. & Ciechanover, A. The ubiquitin system. *Annu Rev Biochem* **67**, 425–479 (1998).
- 62. Peng, J. *et al.* A proteomics approach to understanding protein ubiquitination. *Nature Biotechnology 2003 21:8* **21**, 921–926 (2003).
- 63. Komander, D. & Rape, M. The ubiquitin code. *Annu Rev Biochem* **81**, 203–229 (2012).
- 64. Ekkebus, R., Flierman, D., Geurink, P. P. & Ovaa, H. Catching a DUB in the act: novel ubiquitin-based active site directed probes. *Curr Opin Chem Biol* **23**, 63–70 (2014).
- 65. Pham, G. H. & Strieter, E. R. Peeling away the layers of ubiquitin signaling complexities with synthetic ubiquitin–protein conjugates. *Curr Opin Chem Biol* **28**, 57–65 (2015).
- 66. Chatterjee, C., McGinty, R. K., Pellois, J. P. & Muir, T. W. Auxiliary-mediated site-specific peptide ubiquitylation. *Angewandte Chemie International Edition* **46**, 2814–2818 (2007).
- 67. El Oualid, F. *et al.* Chemical synthesis of ubiquitin, ubiquitin-based probes, and diubiquitin. *Angewandte Chemie International Edition* **49**, 10149–10153 (2010).
- 68. Kumar, K. S. A., Spasser, L., Erlich, L. A., Bavikar, S. N. & Brik, A. Total Chemical Synthesis of Di-ubiquitin Chains. *Angewandte Chemie International Edition* **49**, 9126–9131 (2010).
- 69. Erlich, L. A., Kumar, K. S. A., Haj-Yahya, M., Dawson, P. E. & Brik, A. N-Methylcysteine -mediated total chemical synthesis of ubiquitin thioester. *Org Biomol Chem* **8**, 2392–2396 (2010).
- 70. Shanmugham, A. *et al.* Nonhydrolyzable ubiquitin-isopeptide isosteres as deubiquitinating enzyme probes. *J Am Chem Soc* **132**, 8834–8835 (2010).
- 71. Ji, E. J. *et al.* Functional ubiquitin conjugates with lysine-ε-amino-specific linkage by thioether ligation of cysteinyl-ubiquitin peptide building blocks. *Bioconjug Chem* **20**, 1152–1162 (2009).
- 72. Valkevich, E. M. *et al.* Forging isopeptide bonds using thiol-ene chemistry: Site-specific coupling of ubiquitin molecules for studying the activity of isopeptidases. *J Am Chem Soc* **134**, 6916–6919 (2012).
- 73. Trang, V. H. *et al.* Nonenzymatic Polymerization of Ubiquitin: Single-Step Synthesis and Isolation of Discrete Ubiquitin Oligomers. *Angewandte Chemie International Edition* **51**, 13085–13088 (2012).

- 74. Vijay-kumar, S., Bugg, C. E. & Cook, W. J. Structure of ubiquitin refined at 1.8 A resolution. *J Mol Biol* **194**, 531–544 (1987).
- 75. Ciechanover, A., Elias, S., Heller, H., Ferber, S. & Hershko, A. Characterization of the heat-stable polypeptide of the ATP-dependent proteolytic system from reticulocytes. *Journal of Biological Chemistry* **255**, 7525–7528 (1980).
- 76. Butt, T. R. *et al.* Ubiquitin fusion augments the yield of cloned gene products in Escherichia coli. *Proceedings of the National Academy of Sciences* **86**, 2540–2544 (1989).
- 77. Baker, R. T., Smith, S. A., Marano, R., McKee, J. & Board, P. G. Protein expression using cotranslational fusion and cleavage of ubiquitin. Mutagenesis of the glutathione-binding site of human Pi class glutathione S-transferase. *Journal of Biological Chemistry* **269**, 25381–25386 (1994).





# Ubiquitin as a conjugation tag for labeling and multimerization of antibodies

2

This chapter is part of the publication:

A.F. Elhebieshy\*, Z. Wijfjes\*, et al. Site-directed multivalent conjugation of antibodies to ubiquitinated payloads. Accepted for publication: Nature Biomedical Engineering.



### Ubiquitin as a conjugation tag for labeling and multimerization of antibodies

Angela F. el Hebieshy, Johan M. S. van Der Schoot, Jim Middelburg, Marjolein Sluijter, Thorbald van Hall, Douwe J. Dijkstra, Leendert A. Trouw, Cami M. P. Talavera Ormeño, Bjorn R. van Doodewaerd, Paul W. H. I. Parren, Gerbrand J. van der Heden van Noort, Martijn Verdoes, Ferenc A. Scheeren, Huib Ovaa.

#### **Abstract**

Antibody conjugates form a foundation for many research-, diagnostic-, and therapeutic applications. Despite the robustness and efficiency of existing antibody conjugation techniques, the challenge of efficiently obtaining homogeneous products remains. Here, we developed a versatile modular method for site-directed antibody conjugation using the small protein ubiquitin. We show that ubiquitin, when fused to antibodies or antibody fragments, is conjugated using in vitro ubiquitin ligation with an average efficiency of 94%. We effectively applied this method, which we named ubi-tagging, to conjugate chemically synthesized ubiquitin with a site-specifically incorporated payload (fluorophore) to ubi-tagged Fab fragments. Additionally, we show that this method can be efficiently used to generate di-, tri-, and multi-valent antibody complexes and to generate a bi-specific T cell activator. The combined use of both recombinant ubitags and synthetic ubiquitin allows homogeneous site-directed antibody conjugation with defined conjugates incorporating precise functionalities while retaining antibody functionality.

#### Introduction

Antibodies are indispensable tools in the fields of chemical biology, diagnostics and therapeutics, owing to their high selectivity and affinity towards specific target molecules.

Over the past decade, the interest in antibody-based reagents and therapeutics of higher complexity than monoclonal antibodies has been growing steeply. This led to the soaring development of antibody engineering technologies for the production of antibody conjugates and multivalent antibody formats such as antibodies conjugated to fluorophores for analytical or diagnostic applications, antibodies conjugated to small molecules forming antibody-drug conjugates (ADCs), and bi- or multi-specific antibodies targeting multiple targets simultaneously.

Conventional antibody conjugation strategies rely on the random attachment to certain amino acid residues along the antibody. These techniques make use of the chemical properties of the side chain of lysine or cysteine residues through NHS labeling or thiol-reactive maleimide groups, respectively<sup>1–3</sup>. Despite being used in clinical-grade antibody products, such random modifications result in highly heterogeneous products,

with limited control over the number and site of modifications, often compromising antibody functionality and pharmacokinetics<sup>4-7</sup>. Remarkable advances have been made in developing site-specific conjugation techniques to overcome these challenges, including the incorporation of non-natural amino acids in the antibody sequence carrying reactive groups for bio-orthogonal chemistry 8-12, glycan-remodeling of native glycans to install an unnatural sugar containing a conjugation handle<sup>13-15</sup>, and the fusion of a peptide tag to the antibody that can be specifically modified enzymatically. Well-exemplified in the latter category are ligation strategies based on enzymes such as transglutaminase, formylglycine-generating enzyme (FGE), and sortase. Microbial transglutaminase (mTG) recognizes a specific glutamine-containing sequence and covalently attaches an amine-functionalized linker carrying a payload or conjugation handle to the glutamine residue while expelling ammonia<sup>5,16</sup>. Formylglycine-generating enzyme (FGE) converts the cysteine residue present in its recognition motif to an aldehyde functional group which serves as a conjugation handle 17,18, while sortase mediates the ligation of its recognition sequence to an oligoglycine peptide attached to a payload, peptide or conjugation handle 19-22. These techniques are site-specific and modular for the ligation of synthetic payloads to antibodies or antibody fragments, however, significant challenges remain. In particular, long reaction times on the order of hours and even days, limited reaction efficiency, and poor yields are key limitations to using these techniques<sup>5,17,21–23</sup>. Additionally, a two-step approach is required when using these techniques for protein-protein conjugation, for example to generate a bispecific antibody<sup>23,24</sup>, which is time consuming and often leads to reduced yields.

To address these limitations, here we introduce a novel versatile modular approach for site-specific antibody conjugation based on ubiquitin biochemistry and the chemical synthesis of ubiquitin-related tools. We set out to determine the use of ubiquitin as a conjugation tag for the site-selective attachment of different moieties to antibodies and the generation of multivalent antibody complexes in a controlled manner using ubiquitinating enzymes (Fig. 1a).

Ubiquitin (Ub) is a small protein tag involved in almost all cellular processes<sup>25–28</sup>. It is a 76-amino acid post-translational modifier that is covalently attached to target proteins in a highly regulated process called ubiquitination. This process is coordinated by an enzymatic cascade involving ubiquitin-activating (E1)<sup>29</sup>, ubiquitin-conjugating (E2)<sup>30</sup>, and ubiquitin-ligating (E3)<sup>31,32</sup> enzymes, resulting in the covalent attachment of the C-terminal glycine residue of ubiquitin to the N-terminus or lysine residues of target proteins. Ubiquitin molecules also have the ability to be conjugated to each other at one of the seven internal lysine residues or at the N-terminal methionine residue. This results in the formation of ubiquitin chains with different linkage types<sup>26</sup>. Notably, the linkage type involved in ubiquitin chain-formation is regulated by different E2 and E3 enzymes<sup>31–34</sup>. Linkage-specific ubiquitin chains of all types can therefore be efficiently

ligated *in vitro* using the appropriate recombinant E1, E2, and E3 enzymes<sup>35</sup>. The E2 and E3 can be provided as a fusion protein<sup>36</sup> to increase ligation activity (Fig. 1a). In addition, using specific ubiquitin mutants, the process of ubiquitin chain formation can be fully controlled<sup>35,37</sup>. These features combined make the exploitation of ubiquitin and the ubiquitination machinery an interesting approach to selectively generate antibody conjugates that are site-specifically joined through ubiquitin chains of a specific ubiquitin-linkage type. Fusing ubiquitin to an antibody at a position not affecting its binding, hereafter referred to as ubi-tagging, would allow the precise *in vitro* engineering of this ubiquitin at specific lysine residues depending on the E2 and E3 used. Ubi-tagged antibodies can be conjugated to another ubiquitin fused-antibody, making a bispecific antibody, or to a chemically synthesized ubiquitin carrying selected modifications such as a fluorophore, label, or cytotoxic drug. This provides a modular platform for the generation of ubiquitin-based antibody conjugates of limitless different architectures, marrying the advantages of (therapeutic) protein engineering and synthetic chemistry.

The vast potential of ubi-tagging is exemplified by the generation of homogeneous conjugates, including fluorescently-labeled Fab fragments and defined Fab multimers. Moreover, we demonstrate ubiquitin chain elongation of Fab hetero-dimers to form hetero-trimers and show that ubi-tagged conjugates can be site-specifically cleaved using deubiquitinating enzymes.

#### Results

#### Generation and characterization of ubi-tagged antibody fragments

As a proof of principle, we selected monovalent Fab fragments to characterize ubiquitin conjugation in the context of antibody-ubiquitin fusion. The Fab fragment is produced as a fusion protein with a ubi-tag followed by a His-tag at the C-terminus of its heavy chain (Fig. 1b). We generated recombinant ubi-tagged Fab fragments using CRISPR/HDR, which we recently developed for the production of modified recombinant antibodies<sup>38</sup>. The IgH locus of parental hybridoma cell line anti-CD3 (KT3, mlgG2a) WT was genetically modified to switch production from WT mAbs to ubiquitin-His-tagged Fabs (Fig. 1c). The genetically-modified monoclonal cell lines were assessed for the secretion of Ubiquitin-His-tagged Fab fragments using an anti-his secondary antibody. The supernatant of over 80% of the single-cell colonies that grew out after antibiotic selection were positive for the His-tag, indicating that these edited monoclonal cell lines produced a ubi-tagged Fab fragment (Fig. 1d). Next, we selected a monoclonal cell line highly expressing the ubi-tagged Fab and expanded it for further characterization. The Fab fragments isolated from the supernatants were validated for the presence of the ubi-tag on the heavy chain by resolving on SDS-PAGE, with or without prior reduction using β-mercaptoethanol, followed by anti-ubiquitin western blotting (Fig. 1e).

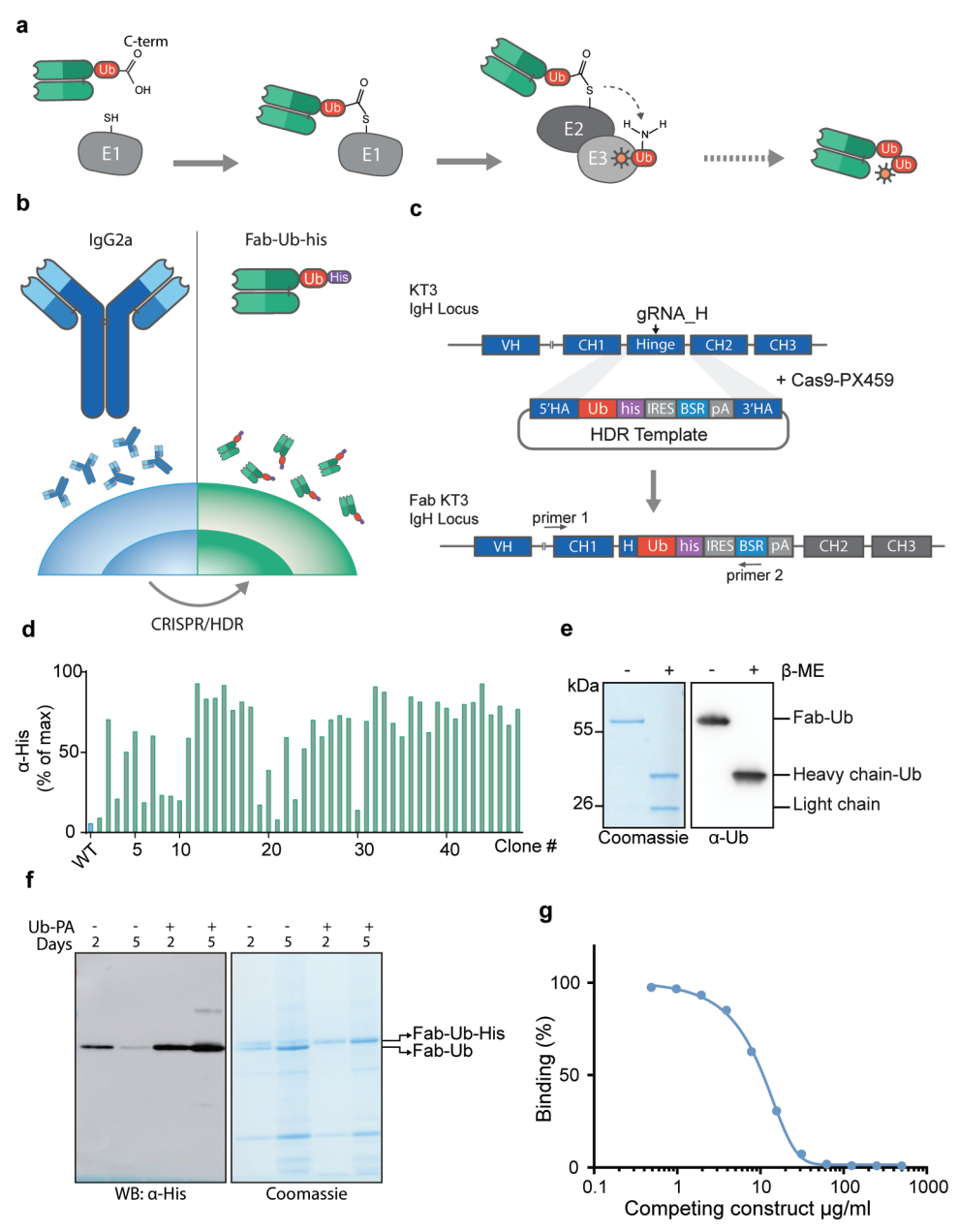


Figure 1| Generation and site-specific labeling of ubi-tagged antibody fragments. (a) Schematic illustration of ubi-tag conjugation using the ubiquitination cascade. The ubi-tag C-terminus is activated by the E1 enzyme to form a thioester bond. The activated ubi-tag is then transferred to an E2 enzyme which then, with the help of an E3 enzyme, specifically transfers it to a lysine residue of another ubiquitin or ubi-tag, forming a ubi-tag dimer linked via an iso-peptide bond. (b) Schematic representation of the general CRISPR/HDR hybridoma genome editing approach for the generation of ubi-tagged Fab fragments where ubiquitin (red) is fused to the C-terminus of the heavy chain of a Fab (green) followed

by a His-tag (purple). (c) The IgH locus of KT3 is targeted for double strand break by gRNA\_H to allow the integration of the homology directed repair (HDR) template consisting of a ubi-tag, His-tag, an internal ribosomal entry site (IRES) and blasticidin resistance gene (BSR) (d) Flow cytometry screening of clonal supernatants of the CRISPR/HDR targeted cells following limiting dilution, showing EL4 cells expressing mCD3 incubated with the supernatants followed by anti-his secondary antibody. (e) SDS-PAGE analysis of purified Fab-Ub in the absence or presence of  $\beta$ -mercaptoethanol, stained with Coomassie Blue and analyzed by western blot using an anti-Ub antibody. (f) Coomassie staining and western blot analysis of hybridoma culturing media containing ubi-tagged Fab after 2 and 5 days in presence or absence of Ubiquitin-propargylamide (Ub-PA). (g) Antigen binding competition assay of murine CD3 Fab-Ub against fluorescently-labeled parental mAb of the same clone. Representative of n=3 independent experiments.

### Isolation and functional characterization of ubi-tagged antibody fragments

After expansion, the modified hybridoma cells were cultivated for antibody fragment production for 7 to 10 days. After cultivation, we observed that the ubi-tagged Fabs partially or fully lost the C-terminal His-tag, depending on the duration in which the hybridoma cells were cultivated. We hypothesized that the C-terminal His-tag is possibly lost during culture due to deubiquitinating enzymes (DUBs) released by dying cells into the culturing media cleaving the His-tag from the C-terminus of ubiquitin<sup>39–41</sup>. To test this, we cultivated the modified hybridoma cells in presence or absence of C-terminally propargylated ubiquitin (Ub-PA), known to selectively inhibit cysteine DUBs, and detected the presence of the His-tag on the ubi-tagged Fab secreted in the supernatant at day 2 and 5 of cultivation by anti-his western blot analysis. In absence of Ub-PA in the culture media, on day 2 a thin band was observed by western blot analysis which decreased in intensity by day 5 (Fig 1f). Also when the ubi-tagged Fab containing supernatants were visualized by coomassie, in absence of Ub-PA, two bands were observed corresponding to Fab-Ub-his and Fab-Ub. However, in presence of Ub-PA in the culture media, a single band is observed by Coomassie and on western blot the intensity of the band increased, indicating that indeed the loss of the His-tag during cultivation can be resolved by supplementing the culture medium with 1 μM Ub-PA (Fig. 1f). Following cultivation and isolation of the ubi-tagged Fab-fragment, we performed a competitive antigen binding assay to confirm that the ubi-tagged Fab-fragment retained antigen binding. Here, we used the CD3 expressing cell line EL442 to compete a fixed concentration of fluorescently labeled parental antibody against increasing concentrations of unlabeled ubi-tagged Fab CD3. The ubi-tagged Fab competed with the fluorescent parental antibody in a dose-dependent manner, indicating that antigen binding was retained (Fig. 1g).

## Site-specific fluorescent labeling of ubi-tagged Fab fragments

Having validated that the binding of a ubi-tagged antibody fragment to its cognate antigen is retained, we next set out to determine the feasibility of using ubiquitin as a conjugation tag. Three main determinants crucial for the specificity of ubi-tag conjugation are: (1) the ubiquitinating enzymes specific for a single lysine linkage-

type, (2) the acceptor ubi-tag (ub<sup>acc</sup>) carrying the corresponding lysine residue while having an unavailable C-terminal glycine, and (3) the donor ubi-tag (Ub<sup>don</sup>) having a free C-terminal glycine while the conjugating enzyme-specific lysine is mutated. This design ensures that the two different ubi-tagged moieties are only conjugated to one another and prevents either of them from being conjugated to a similar ubi-tag moiety (Fig. 2a).

To assess the efficiency of using ubiquitin as a conjugation tag for the introduction of a payload to the ubi-tagged Fab, we used a donor ubi-tagged Fab, hereafter referred to as Fab-Ubdon, and a chemically synthesized acceptor ubiquitin carrying a rhodamine fluorophore on its N-terminus, hereafter referred to as Rho-Ubacc (Fig. 2a and Supplementary Fig. 1). For this conjugation reaction, the lysine-48 (K48)-specific ubiquitin E2-E3 fusion protein gp78RING-Ube2g2 was used36. To validate our design and confirm that no self-tagging occurs, the ubi-tag conjugation was carried out in the presence or absence of the donor and acceptor ubi-tag, respectively. In the presence of both Rho-Ubacc and Fab-Ubdon, a single fluorescent band was observed after 30 minutes, indicating the formation of a single product corresponding to a Fab attached to a fluorescent label through ubiquitin chain formation (Fig. 2b). In the absence of either Rho-Ubacc or Fab-Ubdon, no product formation was observed. In the absence of Rho-Ubacc, the band shifting upwards at around 90 kDa after 30 minutes on Coomassie corresponds to the molecular weight of Fab-Ubdon loaded on the E2-E3 enzyme. The product of the conjugation reaction, fluorescently labeled Fab (hereafter Rho-Ub<sub>3</sub>-Fab), was purified using Protein G affinity purification and analyzed using ESI-TOF mass spectrometry (Fig. 2b). The disappearance of the mass peak corresponding to the mass of Fab-Ub<sup>don</sup> indicated that it was completely consumed in the conjugation reaction and the mass observed corresponded to the calculated mass of the covalently attached Rho-Ub<sub>2</sub>-Fab (Fig. 2b). The efficiency of ubi-tag conjugation reactions carried out in the scope of this study were quantified, showing an average efficiency of 94% for all reactions involving ubi-tagged Fab fragments (Supplementary Fig. 2). To assess the effect of ubi-tag conjugation on protein stability, we compared the thermal unfolding profiles of Rho-Ub<sub>2</sub>-Fab to that of the unconjugated Fab-Ub<sup>don</sup>. We monitored the temperature-dependent change in intrinsic protein fluorescence to determine the infliction temperature at which the protein unfolds. Both conjugated and unconjugated ubi-tag Fab showed an infliction temperature of about 75 °C, indicating that ubi-tagging does not alter protein stability (Fig. 2c). Next, we used flow cytometry to compare the staining of CD3 positive mouse splenocytes with Rho-Ub<sub>3</sub>-Fab CD3 to the staining with FITC-labeled parental antibody (Fig. 2d). Both Rho-Ub<sub>3</sub>-Fab CD3 and FITC labeled parental antibody showed a comparable percentage of CD3-positive cells, illustrating that ubi-tag conjugation does not hinder antigen binding.

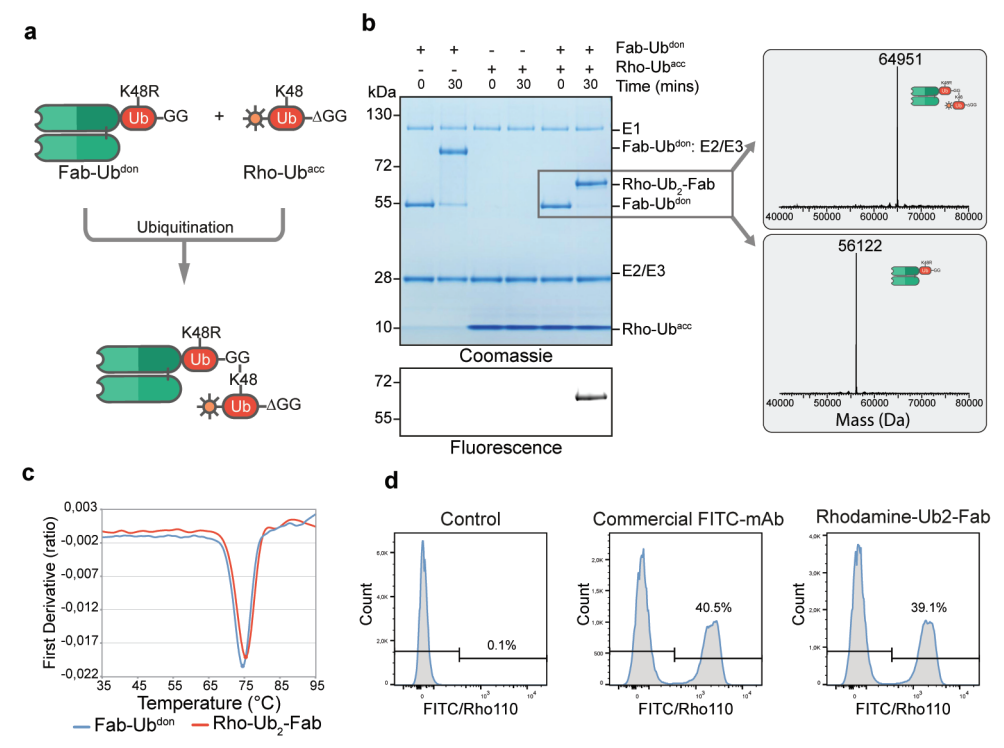
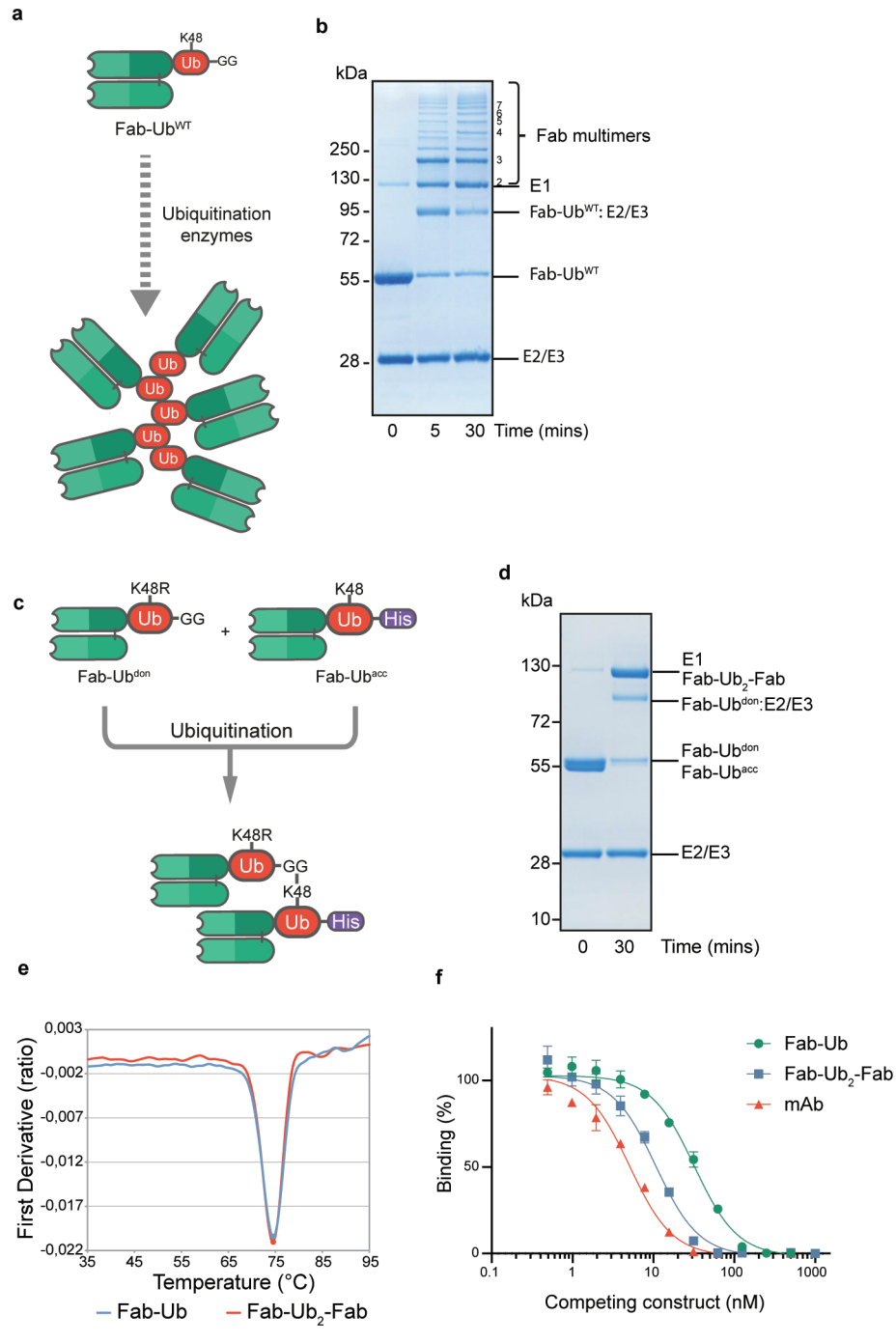


Figure 2 | Ubi-tag conjugation for the site-specific fluorescent labeling of a ubi-tagged Fab fragment (a) Schematic representation of the concept of K48-specific ubi-tag conjugation for the fluorescent labeling of Fab-Ub. (b) Labeling of Fab-Ub<sup>don</sup> with Rho-Ub<sup>acc</sup> using K48-specific ubiquitination enzymes shown by non-reducing SDS-PAGE followed by fluorescent imaging and Coomassie Blue staining. The deconvoluted ESI-TOF mass spectrum of the Fab fragments isolated from the reaction mixture confirmed the conjugation of all Fab-Ub<sup>don</sup> to form Rho-Ub<sub>2</sub>-Fab. (c) Thermal unfolding profiles of Fab-Ub (blue) and the conjugated Rho-Ub<sub>2</sub>-Fab (red) showing similar thermostability. (d) Histograms of mouse splenocytes showing the percentage CD3 positive cells stained with Rho-Ub<sub>2</sub>-Fab CD3 or FITC-mAb CD3 analyzed by flow cytometry.

#### Bi-and tri-valent antibody formats using ubi-tag conjugation

Having established and validated ubi-tag conjugation for antibody fragments, we next decided to assess the production of multimeric antibody formats using ubi-tag conjugation. We first evaluated the upper limit for the multimerization reaction efficiency, using a ubi-tagged Fab where the fused ubiquitin has both the acceptor lysine available as well as a free C-terminal glycine (hereafter referred to as Fab-Ub<sup>WT</sup>) to allow the formation of higher-order ubiquitin chains (Fig. 3a). Within 30 minutes of the conjugation reaction, the majority of Fab-Ub<sup>WT</sup> was converted to multimeric Fab-Ub chains, showing the feasibility of the ubiquitination enzymes to elongate the Fab-Ub chains forming multimers as high as the 11<sup>th</sup> order and beyond, indicating that a large cargo such as a Fab of 50 kDa does not hamper ubi-tag conjugation (Fig. 3b and Supplementary Fig. 3).



**Figure 3| Site-specific Fab multimerization and dimerization through ubi-tag conjugation.** (a) Schematic overview of ubi-tag based multimerization reaction of Fab-Ub<sup>WT</sup>, where both the C-terminal glycine residue as well as lysine 48 are available for conjugation. (b) Non-reducing SDS-

PAGE gel stained with Coomassie Blue visualizing multimerization of Fab-UbWT in 30 minutes. (c) Schematic diagram of site-specific heterodimerization of ubi-tagged Fab-fragments. (d) Non-reducing SDS-PAGE analysis of site-specific conjugation to generate Fab-Ub2-Fab. Here, both ubi-tagged Fab moieties target mCD3. (e) Thermal unfolding of Fab-Ub2-Fab (red) compared to Fab-Ub (blue) showing that dimerization does not compromise the stability of the ubi-tagged Fab fragment. (f) Competition binding assay of each of Fab-Ub (green), Fab-Ub2-Fab (blue), and parental mAb (red) targeting mCD3 against fluorescently labeled parental mAb. Representative experiment of n=3, each condition performed in triplicates. Data are shown as mean ±SD.

Next, we set out to make a bivalent monospecific Fab-Ub<sub>3</sub>-Fab against mouse CD3. The monospecific Fab heterodimer was efficiently generated by conjugating a Fab CD3-Ubacc, with a His-tag blocking the C-terminal glycine, to a Fab CD3-Ubdon with a UbK48R mutation (Fig. 3c and 3d). The resulting Fab-Ub<sub>2</sub>-Fab was assessed for its thermostability compared to the Fab-Ub monomer. Indeed, dimerization did not influence the thermostability compared to the monomer (Fig. 3e). To validate the functionality and assess the avidity effect of the bivalent antibody format compared to the monovalent Fab-Ub, a competition binding assay was performed using EL4 cells expressing mouse CD3 (Fig. 3f). For this, we competed a fixed concentration of fluorescentlylabeled parental antibody against increasing concentrations of Fab-Ub, Fab-Ub<sub>2</sub>-Fab, and unlabeled parental antibody. Fab-Ub<sub>3</sub>-Fab showed a lower IC<sub>50</sub> compared to the monovalent Fab-Ub which we attribute to the increased avidity of the bi-valent format. Next, we set out to investigate the feasibility of site-specific ubiquitin chain elongation of the hetero-dimeric Fab-Ub<sub>2</sub>-Fab to form a hetero-trimer. We reasoned that exposing the C-terminal glycine of the Ubacc of the Fab dimer would transform it into a Fab-Ub<sub>a</sub>don-Fab, allowing it to be available for conjugation to a third Ubacc moiety (Fig. 4a). For this purpose, we used the deubiquitinating enzyme (DUB) UCHL3, known to exclusively liberate the C-terminus of Ub and not the isopeptide linkage in the Ub,, to cleave the His-tag from the C-terminus of the Ub, 40,41,43. The cleavage reaction was monitored by mass spectrometry, detecting a decrease in mass of the heavy chain dimer of 1371 Da, corresponding to the His, tag being cleaved off (Fig. 4b). Following isolation from the reaction mixture, the Fab-Ub<sub>2</sub>don-Fab, now carrying an available C-terminus, was conjugated to Rho-Ubacc . Also this reaction showed to be highly efficient, where after 30 minutes almost all heavy chain dimer was conjugated to Rho-Ubacc as shown by Coomassie staining and fluorescent scan of the protein gel ran in reducing conditions (Fig. 4c). Similarly, the heterotrimer formation by conjugating Fab-Ub<sub>2</sub>don-Fab to a third Fab fused to a Ubacc proved to be efficient, showing that the majority of the dimer converted into a trimer after 30 minutes (Fig. 4d).

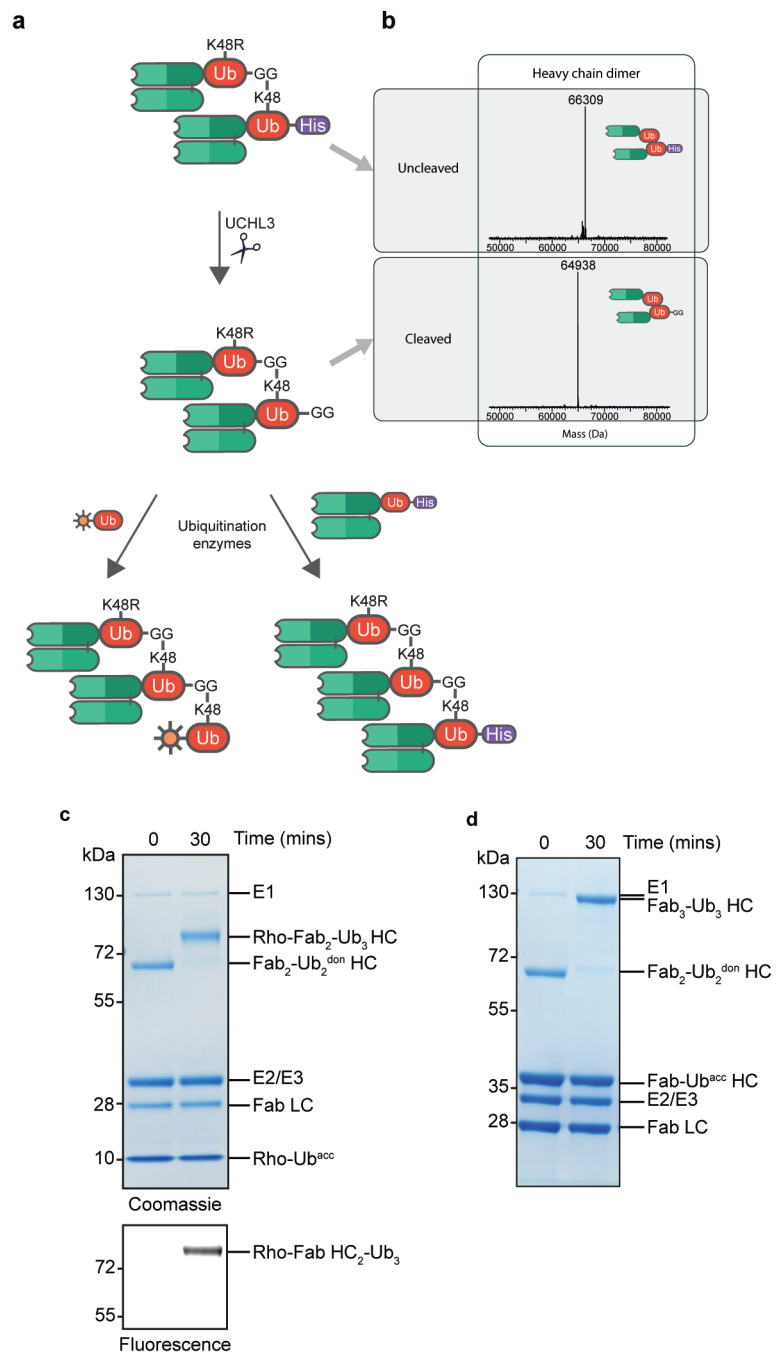


Figure 4| Generation of heterotrimeric ubi-tagged antibody complexes (a) Schematic illustration of ubiquitin chain elongation to form hetero-trimeric antibody complexes (b) Deconvoluted ESI-TOF mass spectra of the heavy chain dimer of Fab-Ub<sub>2</sub>-Fab and Fab-Ub<sub>2</sub><sup>don</sup>-Fab, showing the liberation of the His<sub>10</sub>-tag from Fab-Ub<sub>2</sub>-Fab by UCHL3 (calculated mass different = 1371 Da, observed mass difference =

1371 Da). (c) Conjugation of Fab-Ub<sub>2</sub><sup>don</sup>-Fab to Rho-Ub<sup>acc</sup> analyzed by SDS-PAGE in reducing conditions followed by fluorescent imaging and Coomassie Blue staining. (d) Reducing SDS-PAGE analysis showing the conjugation of the heterodimer Fab-Ub<sub>3</sub><sup>don</sup>-Fab to Fab-Ub<sup>acc</sup> to form a Fab heterotrimer.

# Ubi-tag conjugation is site-specifically reversible by DUBs

Lastly, we set out to investigate whether the internal isopeptide bond in the generated ubi-tagged conjugates were recognized and processed by deubiquitinating enzymes. We reasoned that cleaving ubi-tagged conjugates could potentially further expand the applications of this technology when used in a context where the controlled disassembly of the conjugate is desirable (Fig. 5a). However, the presence of DUBs in a biological setting could also be detrimental to the stability and functionality of the ubi-tagged conjugates. To investigate whether DUBs are capable of cleaving ubi-tagged conjugates, we selected OTUB1, a DUB known to have a preference for cleaving K48-linked ubiquitin chains<sup>44</sup>, and assessed its effect on the K48-linked Rho-Ub<sub>3</sub>-Fab when incubated together over time by Coomassie staining and fluorescent scan of the protein gel. As shown in figure 5b, the fluorescence intensity of the upper band corresponding to Rho-Ub<sub>2</sub>-Fab decreases over time while a lower band running around 10kDa corresponding to Rho-Ub appears and increases in intensity. Similarly, on Coomassie over time the upper band corresponding to Rho-Ub,-Fab decreases in intensity while two bands at around 55kDa and 10 kDa appear and increase in intensity, corresponding to Fab-Ub and Rho-Ub respectively. This indicated that the K48-linked Rho-Ub<sub>2</sub>-Fab was processed and cleaved by OTUB1. Next, we investigated the stability of Rho-Ub<sub>3</sub>-Fab in human serum in vitro as a preliminary indication for the usability of ubi-tag conjugation for diagnostic or therapeutic applications. Here, we monitored the stability of Rho-Ub<sub>3</sub>-Fab when incubated in human serum in vitro at 37°C over 24 hours (Fig. 5c). Notably, the band corresponding to Rho-Ub<sub>3</sub>-Fab remained equal in intensity over time while no new bands appeared indicating that Rho-Ub<sub>2</sub>-Fab remained stable in human serum in vitro for more than 24 hours. To validate that a ubi-tagged Fab conjugate carrying a larger cargo such as a ubi-tagged Fab-dimers could still be processed by DUBs, we incubated the K48-linked Fab-Ub,-Fab with OTUB1 and monitored its stability over time (Fig. 5d and 5e). After 90 minutes, the majority of Fab-Ub<sub>3</sub>-Fab was cleaved and a band corresponding to the Fab-Ub monomers could be observed indicating that larger ubitagged conjugates such as Fab-Ub<sub>3</sub>-Fab are still recognized and cleaved by OTUB1.

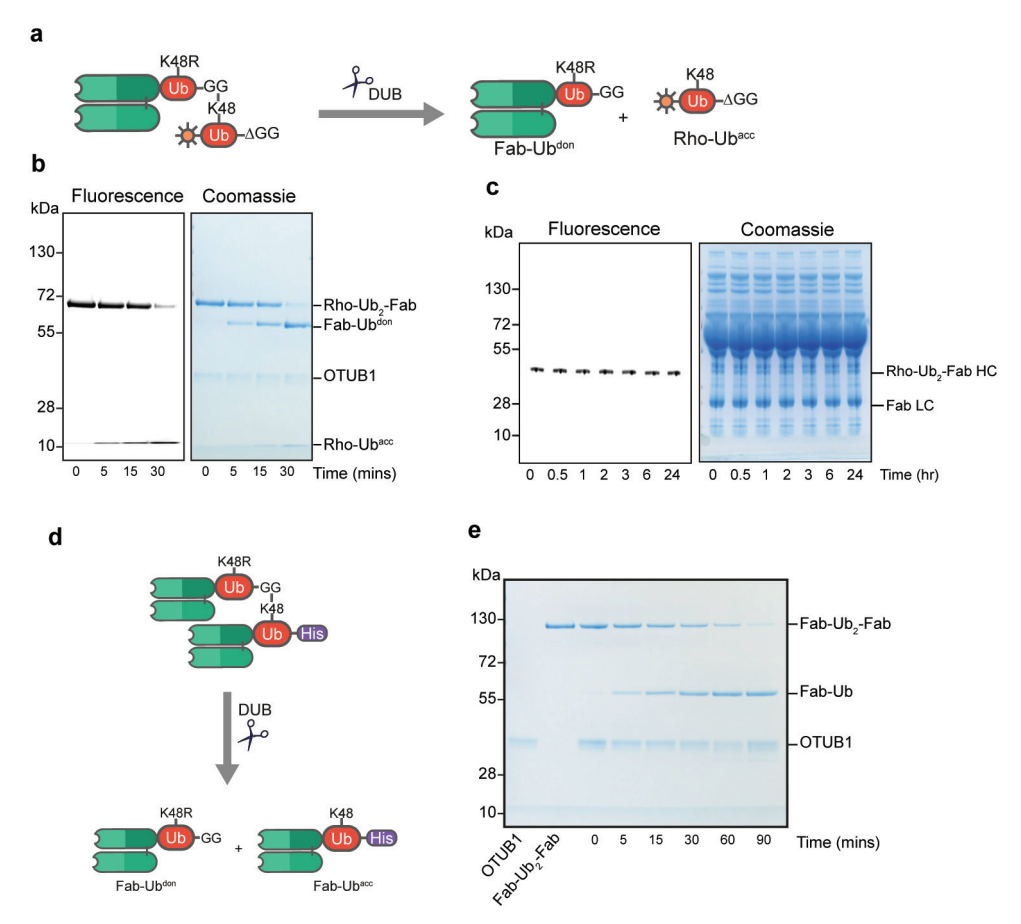


Figure 5| Site-specific disassembly of ubi-tagged antibody conjugated by DUBs. (a) Schematic representation of the disassembly of K48 linked Rho-Ub<sub>2</sub>-Fab by deubiquitinating enzymes to form the monomers Fab-Ub<sup>don</sup> and Rho-Ub<sup>acc</sup>. (b) Cleavage of Rho-Ub<sub>2</sub>-Fab by the K48-specific DUB OTUB1 shown by non-reducing SDS-PAGE followed by fluorescent imaging and Coomassie Blue staining. (c) In vitro stability of Rho-Ub<sub>2</sub>-Fab in human serum analysed by SDS-PAGE in reducing conditions, visualized by fluorescent imaging and Coomassie Blue staining. (d) Schematic illustration of Fab-Ub<sub>2</sub>-Fab cleaved by DUBs to form the Fab-Ub<sup>don</sup> and Fab-Ub<sup>acc</sup> monomers. (e) K48-linked Fab-Ub<sub>2</sub>-Fab cleavage by OTUB1 analyzed by non-reducing SDS-PAGE followed by Coomassie blue staining.

# mAb conjugation and Tetravalent antibody formats

To show that ubi-tagging is not restricted to antibody fragments but can also be applied to full mAbs, we produced recombinant mAbs with a ubi-tag fused to the C-terminus of each heavy chain. We produced two ubi-tagged mAbs, TA99 anti-TRP1 carrying an acceptor ubi-tag and 2C11 anti-mCD3 carrying a donor ubi-tag. We generated the ubi-tagged anti-TRP1 mAb using the hybridoma genome editing technology<sup>38</sup>, where we targeted the hinge region of the TA99 anti-TRP1 hybridoma to introduce an Fc-silent domain to which acceptor ubiquitin (Ub $\Delta$ GG) was fused. The Fc-silent domain

was introduced to avoid Fc-mediated immune activation in the following applications. Stable ubi-tagged antibody-producing hybridoma clones were obtained, and Ubi-tagged mAbs were validated for the presence of the ubi-tag using western blot analysis (Supplementary Fig. 4). The ubi-tagged 2C11 anti-mCD3 mAbs were generated by overexpression of the mAbs in HEK-293 cells. Here, the Fc-silent domain was also introduced to which the donor ubi-tag was fused. Both ubi-tagged mAbs were purified

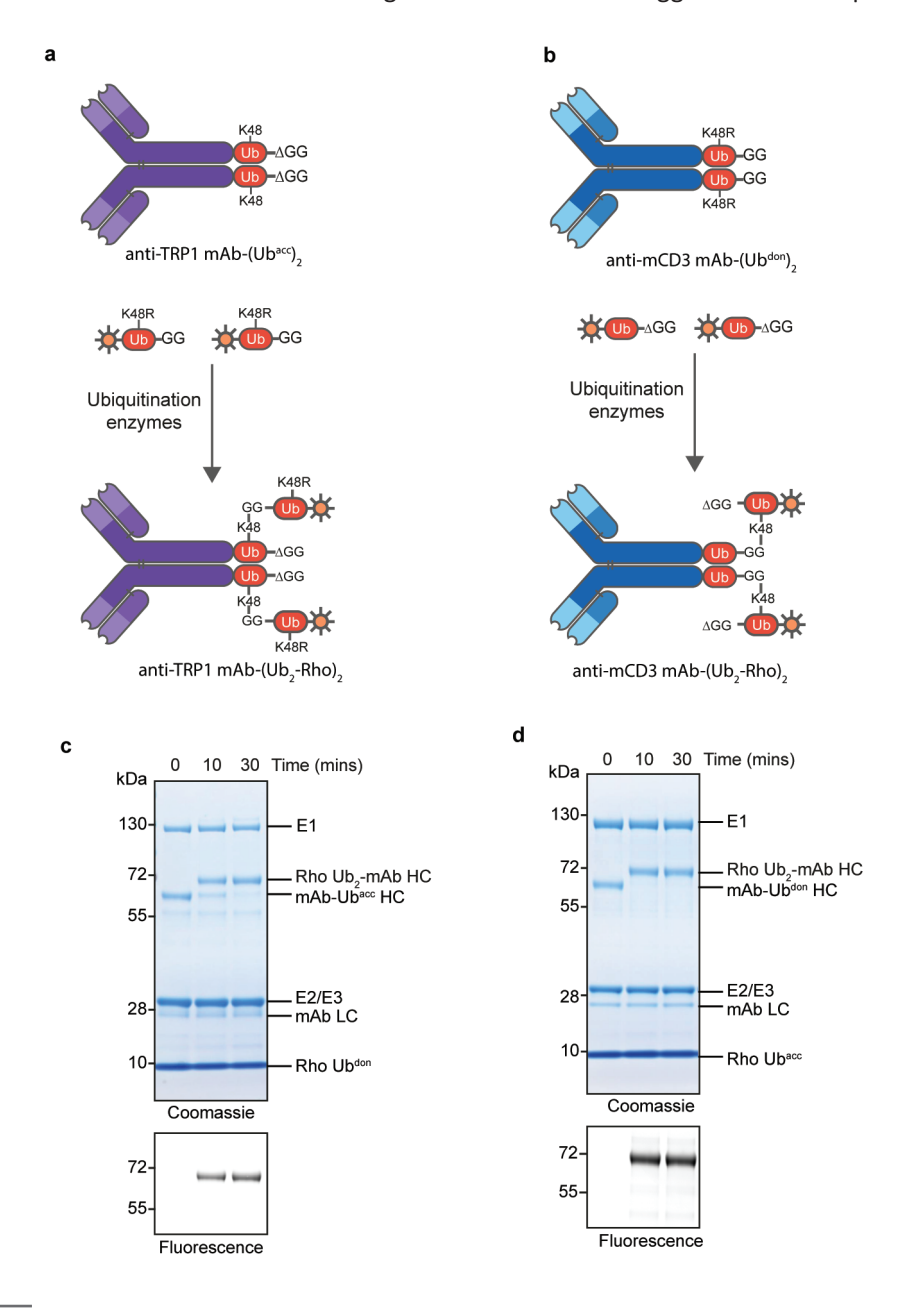


Figure 6| Ubi-tag conjugation for the fluorescent labeling of ubi-tagged mAbs (a) Schematic representation of the K48-specific ubi-tag conjugation for the fluorescent labeling of anti-TRP1 mAb-Ubacc to Rho-Ubdon. (b) Schematic representation of the ubi-tag conjugation of anti-mCD3 mAb-Ubdon to Rho-Ubdon to anti-TRP1 mAb-(Ubacc), analyzed by SDS-PAGE under reducing conditions and visualized by fluorescent imaging and Coomassie Blue staining. (d) Conjugation of Rho-Ubdoc to anti-mCD3 mAb-(Ubdon), analyzed by SDS-PAGE under reducing conditions and visualized by fluorescent imaging and Coomassie Blue staining.

using Protein A affinity purification and the purified ubi-tagged mAbs were assessed by mass spectrometry (Supplementary Fig. 5).

To assess the conjugation efficiency of ubi-tagged mAbs and determine if full conjugation is achievable, we decided to first test the ubi-tag conjugation of both donor and acceptor ubi-tagged mAbs to a ubitag carrying a small cargo, a rhodamine moiety, to either an acceptor or donor respectively (Fig. 6a-b). We tested the conjugation of the mAb fused to an acceptor ubiquitin, hereafter mAb-(Ubacc), to Rho-Ubdon. After 30 minutes, the heavy chains of mAb-(Ubacc), were fluorescently labeled as shown by Coomassie staining and fluorescent scan in figure 6c. The protein gel was run in reducing conditions, and it can be appreciated that the complete upward shift of the band corresponding to the ubi-tagged heavy chain indicates that both ubi-tags on each of the heavy chains were conjugated to Rho-Ub. To confirm that ubi-tagged mAbs can be efficiently conjugated in both acceptor and donor ubi-tag formats, we conjugated a mAb-(Ubdon), to Rho-Ubacc. Indeed, both ubi-tagged mAb formats showed similarly high conjugation efficiency (Fig. 6d).

Next, we attempted to form a tetravalent bispecific-antibody conjugate applying ubi-tagging. We aimed for a bispecific T cell engager (BiTE) in two ubi-tagged formats, one by conjugating anti-TRP1 Fc-silent mAb-(Ubacc), to anti-mCD3 (clone 145-2C11) Fab-Ubdon and the other by conjugating anti-mCD3 Fc-silent mAb-(Ubdon), to anti-TRP1 Fab-Ubdon (Fig 7a-b). The conjugation reactions reached near completion in 60 minutes (Fig. 7c-d) in which the majority of the unconjugated mAb-(Ub), were converted to the tetravalent bispecific-antibody conjugate mAb-(Ub3-Fab)3. After purification the functionality of these two ubi-tagged BiTEs were evaluated in an in vitro T cell activation and cytotoxicity assay. Here, WT or TRP1 transfected KPC3 cells (KPC3-TRP1) were co-cultured with CD8 T cells from WT C57BL6/J mice and incubated with increasing concentrations of either of the two bispecific antibody complexes or the combination of their corresponding unconjugated mAb-(Ubacc), and Fab-Ubdon(Fig.7e-f). Flow cytometry analysis revealed that both ubi-tagged BiTEs induced a dose-dependent T cell activation as measured by the increased expression of Ki67, granzyme B, CD69 and 4-1BB (CD137) by the T cells, only when co-cultured with KPC3-TRP1 cells and not with KPC3 WT cells (Fig. 7e-f and Supplementary Fig. 6). Additionally, the ubi-tagged BiTEs showed a dosedependent cell killing in an LDH release assay with TRP1 expressing KPC3 cells, while the WT cells and KPC3-TRP1 incubated with the unconjugated mAb-(Ubacc), and Fab-Ubdon showed no induction of killing (Fig. 7e-f and Supplementary Fig. 7). Altogether these results demonstrate the flexibility and efficiency of the ubi-tagging approach, and the functionality of ubi-tagged tetravalent bispecific-antibody complexes.

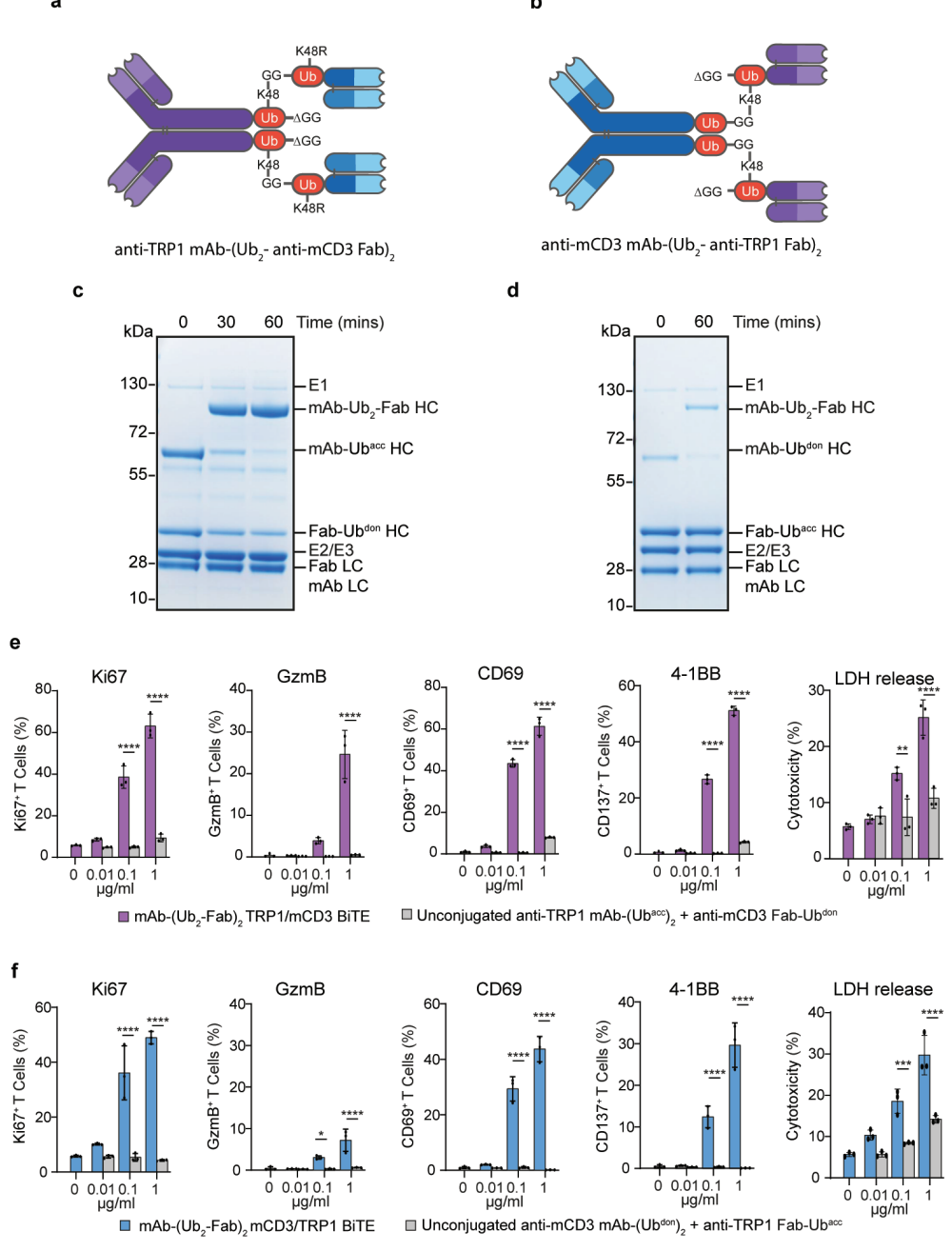


Figure 7 | Conjugation of ubi-tagged mAbs for the generation of a bispecific tetravalent antibody

complexes. (a) Schematic representation of anti-TRP1 mAb-(Ub<sub>2</sub>-anti-mCD3 Fab)<sub>2</sub> generated by ubitag conjugation of anti-TRP1 mAb-(Ubacc), to two moieties of anti-mCD3 Fab-Ubdon. (b) Schematic representation of the bispecific tetravalent antibody complex anti-mCD3 mAb-(Ub<sub>2</sub>-anti-TRP1 Fab) by ubi-tag conjugation of anti-mCD3 mAb-(Ubdon), to two moieties of anti-TRP1 Fab-Ubacc. (c) SDS-PAGE analysis of the generation of the bispecific tetravalent antibody complex anti-TRP1 mAb-(Ub.anti-mCD3 Fab), by ubi-tag conjugation of anti-TRP1 mAb-(Ubacc), to two moieties of anti-mCD3 Fab-Ubdon. (d) SDS-PAGE analysis of the generation of the bispecific tetravalent antibody complex antimCD3 mAb-(Ub,-anti-TRP1 Fab), by ubi-tag conjugation of anti-mCD3 mAb-(Ubdon), to two moieties of anti-TRP1 Fab-Ubacc, (d-h) In vitro T cell activation and cytotoxicity by the ubi-tagged bispecific TRP1xmCD3 complexes. Primary mouse (C57BL/6) CD8+T cells were added in a 10:1 ratio to KPC3-Trp1 followed by addition of  $0 - 1 \mu g/mL$  of either mAb-(Ub,-Fab), or unconjugated mAb-(Ub), and two Fab-Ubdon, and incubated for two days. T cell activation was assessed using flow cytometry for Ki67, Granzyme B, CD69, and 4-1BB. Data (n=3) are shown as percentage positive T cells ±SD. T tests, \*\*\*\*P<0.0001, \*\*P<0.01. Full statistical analysis is provided in supplementary table S5. Cytotoxicity was assessed using a LDH cytotoxicity assay. Data (n=3) are shown as percentage cytotoxicity ±SD. T tests, \*\*\*\*P<0.0001, \*\*P<0.01. Full statistical analysis is provided in supplementary table S5.

#### Discussion

Over the past decade, tremendous advances have been made in the field of antibody conjugation to facilitate the generation of antibody conjugates and multivalent antibody formats for a broad spectrum of applications in research, diagnostics and therapy. Traditional conjugation methods rely on chemical modification of primary amines or thiol groups along the antibody sequence resulting in heterogenous mixtures with multiple uncontrolled modification sites.<sup>1–3</sup> This often results in batch-to-batch variability, reduced antigen binding and impaired stability.

Significant progress has been made in the development of site-specific conjugation methods, contributing to innovation in the generation of antibody conjugates of diverse formats. However, slow reaction kinetics, low yield and time-consuming multistep conjugation procedures remain problematic.<sup>5,17,22</sup> Hence, substantial efforts are currently still being focused on developing new or improved antibody conjugation strategies.

Here we report the use of ubiquitin conjugation (ubi-tagging), as a highly-specific and broadly applicable antibody conjugation platform. We demonstrate that this approach is an efficient technology for the site-specific, and flexible ubi-tag conjugation. In this study we addressed four main aspects of this technique: (1) Ubi-tag conjugation reactions result in a highly defined homogenous product that is covalently attached at a specific position. For the conjugation reactions, we used an E2-E3 fusion enzyme specific for ubiquitin conjugation on lysine 48 and a single product was formed in each reaction (Fig. 2b). This indicates that the conjugation only took place on lysine 48 and that a defined antibody conjugate was produced that, in contrast to commonly used conjugation techniques, is consistent from batch-to-batch. (2) Ubi-tag conjugation reactions are fast and highly efficient process. The efficiency of ubi-tag conjugation reactions in this study at timepoint 30 minutes were quantified and plotted (Supplementary Fig. 2).

Conjugation reactions involving ubi-tagged Fab fragments or ubi-tagged mAbs showed an average reaction efficiency of 93% and 96%, respectively. This indicates that the ubitag conjugation reaction efficiency was not hampered, neither as donor nor acceptor ubi-tag, by fusion to a protein with molecular weight as high as a mAb of 150 kDa. (3) The specificity and efficiency of ubi-tag conjugation facilitates the generation of multimeric antibody complexes with an unprecedented ease. The level of control in this conjugation reaction, with a defined donor ubi-tag and acceptor ubi-tag each fused to a different moiety, allows the generation of defined hetero-multimeric antibody complexes (Fig 3, 4 and 7). (4) The established full chemical synthesis of ubiquitin<sup>45–47</sup> further expands its potential applications as an antibody conjugation tag. This facilitates the attachment of chemical modifications such as small molecules, fluorophores, tags or chemical warheads at one or more position in a defined manner (Fig. 2, 6 and Supplementary Fig. 1).

Although, in this study the K48 specific E2-E3 pair gp78RING-Ube2g2 was used<sup>36</sup>, ubi-tag conjugation is not limited to this pair of ubiquitin E2 and E3 enzymes or linkage type. Other E2 and E3 enzymes also proved to be exploitable for ubi-tag conjugation of proteins and antibodies, including the E2-E3 pair UbcH7 and NIeL<sup>48</sup> for the generation of K6-linked ubi-tagged antibody conjugates (Supplementary Fig. 8). The variety in ubiquitin linkage types and linkage specific ubiquitination enzymes provide additional flexibility to this conjugation platform. Additionally, ubiquitin chains of different linkage types are known to have different conformations<sup>26</sup>. This could be exploited in future research for applications where it is of value to gain control over the spatial orientation of the antibodies conjugated to each other<sup>49</sup>. Furthermore, another promising aspect of ubi-tag conjugation is its specific reversibility using deubiquitinating enzymes<sup>50</sup>(Fig. 5). Conditional cleavage using DUBs, could provide dynamic control over the activity of ubi-tagged antibody complexes.

In summary, ubi-tag conjugation provides a fast, efficient, and modular technique to generate well-characterized antibody conjugates of limitless formats and combinations. We expect the widespread adoption of this conjugation technique and its contribution to improving and developing antibody conjugates for preclinical research, diagnostic, and therapeutic applications.

#### Methods

#### General cell culture conditions

The hybridoma cell line KT3, kindly provided by dr. Ramon Arens (LUMC, The Netherlands), was modified for the stable expression of ubi-tagged antibodies or antibody fragments. Other cell lines used in this study were EL4 (kindly provided by dr. Jacques Neefjes (LUMC, The Netherlands) KPC3 and KPC3-TRP1. KT3 and EL4 cells were cultured in Dulbecco's modified Eagle's medium (DMEM) (Gibco) supplemented with 7.5% FCS. The KPC3 cell line was obtained from a primary pancreatic KPC tumor with mutant p53 and K-ras<sup>51</sup>

from a female C57BL/6 mouse. KPC3-Trp1 was generated as described  $^{52}$  and purified using cell sorting with the TA99 antibody. Cells were cultured in IMDM supplemented with 7.5% FCS. All the cell lines used in the study were maintained at 37 °C and 5% CO $_{2}$ , routinely examined by morphology analysis and tested for mycoplasma.

## **Cloning of CRISPR-Cas9 and donor constructs**

The genomic sequence of the rlgG2a heavy chain locus, mlgG2a heavy chain locus, were identified via the Ensembl rate genome build Rnor 6.0 and used for the design of the different HDR donor templates. gRNA for the rlgG2a constructs were previously described; for Hinge HDR constructs, gRNA-H, GACTTACCTGTACATCCACA, Addgene 124808; for isotype switch, gRNA-ISO (TGTAGACAGCCACAGACTTG, Addgene 124811). For the hinge region of mlgG2a gRNA-85 (TGGAGGACAGGGCTTGATTG), gRNA-76 (GGGCTTGATTGTGGGCCCTC) and gRNA-102 (TTACCTGGGCATTTGCATGG) were designed using the CRISPR tool from the Zhang laboratory (http://crispr.mit.edu) and ordered as single-stranded oligos from Integrated DNA Technologies (IDT) with the appropriate overhangs for cloning purposes. The oligos were phosphorylated with T4 PNK enzyme by incubation at 37 °C for 30 minutes and annealed by incubation at 95 °C for 5 minutes followed by gradually cooling to 25 °C using a thermocycler. The annealed oligos were cloned into the plasmid pSpCas9(BB)-2A-Puro (PX459), which was obtained as gifts from F. Zhang (Addgene plasmids 62988)<sup>53</sup>. Synthetic gene fragments containing homologous arms and desired insert were obtained via Twistbioscience and cloned into the PCR4 TOPO TA vector (Thermo Fisher Scientific). All CRISPR-Cas9 and HDR constructs were purified with the NucleoBond Xtra Midi Kit (740410.100, Machery-Nagel) according to the manufacturer's protocol.

## Hybridoma nucleofection with HDR and CRISPR-Cas9

Nucleofection of the HDR template and CRISPR-Cas9 vectors was performed with Cell Line Nucleofector Kit R (Lonza, VCA-11001) nucleofector 2b device. Before nucleofection hybridoma cells were assessed for viability and centrifuged (90g, 5 minutes), resuspended in PBS supplemented with 1% FBS and centrifuged again (90g, 5 minutes). 1x10<sup>6</sup>cells were resuspended in 100 μL Nucleofector medium with 1 μg of HDR template and 1 μg of CRISPR-Cas9 vectors or 2 μg of GFP vector (control) and transferred to cuvettes for nucleofection with the 2b Nucleofection System from Lonza (Program X001). Transfected cells were transferred to a 6-well plate in 4 mL of prewarmed complete medium. The following day the cells were transferred to a 10 cm petridish in 10 mL of complete medium, supplemented with 10-20 μg/mL of blasticidin (Invivogen, anti-bl-05). Antibiotic pressure was sustained until GFP-transfected hybridomas were dead and HDR transfections were confluent (typically between day 10-14). Cells were subsequently clonally expanded by seeding the hybridomas in 0.3

cells/well in round-bottom 96-well plates in 100  $\mu L$  of complete medium. After one-two weeks, supernatant from wells with a high cell density were obtained for further characterization and selected cloned were expanded.

### Solid-phase peptide synthesis

Solid-phase peptide synthesis (SPPS) of Rho-Ub was performed on a Syro II Multisyntech Automated Peptide synthesizer (SYRO robot; Part Nr: S002PS002; MultiSyntech GmbH, Germany) on a 25  $\mu$ mol scale using standard 9-fluorenylmethoxycarbonyl (Fmoc) based solid phase peptide chemistry based on the procedure described by El Oualid *et al.*<sup>45</sup> using a fourfold excess of amino acids relative to pre-loaded Fmoc amino acid trityl resin (between 0.17 and 0.20 mmol/g, Rapp Polymere, Germany). To prepare Rho-Ub, 5-carboxyrhodamine110 (Rho) was coupled to the N-terminus of Ub following SPPS as described by Geurink *et al.*<sup>54</sup>. All synthetic products were purified by RP-HPLC on a Waters preparative RP-HPLC system equipped with a Waters C18-Xbridge 5  $\mu$ m OBD (10 x 150 mm) column. The purified products were lyophilized and assayed for purity by high resolution mass spectrometry on a Waters Acquity H-class UPLC with XEVO-G2 XS Q-TOF mass spectrometer and by SDS-PAGE analysis.

## Thermal unfolding assay

For each of the Ubi-tagged Fab and conjugates, 10  $\mu$ L samples were prepared with a concentration ranging from 0.5 to 1 mg/mL and loaded into the capillaries (NanoTemper Technologies). Changes in tryptophan fluorescence intensity upon protein unfolding was measured using the NanoTemper Tycho NT.6 (NanoTemper Technologies) using an increasing temperature gradient from 35 °C to 95 °C at a rate of 20 °C/min. The Inflection temperatures ( $T_i$ ) of the proteins was determined from the first derivative of the fluorescence ratios ( $F_{350}/F_{330}$ ).

### Mass spectrometry

Mass spectrometry analysis was carried out on Waters ACQUITY UPLC-MS system equipped with a Waters ACQUITY Quaternary Solvent Manager (QSM), Waters ACQUITY FTN AutoSampler, Waters ACQUITY UPLC Protein BEH C4 Column (300 Å, 1.7  $\mu$ m, 2.1 x 50 mm) and XEVO-G2 XS QTOF Mass Spectrometer (m/z = 200-2500) in ES+ mode. Sample were run using 2 mobile phases: A = 1% MeCN, 0.1% formic acid in water and B = 1% water and 0.1% formic acid in MeCN with a runtime of 14 minutes. In the first 4 minutes, salts and buffer components were flushed from LC column using 98% A and 2% B. In the next 7.5 minutes, a gradient of 2-100% B was used, followed by 0.5 minutes of 100% B and subsequent reduction to 2% B and 98% A in 2 minutes. Data processing was performed using Waters MassLynx Mass Spectrometry Software 4.1, where the mass was obtained by deconvolution with the MaxEnt1 function.

## Protein expression and purification

The E1 ubiquitin-activating enzyme UBE1 carrying an N-terminal His-tag was expressed from a pET3a vector in E. coli BL21(DE3) in autoinduction media for 2-3 hours at 37 °C, after which the bacteria were allowed to grow overnight at 18 °C. Next, bacteria were harvested and lysed by sonication, followed by His-affinity purification using Talon metal affinity resin (Clontech Inc., Palo Alto, CA, USA). Subsequently, the protein was further purified by anion exchange using a Resource Q column (GE Healthcare), followed by size exclusion using a Superdex 200 column (GE Healthcare).

The E2/E3 enzyme chimera plasmid was obtained as a gift from dr. Vincent Chau (Penn State, USA). The expression plasmid consists of the RING domain of the E3 ubiquitin ligating enzyme gp78 fused to the N-terminus of the E2 ubiquitin-conjugating enzyme Ube2g2 in a PET28a-TEV vector.

The E2/E3 enzyme chimera was expressed and purified as described $^{36}$ . In brief, the fusion protein was expressed in E. coli BL21(DE3) cells grown in LB at 37°C until OD $_{600}$  = 0.4-0.6 and induced with 0.4 mM IPTG for 4 hours at 30 °C. The harvested cells were lysed with Bugbuster protein extraction reagent (Millipore) according to manufacturer's protocol. The fusion protein was purified on Ni-NTA resin followed by size exclusion using a Superdex 200 column (GE Healthcare). Next, TEV protease cleavage was carried out overnight, and the cleaved fusion protein was further purified using a Resource Q column (GE Healthcare).

Ubi-tagged Fabs were produced in hybridoma cell lines engineered to produce Fabs fused at the C-terminus of the heavy chain to ubiquitin, followed by a His-tag at the C-terminus of ubiquitin. The modified hybridoma cells were cultivated for antibody production in CD Hybridoma medium supplemented with 2 mM ultraglutamine and 50 μΜ β-mercaptoethanol for 7 to 10 days. To prevent the cleavage of the His-tag during cultivation, which is essential for blocking the C-terminal glycine residue of acceptor ubi-tags, antibodies fused to an acceptor ubi-tag were secreted in culture media supplemented with Ub-PA. However, donor ubi-tags require a free C-terminus; thus, antibodies fused a donor ubi-tag intended for conjugation were cultured without a DUB inhibitor. After 7 to 10 days, the culture media containing the ubi-tagged Fabs was centrifugated to remove cells. The supernatant was filtered through a 0.22 μm filter (GE Healthcare) and loaded on a pre-equilibrated HiTrap Protein G HP column (GE Life Science), and the ubi-tagged antibodies were purified according to the manufacturer's protocol. Elution fractions containing the ubi-tagged antibodies were pooled and dialyzed against PBS. Acceptor ubi-tagged antibodies, carrying a His-tag at the C-terminus of ubiquitin, were purified by Ni-NTA affinity purification prior to Protein G affinity purification (Supplementary Fig. 9).

# **Ubi-tag conjugation reaction**

Ubi-tag conjugation reactions were carried out in the presence of 0.25 μM E1 enzyme, 20 μM E2/E3 hybrid enzyme, 10 mM MgCl, and 5 mM ATP in PBS. For analysis of the reaction efficiency by SDS-PAGE, an initial reaction sample was taken from the reaction mixture prior to the addition of ATP. After the addition of ATP, the reaction was incubated at 37 °C for 30 minutes while shaking. Conjugation reaction samples were analyzed by quenching 2-5 µL of the reaction mixture in sample buffer and run on 4-12% Bis-Tris gels (Invitrogen) by SDS-PAGE with MOPS as running buffer. All conjugation reactions were run in non-reducing conditions except for conjugation reactions involving constructs of high molecular weight such as Fab trimers, where the sample buffer was supplemented with β-mercaptoethanol. Gels were stained using InstantBlue Coomassie Protein Stain (abcam) and imaged using Amersham600. Fluorescently labeled proteins were visualized by in-gel fluorescence using Typhoon FLA 9500 imaging system (GE Life Sciences) prior to staining with Coomassie. Small-scale reactions were carried out on a scale corresponding to 2.5 µg ubi-tagged antibody fragments, while large-scale reactions were carried out on a 200 μg to 1 mg scale. Ubi-tagged Fab conjugates were purified from the reaction mixture by protein G affinity purification using a HiTrap Protein G HP column (GE Life Science) according to the manufacturer's protocol. The elution fractions containing purified conjugates were pooled, dialyzed against PBS, and concentrated using a 10 kDa Amicon Ultra centrifugal filter unit (Millipore). The purity of the ubitagged conjugates was assessed by SDS-PAGE and high-resolution mass spectrometry on a Waters Acquity H-class UPLC with XEVO-G2 XS Q-TOF mass spectrometer.

For conjugation of  $\alpha$ -CD3 Fab-Ub<sup>don</sup> to Rho-Ub<sup>acc</sup>, 10  $\mu$ M of Fab-Ub<sup>don</sup> and 50  $\mu$ M Rho-Ub<sup>acc</sup> were used in the reaction. Multimerization of ubi-tagged Fab fragments was carried out using 30  $\mu$ M of Fab-Ub<sup>WT</sup>. For site-specific dimerization of  $\alpha$ -CD3 ubi-tagged Fab-fragments, 15  $\mu$ M of the Fab-Ub<sup>don</sup> and 10  $\mu$ M Fab-Ub<sup>acc</sup> were used, and the conjugates were further purified using Ni-NTA prior to dialysis. Rhodamine labeling of ubi-tagged mAbs was carried out using 5  $\mu$ M mAbs and 50  $\mu$ M Rho-Ub, while bispecific antibody conjugates were generated using 3.5  $\mu$ M mAbs and 10  $\mu$ M Fab.

## Conjugation of a third moiety to ubi-tagged Fab dimer

To prepare Fab-Ub $_2$ -Fab for conjugation, the C-terminal glycine was exposed using the DUB UCHL3. For this, 2.5  $\mu$ M Fab dimer was incubated with 50 nM UCHL3 in PBS at 37 °C for 30 minutes. The cleavage efficiency was assessed by high-resolution mass spectrometry on a Waters Acquity H-class UPLC with XEVO-G2 XS Q-TOF mass spectrometer. Following cleavage, UCHL3 was precipitated by 10-fold dilution with 50 mM sodium acetate pH 4.5 and 100 mM sodium chloride, followed by centrifugation. The supernatant containing Fab-Ub $_2$  don-Fab was concentrated, and buffer exchanged to PBS using a 50 kDa Amicon Ultra centrifugal filter unit (Millipore).

For the conjugation of Fab-Ub $_2^{don}$ -Fab to Rho-Ub $_2^{acc}$ , 4  $\mu$ M Fab-Ub $_2^{don}$ -Fab and 100  $\mu$ M Rho-Ub $_2^{acc}$  were reacted in the presence of 0.25  $\mu$ M E1 enzyme, 20  $\mu$ M E2/E3 hybrid enzyme, 10 mM MgCl $_2$  and 5 mM ATP in PBS for 30 minutes at 37 °C. For the generation of a ubi-tagged Fab trimer, 4  $\mu$ M Fab dimer and 30  $\mu$ M Fab-Ub $_2^{acc}$  were used for conjugation in the presence of 0.25  $\mu$ M E1 enzyme, 20  $\mu$ M E2/E3 hybrid enzyme, 10 mM MgCl $_2$  and 5 mM ATP in PBS for 30 minutes at 37 °C. Conjugation reaction samples were analyzed by quenching 3  $\mu$ L of the reaction mixture in sample buffer and run on 4-12% Bis-Tris gels (Invitrogen) by SDS-PAGE with MOPS as running buffer.

# Flow cytometry

The binding of Rho-Ub $_2$ -Fab targeting mCD3 and FITC-labeled parental antibody (ThermoScientific, MA1-80640) to mCD3 positive EL4 cells was compared by staining 50,000 EL4 cells with 50  $\mu$ L of  $1\mu$ g/mL Rho-Ub $_2$ -Fab or FITC-labeled parental antibody for 30 minutes at 4 °C. Next, the cells were washed twice with PBS supplemented with 5% FCS and fluorescence intensity was measured on an LSR II flow cytometer (BD). A competitive binding assay was performed to assess the antigen binding of ubi-tagged antibody fragments and conjugates. Here, 50.000 EL4 cells per well were stained with 50  $\mu$ L of mCD3 targeting Fab-Ub, Fab-Ub2-Fab, or unlabeled parental antibody (ThermoScientific, MA1-80783), in increasing concentrations ranging from 0.01 to 1000 nM for 15 minutes at 4 °C. Next, the cells were washed with PBS supplemented with 5% FCS, followed by incubation with  $1\mu$ g/mL in 50  $\mu$ L of FITC-labeled parental antibody (ThermoScientific, MA1-80640) for 30 minutes at 4 °C. Cells were washed twice, and fluorescence intensity was measured by flow cytometry on an LSR II flow cytometer (BD).

## In vitro serum stability assay

Human serum (Sigma-Aldrich, H4522) was diluted in PBS to 25% (v/v) and incubated at 37 °C for 15 minutes. Next, Rho-Ub $_2$ -Fab was added at a final concentration of 10 μM, and the mixture was incubated at 37 °C. The stability of Rho-Ub $_2$ -Fab over time was analyzed by quenching 5 μL of the reaction mixture in sample buffer supplemented with β-mercaptoethanol at specific time points (0, 0.5, 1, 2, 3, 6, and 24 hours). Samples were run on 4-12% Bis-Tris gels (Invitrogen) by SDS-PAGE with MOPS as running buffer. Serum stability of Rho-Ub $_2$ -Fab was visualized by in-gel fluorescence using Typhoon FLA 9500 imaging system (GE Life Sciences), followed by staining with InstantBlue Coomassie Protein Stain (abcam).

## **DUB** cleavage assay

DUB cleavage of ubi-tagged Fab conjugates by OTUB1 was carried out using 5  $\mu$ M of either Rho-Ub<sub>3</sub>-Fab and Fab-Ub<sub>3</sub>-Fab and 1  $\mu$ M OTUB1 in PBS at 37 °C for 30-90 minutes.

The reaction efficiency was monitored by SDS-PAGE where samples were quenched at different time-point in sample buffer and run on 4-12% Bis-Tris gels (Invitrogen) by SDS-PAGE with MOPS as running buffer. Gels were stained using InstantBlue Coomassie Protein Stain (abcam) and imaged using Amersham600. Fluorescently labeled proteins were visualized by in-gel fluorescence using Typhoon FLA 9500 imaging system (GE Life Sciences) prior to staining with Coomassie.

#### Mice

All mice were purchased from Charles River Laboratories, France. All animal studies were approved by the local authority for the Ethical Evaluation of Animal Experiments and Animal Welfare (Instantie voor Dierenwelzijn Radboudumc). All mice were kept in accordance with federal and state policies on animal research and Annex III of the EU Directive (Directive 2010-63-EU). Female C57BL/6 WT and OTI (Tg(TcraTcrb)1100Mjb/Crl) between 8-12 weeks of age and 18-25 g body weight were used for *in vitro* and *in vivo* experiments. Mice were sacrificed by cervical dislocation.

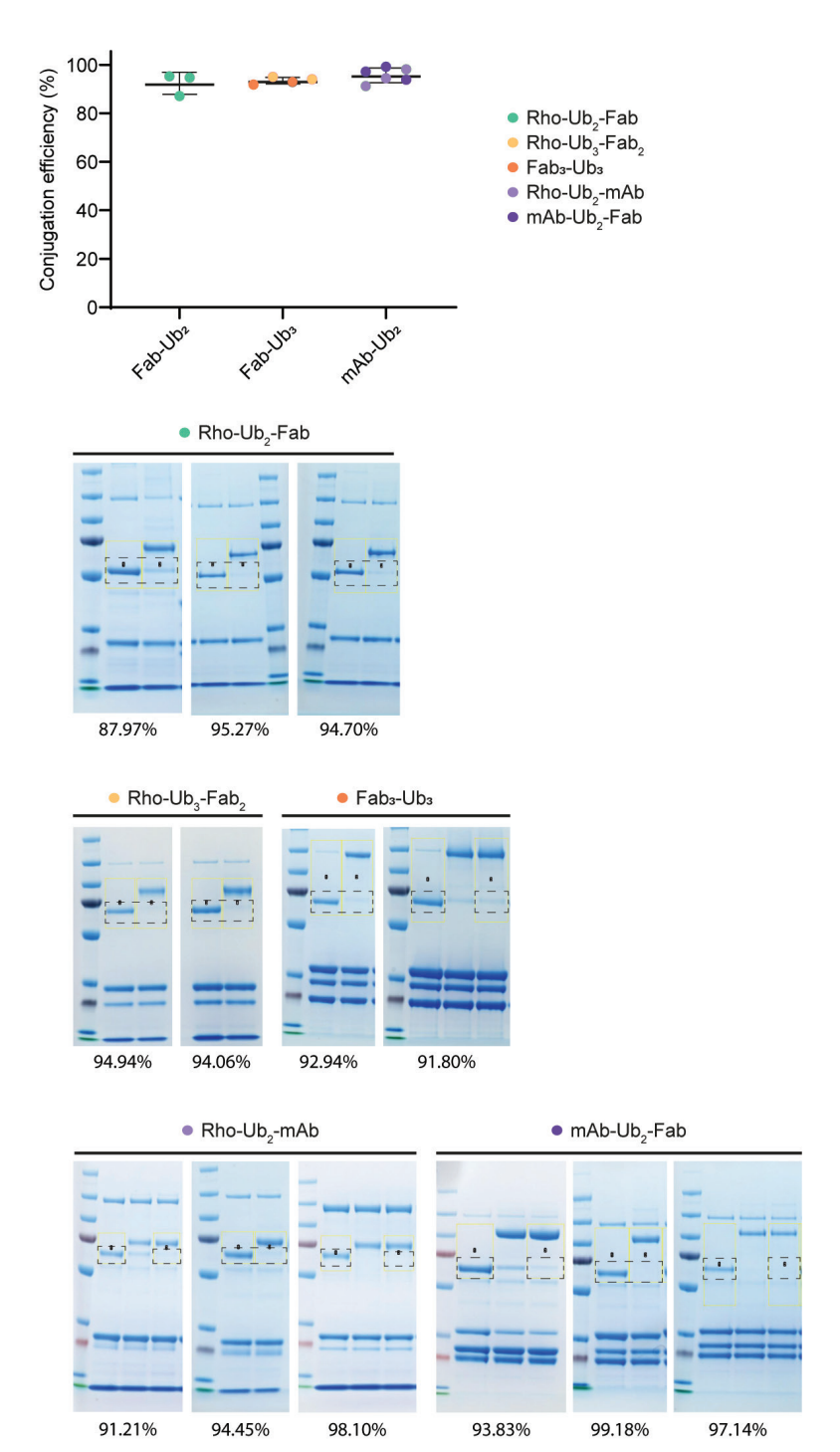
# LDH assay

KPC3 or KPC3-Trp1 cells were irradiated with 6000 Rad to prevent proliferation, added to a 96-well plate, and incubated for 4 hours at 37 °C to facilitate adherence. Splenocytes were obtained from naïve C57BL/6 mice and CD8 T cells were purified using a CD8 enrichment kit (BD Biosciences, 558471). CD8 T cells were added in a 10:1 E:T ratio to the 96-well plate, followed by the addition of 0-1μg/mL of either the ubiconjugated TRP1xmCD3 bispecific or the unconjugated ubi-tagged TRP1 mAb + mCD3 Fab, and incubated for 48 hours. Tumor cell killing was assessed using the CyQUANT TM LDH cytotoxicity assay (ThermoFisher, C20301) following manufacturer's instructions. In parallel, CD8 T cells were stained with Zombie Aqua fixable viability dye (BioLegend, 423102), CD69 FITC (Invitrogen, 11-0691-82), and CD137 APC (BioLegend, 106110), and fluorescence was measured on the LSR II flow cytometer (BD) to determine T-cell activation. Fluorescence data were analyzed using FlowJo software.

# **Supplementary information**

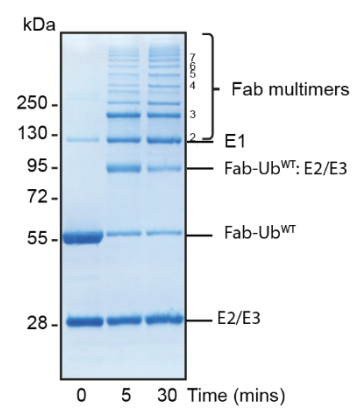


S1 Total chemical synthesis of Rho-Ubacc. The Ubacc lacking G75 and G76 (Ub $\Delta$ GG) was synthesized by linear solid-phase peptide synthesis (SPPS) on a trityl resin followed by coupling of diBoc-protected rhodamine (Rho) to the N-terminus. Next, removal of the protection groups (PG) and cleavage of Rho-Ubacc from resin was performed under strong acidic conditions. Reagents and conditions: a) N,N'-Boc-protected 5-carboxyrhodamine, PyBOP, DIPEA, NMP overnight at RT; b) TFA/H<sub>2</sub>O/phenol/iPr<sub>3</sub>SiH (90.5:5:2.5:2; v/v/v/v) for 3 h. at RT.

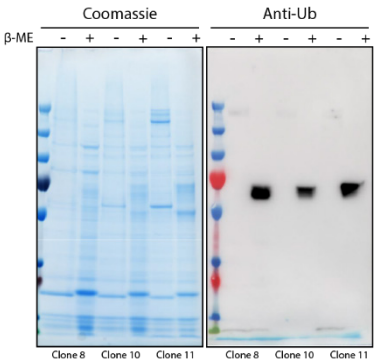


**S2** The efficiency of ubi-tag conjugation reactions conducted in this study. Conjugation reactions involving ubi-tagged Fab fragments forming di-ubiquitin chains showed an average reaction efficiency

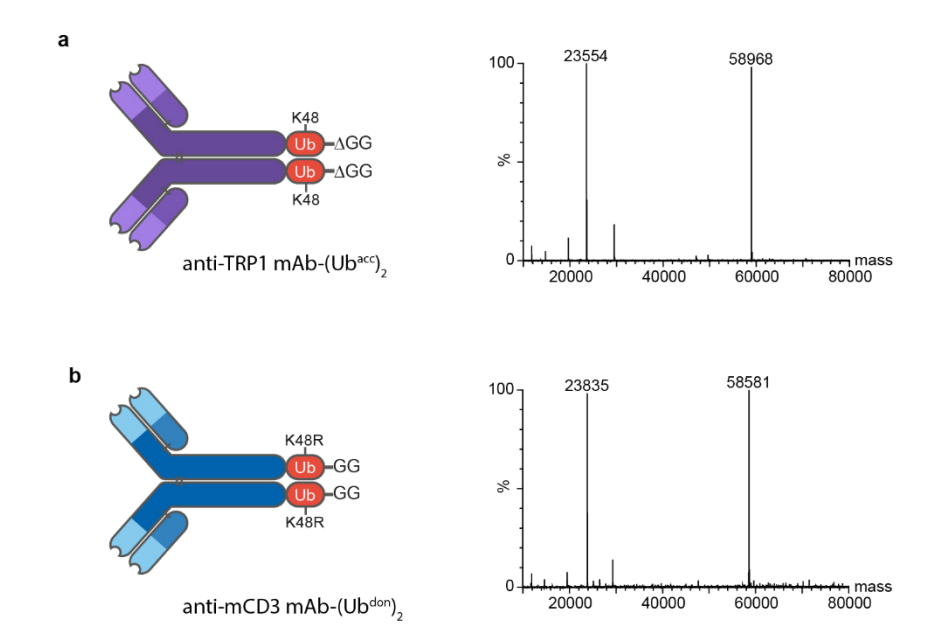
of 94.2% while conjugation reactions involving ubi-tagged Fabs forming tri-ubiquitin chains showed an average efficiency of 93.4%. Conjugation of ubi-tagged mAbs showed an average reaction efficiency of 95.7% within 60 mins. The conjugation reaction efficiency is calculated by quantifying the gel bands corresponding to the limiting reactant at the start and end of the reaction (indicated in the dashed boxes) and calculating the percentage of limiting reactant consumed.



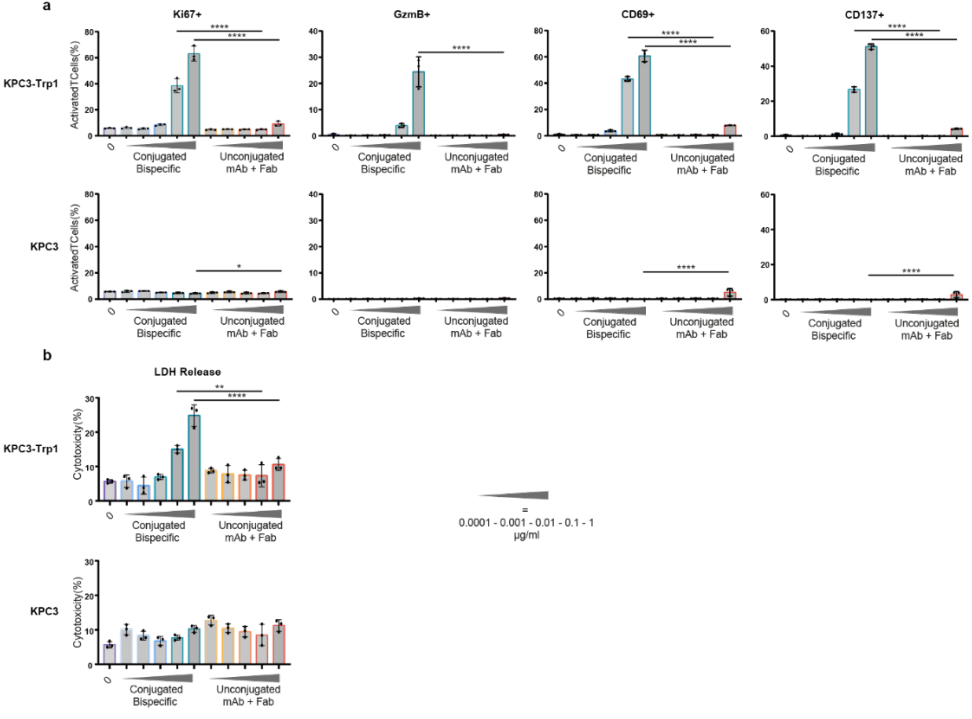
**S3** Generation of multimeric Fab complexes using ubi-tag conjugation. Non-reducing SDS-PAGE stained with Coomassie staining of multimerization of Fab-Ub<sup>WT</sup> showing the formation of multimers beyond the 11<sup>th</sup> order.



**S4Validation of mAb-Ub producing hybridoma clones.** SDS-PAGE analysis of hybridoma supernatants containing mAb-Ub in the absence or presence of  $\beta$ -mercaptoethanol, stained with Coomassie Blue and analyzed by western blot using an anti-Ub antibody.

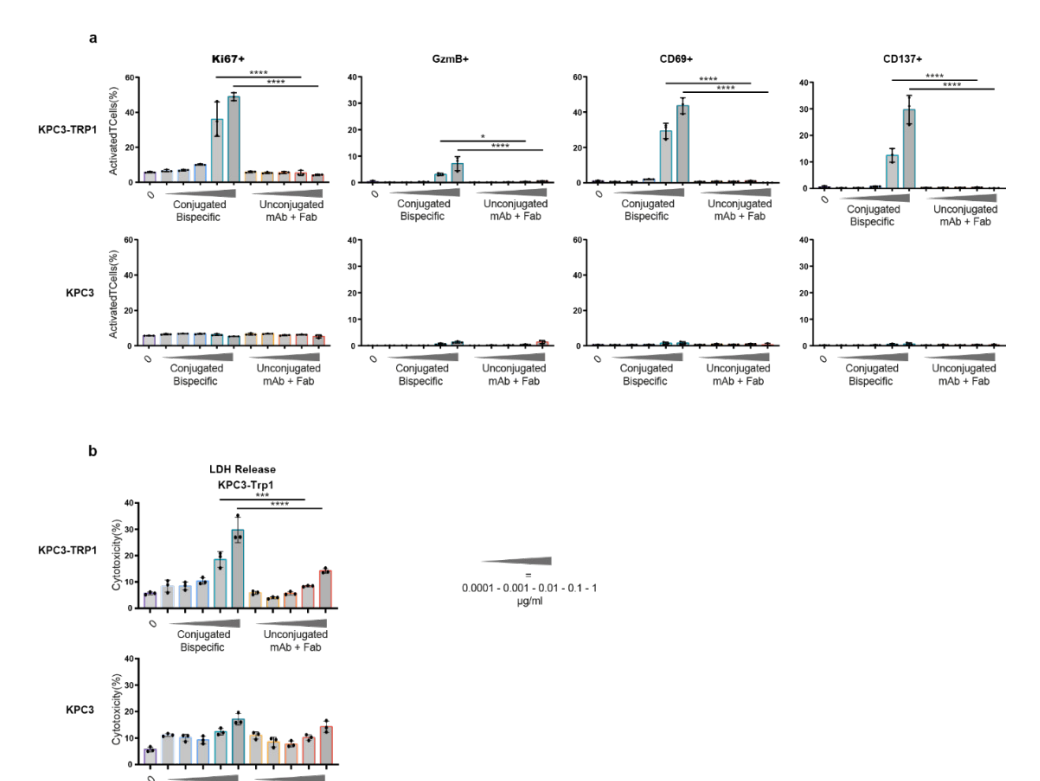


S5 LC-MS analysis showing the deconvoluted ESI-TOF mass spectra of (a) anti-TRP1 mAb- $(Ub^{acc})_2$  and (b) anti-mCD3 mAb- $(Ub^{don})_2$ .

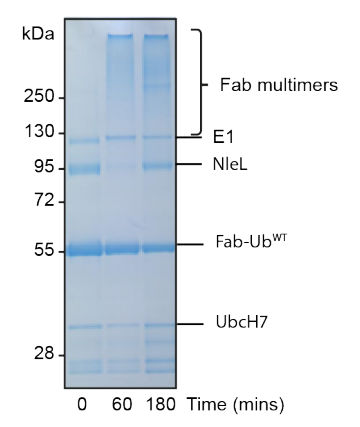


S6 In vitro T cell activation and tumor cell killing assay to validate the functionality of ubi-conjugated bispecific TRP1 mAb x mCD3 Fab antibody complex. CD8\* T cells in the presence of KPC3-TRP1 cells

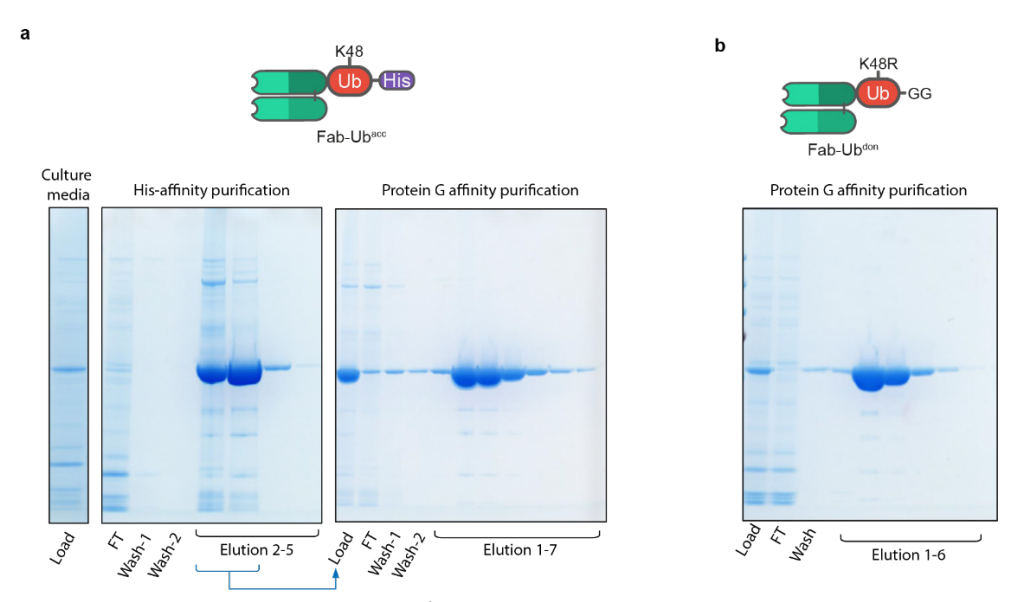
or control cells KPC1, were treated with increasing concentrations (0 – 1  $\mu$ g/mL) of the ubi-conjugated TRP1 mAb x mCD3 Fab bispecific or the unconjugated ubi-tagged TRP1 mAb and mCD3 Fab. (a) Surface expression of T cell activation markers Ki67, granzyme B, CD69 and CD137 were analyzed by flow cytometry. (b) Tumor cell killing was assessed using the CyQUANT TM LDH cytotoxicity assay. (a-b) Ordinary one-way Anova test was applied to the ubi-conjugated bispecific TRP1 mAb x mCD3 Fab vs. the unconjugated ubi-tagged TRP1 mAb and mCD3 Fab of the same concentration, showing only the significant values. All statistical values are shown in table S5. n=1 independent experiments, each condition performed in triplicates.



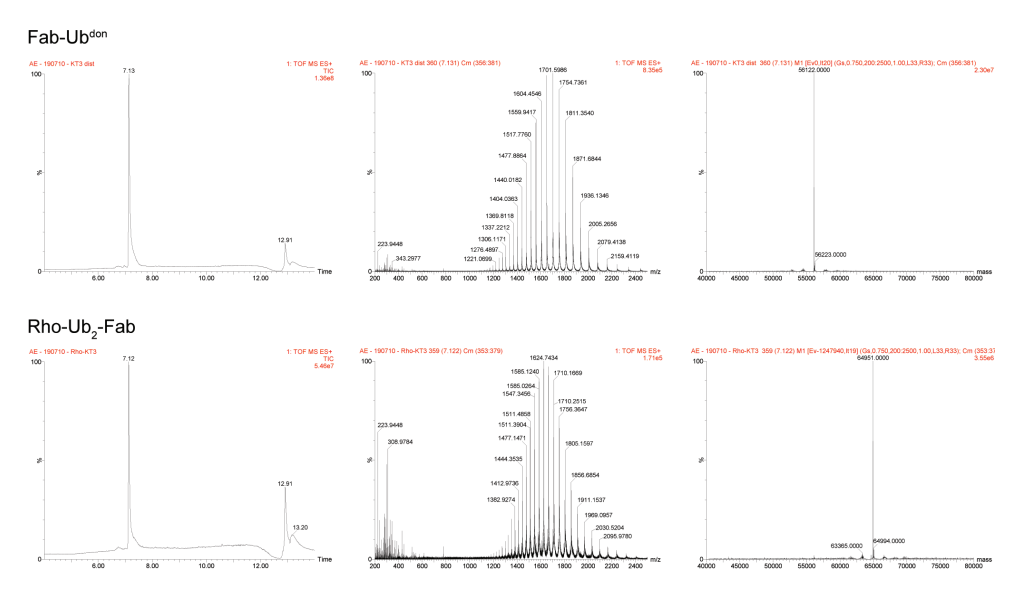
S7 In vitro T cell activation and tumor cell killing assay to validate the functionality of ubi-conjugated bispecific mCD3mAb x TRP1 Fab antibody complex. CD8+ T cells in the presence of KPC3-TRP1 cells or control cells KPC1, were treated with increasing concentrations (0 - 1  $\mu$ g/mL) of the ubi-conjugated bispecific mCD3 mAb x TRP1 Fab or the unconjugated ubi-tagged mCD3 mAb and TRP1 Fab. (a) Surface expression of T cell activation markers Ki67, granzyme B, CD69 and CD137 were analyzed by flow cytometry. (b) Tumor cell killing was assessed using the CyQUANT TM LDH cytotoxicity assay. (a-b) Ordinary one-way anova test was applied to the ubi-conjugated bispecific mCD3 mAb x TRP1 Fab vs. the unconjugated ubi-tagged mCD3 mAb and TRP1 Fab. of the same concentration, showing only the significant values. All statistical values are shown in table S5. n=3 independent experiments, each condition performed in triplicates.



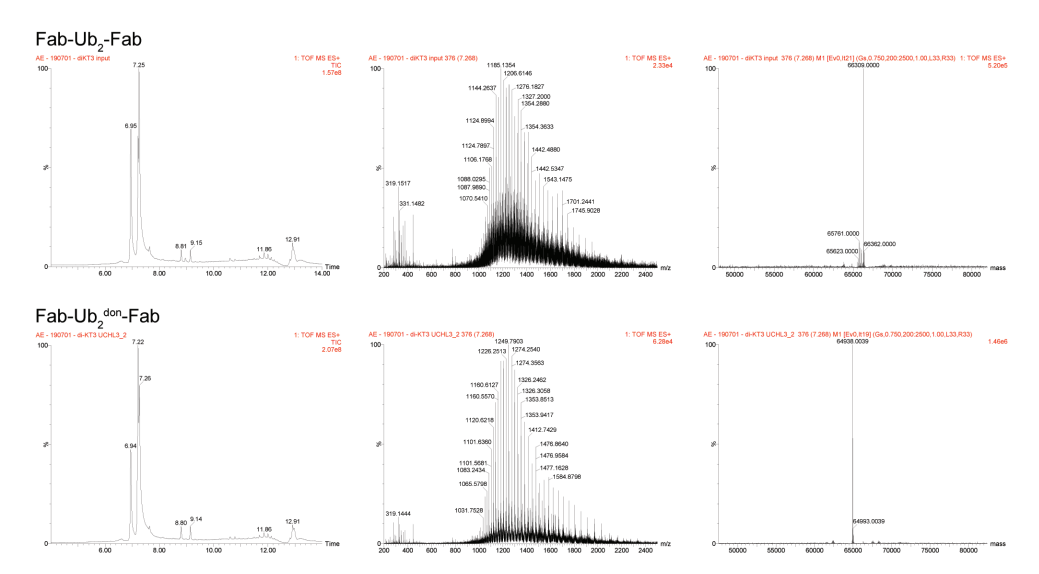
**\$8** UbcH7 and NIeL for the generation of K6-linked ubi-tagged antibody multimers.



**S9 Purification of Fab-Ub**<sup>acc</sup> and **Fab-Ub**<sup>don</sup> from hybridoma culturing media. (a) Hybridoma cells secreting Fab-Ub<sup>acc</sup> are cultured in presence of Ub-PA and Fab-Ub<sup>acc</sup> is isolated from the culturing media by Ni-NTA followed by Protein G affinity purification to ensure the His-tag is present on all purified Fab-Ub<sup>acc</sup>. (b) Hybridoma cells secreting Fab-Ub<sup>don</sup> are cultured in absence of Ub-PA and Fab-Ub<sup>don</sup> is purified from culturing media by Protein G affinity purification.



**S10 LC-MS analysis of Fab-Ub**<sup>don</sup> **conjugation to Rho-Ub**<sup>acc</sup> **forming Rho-Ub**<sub>2</sub>-**Fab.** Total ion chromatograms (left), ESI-TOF spectra (middle) and deconvoluted ESI-TOF mass spectra (right).



**S11 LC-MS** analysis of the cleavage of His-tag from C-terminus of Fab-Ub<sub>2</sub>-Fab by UCHL3. Total ion chromatograms (left), ESI-TOF spectra (middle) and deconvoluted ESI-TOF mass spectra (right).

**Table S1 Rat IgG2A ubi-tagged Fab: donor and acceptor.** Design HDR-template used to obtain the antimCD3 Fab-Ub<sup>don</sup> and anti-mCD3 Fab-Ub<sup>acc</sup>.

PCR4 TOPO	sequence
5'HA	CCTGGAACTCTGGAGCCCTGTCCAGCGGTGTGCACACCTTCCCAGCTGTCCTG-CAGTCTGGACTCTACACTCTCACCAGCTCAGTGACTGTACCCTCCAGCACCTGGTC-CAGCCAGGCCGTCACCTGCAACGTAGCCCACCCGGCCAGCACCAAGGTGGA-CAAGAAAATTGGTGAGAGAACAACCAGGGGATGAGGGCCACCAGGGAGGG
Linker - Ub <sub>1-76</sub> -His <sub>10x</sub> (acceptor)	TGCCAAGGGAATGCGGAGGCGGTGGATCTATGCAAATTTTCGTTAAGACTCT-GACAGGGAAGACTATTACACTGGAGGTTGAGCCATCAGATACGATTGAGAAT-GACAGGGAAGATACAGATACAGAAAGAAGGGTTCAAGGCCAACAAAGGCT-GATCTTCGCTGGGAAGCAACTGGAAGATGGCCGAACACTGAGCGATTATAACATA-CAAAAGGAGTCTACACTGCATTTGGTTCTGCGCCTTCGAGGCGGGCATCACCACCACCACCACCACCACCACCACCACCACCACC
Linker - Ub <sub>K48R</sub> -His <sub>10x</sub> (Donor)	TGCCAAGGGAATGCGGAGGCGGTGGATCTATGCAAATATTCGTAAAGACTCTGACC- GGGAAAACCATTACACTTGAAGTGGAGCCGTCAGACACGATTGAGAATGTTAAGGC- TAAGATTCAGGACAAGGAAGGTATCCCGCCAGACCAACAACGCCTGATCTTCGCCG- GACGACAATTGGAGGATGGTAGGACTTTGAGCGATTACAACATACAGAAAGAA
IRES Bsr polyA	CCGGTGAGCTCTCCCCCCCCCCCCTAACGTTACTGGCCGAAGCCGCTTGGAATAAGGCCGGTGTGCGTTTGTCTATATGTTATTTTCCACCATATTGCCGAATAAGGCCGGTGTGCGTTTGTCTATATGTTATTTTCCACCATATTGCCGTCTTTTTGGCAATGTGAGGGCCCGGAAACCTGGCCCTGTCTTCTTGACGAGGCATTCCTAGGGGGTCTTTCCCCTCTCGCCAAAGGAATGCAAGGTCTGTTGAATGCGTGGAAGCAAGGAAGAACAACGTCTGGAAGCACCCCACCTGGCGAAAGCAACCACCCAGTGCGGCAAAAGCCACCCAGTGAAAAGCCACCTGGCAAAAGCCACCCAGTGCTCCAAAAGCCACCGTGTATAAAGAATACACCTGCAAAAGCCACCCAGTGCCAAAAGCCACCGTGTATTCAACAAGGGGCTGAAAGGCCACCAAGCCCCAGTGCCAACCCCAGTGCTATTCAACAAGGGGCTGAAAGGATGCCCAAAGGCCCCAATTGTATGGGATCTGAATCAACAAGGGGCCTCAAAGCCCAATTGTATGGGATCTGAACAAGGGCCCCCGAACCACGGGGACCCCAGAAGGTACCCCATTTGTATGGGATCTGAACAAAAAACCGATGATAATTCAACAAGGGCCCCCGAACCACGGGGACGTGGTTTTCCTTTGAAAAAAACACGATGATAATTAAAAAAACACGATGATAAAAAACCGATGATAAAAAACACGATGATAAAAAAACACGATGATAAAAAAACACGATGATAAAAAAACACGATGATAAAAAAACACGATGATAAAAAAACACGATGATAAAAAAACACGATGATAAAAAAAA

3'HA	GGTAAGTCACTAGGACTATTACTCCAGCCCCAGATTCAAAAAATATCCTCAGAG-
	GCCCATGTTAGAGGATGACACAGCTATTGACCTATTTCTACCTTTCTTCATC-
	TACAGGCTCAGAAGTATCATCTGTCTTCATCTTCCCCCCAAAGACCAAAGATGT-
	GCTCACCATCACTCTGACTCCTAAGGTCACGTGTGTTGTGGTAGACATTAGC-
	CAGAATGATCCCGAGGTCCGGTTCAGCTGGTTTATAGATGACGTGGAAGTCCA-
	CACAGCTCAGACTCATGCCCCGGAGAAGCAGTCCAACAGCACTTTACGCTCAGT-
	CAGTGAACTCCCCATCGTGCACCGGGACTGGCTCAATGGCAAGACGTTCAAATG-
	CAAAGTCAACAGTGGAGCATTCCCTGCCCCCATCGAGAAAAGCATCTCCAAACCC-
	GAAGGTGGGAGCAGCAGGTGTGTGTGTAGAAGCTGCAGTAGGCCATAGA-
	CAGAGCTTGACTTAACTAGACTTAAGGGCGAATTCGCGGCCGCGCGGCCGC

#### Table S2 mlgG2a Hinge targeted to mlgG2a-Fc silent – ubiquitin.

Mus musculus strain 129S1/SvImJ chromosome 12 genomic scaffold, GRCm38.p4 alternate locus group 129S1/SvImJ 129S1/SVIMJ MMCHR12 CTG1

Sequence ID: NT\_114985.3 Length: 1714434 Number of Matches: 7

CCAGGGACAAAGTCCCTGGTTTGGTGCCTTTCTCCTTCAAACTTGAGTAACCCCCAGCCTTCTCTCTGCAGAGGCCCAGAGGGCCCACAATCAAGCCCTGTCCTCCATGCAAATGCCCAGGTAAGTCACTAGACCAGAGCTCCACTCCCGGGAGAATGGTAAGTGCTGTAAACATCCCTGCACTAGAGGATAAGCCATGTACAGATCCATTTCCATCTCT(85) TGGAGGACAGGGCTTGATTG TGG

Genomic Sequence and annotated base pair sequence of mlgG2a constant domains. The genomic annotated basepair sequence and of the lgH locus of murine lgG2a located on chromosome 12 are given. The Hinge region is indicated (grey highlight) with splice acceptor and donor sites (underlined, cursive). The targeted protospacer adjacent motifs (PAMs) for gRNA-6 (yellow, underlined) and gRNA-2 (red. underlined) are indicated.

PCR4 TOPO	sequence
5'HA mlgG2a	ACTAGTGATCCCTGTCCAGTGGTGTGCACACCTTCCCAGCTGTCCTG-CAGTCTGACCTCTACACCCTCAGCAGCTCAGTGACTGTAACCTCGAG-CAGTCTGACCTCAGCAGCCCAGCC
Fc silent mlgG2a	GCCCCAAATGCCGCCGGTGGTCCTAGCGTCTTCATCTTCCCCCCCAAGATTA- AGGATGTGCTGATGATTTCATTGAGCCCAATTGTCACATGTGTGGTCGTGGATGT- GTCAGAGGATGACCCTGACGTGCAAATATCTTGGTTTGTAAATAACGTAGAGGTG- CATACCGCTCAGACTCAGACTCACCGGGAGGACTATGCCAGCACTCTCAGGGTG- GTCTCCGCACTTCCAATTCAGCACCAGGACTGGATGTCCGGCAAAGAGTTCAAGTG- TAAAGTCAATAACAAGGATTTGCCCGCACCAATAGAACGGACCATCTCTAAACCTA- AAGGGAGTGTACGCGCCCCACAGGTTTACGTGCTGCCCCCACCCGAGGAGGAAAT- GACCAAAAAGCAGGTGACACTCACCTGCATGGTTACCGATTTTATGCCCGAAGA- CATATATGTTGAGTGGACTCACACGGGAAGACCGAGCTGAATTATAAAAATAC- CGAACCCGTTTTGGACTCAGATGGCTCATACTTCATGTACTCCAAACTCCGGG- TAGAGAAAAAGAACTGGGTTGAAAGAACAGCTACTCATGCAGCGTGGTGCATGAG- GGGCTCCACAATCATCATACCACCAAGTCTTTCTCACGGACACCTGGGAAA

Linker - Ub	GGCGGGGGGATCCGGGGGAGGCGGAAGTGGGGGCGGAGGCTCCATG-
(acceptor)	CAAATTTTCGTTAAGACTCTGACAGGGAAGACTATTACACTGGAGGTTGAGCCAT-CAGATACGATTGAGAATGTCAAGGCAAAGATACAGGACAAAGAAGGGATACCCCC-GGACCAACAAAGGCTGATCTTCGCTGGGAAGCAACTGGAAGATGGCCGAACACT-GAGCGATTATAACATACAAAAGGAGTCTACACTGCATTTGGTTCTGCGCCTTC
IRES Bsr polyA	TCCCTCCCCCCCCTAACGTTACTGGCCGAAGCCGCTTGGAATAAGGC-CGGTGTGCGTTTGTCTATATGTTATTTTCCACCATATTGCCGTCTTTTG-GCAATGTGAGGGCCCGGAAACCTGGCCCTGTCTTCTTGACGAGCATTCCTAGGGGTCTTTTCCCCTCTCGCCAAAGGAATGCAAGGTCTGTTGAATGTCGT-GAAGGAAGCAGCTCCTCTGGCAAAGGAATGCAAGGTCTGTTGAATGTCGT-GAAGGAAGCAGCACCCCCCCCCC
3'HA mIgG2a	GGTAAGTCACTAGACCAGAGCTCCACTCCCGGGAGAATGGTAAGTGCTGTAAA- CATCCCTGCACTAGAGGATAAGCCATGTACAGATCCATTTCCATCTCCTCAT- CAGCACCTAACCTCTTGGGTGGACCATCCGTCTTCATCTTCCCTCCAAAGAT- CAAGGATGTACTCATGATCTCCCTGAGCCCCATAGTCACATGTGTGGTGGTGGAAG- GTGAGCGAGGATGACCCAGATGTCCAGATCAGCTGGTTTTGTGAACAACGTGGAAG- TACACACAGCTCAGACCACAAACCCATAGAGAGGATTACAACAGTACTCTCCGGGTG- GTCAGTGCCCTCCCCATCCAGCACCAGGACTGGATGAGTGGCAAGGAGTTCAAAT- GCAAGGTCAACAACAAAGACCTCCCAGCCCCATCGAGAGAACCATCT- CAAAACCCAAAGGTGAGAGCTGCAGCCTGACTGCATGGGGGCTGGGATGGCCATA- AGGATAAAGGTCTGTGTGGACAGC GCGGCCGC

**Table S3 Rat IgG2a intron targeted to mIgG1-ubiquitin.** Isotype donor constructs for HDR introducing synthetic exon. Table displays sequences of each feature of donor constructs used to change the isotype of rat IgG2a hybridomas to mIgG1 fused to Ubiquitin with a HIS tag. The gRNA-ISO and sequences of 5' HA, IRES-Bsr-PolyA and 3' HA of the HDR plasmid are previous published<sup>38</sup>.

5 111 y 11125 251 1 51 y 1 1	Someone
	Sequence
5'HA rIgG2a	AGAAAGATCTGAGTAGAACCAAGGTAAAAAGTGTGGGTAAAAACACATGTTCA- CAGGCCTGGCTGACATGATGCTGGGCACGTATGAGGCCAAAGTCAAGAGGGCAGT- GTAAGGGCCAGAAGTGAATCCTGACCCAAGAAATAGAGAGTGCTAAACCTACG- TAGATCGAAGCCAACTAAAAAGACAAGCTACAAACGAAGCTAAGGCCAGA- GATCTTGGACTGTGAAGAGTTCAGAGACCTAGGATCAGGAACCATTAGTAA- CAGGCCAAGGAAGATAGAAGCTGCCTAGGACTTGGCAACATGGTTG- GACTGGAAAAGAAAGGAGGAGACAGAAGACAGGAGAGATATGGCCAACTT- GATTTTGGGCTTCACTGTTGTCCATACTGTTGCAGCCATATGGCCCACAGATAA- CAGGTTTAGCCGAGGAACACAGATACCCACATTTGGACAATGGTGGGGGAACA- CAGATACCCATACTACAGGGCTCTTTAGGGCATTTCCTGAAAGTGTACTAG- GAGTGGGACTGGGCTCAAAGGGATTAGGTTGGCCTGGTGAGGCT- GACATTGGCAAGCCCAATGGTTGGCCTCCTCCATGT
Splice Acceptor	GCTAGCgatcgcaggcgcaatcttcgcatttcttttttccag
mlgG1	CAAAGACCACCACCTTCTGTGTACCCACTCGCACCAGGCAGCGCCGCTCAAACCCAACAGTATGGTGACCTTGGGGTGTCTTGTGAAGGGCTACTTTCCCGAGCCCGTTACCGTCACCTGGAACTCCGGGTTCTCTCAAGCGGCGTTCACACCTTCCCCGCCGTACTGCAATCAGACTCCTATACCCTGTCTTCCAGCGGTCACTGTACCCAGTTCCACCTTGCCAGTTCCACCTTGCCAGTTCCACCTTGCCAGTTCCACCTTGCCAGTTCCACCTTGCCCAGTTCCACCTTGCCCAGTTCCACCTTGCCCAGTTCCACCTTGCCCAGTTGAAACAGTGCACAAAAAAAA
Linker - Ub <sub>K48R</sub> - His <sub>10x</sub>	CGTACGGGAGGTGGCGGTTCCGGGGGAGGTGGATCTGGAGGGGGCGGAAGTG-GCGGTGGTGGATCAATGCAAATATTCGTAAAGACTCTGACCGGGAAAACCATTA-CACTTGAAGTGGAGCCGTCAGACACGATTGAGAATGTTAAGGCTAAGATTCAG-
(Donor)	GACAAGGAAGGTATCCCGCCAGACCAACAACGCCTGATCTTCGCCGGACGA- CAATTGGAGGATGGTAGGACTTTGAGCGATTACAACATACAGAAAGAA

IDEC Daniela	GCCCCTCTCCCTCCCCCCCCCTAACGTTACTGGCCGAAGCCGCTTG-
IRES Bsr polyA	GAATAAGGCCGGTGTGCGTTTGTCTATATGTTATTTTCCACCATATTGCC-
	GTCTTTTGGCAATGTGAGGGCCCGGAAACCTGGCCCTGTCTTCTTGACGAG-
	CATTCCTAGGGGTCTTTCCCCTCTCGCCAAAGGAATGCAAGGTCTGTTGAAT-
	GTCGTGAAGGAAGCAGTTCCTCTGGAAGCTTCTTGAAGACAAACAA
	TAGCGACCCTTTGCAGGCAGCGGAACCCCCCACCTGGCGACAGGTGCCTCTGC-
	GGCCAAAAGCCACGTGTATAAGATACACCTGCAAAGGCGGCACAACCCCAGT-
	GCCACGTTGTGAGTTGGATAGTTGTGGAAAGAGTCAAATGGCTCTCCT-
	CAAGCGTATTCAACAAGGGGCTGAAGGATGCCCAGAAGGTACCCCATTG-
	TATGGGATCTGATCTGGGGCCTCGGTGCACATGCTTTACATGTGTTTAGTC-
	GAGGTTAAAAAAACGTCTAGGCCCCCCGAACCACGGGGACGTGGTTTTCCTTT-
	GAAAAACACGATGATAATATGGCCACAGAATTCGCCACCATGGCCAAGCCTTT-
	GTCTCAAGAAGAATCCACCCTCATTGAAAGAGCAACGGCTACAATCAACAG-
	CATCCCCATCTCTGAAGACTACAGCGTCGCCAGCGCAGCTCTCTCT
	GGCCGCATCTTCACTGGTGTCAATGTATATCATTTTACTGGGGGACCTTGTG-
	CAGAACTCGTGGTGCTGGGCACTGCTGCTGCTGCGGCAGCTGGCAACCTGACTT-
	GTATCGTCGCGATCGGAAATGAGAACAGGGGCATCTTGAGCCCCTGCGGACG-
	GTGCCGACAGGTGCTTCTCGATCTGCATCCTGGGATCAAAGCCATAGTGAAGGA-
	CAGTGATGGACAGCCGACGGCAGTTGGGATTCGTGAATTGCTGCCCTCTGGT-
	TATGTGTGGGAGGGCTAAGTACTAGTCGAGTGTGCCTTCTAGTTGCCAGCCA
	GTTGTTTGCCCCTCCCCCGTGCCTTCCTTGACCCTGGAAGGTGCCACTCCCACT-
	GTCCTTTCCTAATAAAATGAGGAAATTGCATCGCATTGTCTGAGTAGGTGCCACTC
	TATTCTGGGGGGTGGGGCAGGACAGCAAGGGGGAGGATTGGGAAGACAATAG-
	CAGGCATGCTGGGGATGCGGTGGGCTCTATGGAGATCT
3'HA rlgG2a	TGTACAACTTGGGGAGGGTACAAAATGGAGGACTTGTAGGAGCTTGGGTC-
	CAGACCTGTCAGACAAAATGATCACGCATACTTATTCTTGTAGCTGAAACAA-
	CAGCCCCATCTGTCTATCCACTGGCTCCTGGAACTGCTCTCAAAAGTAACTC-
	CATGGTGACCCTGGGATGCCTGGTCAAGGGCTATTTCCCTGAGCCAGTCACCGT-
	GACCTGGAACTCTGGAGCCCTGTCCAGCGGTGTGCACACCTTCCCAGCTGTCCT-
	GCAGTCTGGACTCTACACTCTCACCAGCTCAGTGACTGTACCCTCCAGCACCTG-
	GTCCAGCCAGGCCGTCACCTGCAACGTAGCCCACCCGGCCAGCAGCACCAAGGTG-
	GACAAGAAATTGGTGAGAGAACAACCAGGGGATGAGGGGCTCACTAGAG-
	GTGAGGATAAGGCATTAGATTGCCTACACCAACCAGGGTGGGCAGACATCAC-
	CAGGGAGGGGCCTCAGCCCAGGAGACCAAAAATTCTCCTTTGTCTCCCTTCTGGA-
	GATTTCTATGTCCTTTACACCCATTTATTAATATTCT

**Table S4 Recombinant ubitagged Fab fragments produced by Genscript.** Table displays protein sequence of recombinant constructs used. Clone TA99 is directed against Tryp-1 and clone 145-2C11 is against mCD3.

	Sequence
IgH chain TA99	MGWSCIILFLVATATGVHSEVQLQQSGAELVRPGALVKLSCKTSGFNIKDY-FLHWVRQRPDQGLEWIGWINPDNGNTVYDPKFQGTASLTADTSSNTVYLQLS-GLTSEDTAVYFCTRRDYTYEKAALDYWGQGTTVTVSTAKTTAPSVYPLAPVC-GDTTGSSVTLGCLVKGYFPEPVTLTWNSGSLSSGVHTFPAVLQSDLYTLSSS-VTVTSSTWPSQSITCNVAHPASSTKVDKKI
Linker-ubi	GGGGSGGGGGGGGMQIFVKTLTGKTITLEVEPSDTIENVKAKIQDKEGIP- PDQQRLIFAGKQLEDGRTLSDYNIQKESTLHLVLRLR
His-tag	ннинин*

IgL chain TA99	MGWSCIILFLVATATGVHSDIQMSQSPASLSASVGETVTITCRASGNIYNYL- AWYQQKQGKSPHLLVYDAKTLADGVPSRFSGSGSGTQYSLKISSLQTEDS- GNYYCQHFWSLPFTFGSGTKLEIKRADAAPTVSIFPPSSEQLTSGGASVVC- FLNNFYPKDINVKWKIDGSERQNGVLNSWTDQDSKDSTYSMSSTLTLTKDEY- ERHNSYTCEATHKTSTSPIVKSFNRNEC*
IgH chain 145-2C11	MGWSCIILFLVATATGVHSEVQLVESGGGLVQPGKSLKLSCEASGFTFS-GYGMHWVRQAPGRGLESVAYITSSSINIKYADAVKGRFTVSRDNAKNLL-FLQMNILKSEDTAMYYCARFDWDKNYWGQGTMVTVSSAKTTAPSVYPLAPVC-GDTTGSSVTLGCLVKGYFPEPVTLTWNSGSLSSGVHTFPAVLQSDLYTLSSS-VTVTSSTWPSQSITCNVAHPASSTKVDKKI
Linker-Ub <sup>don</sup>	GGGGSGGGSGGGSMQIFVKTLTGKTITLEVEPSDTIENVKAKIQDKEGIP- PDQQRLIFAGRQLEDGRTLSDYNIQKESTLHLVLRLRGG
His-tag	ннинин*
IgL chain 145-2C11	MGWSCIILFLVATATGVHSDIQMTQSPSSLPASLGDRVTINCQASQDISNYL- NWYQQKPGKAPKLLIYYTNKLADGVPSRFSGSGSGRDSSFTISSLESEDIG- SYYCQQYYNYPWTFGPGTKLEIKRADAAPTVSIFPPSSEQLTSGGASVVC- FLNNFYPKDINVKWKIDGSERQNGVLNSWTDQDSKDSTYSMSSTLTLTKDEY- ERHNSYTCEATHKTSTSPIVKSFNRNEC

**Table S5 Statistics for figure 3 and supplemental figure 7 and 8.** \*\*\*\*P<0.0001, \*\*\*P<0.001, \*\*P<0.001, \*\*P<0.005 and ns= non-significant in a One-way ANOVA followed by Tukey post-hoc test.

	_	•	•		
	KPC3-TRP1 cells				
	Conjugated TRP1	mAb x mCD3Fab vs	s. the unconjugated	TRP1mAb and mC	D3Fab
Conc. (µg/mL)	0.0001	0.001	0.01	0.1	1
Ki67	0.9997, ns	>0.9999, ns	0.7607, ns	<0.0001, ****	<0.0001, ****
GzmB	>0.9999, ns	>0.9999, ns	>0.9999, ns	0.2771, ns	<0.0001, ****
CD69	>0.9999, ns	>0.9999, ns	0.331, ns	<0.0001, ****	<0.0001, ****
4-1BB	>0.9999, ns	>0.9999, ns	0.8061, ns	<0.0001, ****	<0.0001, ****
LDH	0.7266, ns	0.6012, ns	>0.9999, ns	0.0037, **	<0.0001, ****

	KPC3 cells  Conjugated TRP1mAb x mCD3Fab vs. the unconjugated TRP1mAb and mCD3Fab				
Conc. (µg/mL)	0.0001	0.001	0.01	0.1	1
Ki67	0.2068, ns	0.8187, ns	0.9917, ns	0.9991, ns	0.0337, *
GzmB	>0.9999, ns	>0.9999, ns	>0.9999, ns	0.9991, ns	0.9852, ns
CD69	>0.9999, ns	>0.9999, ns	>0.9999, ns	>0.9999, ns	<0.0001, ****
4-1BB	>0.9999, ns	>0.9999, ns	>0.9999, ns	>0.9999, ns	<0.0001, ****
LDH	0.5391, ns	0.7981, ns	0.5747, ns	0.9998, ns	0.9991, ns

	KPC3-TRP1 cells						
	Conjugated mCD3mAb x TRP1Fab vs. the unconjugated mCD3mAb and TRP1Fab						
Conc. (µg/mL)	0.0001	0.0001 0.001 0.01 1					
Ki67	>0.9999, ns	0.9999, ns	0.7703, ns	<0.0001, ****	<0.0001, ****		
GzmB	>0.9999, ns	>0.9999, ns	>0.9999, ns	0.0209, *	<0.0001, ****		
CD69	>0.9999, ns	>0.9999, ns	0.9987, ns	<0.0001, ****	<0.0001, ****		

4-1BB	>0.9999, ns	>0.9999, ns	>0.9999, ns	<0.0001, ****	<0.0001, ****
LDH	0.8808, ns	0.2477, ns	0.2104, ns	0.0002, ***	<0.0001, ****

	KPC3 cells				
	Conjugated mCD3mAb x TRP1Fab vs. the unconjugated mCD3mAb and TRP1Fab				
Conc. (µg/mL)	0.0001	0.001	0.01	0.1	1
Ki67	>0.9999, ns	>0.9999, ns	0.3557, ns	>0.9999, ns	>0.9999, ns
GzmB	>0.9999, ns	>0.9999, ns	0.9997, ns	0.9447, ns	>0.9999, ns
CD69	>0.9999, ns	0.9878, ns	>0.9999, ns	0.9183, ns	0.1305, ns
4-1BB	>0.9999, ns	0.9862, ns	>0.9999, ns	0.9966, ns	0.3262, ns
LDH	>0.9999, ns	0.9439, ns	0.9547, ns	0.7421, ns	0.4074, ns

#### References

- 1. Sun, M. M. C. *et al.* Reduction-alkylation strategies for the modification of specific monoclonal antibody bisulfides. *Bioconjug Chem* **16**, 1282–1290 (2005).
- 2. Junutula, J. R. *et al.* Site-specific conjugation of a cytotoxic drug to an antibody improves the therapeutic index. *Nature Biotechnology 2008 26:8* **26**, 925–932 (2008).
- 3. Yamada, K. & Ito, Y. Recent Chemical Approaches for Site-Specific Conjugation of Native Antibodies: Technologies toward Next-Generation Antibody–Drug Conjugates. *ChemBioChem* **20**, 2729–2737 (2019).
- 4. Wang, L., Amphlett, G., Blättler, W. A., Lambert, J. M. & Zhang, W. Structural characterization of the maytansinoid-monoclonal antibody immunoconjugate, huN901-DM1, by mass spectrometry. *Protein Sci* **14**, 2436–2446 (2005).
- 5. Strop, P. *et al.* Location Matters: Site of Conjugation Modulates Stability and Pharmacokinetics of Antibody Drug Conjugates. *Chem Biol* **20**, 161–167 (2013).
- 6. Shen, B. Q. *et al.* Conjugation site modulates the in vivo stability and therapeutic activity of antibody-drug conjugates. *Nature Biotechnology 2012 30:2* **30**, 184–189 (2012).
- 7. Agarwal, P. & Bertozzi, C. R. Site-specific antibody-drug conjugates: The nexus of bioorthogonal chemistry, protein engineering, and drug development. *Bioconjug Chem* **26**, 176–192 (2015).
- 8. Axup, J. Y. *et al.* Synthesis of site-specific antibody-drug conjugates using unnatural amino acids. *Proc Natl Acad Sci U S A* **109**, 16101–16106 (2012).
- 9. Oller-Salvia, B., Kym, G. & Chin, J. W. Rapid and Efficient Generation of Stable Antibody—Drug Conjugates via an Encoded Cyclopropene and an Inverse-Electron-Demand Diels—Alder Reaction. *Angewandte Chemie International Edition* **57**, 2831—2834 (2018).

- 10. Kim, C. H. *et al.* Synthesis of bispecific antibodies using genetically encoded unnatural amino acids. *J Am Chem Soc* **134**, 9918–9921 (2012).
- 11. Hofer, T., Skeffington, L. R., Chapman, C. M. & Rader, C. Molecularly defined antibody conjugation through a selenocysteine interface. *Biochemistry* **48**, 12047–12057 (2009).
- 12. Zimmerman, E. S. *et al.* Production of site-specific antibody-drug conjugates using optimized non-natural amino acids in a cell-free expression system. *Bioconjug Chem* **25**, 351–361 (2014).
- 13. van Geel, R. *et al.* Chemoenzymatic Conjugation of Toxic Payloads to the Globally Conserved N-Glycan of Native mAbs Provides Homogeneous and Highly Efficacious Antibody-Drug Conjugates. *Bioconjug Chem* **26**, 2233–2242 (2015).
- 14. Ruhe, L., Ickert, S., Beck, S. & Linscheid, M. W. A new strategy for metal labeling of glycan structures in antibodies. *Anal Bioanal Chem* **410**, 21–25 (2018).
- 15. Toftevall, H., Nyhlén, H., Olsson, F. & Sjögren, J. Antibody Conjugations via Glycosyl Remodeling. *Methods in Molecular Biology* **2078**, 131–145 (2020).
- 16. Strop, P. Versatility of microbial transglutaminase. *Bioconjug Chem* **25**, 855–862 (2014).
- 17. Drake, P. M. *et al.* Aldehyde tag coupled with HIPS chemistry enables the production of ADCs conjugated site-specifically to different antibody regions with distinct in vivo efficacy and PK outcomes. *Bioconjug Chem* **25**, 1331–1341 (2014).
- 18. Zang, B. *et al.* Freezing-assisted synthesis of covalent C–C linked bivalent and bispecific nanobodies. *Org Biomol Chem* **17**, 257–263 (2019).
- 19. Beerli, R. R., Hell, T., Merkel, A. S. & Grawunder, U. Sortase Enzyme-Mediated Generation of Site-Specifically Conjugated Antibody Drug Conjugates with High In Vitro and In Vivo Potency. *PLoS One* **10**, e0131177 (2015).
- 20. Swee, L. K. *et al.* Sortase-mediated modification of aDEC205 affords optimization of antigen presentation and immunization against a set of viral epitopes. *Proc Natl Acad Sci U S A* **110**, 1428–1433 (2013).
- 21. Bridoux, J. *et al.* Anti-Human PD-L1 Nanobody for Immuno-PET Imaging: Validation of a Conjugation Strategy for Clinical Translation. *Biomolecules 2020, Vol. 10, Page 1388* **10**, 1388 (2020).
- 22. Morgan, H. E., Turnbull, W. B. & Webb, M. E. Challenges in the use of sortase and other peptide ligases for site-specific protein modification. *Chem Soc Rev* **51**, 4121–4145 (2022).
- 23. Bartels, L., Ploegh, H. L., Spits, H. & Wagner, K. Preparation of bispecific antibody-protein adducts by site-specific chemo-enzymatic conjugation. *Methods* **154**, 93–101 (2019).

- 24. Wagner, K. *et al.* Bispecific antibody generated with sortase and click chemistry has broad antiinfluenza virus activity. *Proc Natl Acad Sci U S A* **111**, 16820–16825 (2014).
- 25. Hershko, A. & Ciechanover, A. The ubiquitin system. *Annu Rev Biochem* **67**, 425–479 (1998).
- 26. Komander, D. & Rape, M. The ubiquitin code. *Annu Rev Biochem* **81**, 203–229 (2012).
- 27. Yau, R. & Rape, M. The increasing complexity of the ubiquitin code. *Nature Cell Biology 2016 18:6* **18**, 579–586 (2016).
- 28. Damgaard, R. B. The ubiquitin system: from cell signalling to disease biology and new therapeutic opportunities. *Cell Death & Differentiation 2021 28:2* **28**, 423–426 (2021).
- 29. Schulman, B. A. & Wade Harper, J. Ubiquitin-like protein activation by E1 enzymes: the apex for downstream signalling pathways. *Nature Reviews Molecular Cell Biology 2009 10:5* **10**, 319–331 (2009).
- 30. Ye, Y. & Rape, M. Building ubiquitin chains: E2 enzymes at work. *Nature Reviews Molecular Cell Biology 2009 10:11* **10**, 755–764 (2009).
- 31. Buetow, L. & Huang, D. T. Structural insights into the catalysis and regulation of E3 ubiquitin ligases. *Nature Reviews Molecular Cell Biology 2016 17:10* **17**, 626–642 (2016).
- 32. Zheng, N. & Shabek, N. Ubiquitin Ligases: Structure, Function, and Regulation. *Annu Rev Biochem* **86**, 129–157 (2017).
- 33. Mattiroli, F. & Sixma, T. K. Lysine-targeting specificity in ubiquitin and ubiquitin-like modification pathways. *Nature Structural & Molecular Biology 2014 21:4* **21**, 308–316 (2014).
- 34. Deol, K. K., Lorenz, S. & Strieter, E. R. Enzymatic Logic of Ubiquitin Chain Assembly. *Front Physiol* **10**, 1–14 (2019).
- 35. Michel, M. A., Komander, D. & Elliott, P. R. Enzymatic assembly of ubiquitin chains. *Methods in Molecular Biology* **1844**, 73–84 (2018).
- 36. Blythe, E. E., Olson, K. C., Chau, V. & Deshaies, R. J. Ubiquitin- A nd ATP-dependent unfoldase activity of P97/VCP•NPLOC4•UFD1L is enhanced by a mutation that causes multisystem proteinopathy. *Proc Natl Acad Sci U S A* **114**, E4380–E4388 (2017).
- 37. Faggiano, S., Alfano, C. & Pastore, A. The missing links to link ubiquitin: Methods for the enzymatic production of polyubiquitin chains. *Anal Biochem* **492**, 82–90 (2016).
- 38. van der Schoot, J. M. S. *et al.* Functional diversification of hybridoma-produced antibodies by CRISPR/HDR genomic engineering. *Sci Adv* **5**, eaaw1822 (2019).

- 39. Luchansky, S. J., Lansbury, P. T. & Stein, R. L. Substrate recognition and catalysis by UCH-L1. *Biochemistry* **45**, 14717–14725 (2006).
- 40. Larsen, C. N., Krantz, B. A. & Wilkinson, K. D. Substrate specificity of deubiquitinating enzymes: Ubiquitin C-terminal hydrolases. *Biochemistry* **37**, 3358–3368 (1998).
- 41. Navarro, M. F., Carmody, L., Romo-Fewell, O., Lokensgard, M. E. & Love, J. J. Characterizing substrate selectivity of ubiquitin C-terminal hydrolase-L3 using engineered  $\alpha$ -linked ubiquitin substrates. *Biochemistry* **53**, 8031–8042 (2014).
- 42. Gays, F. et al. The Mouse Tumor Cell Lines EL4 and RMA Display Mosaic Expression of NK-Related and Certain Other Surface Molecules and Appear to Have a Common Origin. *The Journal of Immunology* **164**, 5094–5102 (2000).
- 43. van Tilburg, G. B. A. *et al.* K27-Linked Diubiquitin Inhibits UCHL3 via an Unusual Kinetic Trap. *Cell Chem Biol* **28**, 191-201.e8 (2021).
- 44. Mevissen, T. E. T. *et al.* OTU deubiquitinases reveal mechanisms of linkage specificity and enable ubiquitin chain restriction analysis. *Cell* **154**, 169 (2013).
- 45. el Oualid, F. *et al.* Chemical synthesis of ubiquitin, ubiquitin-based probes, and diubiquitin. *Angewandte Chemie International Edition* **49**, 10149–10153 (2010).
- 46. Hameed, D. S., Sapmaz, A. & Ovaa, H. How Chemical Synthesis of Ubiquitin Conjugates Helps to Understand Ubiquitin Signal Transduction. *Bioconjug Chem* **28**, 805–815 (2017).
- 47. Huppelschoten, Y. & van der Heden van Noort, G. J. State of the art in (semi-) synthesis of Ubiquitin- and Ubiquitin-like tools. *Semin Cell Dev Biol* (2021) doi:10.1016/J. SEMCDB.2021.11.025.
- 48. Hospenthal, M. K., Freund, S. M. v & Komander, D. Assembly, analysis and architecture of atypical ubiquitin chains. doi:10.1038/nsmb.2547.
- 49. Jendroszek, A. & Kjaergaard, M. Nanoscale spatial dependence of avidity in an IgG1 antibody. *Scientific Reports 2021 11:1* **11**, 1–10 (2021).
- 50. Clague, M. J., Urbé, S. & Komander, D. Breaking the chains: deubiquitylating enzyme specificity begets function. *Nature Reviews Molecular Cell Biology 2019 20:6* **20**, 338–352 (2019).
- 51. Hingorani, S. R. *et al.* Trp53R172H and KrasG12D cooperate to promote chromosomal instability and widely metastatic pancreatic ductal adenocarcinoma in mice. *Cancer Cell* **7**, 469–483 (2005).
- 52. Benonisson, H. *et al.* CD3-Bispecific Antibody Therapy Turns Solid Tumors into Inflammatory Sites but Does Not Install Protective Memory. *Mol Cancer Ther* **18**, 312–322 (2019).
- 53. Ran, F. A. et al. Genome engineering using the CRISPR-Cas9 system. Nature

Protocols 2013 8:11 8, 2281-2308 (2013).

54. Geurink, P. P. *et al.* Development of Diubiquitin-Based FRET Probes To Quantify Ubiquitin Linkage Specificity of Deubiquitinating Enzymes. *ChemBioChem* **17**, 816–820 (2016).



# Targeted dendritic cell vaccination through ubi-tag-based peptide delivery

3

This chapter is part of the publication:

A.F. Elhebieshy\*, Z. Wijfjes\*, et al. Site-directed multivalent conjugation of antibodies to ubiquitinated payloads. Accepted for publication: Nature Biomedical Engineering.



## Targeted Dendritic Cell vaccination through ubi-tag-based peptide delivery

Angela F. el Hebieshy, Zacharias Wijfjes, Camille M. Le Gall, Felix L. Fennemann, Cami M. P. Talavera Ormeño, Bjorn R. van Doodewaerd, Gerbrand J. van der Heden van Noort, Paul W. H. I. Parren, Martijn Verdoes, Huib Ovaa, Ferenc A. Scheeren.

#### **Abstract**

Targeted dendritic cell (DC) vaccination enhances antigen uptake and presentation, leading to more robust T cell responses against specific pathogens or tumor cells. In this study, we explored ubi-tagging as a promising conjugation technique for DC-targeted antigen delivery and compared its efficacy with that of the established sortagging method. We engineered the NLDC-145 hybridoma using the CRISPR/HDR platform to produce anti-mDEC205 Fab fragments fused to either a donor Ubi-tag or a sortag motif. We proceeded to conjugate the Fab fragments to the ovalbumin antigenic peptide SIINFEKL (OVAp) using ubitagging or sortagging respectively. In vitro assessments revealed that the ubitagged conjugates induced significantly higher levels of T cell activation markers and cytokine secretion compared to their sortagged counterparts. Encouraged by these results, we further evaluated the in vivo efficacy of both conjugates. Mice treated with ubi-tagged conjugates displayed a strong OT-I cell proliferation response, whereas sortagged conjugates showed minimal proliferation induction at this concentration. Biodistribution studies indicated that the ubi-tagged conjugates were preferentially taken up by CD11c+ dendritic cells, suggesting that this enhanced uptake contributes to improved T cell activation. Overall, our findings demonstrate the feasibility of ubi-tagging for DC-targeted antigen delivery, highlighting its potential advantages over traditional methods and its promise for future therapeutic applications.

#### Introduction

Dendritic cell (DC)-based immunotherapy has emerged as a promising approach to harness the immune system's capacity to target and eliminate cancer cells.¹ DCs are professional antigen-presenting cells that play a central role in linking innate and adaptive immunity by capturing, processing, and presenting antigens to T cells.²,³ Through this interaction, DCs can initiate a potent anti-tumor immune response by presenting antigenic peptides on major histocompatibility complex (MHC) molecules to T cell receptors (TCRs) on both CD4+ helper and CD8+ cytotoxic T cells.⁴,⁵ Moreover they provide co-stimulatory signals which strengthen the TCR mediated signals. This recognition process triggers the differentiation and proliferation of T cells, leading to targeted destruction of tumor cells and the secretion of cytokines that amplify the immune response.<sup>6-9</sup>

Traditionally, DC-based vaccines are generated by isolating DCs from a patient's blood, loading them with tumor antigens ex vivo, and reinfusing them back into the patient to stimulate a tumor-specific T cell response. 10-12 Since antigen presentation is highly dependent on the patient's unique HLA molecules (both MHC-II), using autologous DCs ensures compatibility and avoids the risk of immune rejection or suboptimal activation. 12,13 However, this ex vivo cellular therapy method is labor-intensive, time-consuming, and difficult to standardize, making it challenging for widespread clinical application. 12 To overcome these limitations, in vivo strategies have been developed to directly target DCs within patients, bypassing the need for cell isolation and manipulation. These approaches include the use of nanoparticles, liposomes, mRNA, and synthetic peptides for antigen delivery. 1,14-16 Additionally, antibodies that specifically bind to DC surface receptors have shown great potential for enhancing targeted delivery and improving T cell activation. 17-21

Among DC-specific targets, the C-type lectin receptor DEC205 (CD205) is of particular interest for DC targeted therapies, due to its specific expression on murine myeloid DCs.<sup>22</sup> Targeting DEC205 with antibodies facilitates receptor-mediated endocytosis and subsequent antigen presentation, making it an attractive target for DC-focused vaccination strategies.<sup>23,24</sup> Furthermore, targeted DC vaccination has been shown to promote cross-presentation—a unique process where DCs can present extracellular antigens on MHC-I molecules, which are typically used for presenting intracellular antigens.<sup>22–24</sup> This ability enables DCs to simultaneously activate both CD4+ helper T cells (via MHC-II presentation) and CD8+ cytotoxic T cells (via MHC-I presentation), leading to a stronger and more coordinated anti-tumor response.<sup>24</sup>

For effective DC targeting, peptide antigens need to be stably and specifically conjugated to antibodies that bind to DC surface receptors. However, current antigenantibody conjugation methods, such as thiol-based strategies, often result in conjugates with inconsistent antigen-to-antibody ratios and reduced binding affinity due to non-specific attachment.<sup>25</sup> More sophisticated approaches, such as recombinant fusion expression or site-specific chemo-enzymatic ligation (e.g., sortagging), have been developed to address these issues.<sup>17</sup> Although these techniques offer better conjugation efficiency and maintain antibody functionality, they require additional reagents and complex purification steps, which can lower yields and complicate production processes.

To address these limitations, we used the ubi-tagging technology for the development of antibody-peptide conjugates for DC targeted vaccination. We used the anti-DEC205 antibody-producing hybridoma cell line NLDC-145, and engineered it to secrete monovalent Fab fragments fused to a donor ubi-tag. This donor ubi-tag was then subsequently used for conjugation to a fully chemically synthesized acceptor-ubitag carrying the ovalbumin-derived antigenic peptide SIINFEKL (OVAp) at its C-terminus. For comparison, we also generated conjugates using the same OVAp peptide fused to the

sortag motif through its respective conjugation enzymes. This design ensures precise site-specific conjugation and maintains the antibody's binding affinity for DEC205. Furthermore, using monovalent Fab fragments minimizes non-specific uptake via Fc receptors and enhances tissue penetration.

In this study, we evaluated the effectiveness of ubi-tagged and sortagged conjugates in terms of their ability to activate T cells and in vivo biodistribution. Our findings demonstrated that the ubi-tagged conjugates significantly enhanced T cell activation markers and cytokine secretion compared to the sortagged versions. Biodistribution studies revealed that the ubi-tagged conjugates were more selectively taken up by CD11c+ DCs in the spleen, which express DEC205, while the sortagged conjugates, despite using the same anti-DEC205 Fab fragment, were more frequently taken up by CD11b+ cells (likely macrophages, which do not express DEC205) and other splenocytes. The anti-DEC205 Fab ubiquitin conjugates showed therefore high target specificity. This differential uptake may be explained by variations in the solubility and aggregation tendencies of the two conjugates, which could affect their distribution and cellular interactions in vivo.

We hypothesize that the enhanced solubility and stability of ubi-tagged conjugates contribute to their improved targeting efficiency and T cell activation. Given these advantages, our platform has the potential to support the development of personalized DC-targeted vaccines incorporating multiple patient-specific tumor neoantigens. Such vaccines could enhance therapeutic efficacy by addressing the diverse mutational landscape and heterogeneity of tumors, thus paving the way for improved cancer immunotherapy strategies.

#### Results

#### Ubi-tagging for DC-targeted antigen delivery induces T cell activation in vitro

We explored ubi-tagging as a conjugation technique for dendritic cell (DC)-targeted antigen delivery and compared it to the alternative state-of-the-art chemoenzymatic conjugation technique, sortagging<sup>26,27</sup>. To compare ubi-tagged-based and sortagged-based DC-targeted antigen delivery, we modified the NLDC-145 hybridoma using the CRISPR/HDR platform to produce anti-mDEC205 Fab fragments either linked to a Ub(K48R)<sup>don</sup>-tag (Fig. 1a)or containing the LPESGG sortag-motif (Fab-Srt)<sup>28,29</sup>. We selected the well-studied model ovalbumin epitope SIINFEKL (OVA<sub>p</sub>, OVA<sub>257-264</sub>)<sup>17,30</sup>, which was attached to the C-terminus of either ubiquitin (Ub<sup>acc</sup>-OVA<sub>p</sub>) or a triglycine motif, via solid-phase peptide synthesis, with or without the FR-motif (Fig. 1b). This dipeptide motif was reported to enhance proteasome dependent cross-presentation for antigens delivered using NLDC-145 mAb<sup>17</sup>. After conjugation and purification, the OVA<sub>p</sub> conjugates (Fig. 2a and Supplementary Fig. S1) were tested for their ability to induce antigen cross-presentation by DCs, as measured by their ability to activate SIINFEKL-specific CD8<sup>+</sup> OT-I T cells *in vitro* (Fig. 2b). We observed high levels of activation markers

CD25, 4-1BB and CD44 on OT-I cells, as well as secretion of the pro-inflammatory cytokines interferon  $\gamma$  (IFN $\gamma$ ) and interleukin-2 (IL-2) in the Fab-Ub $_2$ -OVA $_p$  conditions, irrespective of the presence of the FR-motif (Fig. 2c-e and Supplementary Fig. S2). For the sortagged conjugates, the FR-motif appears crucial for T cell activation, consistent with earlier work<sup>17</sup>. The observed expression levels of activation markers and cytokine secretion suggest a more potent T cell activation by the Fab-Ub $_2$ -OVA $_p$  conjugates compared to the Fab-Srt-OVA $_p$  conjugates *in vitro* irrespective of the FR-motif (Fig. 2c-e).

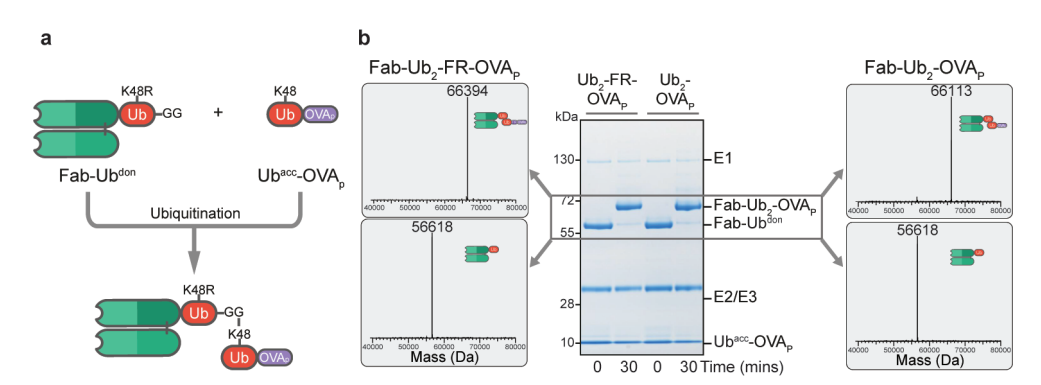


**Figure 1** | **Ubi-tag conjugation of Fab-Ub**<sup>don</sup> **to Ub**<sup>acc</sup>-**OVA**<sub>p</sub> (a) Schematic representation of ubi-tag conjugation of DEC205 Fab-Ub<sup>don</sup> to chemically synthesized acceptor ubiquitin of which ovalbumin(257-264) peptide is attached to the C-terminus (Ub<sup>acc</sup>-OVA<sub>p</sub>). (b) Non-reducing SDS-PAGE analysis of the conjugation of Fab-Ub<sup>don</sup> to either Ub<sup>acc</sup>-FR-OVA<sub>p</sub> or Ub<sup>acc</sup>-OVA<sub>p</sub>. The generated conjugates were isolated from the reaction mixture and the purity assessed using ESI-TOF mass spectrometry.

Ubi-tagged Fab-OVA $_{\rm p}$  conjugates targeting DCs result in potent T cell activation in vivo Encouraged by these results, we evaluated the ability of both Fab-Ub $_2$ -OVA $_{\rm p}$  and Fab-Srt-FR-OVA $_{\rm p}$  conjugates to induce OT-I activation *in vivo*. The day after adoptive transfer of CellTrace Violet (CTV)-labeled OT-I cells, mice were injected with a low dose (5 pmol,  $\pm 12.5$  ng/g + 10 µg LPS) of either conjugated anti-DEC205 Fab-Ub $_2$ -OVA $_{\rm p}$ , Fab-Ub $_2$ -FR-OVA $_{\rm p}$ , Fab-Srt-FR-OVA $_{\rm p}$ , or a combination of unconjugated Fab-Ub(K48R)<sup>don</sup> and Ub<sup>acc</sup>-OVA $_{\rm p}$  or Ub<sup>acc</sup>-FR-OVA $_{\rm p}$  (Fig. 2a). Two days after vaccination we evaluated the progressive dilution of CTV in the OT-I cells in the spleens and inguinal lymph nodes (Fig. 2b,c and Supplementary Fig. S3). We observed strong OT-I cell proliferation in the mice treated with the ubi-tagged conjugates, whereas the sortagged conjugate induced minimal OT-I proliferation at the dose used in this experiment. The ubi-tagged conjugates also induced stronger proliferation compared to the conditions in which unconjugated Fab-Ub and Ub-OVA $_{\rm p}$ s were given. This demonstrates the benefit of ubi-tagging of the targeting moiety, as well as the stability of the Fab-Ub $_{\rm p}$  conjugates *in vivo*.

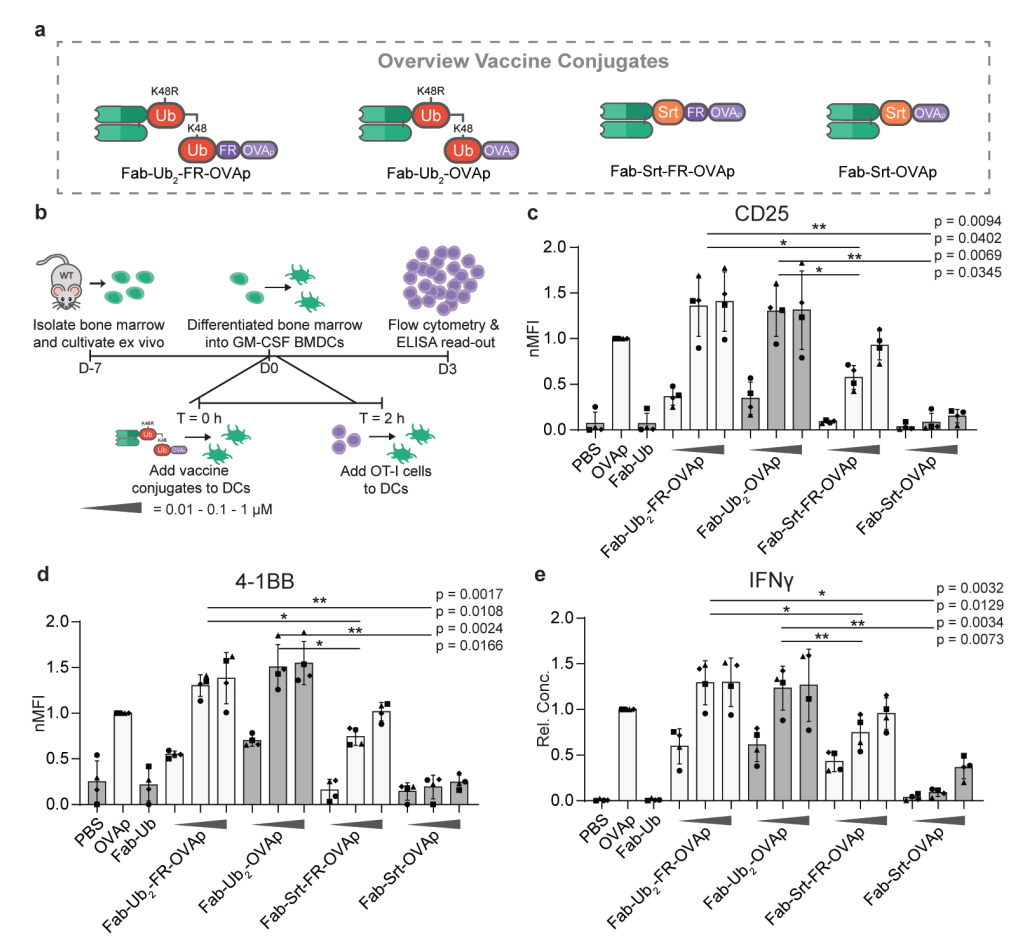


Figure 2 | Fab-Ub $_2$ -OVA $_p$  conjugates elicit potent T cell responses in vitro. (a) Schematic representation of anti-mDEC205 vaccine conjugates used in this experiment; Fab-Ub $_2$ -FR-OVA $_p$ , Fab-Ub $_2$ -OVA $_p$ , Fab-Ub $_2$ -

#### Biodistribution of ubi-tagged conjugates compared to sortagged conjugates

To gain insight into the observed differences in vaccine efficacy, we synthesized Fab-Ub $_2$ -K(DOTA-GA)-FR-OVA $_p$  and Fab-Srt-K(DOTA-GA)-FR-OVA $_p$  (Fig. 4a), which differ molecularly only in the linker type (ubi-tag vs sortag). Having these chelator-functionalized targeted vaccines in hand, we labeled them with radioactive  $^{111}$ In and injected mice with the same

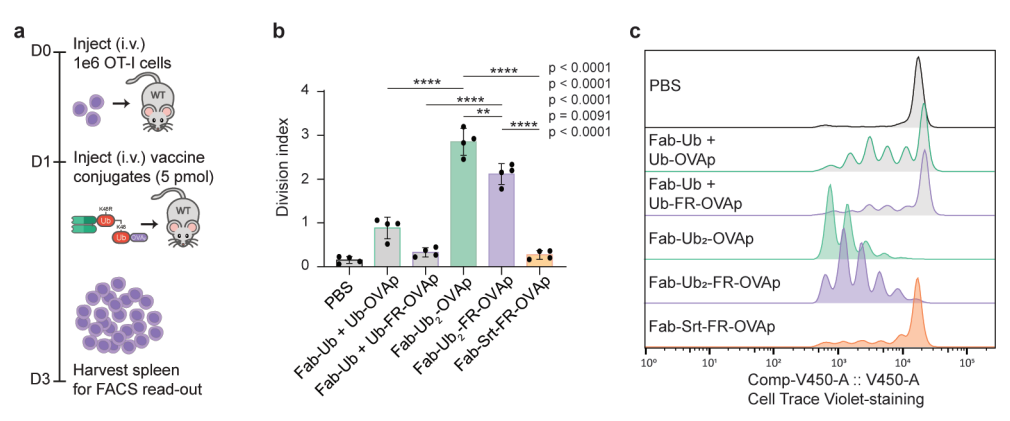


Figure 3 | Fab-Ub $_2$ -OVA $_p$  conjugates elicit potent T cell responses in vivo. (a) Schematic overview of in vivo OT-I cell activation assay. Mice (C57BL/6) received 1e6 CTV-labeled OT-I cells on day 0, followed by 5 pmol vaccine conjugate + 10  $\mu$ g LPS on day 1. Spleens were harvested on day 3. (b) Division index obtained by flow cytometry analysis (n = 4) of OT-I cells isolated from spleen. Data are shown as mean  $\pm$ SD. Unpaired T tests, p-values are noted in figure \*\*\*\*P<0.0001, \*\*P<0.01. (c) Representative histograms of OT-I cell proliferation in spleen.

dose used for the vaccination experiments (5 pmol, ±12.5 ng/g vaccine + 10 µg LPS). Blood samples were taken over time until 24 hours post injection, at which point the biodistribution was determined. The blood clearance kinetics (Ub: fast t<sub>1/2</sub>: 12.09 min., slow  $t_{1/2}$ : 139 min., Srt: fast  $t_{1/2}$ : 10.16 min, slow  $t_{1/2}$ : 88.79 min.) for the targeted vaccines are not significantly different (P=0.1179, F-test) (Fig. 4b and Supplementary Table S2a). A slightly higher concentration in the blood is observed at later time points for the ubitagged vaccine compared to the sortagged derivative, which we do not expected to be biologically relevant. The biodistribution data indicates that the ubi-tagged conjugate (molecular weight ~66 kDa) is primarily cleared via the liver and the sortagged conjugate (molecular weight ~52 kDa) through renal clearance (Fig. 4c and Supplementary Table S2b). This is in line with the molecular weight cutoff for glomerular filtration of 30-50 kDa<sup>35</sup>. The remaining biodistribution data is very similar, with the exception of the higher uptake of the sortagged conjugate observed in the inguinal lymph node. To assess differences in cellular uptake within the spleen, different cell populations where isolated from the splenocytes, followed by measurement of the radioactivity in these isolated populations (Fig. 4d and Supplementary Table S2c). Interestingly, although the conjugates are equipped with the same DEC205-targeting Fab fragment, the ubi-tagged conjugate was more specifically taken up by the CD11c+ "dendritic cell" population, compared to the sortagged conjugate. The latter was taken up by the CD11c /CD11b+ population to a significantly higher degree. These data demonstrate superior in vivo target cell engagement of the ubi-tagged DC targeted vaccines, which helps explain the difference between the two conjugates in their ability to induce antigen-specific CD8<sup>+</sup> T cell activation in the spleen (Fig. 3).

These results, together with the *in vivo* functionality of the anti-DEC205 Fab-Ub $_2$ -OVA $_p$  conjugates, demonstrate the feasibility of ubi-tagging as conjugation technique for DC-targeted antigen delivery, highlight the potential of ubi-tagging compared to the current state-of-the-art and provide a positive outlook for the use of ubi-tagged conjugates for other *in vivo* therapeutic applications.

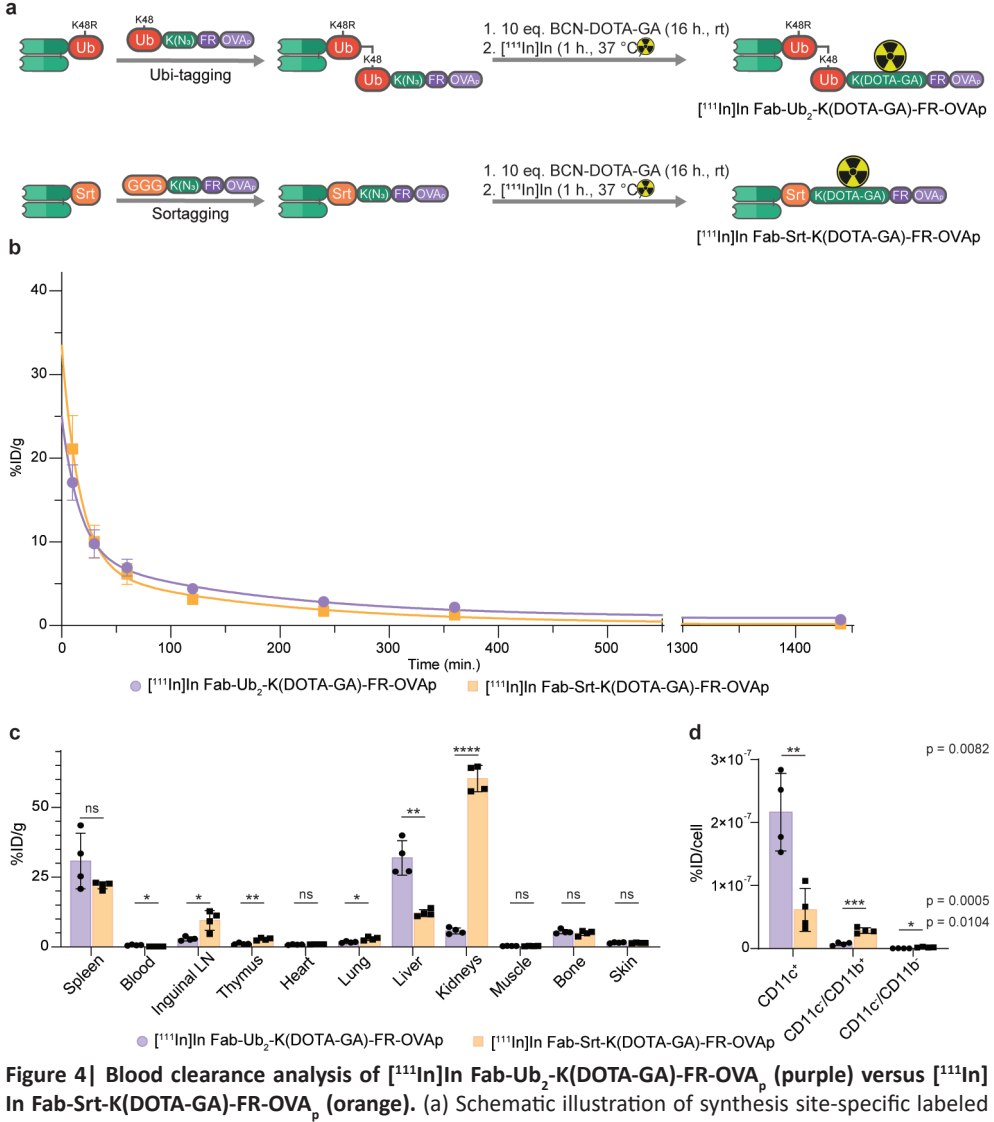


Figure 4| Blood clearance analysis of [ $^{111}$ In]In Fab-Ub $_2$ -K(DOTA-GA)-FR-OVA $_p$  (purple) versus [ $^{111}$ In] In Fab-Srt-K(DOTA-GA)-FR-OVA $_p$  (orange). (a) Schematic illustration of synthesis site-specific labeled DOTA-GA-conjugates. (b) Blood clearance analysis of [ $^{111}$ In]In Fab-Ub $_2$ -K(DOTA-GA)-FR-OVAp vs. [ $^{111}$ In] In Fab-Srt-K(DOTA-GA)-FR-OVAp. Data is depicted as mean percentage injected dose per gram (%ID/g) at several time-points with a two-phase decay curve fit ( $^{2}$ = 0.9640 for Ub-conjugate,  $^{2}$ = 0.9507 for Srt-conjugate). F-testing indicates no significant differences between the two curve fits ( $^{2}$ = 0.1187). The calculated fast  $^{1}$ <sub>1/2</sub> for the Ub-conjugate is 12.09 min. and for the Srt-conjugate is 88.79 min. (c) Mice

(C57BL/6) were injected with 5 pmol  $^{111}$ In-labeled Fab-Ub $_2$ -K(DOTA-GA)-FR-OVAp or Fab-Srt-K(DOTA-GA)-FR-OVAp + 10 µg LPS. Biodistribution was determined ex vivo 24 hours after injection (n = 4). Values are presented as percentage injected dose per gram (%ID/g). Data are shown as mean  $\pm$ SD. Unpaired T tests, p-values are noted in figure. \*\*\*\*P<0.0001, \*\*P<0.001, \*P<0.01, \*P<0.05, ns P>0.05. (d) The spleens from (c) were dissociated and subsequently the CD11c $^+$  and CD11b $^+$  populations were isolated using MACS from the splenocytes, after which the radioactivity in all fractions was measured. Values are presented as percentage injected dose per cell (%ID/cell). Data are shown as mean  $\pm$ SD. Unpaired T tests, p-values are noted in figure. \*\*\*P<0.001, \*P<0.01.

#### Discussion

In this work we explore the significance of ubi-tagging in the field of targeted antigen delivery. We also demonstrate the benefit of ubi-tag conjugation compared to the state-of-the-art ligation technique sortagging on potency to activate T cells in vitro and in vivo. Comparative blood clearance, biodistribution and in vivo target cell engagement data reveal that the ubi-tagged DC-targeted vaccines are more selectively taken up by DCs in the spleen, and show a higher on-target effect where they predominantly target DCs and not CD11b+ cells (presumably macrophages). However, the sortagged vaccine equipped with the same anti-DEC205 Fab fragment, was observed to be taken up by CD11b<sup>+</sup> cells and other splenocytes showing a higher off-target effect. Differences in solubility and propensity to aggregation could be an explanation for this observation, but remains to be verified. The redundancy of the proteasomal cleavage FR-motif in these experiments hints towards different intracellular routing and processing, possibly by deubiquitinating enzymes. An alternative explanation could be that proteasome targeting is induced by the K48-linked di-ubiquitin. K48 tetra-ubiquitination is a well-known signal for proteasomal degradation. Yet, shorter ubiquitination-motifs also signal for proteasomal degradation<sup>31,32</sup>. Follow-up studies will focus on further elucidation of the observed benefit in efficacy of ubi-tagged conjugates and will expand the use of ubi-tagging for targeted antigen delivery.

In summary, ubi-tagging provides a fast, efficient, and modular technique to generate well-characterized antibody conjugates of a wide variety of formats and combinations. Furthermore, significant improvements in T cell activation are observed when utilizing ubi-tagging as platform for antigen delivery compared to current state-of-the-art conjugation techniques. We expect the widespread adoption of this conjugation technique and its contribution to improving and developing protein conjugates, in particular antibody conjugates for preclinical research, diagnostic, and therapeutic applications.

#### **Methods**

#### General cell culture conditions

The hybridoma cell line NLDC-145 (ATCC HB-290) was modified for the stable expression of ubi-tagged antibodies or antibody fragments. Other cell lines used in this study were

EL4 (kindly provided by dr. Jacques Neefjes (LUMC, The Netherlands). The cell line NLDC-145 was cultured in Iscove's modified Dulbecco's medium (IMDM) (Gibco) supplemented with 7.5% fetal calf serum (FCS, Greiner). The cells were maintained at 37 °C and 5% CO<sub>2</sub>, routinely examined by morphology analysis and tested for mycoplasma.

#### Cloning of CRISPR-Cas9 and donor constructs

The genomic sequence of the rlgG2a heavy chain locus was identified via the Ensembl rate genome build Rnor\_6.0 and used for the design of the different HDR donor templates. gRNA for the rlgG2a constructs were previously described; for Hinge HDR constructs, gRNA-H, GACTTACCTGTACATCCACA, Addgene 124808; for isotype switch, gRNA-ISO (TGTAGACAGCCACAGACTTG, Addgene 124811) and ordered as single-stranded oligos from Integrated DNA Technologies (IDT) with the appropriate overhangs for cloning purposes. The oligos were phosphorylated with T4 PNK enzyme by incubation at 37 °C for 30 minutes and annealed by incubation at 95 °C for 5 minutes followed by gradually cooling to 25 °C using a thermocycler. The annealed oligos were cloned into the plasmid pSpCas9(BB)-2A-Puro (PX459), which was obtained as gifts from F. Zhang (Addgene plasmids 62988)<sup>33</sup>. Synthetic gene fragments containing homologous arms and desired insert were obtained via Twistbioscience and cloned into the PCR4 TOPO TA vector (Thermo Fisher Scientific). All CRISPR-Cas9 and HDR constructs were purified with the NucleoBond Xtra Midi Kit (740410.100, Machery-Nagel) according to the manufacturer's protocol.

#### Hybridoma nucleofection with HDR and CRISPR-Cas9

Nucleofection of the HDR template and CRISPR-Cas9 vectors was performed with Cell Line Nucleofector Kit R (Lonza, VCA-11001) nucleofector 2b device. Before nucleofection hybridoma cells were assessed for viability and centrifuged (90g, 5 minutes), resuspended in PBS supplemented with 1% FBS and centrifuged again (90g, 5 minutes). 1x10<sup>6</sup>cells were resuspended in 100 μL Nucleofector medium with 1 μg of HDR template and 1 µg of CRISPR-Cas9 vectors or 2 µg of GFP vector (control) and transferred to cuvettes for nucleofection with the 2b Nucleofection System from Lonza (Program X001). Transfected cells were transferred to a 6-well plate in 4 mL of prewarmed complete medium. The following day the cells were transferred to a 10 cm petridish in 10 mL of complete medium, supplemented with 10-20 µg/mL of blasticidin (Invivogen, anti-bl-05). Antibiotic pressure was sustained until GFP-transfected hybridomas were dead and HDR transfections were confluent (typically between day 10-14). Cells were subsequently clonally expanded by seeding the hybridomas in 0.3 cells/well in round-bottom 96-well plates in 100 µL of complete medium. After onetwo weeks, supernatant from wells with a high cell density were obtained for further characterization and selected cloned were expanded.

#### **Ubi-tag conjugation reaction**

Ubi-tag conjugation reactions were carried out using 20 μM of aDEC205 Fab-Ub<sup>don</sup> and 100  $\mu$ M of Ubacc-OVA in the presence of 0.25  $\mu$ M E1 enzyme, 20  $\mu$ M E2/E3 hybrid enzyme, 10 mM MgCl<sub>2</sub> and 5 mM ATP in PBS. For analysis of the reaction efficiency by SDS-PAGE, an initial reaction sample was taken from the reaction mixture prior to the addition of ATP. After the addition of ATP, the reaction was incubated at 37 °C for 30 minutes while shaking. Conjugation reaction samples were analyzed by quenching 2-5 μL of the reaction mixture in sample buffer and run in non-reducing conditions on 4-12% Bis-Tris gels (Invitrogen) by SDS-PAGE with MOPS as running buffer. Gels were stained using InstantBlue Coomassie Protein Stain (abcam) and imaged using Amersham600. Small-scale reactions were carried out on a scale corresponding to 2.5 µg ubi-tagged antibody fragments, while large-scale reactions were carried out on a 200 µg to 1 mg scale. Ubi-tagged Fab conjugates were purified from the reaction mixture by protein G affinity purification using a HiTrap Protein G HP column (GE Life Science) according to the manufacturer's protocol. The elution fractions containing purified conjugates were pooled, dialyzed against PBS, and concentrated using a 10 kDa Amicon Ultra centrifugal filter unit (Millipore). The purity of the ubi-tagged conjugates was assessed by SDS-PAGE and high-resolution mass spectrometry on a Waters Acquity H-class UPLC with XEVO-G2 XS Q-TOF mass spectrometer.

#### Solid-phase peptide synthesis

Solid-phase peptide synthesis (SPPS) of Rho-Ub was performed on a Syro II Multisyntech Automated Peptide synthesizer (SYRO robot; Part Nr: S002PS002; MultiSyntech GmbH, Germany) on a 25  $\mu$ mol scale using standard 9-fluorenylmethoxycarbonyl (Fmoc) based solid phase peptide chemistry. It was synthesized based on the procedure described by El Oualid *et al.*<sup>34</sup> using a fourfold excess of amino acids relative to pre-loaded Fmoc amino acid trityl resin (between 0.17 and 0.20 mmol/g, Rapp Polymere, Germany). All synthetic products were purified by RP-HPLC on a Waters preparative RP-HPLC system equipped with a Waters C18-Xbridge 5  $\mu$ m OBD (10 x 150 mm) column. The purified products were lyophilized and assayed for purity by high resolution mass spectrometry on a Waters Acquity H-class UPLC with XEVO-G2 XS Q-TOF mass spectrometer and by SDS-PAGE analysis.

#### Mass spectrometry

Mass spectrometry analysis was carried out on Waters ACQUITY UPLC-MS system equipped with a Waters ACQUITY Quaternary Solvent Manager (QSM), Waters ACQUITY FTN AutoSampler, Waters ACQUITY UPLC Protein BEH C4 Column (300 Å,  $1.7 \mu m$ ,  $2.1 \times 50 \text{ mm}$ ) and XEVO-G2 XS QTOF Mass Spectrometer (m/z = 200-2500) in ES+ mode.

Sample were run using 2 mobile phases: A = 1% MeCN, 0.1% formic acid in water and B = 1% water and 0.1% formic acid in MeCN with a runtime of 14 minutes. In the first 4 minutes, salts and buffer components were flushed from LC column using 98% A and 2% B. In the next 7.5 minutes, a gradient of 2-100% B was used, followed by 0.5 minutes of 100% B and subsequent reduction to 2% B and 98% A in 2 minutes. Data processing was performed using Waters MassLynx Mass Spectrometry Software 4.1, where the mass was obtained by deconvolution with the MaxEnt1 function.

#### Protein expression and purification

The E1 ubiquitin-activating enzyme UBE1 carrying an N-terminal His-tag was expressed from a pET3a vector in E. coli BL21(DE3) in autoinduction media for 2-3 hours at 37 °C, after which the bacteria were allowed to grow overnight at 18 °C. Next, bacteria were harvested and lysed by sonication, followed by His-affinity purification using Talon metal affinity resin (Clontech Inc., Palo Alto, CA, USA). Subsequently, the protein was further purified by anion exchange using a Resource Q column (GE Healthcare), followed by size exclusion using a Superdex 200 column (GE Healthcare).

The E2/E3 enzyme chimera plasmid was obtained as a gift from dr. Vincent Chau (Penn State, USA). The expression plasmid consists of the RING domain of the E3 ubiquitin ligating enzyme gp78 fused to the N-terminus of the E2 ubiquitin-conjugating enzyme Ube2g2 in a PET28a-TEV vector.

The E2/E3 enzyme chimera was expressed and purified as described $^{36}$ . In brief, the fusion protein was expressed in E. coli BL21(DE3) cells grown in LB at 37°C until OD $_{600}$  = 0.4-0.6 and induced with 0.4 mM IPTG for 4 hours at 30 °C. The harvested cells were lysed with Bugbuster protein extraction reagent (Millipore) according to manufacturer's protocol. The fusion protein was purified on Ni-NTA resin followed by size exclusion using a Superdex 200 column (GE Healthcare). Next, TEV protease cleavage was carried out overnight, and the cleaved fusion protein was further purified using a Resource Q column (GE Healthcare).

Ubi-tagged Fabs were produced in hybridoma cell lines engineered to produce Fabs fused at the C-terminus of the heavy chain to ubiquitin, followed by a His-tag at the C-terminus of ubiquitin. The modified hybridoma cells were cultivated for antibody production in CD Hybridoma medium supplemented with 2 mM ultraglutamine and 50  $\mu$ M  $\beta$ -mercaptoethanol for 7 to 10 days. To prevent the cleavage of the his-tag during cultivation, which is essential for blocking the C-terminal glycine residue of acceptor ubi-tags, antibodies fused to an acceptor ubi-tag were secreted in culture media supplemented with Ub-PA. However, donor ubi-tags require a free C-terminus; thus, antibodies fused a donor ubi-tag intended for conjugation were cultured without a DUB inhibitor. After 7 to 10 days, the culture media containing the ubi-tagged Fabs was centrifugated to remove cells. The supernatant was filtered through a 0.22  $\mu$ m

filter (GE Healthcare) and loaded on a pre-equilibrated HiTrap Protein G HP column (GE Life Science), and the ubi-tagged antibodies were purified according to the manufacturer's protocol. Elution fractions containing the ubi-tagged antibodies were pooled and dialyzed against PBS. Acceptor ubi-tagged antibodies, carrying a His-tag at the C-terminus of ubiquitin, were purified by Ni-NTA affinity purification prior to Protein G affinity purification (Supplementary Fig. 9).

#### Sortase-mediated chemoenzymatic ligation

aDEC205 Fab-Srt (1 eq., 20 nmol, 1 mg), 4s9 sortase (0.5 eq., 10 nmol, 0.18 mg) and GGG(FR)SIINFEKL (40 eq., 800 nmol, 0.91 mg) were added in sortase buffer (10% DMSO in 50 mM Tris HCl, 150 mM NaCl, 2 mM CaCl<sub>2</sub>, pH = 7.5) and incubated (2 h., 37 °C). 100  $\mu$ L HisPur<sup>TM</sup> Ni-NTA Resin was added to the completed reaction and the mixture was incubated (15 min., rt) and centrifuged (10,000 rcf, 1 min., rt). The clear supernatant was purified by size exclusion chromatography (NGC, BioRad). The product was concentrated over a 10-kDa filter (Millipore). Concentration was determined using a NanoDrop<sup>TM</sup> 2000 (ThermoFisher) and purity was assessed by SDS-PAGE (12%) analysis.

#### Site-specific generation DOTA-GA conjugates

Fab-Ub<sub>2</sub>-K(N<sub>3</sub>)-FR-OT-I (5 nmol, 0.33 mg) and Fab-Srt-K(N<sub>3</sub>)-FR-OT-I (5 nmol, 0.25 mg) were conjugated as described above using ubi-tagging or sortase-mediated chemoenzymatic ligation respectively. After ligation, buffer was exchanged to metal-free PBS using Zeba spin desalting columns (0.5 mL, 7 kDa MW cut-off, Pierce Biotechnology). BCN-DOTA-GA (10 eq., 50 nmol, 14 μg) (C130, CheMatech) was added as 10 mM stock solution in DMSO and the final DMSO concentration was set at 10%. The reaction was incubated (16 h., rt) and purified using Zeba spin desalting columns (0.5 mL, 7 kDa MW cut-off, Pierce Biotechnology). Concentration was determined using a NanoDrop™ 2000 (ThermoFisher) and purity was assessed by SDS-PAGE (12%) analysis.

#### Radiolabeling

Conjugates (10 µg) were labeled under metal-free conditions with In-111 (Curium) (0.5 MBq/µg) in MES buffer (0.5 M, pH 5.5, 2x volume of 111InCl $_3$  solution). The mixture was incubated at 37 °C for 60 min. after which EDTA (final conc. 5 mM) was added. Radiochemical yield (RCY) of [ $^{111}$ In]In-Srt and [ $^{111}$ In]In-Ub conjugates was determined by instant thin-layer chromatography (iTLC) using silica gel coated paper (Agilent Technologies) with 0.1 M NH $_4$ OAc containing 0.1 M EDTA as mobile phase. iTLC strips were imaged using phosphor-luminescent plates on a phosphor imager (Typhoon FLA 7000, GE Healthcare). Purification was performed for all conjugates using Zeba spin desalting columns (0.5 mL, 7 kDa MW cut-off, Pierce Biotechnology). Purification was repeated once to obtain a radiochemical purity of >90%. Purified conjugates were

diluted in PBS for injection.

#### Mice

All mice were purchased from Charles River Laboratories, France. Female C57BL/6 WT and OT-I (Tg(TcraTcrb)1100Mjb/Crl) between 8-12 weeks of age and 18-25 g body weight were used for *in vitro* and *in vivo* experiments. Mice were sacrificed by cervical dislocation.

#### In vitro OT-I cell activation assay

BMDCs were generated as described below and plated at 10,000 cells per condition. Vaccine conjugates (1000 nM, 100 nM, 10 nM) were added to the BMDCs in 1:1 ratio of complete medium and PBS supplemented with LPS (0.3 μg/mL final concentration), and the BMDCs were incubated (2 h., 37 °C). In tandem, OT-I CD8+ cells were isolated as described below. After incubation with the vaccine conjugates, the BMDCs were washed and 50,000 OT-I cells were added to each condition. The BMDCs-OT-I cell coculture was incubated (3 d., 37 °C). The cells were spun down (1700 rpm., 2 min., 4 °C), supernatant was stored for ELISA analysis, and the cells were analyzed using a FACSVerse<sup>TM</sup> (BD Biosciences).

#### In vivo OT-I cell activation assays

OT-I CD8 $^{+}$  cells were isolated as described below and injected intravenously (1e6 cells, 100  $\mu$ L) into WT C57BL/6 mice (Charles River). After 24 h., the different vaccine conjugates (5 pmol) supplemented with LPS (10  $\mu$ g) in PBS were injected intravenously (100  $\mu$ L). 48 h. after injection of the vaccines, mice were cervical dislocated and the spleen and inguinal lymph nodes were harvested. Spleen cells were filtered and an ACK lysis was performed to remove red blood cells. Cells from the lymph nodes were filtered and pooled with the spleen cells to be analyzed using a FACSLyric (BD Biosciences).

#### **GM-CSF BMDCs generation**

Hindlegs of C57BL/6 (Charles River) were dissected. Tibia and femur were cleaned and cut open with a scalpel. Bone marrow cells were flushed out and collected in a petridish. 10 mL complete RPMI 1640 medium (ThermoFisher) supplemented with 50  $\mu$ M 2-mercaptoethanol and 25 ng/mL GM-CSF was added per 10e6 cells. On day 3, 5 mL fresh media (+ 50  $\mu$ M 2-mercaptoethanol, 25 ng/mL GM-CSF) was added. On day 8, non-adherent dendritic cells were harvested.

#### OT-I cell isolation

OT-I mice (C57BL/6-Tg(TcraTcrb)1100Mjb/Crl, Charles River) were killed by cervical dislocation and spleen and inguinal lymph nodes were harvested. Both organs were

meshed on a filter and splenocytes underwent ACK lysis. After lysis, splenocytes were pooled with lymphocytes and OT-I cells were isolated using magnetic-assisted cell sorting according to manufacturer's protocol (CD8α T Cell Isolation Kit, mouse, Miltenyi Biotec). Then, OT-I cells were stained with CellTrace™ Violet (ThermoFisher) for 20 min. at 37 °C and recovered in complete medium. Afterwards, cells were spun down (1500 rpm., 4 °C) and resuspended in PBS.

#### Blood kinetics and biodistribution

Mice (n = 4) were injected i.v. via the tail vein with [ $^{111}$ In]In-Srt conjugate or [ $^{111}$ In]In-Ub conjugate (5 pmol, ca. 0.1 MBq in 100  $\mu$ L PBS) pre-mixed with LPS (10 ug). Blood samples (ca. 20  $\mu$ L) were drawn via the vena saphena at various time points (10 min., 30 min., 1 h., 2 h., 4 h., 6 h.). 24 h. post injection, mice were euthanized via CO2 asphyxiation. Blood was obtained by cardiac puncture after which animals were dissected. Blood samples from various time points and isolated organs were weighed and counted in a gamma counter (Wizard 1480, PerkinElmer) along with standards to determine the % injected dose per gram (%ID/g) or % injected dose per organ (%ID). Stomach, small and large intestine were not emptied before y-counting.

#### Splenocyte subset isolation

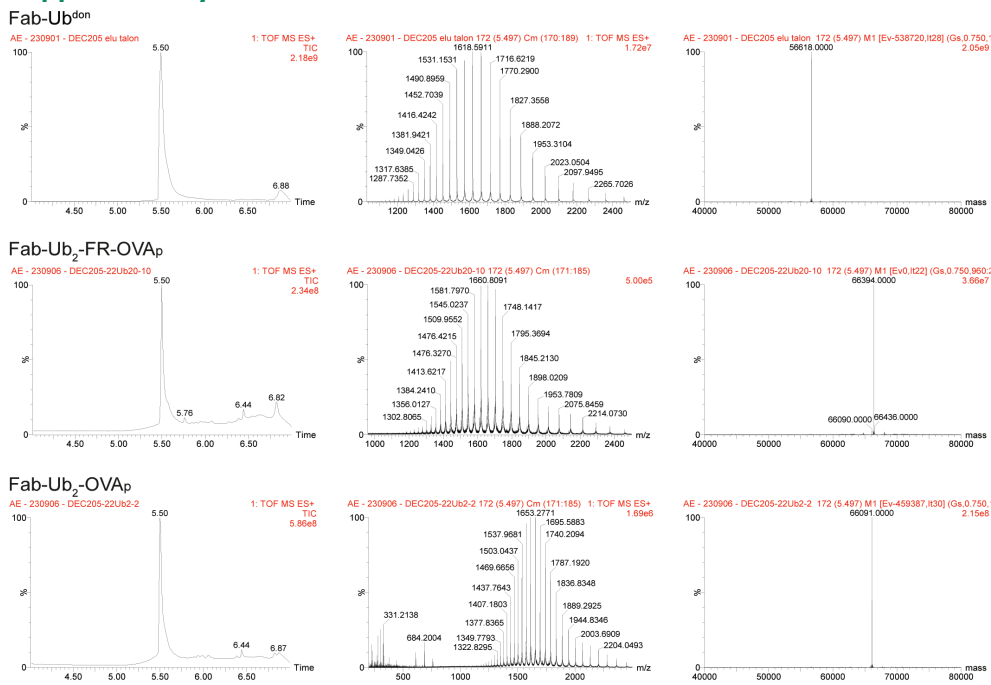
Spleens were recovered after y-counting and meshed on a filter. Splenocytes underwent ACK lysis and subsequently CD11c<sup>+</sup> cells were isolated according to manufacturer's protocol (CD11c MicroBeads UltraPure, mouse, Miltenyi Biotec). In short, splenocytes were dissolved (4 μL buffer per 1e6 splenocytes) in MACS buffer (2 mM EDTA, 2% Fetal Bovine Serum in PBS) and CD11c<sup>+</sup> magnetic beads (1 μL beads per 1e6 splenocytes) were added to the cells. The suspension was incubated at 4 °C for 10 min. and subsequently applied onto a pre-wetted LS column. The flowthrough and wash fractions containing CD11c splenocytes were collected and subjected to CD11b isolation according to the manufacturer's protocol (CD11b MicroBeads, human and mouse, Miltenyi Biotec). The CD11c<sup>+</sup> splenocytes were eluted, counted using trypan blue, and γ-counted in a gamma counter (Wizard 1480, PerkinElmer). The CD11b+ isolation was performed equivalently to the CD11c<sup>+</sup> isolation. The CD11c<sup>-</sup>/CD11b<sup>+</sup> splenocytes were eluted, counted using trypan blue, and y-counted in a gamma counter (Wizard 1480, PerkinElmer). The flowthrough and wash fractions of CD11b<sup>+</sup> isolation were collected and the CD11c<sup>-</sup>/ CD11b<sup>-</sup> splenocytes were counted using trypan blue, and γ-counted in a gamma counter (Wizard 1480, PerkinElmer).

#### Flow cytometry and antibodies

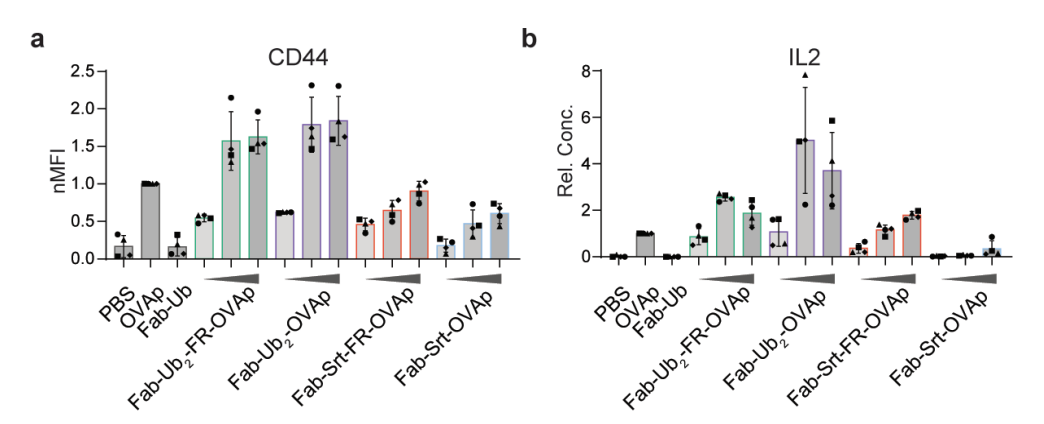
For FACS analysis, cells were washed with PBS, followed by life/death staining (20 min., rt) in 50 µL eBioscience™ Fixable Viability Dye eFluor™ 780 (1:2000, ThermoFisher).

Cells were washed once with PBA and antibody mixes were added (30 min., 4 °C). Cells were washed twice with PBA, taken up in 100 μL PBA and FACS analyses were performed on a FACSLyric<sup>™</sup> (BD Biosciences) or a FACSVerse<sup>™</sup> (BD Biosciences). The following antibodies were used for staining: mCD8α (1:100 dil., PerCP, clone 53-6.7, Biolegend), mCD8α (1:100 dil., FITC, clone 53-6.7, Biolegend), mCD25 (1:100 dil., FITC, clone PC61, Biolegend), mCD25 (1:100 dil., PerCP-Cy5.5, clone PC61, Biolegend), mCD44 (1:50 dil., PE/Cy7, clone IM7, Biolegend), m4-1BB (1:100 dil., APC, clone 17B5, ThermoFisher), mDEC205 (1:1000 dil., PE, clone NLDC-145, Biolegend), hCD8 (1:20 dil., APC, clone RPA-T8, BD Biosciences), hCD25 (1:50 dil., PE/Cy7, clone BC96, BioLegend), hCD69 (1:20 dil., PerCP, clone L78, BD Biosciences), h4-1BB (1:20 dil., PE, clone 4B4-1, BD Pharmingen).

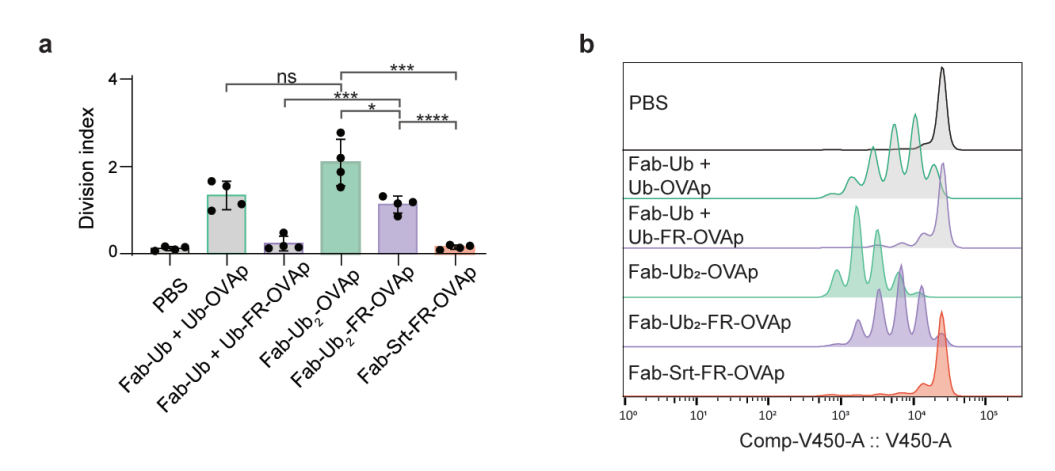
#### Supplementary information



**S1** LC-MS analysis of  $\alpha$ DEC205 Fab-Ub<sup>don</sup> conjugation to either ub<sup>acc</sup>-FR-OVA<sub>p</sub> or Ub<sup>acc</sup>-OVA<sub>p</sub> forming Fab-Ub<sub>2</sub>-FR-OVA<sub>p</sub> or Fab-Ub<sub>2</sub>-FR-OVA<sub>p</sub> respectively. Total ion chromatograms (left), ESI-TOF spectra (middle) and deconvoluted ESI-TOF mass spectra (right).



S2 In vitro OT-I cell activation assay showing data for the T cell activation markers CD44 and IL2. GM-CSF BMDCs were generated and pulsed for 2 h. with 1000-100-10 nM vaccine conjugates or 1000 nM control conditions and 0.3  $\mu$ g/mL LPS. Sequentially, OT-I cells were added in 1:5 ratio and incubated for 3 days. Cells were analyzed using FACS. (c) FACS analysis. Statistics are provided in Table S1. Data (n = 4) are shown as mean  $\pm$ SD normalized MFI to positive control for CD44 (a) and IL2 (b).



**S3 In vivo OT-I cell activation assay** showing (a) flow cytometry analysis (n = 4) of division index of OT-I cells isolated from inguinal lymph nodes. Data are shown as mean ±SD. Paired T tests, \*\*\*\*P<0.0001, \*\*\*P<0.001, \*P<0.005 (b) Representative histograms of OT-I cell proliferation in lymph nodes.

**Table S1 Statistics for figure 2 and supplemental figure 2.** All conditions are tested with a two-sided paired T test between conditions at similar concentrations. P values are notated in tables below, \*\*\*\*P<0.0001, \*\*\*P<0.001, \*\*P<0.001, \*P<0.005, ns P>0.05

Conditions compared		Figure 2C – CD25		
	At 1000 nM	At 100 nM	At 10 nM	
PBS vs Fab-Ub2-FR-OVAp	0.0083, **	0.0101, *	0.0055, **	
PBS vs Fab-Ub2-OVAp	0.0181, *	0.0075, **	0.0169, *	
PBS vs Fab-Srt-FR-OVAp	0.0027, **	0.0026, **	0.8161, ns	

PBS vs Fab-Srt-OVAp	0.2860, ns	0.5382, ns	0.6126, ns
Fab-Ub2-FR-OVAp vs Fab-Ub2-OVAp	0.1842, ns	0.1954, ns	0.7077, ns
Fab-Ub2-FR-OVAp vs Fab-Srt-FR-OVAp	0.1105, ns	0.0402, *	0.0092, **
Fab-Ub2-FR-OVAp vs Fab-Srt-OVAp	0.0075, **	0.0094, **	0.0053, **
Fab-Ub2-OVAp vs Fab-Srt-FR-OVAp	0.2424, ns	0.0345, *	0.0619, ns
Fab-Ub2-OVAp vs Fab-Srt-OVAp	0.0182, *	0.0069, **	0.0336, *
Fab-Srt-FR-OVAp vs Fab-Srt-OVAp	0.0011, **	0.0016, *	0.0313, *

Conditions		Figure 2D – 4-1BB			
Conditions compared	At 1000 nM	At 100 nM	At 10 nM		
PBS vs Fab-Ub2-FR-OVAp	0.0174, *	0.0073, **	0.0534, ns		
PBS vs Fab-Ub2-OVAp	0.0051, **	0.0066, **	0.0197, *		
PBS vs Fab-Srt-FR-OVAp	0.0166, *	0.0158, *	0.05129, ns		
PBS vs Fab-Srt-OVAp	0.9699, ns	0.5262, ns	0.5406, ns		
Fab-Ub2-FR-OVAp vs Fab-Ub2-OVAp	0.1598, ns	0.0863, ns	0.0116, *		
Fab-Ub2-FR-OVAp vs Fab-Srt-FR-OVAp	0.0273, *	0.0108,*	0.0059, **		
Fab-Ub2-FR-OVAp vs Fab-Srt-OVAp	0.0057, **	0.0017, **	0.0071, **		
Fab-Ub2-OVAp vs Fab-Srt-FR-OVAp	0.0098, **	0.0166, *	0.0071, **		
Fab-Ub2-OVAp vs Fab-Srt-OVAp	0.0024, **	0.0024, **	0.0055, **		
Fab-Srt-FR-OVAp vs Fab-Srt-OVAp	0.0020, **	0.0010, **	0.7975, ns		

Conditions compared		Figure 2E - IFNγ		
Conditions compared	At 1000 nM	At 100 nM	At 10 nM	
PBS vs Fab-Ub2-FR-OVAp	0.0022, **	0.0016, **	0.0089, **	
PBS vs Fab-Ub2-OVAp	0.0076, **	0.0020, **	0.0075, **	
PBS vs Fab-Srt-FR-OVAp	0.0017, **	0.0046, **	0.0053, **	
PBS vs Fab-Srt-OVAp	0.0126, *	0.0574, ns	0.2808, ns	
Fab-Ub2-FR-OVAp vs Fab-Ub2-OVAp	0.6742, ns	0.2087, ns	0.6052, ns	
Fab-Ub2-FR-OVAp vs Fab-Srt-FR-OVAp	0.0318, *	0.0129, *	0.0748, ns	
Fab-Ub2-FR-OVAp vs Fab-Srt-OVAp	0.0120, *	0.0032, *	0.0100, **	
Fab-Ub2-OVAp vs Fab-Srt-FR-OVAp	0.1268, ns	0.0073, **	0.0361, *	
Fab-Ub2-OVAp vs Fab-Srt-OVAp	0.0318, *	0.0034, **	0.0086, *	
Fab-Srt-FR-OVAp vs Fab-Srt-OVAp	0.0088, **	0.0065, **	0.0045, **	

Conditions compared		Figure S2 – CD44			
	At 1000 nM	At 100 nM	At 10 nM		
PBS vs Fab-Ub2-FR-OVAp	0.0003, ***	0.0032, **	0.0247, *		
PBS vs Fab-Ub2-OVAp	0.0005, ***	0.0014, **	0.0078, **		
PBS vs Fab-Srt-FR-OVAp	0.0087, **	0.0262, *	0.0764, ns		
PBS vs Fab-Srt-OVAp	0.0450, *	0.0412, *	0.9162, ns		
Fab-Ub2-FR-OVAp vs Fab-Ub2-OVAp	0.0393, *	0.0339, *	0.0592, ns		

Fab-Ub2-FR-OVAp vs Fab-Srt-FR-OVAp	0.0235, *	0.0336, *	0.0464,*
Fab-Ub2-FR-OVAp vs Fab-Srt-OVAp	0.0060, *	0.0020, **	0.0100, *
Fab-Ub2-OVAp vs Fab-Srt-FR-OVAp	0.0227, *	0.0150, *	0.0337, *
Fab-Ub2-OVAp vs Fab-Srt-OVAp	0.0090, **	0.0014, **	0.0024, **
Fab-Srt-FR-OVAp vs Fab-Srt-OVAp	0.0543, ns	0.3228, ns	0.0192, *

Conditions compared	Figure S2 – IL-2		
Conditions compared	At 1000 nM	At 100 nM	At 10 nM
PBS vs Fab-Ub2-FR-OVAp	0.0061, **	<0.0001, ****	0.0165, *
PBS vs Fab-Ub2-OVAp	0.0206, *	0.0211, *	0.0479, *
PBS vs Fab-Srt-FR-OVAp	0.0002, ***	0.0011, **	0.0626, ns
PBS vs Fab-Srt-OVAp	0.1769, ns	0.0474, *	0.8970, ns
Fab-Ub2-FR-OVAp vs Fab-Ub2-OVAp	0.0837, ns	0.1053, ns	0.4949, ns
Fab-Ub2-FR-OVAp vs Fab-Srt-FR-OVAp	0.7317, ns	0.0016, **	0.0197, *
Fab-Ub2-FR-OVAp vs Fab-Srt-OVAp	0.0070, **	<0.0001, ****	0.0179,*
Fab-Ub2-OVAp vs Fab-Srt-FR-OVAp	0.0812, ns	0.0392, *	0.0516, ns
Fab-Ub2-OVAp vs Fab-Srt-OVAp	0.0351, *	0.0221, *	0.0462, *
Fab-Srt-FR-OVAp vs Fab-Srt-OVAp	0.0092, **	0.0016, **	0.0567, ns

**Table S2a Blood clearance data.** Mice were treated as described in figure 5. %ID/g are given for the blood clearance study as shown in .

Timepoint	[111In]In Fab-Ub2-K(DOTA-GA)-FR- OVAp	[111In]In Fab-Srt-K(DOTA-GA)-FR- OVAp
	%ID/g	%ID/g
10 min.	17.1±2.1	21.1±4.01
30 min.	9.79±1.69	10.0±1.99
60 min.	6.92±1.03	6.16±1.25
120 min.	4.40±0.59	3.14±0.46
240 min.	2.84±0.39	1.71±0.20
360 min.	2.19±0.51	1.28±0.20
1440 min.	0.70±0.18	0.20±0.01

**Table S2b Biodistribution data.** Mice were injected as described in figure 5. %ID/g are given for the organs of which the weight was determined or as %ID for the stomach, small intestine, large intestine. Weight was not determined for the latter, as the organs were not emptied.

Tissue	[111In]In Fab-Ub2-K(DOTA-GA)-FR- OVAp	[111In]In Fab-Srt-K(DOTA-GA)-FR- OVAp
	%ID/g	%ID/g
Spleen	30.8±10.0	22.1±1.3
Blood	0.698±0.182	0.200±0.014
Inguinal LN	2.92±0.72	9.51±3.51

Thymus	1.19±0.29	2.88±0.46
Heart	0.888±0.121	0.965±0.025
Lung	1.77±0.29	3.01±0.62
Liver	31.9±6.2	12.2±1.2
Kidneys	5.77±1.10	60.34±4.73
Muscle	0.375±0.025	0.343±0.059
Bone	5.55±0.79	4.96±0.88
Skin	1.57±0.18	1.48±0.11
	%ID (e-3)	%ID (e-3)
Stomach	2.58±0.72	6.49±3.14
Small intestine	11.7±1.0	14.5±2.5
Large intestine	9.31±6.19	20.4±8.43

**Table S2c Distribution data for splenocyte subset isolation.** Mice were treated as described in Figure 5. %ID, cell number and %ID/cell are given for the isolation of the various splenocyte subsets.

Splenocyte	cyte [111In]In Fab-Ub2-K(DOTA-GA)-FR-OVAp		[111In]In Fab-Srt-K(DOTA-GA)-FR-OVAp		A)-FR-OVAp	
subset	%ID (e-5)	# Cells (e6)	%ID/cell (e-9)	%ID (e-5)	# Cells (e6)	%ID/cell (e-9)
CD11c+	25.3±12.5	0.13±0.09	216±62	6.32±1.15	0.13±0.06	61.5±34.1
CD11c-/ CD11b+	5.15±2.44	0.66±0.19	7.51±2.5	22.7±2.77	0.81±0.11	28.4±4.41
CD11c-/ CD11b-	3.88±1.92	11.4±9.1	0.40±0.14	27.4±8.29	13.0±4.11	2.18±0.66

**Table S3 Rat IgG2A ubi-tagged Fab: donor and acceptor.** Design HDR-template used to obtain the anti-DEC205 Fab-Ub<sup>don</sup> and anti-DEC205 Fab-Ub<sup>acc</sup>.

PCR4 TOPO	sequence
5'HA	CCTGGAACTCTGGAGCCCTGTCCAGCGGTGTGCACACCTTCCCAGCTGTCCTG-CAGTCTGGACTCTACACTCTCACCAGCTCAGCACCTGTCACCAGCTCTGACCAGCTCAGCACCTGGTC-CAGCCAGGCCACCTGCAACCTAGCCCAGCCAGCACCAAGGTGGA-CAAGAAAATTGGTGAGAACAACCAGGGGATGAGGGCCACCAGGGAGGG
Linker - Ub <sub>1-76</sub> -His <sub>10x</sub> (acceptor)	TGCCAAGGGAATGCGGAGGCGGTGGATCTATGCAAATTTTCGTTAAGACTCT-GACAGGGAAGACTATTACACTGGAGGTTGAGCCATCAGATACGATTGAGAAT-GTCAAGGCAAAGATACAGATACAGAAAGAAGGCT-GATCTTCGCTGGGAAGCAACAAGGCT-GATCTTCGCTGGGAAGCAACTGGAAGATGGCCGAACACTGAGCGATTATAACATA-CAAAAGGAGTCTACACTGCATTTGGTTCTGCGCCTTCGAGGCGGCATCACCACCACCACCACCACCACCACCACCACCACCACC

Linker - Ub <sub>K48R</sub> -His <sub>10x</sub> (Donor)	TGCCAAGGGAATGCGGAGGCGGTGGATCTATGCAAATATTCGTAAAGACTCTGACC-GGGAAAACCATTACACTTGAAGTGGAGCCGTCAGACACGATTGAGAATGTTAAGGC-TAAGATTCAGGACAAGGAAGGAAGGAAGGTATCCCGCCAGACCAACAACGCCTGATCTTCGCCG-GACGACAATTGGAGGATGGTAGGACTTTGAGCGATTACAACATACAGAAAGAA
IRES Bsr polyA	CCGGTGAGCTCTCCCTCCCCCCCCTAACGTTACTGGCCGAAGCCGCTTG-GAATAAGGCCGGTGTGCGTTTGTCTATATGTTATTTTCCACCATATTGCC-GTCTTTTTGGCAATGTGAGGGCCCGGAAACCTGGCCCTGTCTTCTTGACGAG-CATTCCTAGGGGTCTTTCCCCCCCCAAAGGAATGCAAAGGTCTGTTTGAATGTCGTGAAGGAAG
3'НА	GGTAAGTCACTAGGACTATTACTCCAGCCCCAGATTCAAAAAATATCCTCAGAGGCCCATGTTAGAGGATGACACAGCTATTGACCTATTTCTACCTTTCTTCATCTTACAGGCCCCATGTTAGAGGATGACACAGCTATTGACCTATTCTCCCCCCAAAGACCAAAGATGTGCCCCCCACAGAGACCAAAGATGTGCCCCAGAATGACCCCAGAGTCCACACTTAGGCCCAGAATGACCTTAAGGTCAGCTGGTTTATAGATGACGTGGAAGTCCACACACCTCAGACTCAGACTCCAGCTCAGACTCCAGCTCAGCTCAGTCCAGTCCAGCTCAATGCCCAGTGAACTCCCATCGTGCACCGGGACTGGCTCAATGGCAAAGTCAACACGCTCAAACCCGAAAGTCAACAGGAGCATTCCCTGCCCCCATCGAGAAAAGCATCTCCAAACCCGGAAGGTGGGAGCAGCAGGGTGTGAGAAGCTTCAAATGACTGAGGTGGGAGCAGCAGGGTGTGTGGTGTAGAAGCTGCAGTAGAACCATTAACTAGACTTAAAGGGCGAATTCGCGGCCGCGCCGCCGCCGCCGCCGCCGCCGCCGCCGC

**Table S4 Rat IgG2a SrtA(4s9)-tagged Fab** Design HDR-template used to obtain the anti-DEC205 Fab-Srt.

PCR2.1 TOPO	sequence
5'HA rIgG2a	CCTGGAACTCTGGAGCCCTGTCCAGCGGTGTGCACACCTTCCCAGCTGTCCTG-CAGCTCTGGACTCTACACTCTCACCAGCTCAGCACCTGTACCCTGACCTCACCAGCTCAGCACCTGGACCCAGCACCTGGACCAGCCCAGCACCAAGGTGGA-CAAGAAAATTGGTGAGAGAACAACCAGGGGATGAGGGCTCACTAGAGGTGAGGATA-AGGCATTAGATTGCCTACACCAACCAGGGTGGGCAGACATCACCAGGGAGGG
Linker – Sortag – HIS tag	GGAGGCGGAGCCTGCCGGAATCCGGCGCCACCATCACCATCACCATTGA
IRES Bsr polyA	GGATCCCAATTGCTCGAGGCCCCTCTCCCCCCCCCCTAACGTTACTGCCCGAAGCCGCTTGGAATAAGGCCGGTTGTGCTTTGTCTATATGTTATTTTCACCCATATTGCCGTTTTTGGCAATAGGCCGGTTGTGCTTTGTCTATATGTTATTTTCACCCATATTGCCGTCTTTTTGGCAATGTGAGGGCCCGGAAACCTGGCCCTGTCTTCTTGACGAGGCTTCTTTGAAGAGAAACAAGTCTGAATGTCGAAGGAAG
3'HA rIgG2a	GGTAAGTCACTAGGACTATTACTCCAGCCCCAGATTCAAAAAATATCCTCAGAGGCCCATGTTAGAGGATGACACAGCTATTGACCTATTTCTACCTTTCTTCATCTTACAGGCTCAGAAGTATCATCTGTCTTCATCTTCATCTTACAGGCTCAGAAGTATCATCTGTCTTCATCTTCCCCCCAAAGACCAAAGATGGCTCACCATCACTCTGACTCCTAAGGTCACGTGTGTTGTGGTAGACATTAGCCAGAATGATCCCGAGAGTCCAGCTGGTTTATAGATGACGTGGAAGTCCACAGCTCAGACTCAGTCCAGTCCAGTAGACTCCAACAGCACTTTACGCTCAGTCAG

#### References

- 1. Lee, K. W., Yam, J. W. P. & Mao, X. Dendritic Cell Vaccines: A Shift from Conventional Approach to New Generations. *Cells* **12**, (2023).
- 2. Banchereau, J. & Steinman, R. M. Dendritic cells and the control of immunity. *Nature* **392**, 245–252 (1998).
- 3. Mastelic-Gavillet, B., Balint, K., Boudousquie, C., Gannon, P. O. & Kandalaft, L. E. Personalized Dendritic Cell Vaccines-Recent Breakthroughs and Encouraging Clinical Results. *Front Immunol* **10**, (2019).
- 4. Oliveira, M. M. S. *et al.* Increased cross-presentation by dendritic cells and enhanced anti-tumour therapy using the Arp2/3 inhibitor CK666. *Br J Cancer* **128**, 982–991 (2023).
- 5. Joffre, O. P., Segura, E., Savina, A. & Amigorena, S. Cross-presentation by dendritic cells. *Nat Rev Immunol* **12**, 557–569 (2012).
- 6. Kurts, C., Robinson, B. W. S. & Knolle, P. A. Cross-priming in health and disease. *Nat Rev Immunol* **10**, 403–414 (2010).
- 7. Cabeza-Cabrerizo, M., Cardoso, A., Minutti, C. M., Pereira Da Costa, M. & Reis E Sousa, C. Dendritic Cells Revisited. *Annu Rev Immunol* **39**, 131–166 (2021).
- 8. Kaech, S. M., Wherry, E. J. & Ahmed, R. Effector and memory T-cell differentiation: implications for vaccine development. *Nat Rev Immunol* **2**, 251–262 (2002).
- 9. Curtsinger, J. M. & Mescher, M. F. Inflammatory cytokines as a third signal for T cell activation. *Curr Opin Immunol* **22**, 333–340 (2010).
- 10. Gu, Y. zhuo, Zhao, X. & Song, X. rong. Ex vivo pulsed dendritic cell vaccination against cancer. *Acta Pharmacol Sin* **41**, 959–969 (2020).
- 11. Wimmers, F., Schreibelt, G., Sköld, A. E., Figdor, C. G. & De Vries, I. J. M. Paradigm Shift in Dendritic Cell-Based Immunotherapy: From in vitro Generated Monocyte-Derived DCs to Naturally Circulating DC Subsets. *Front Immunol* **5**, (2014).
- 12. Constantino, J., Gomes, C., Falcão, A., Cruz, M. T. & Neves, B. M. Antitumor dendritic cell-based vaccines: lessons from 20 years of clinical trials and future perspectives. *Transl Res* **168**, 74–95 (2016).
- 13. Aarntzen, E. H. J. G. *et al.* Vaccination with mRNA-electroporated dendritic cells induces robust tumor antigen-specific CD4+ and CD8+ T cells responses in stage III and IV melanoma patients. *Clin Cancer Res* **18**, 5460–5470 (2012).
- 14. Van Lint, S. *et al.* Intratumoral Delivery of TriMix mRNA Results in T-cell Activation by Cross-Presenting Dendritic Cells. *Cancer Immunol Res* **4**, 146–156 (2016).
- 15. Pitt, J. M. *et al.* Dendritic cell-derived exosomes for cancer therapy. *J Clin Invest* **126**, 1224–1232 (2016).
- 16. Chen, Q. *et al.* Photothermal therapy with immune-adjuvant nanoparticles together with checkpoint blockade for effective cancer immunotherapy. *Nat Commun* **7**, (2016).
- 17. Swee, L. K. et al. Sortase-mediated modification of aDEC205 affords optimization

- of antigen presentation and immunization against a set of viral epitopes. *Proc Natl Acad Sci U S A* **110**, 1428–1433 (2013).
- 18. Gardner, A., de Mingo Pulido, Á. & Ruffell, B. Dendritic Cells and Their Role in Immunotherapy. *Front Immunol* **11**, (2020).
- 19. Caminschi, I., Maraskovsky, E. & Heath, W. R. Targeting Dendritic Cells in vivo for Cancer Therapy. *Front Immunol* **3**, (2012).
- 20. Lahoud, M. H. *et al.* Targeting antigen to mouse dendritic cells via Clec9A induces potent CD4 T cell responses biased toward a follicular helper phenotype. *J Immunol* **187**, 842–850 (2011).
- 21. Bonifaz, L. *et al.* Efficient targeting of protein antigen to the dendritic cell receptor DEC-205 in the steady state leads to antigen presentation on major histocompatibility complex class I products and peripheral CD8+ T cell tolerance. *J Exp Med* **196**, 1627–1638 (2002).
- 22. Jiang, W. *et al.* The receptor DEC-205 expressed by dendritic cells and thymic epithelial cells is involved in antigen processing. *Nature* **375**, 151–155 (1995).
- 23. Lehmann, C. H. K. *et al.* Direct Delivery of Antigens to Dendritic Cells via Antibodies Specific for Endocytic Receptors as a Promising Strategy for Future Therapies. *Vaccines 2016, Vol. 4, Page 8* **4**, 8 (2016).
- 24. Bonifaz, L. C. *et al.* In Vivo Targeting of Antigens to Maturing Dendritic Cells via the DEC-205 Receptor Improves T Cell Vaccination. *J Exp Med* **199**, 815 (2004).
- 25. Semmrich, M. *et al.* Directed antigen targeting in vivo identifies a role for CD103+ dendritic cells in both tolerogenic and immunogenic T-cell responses. *Mucosal Immunol* **5**, 150–160 (2012).
- 26. Antos, J. M., Truttmann, M. C. & Ploegh, H. L. Recent advances in sortase-catalyzed ligation methodology. *Curr Opin Struct Biol* **38**, 111–118 (2016).
- 27. Popp, M. W., Antos, J. M., Grotenbreg, G. M., Spooner, E. & Ploegh, H. L. Sortagging: a versatile method for protein labeling. *Nature Chemical Biology 2007 3:11* **3**, 707–708 (2007).
- 28. van der Schoot, J. M. S. *et al.* Functional diversification of hybridoma-produced antibodies by CRISPR/HDR genomic engineering. *Sci Adv* **5**, eaaw1822 (2019).
- 29. Birkholz, K. *et al.* Targeting of DEC-205 on human dendritic cells results in efficient MHC class II-restricted antigen presentation. *Blood* **116**, 2277–2285 (2010).
- 30. Carbone, F. R., Sterry, S. J., Butler, J., Rodda, S. & Moore, M. W. T cell receptor alpha-chain pairing determines the specificity of residue 262 within the Kb-restricted, ovalbumin257-264 determinant. *Int Immunol* **4**, 861–867 (1992).
- 31. Saeki, Y. Ubiquitin recognition by the proteasome. *J Biochem* **161**, 113–124 (2017).
- 32. Carroll, E. C., Greene, E. R., Martin, A. & Marqusee, S. Site-specific ubiquitination affects protein energetics and proteasomal degradation. *Nat Chem Biol* **16**, 866–875 (2020).

- 33. Ran, F. A. *et al.* Genome engineering using the CRISPR-Cas9 system. *Nature Protocols 2013 8:11* **8**, 2281–2308 (2013).
- 34. el Oualid, F. *et al.* Chemical synthesis of ubiquitin, ubiquitin-based probes, and diubiquitin. *Angewandte Chemie International Edition* **49**, 10149–10153 (2010).
- 35. Geurink, P. P. *et al.* Development of Diubiquitin-Based FRET Probes To Quantify Ubiquitin Linkage Specificity of Deubiquitinating Enzymes. *ChemBioChem* **17**, 816–820 (2016).
- 36. Blythe, E. E., Olson, K. C., Chau, V. & Deshaies, R. J. Ubiquitin- A nd ATP-dependent unfoldase activity of P97/VCP•NPLOC4•UFD1L is enhanced by a mutation that causes multisystem proteinopathy. *Proc Natl Acad Sci U S A* **114**, E4380–E4388 (2017).



### Nanobody ubi-tag conjugates for translation to human dendritic cell targeted antigen delivery

4

This chapter is part of the publication:

A.F. Elhebieshy\*, Z. Wijfjes\*, et al. Site-directed multivalent conjugation of antibodies to ubiquitinated payloads. Accepted for publication: Nature Biomedical Engineering.



## Nanobody ubi-tag conjugates for translation to human dendritic cell targeted antigen delivery

Angela F. el Hebieshy, Zacharias Wijfjes, Camille M. Le Gall, Jim Middelburg, Kim E. de Roode, Felix L. Fennemann, Marjolein Sluijter, Thorbald van Hall, Douwe J. Dijkstra, Leendert A. Trouw, Floris J. van Dalen, Andrea Rodgers Furones, Johan M. S. van der Schoot, Ian Derksen, Hans de Haard, Bas van der Woning, Cami M. P. Talavera Ormeño, Bjorn R. van Doodewaerd, Carl G. Figdor, Gerbrand J. van der Heden van Noort, Paul W.H.I. Parren, Sandra Heskamp, Huib Ovaa, Martijn Verdoes, Ferenc A. Scheeren.

#### **Abstract**

Nanobodies, also known as sdAbs or VHHs, hold great potential for the development of dendritic cell (DC)-targeted vaccines due to their small size, high specificity, and ability to penetrate tissues efficiently. In this study, we demonstrate that ubi-tagged VHHs retain their functionality, with the ubi-tag not interfering with VHH antigen binding. Furthermore, we show that the ubi-tag serves as a conjugation tag and also enhances the solubility of the attached peptide, acting as an effective solubility enhancer for hydrophobic epitopes. We then generated an anti-DC-SIGN VHH-Ub<sub>2</sub>-gp100<sub>p</sub> conjugate and demonstrate its functionality *in vitro*, showcasing the potential of ubitagged VHH-peptide epitope conjugates as a vehicle for DC-targeted vaccines in a human setting.

#### Introduction

Nanobodies, or single-domain antibody fragments, are derived from unique heavy-chain-only antibodies found in camelids. Unlike conventional antibodies, which consist of two heavy and two light chains, nanobodies consist solely of the variable heavy-chain domain (VHH), which is responsible for antigen recognition.¹ Despite their small size (approximately 15 kDa), nanobodies maintain antigen-binding capacities comparable to full-sized antibodies, making them highly versatile in biomedical applications¹. Their small size, superior stability, high specificity, and ability to penetrate tissues efficiently, contribute to their effectiveness in both therapeutic and diagnostic applications. For this reason, nanobodies are also attractive to use for the development of dendritic cell (DC)-targeted vaccines, which aim to enhance immune responses against infectious diseases, cancer, and other conditions²-5.

Nanobodies targeting DC cell surface receptors, such as CLEC9A and CD11c, and DC-SIGN, enable targeted delivery of antigens to DCs <sup>3,6,7</sup>. Since VHHs are predominantly produced via recombinant expression in bacterial systems, one approach for generating VHH-peptide epitope conjugates involves recombinant DNA. In this technique, the coding DNA sequences of the VHH and peptide epitopes are linked together within a recombinant plasmid, enabling the co-expression of a single polypeptide chain comprising both the VHH and the peptide epitope. This method facilitates the

production of a bifunctional protein, where the VHH domain and the epitope are expressed in one genetically encoded fusion product, allowing for efficient synthesis in bacterial hosts. While this approach seems straightforward, it often presents challenges due to the hydrophobic nature of antigenic peptides <sup>8</sup>, leading to low expression and improper folding of the resulting fusion proteins. This limits the wide application of bacterial expression for producing VHH-peptide conjugates.

An alternative approach is sortagging, where a VHH is produced with a sortag motif at its C-terminus and then chemoenzymatically conjugated to a chemically synthesized peptide epitope with a polyglycine motif at its N-terminus<sup>9</sup>. Chemical synthesis of the peptide epitope provides more flexibility to attach chemical moieties to enhance the solubility compared to genetic fusions. For instance, the solubility of the highly hydrophobic peptide NY-ESO-1 was improved by chemically attaching polyethylene glycol (PEG) to it.<sup>9</sup>

Ubiquitin has also been shown to enhance the solubility and promote the proper folding of proteins when used as a fusion tag <sup>10</sup>. Encouraged by our data in Chapter 3, where we observed strong T cell activation with ubi-tagged Fab-peptide conjugates, we sought to apply ubi-tag conjugation to generate VHH-peptide epitope conjugates. Our aim was to investigate the impact of the presence of a ubi-tag on the solubility of antigenic peptides, assess the feasibility of ubi-tag conjugation for VHHs, and translate the previously observed effects of the ubi-tagged conjugates for DC-targeted antigen delivery to human applications.

#### **Results**

To explore the applicability of ubi-tagging for DC-targeted antigen delivery, we broadened the scope towards nanobody (VHH)-conjugates (Fig. 1a). The high stability, solubility, and ease of production of nanobodies have raised interest in the use of these small-sized (15 kDa) targeting moieties<sup>1</sup>. We produced two ubi-tagged VHHs (VHH-Ub(K48R)<sup>don</sup>), one targeting hDC-SIGN (CD209)<sup>11</sup> and the other targeting ALFA-tag<sup>12</sup> as a non-targeted control (ntVHH-Ub) (Fig. 1b and Supplementary Fig. S1 and S4, and Supplementary Table S1). As the size of the ubi-tag (16 kDa) is roughly equal to the size of the nanobody, we first verified that ubi-tagging does not hinder target binding. We performed a binding assay on DC-SIGN transfected CHO cells and DC-SIGN expressing monocyte-derived DCs (moDCs) (Fig. 1c and Supplementary Fig. S2). The results revealed a pronounced, DC-SIGN expression- and dose-dependent enhancement in the fluorescent signal for the DC-SIGN targeted Rho-Ub<sub>2</sub>-VHH conjugate. In contrast, no such increase was observed for the Rho-Ub<sub>2</sub>-ntVHH.

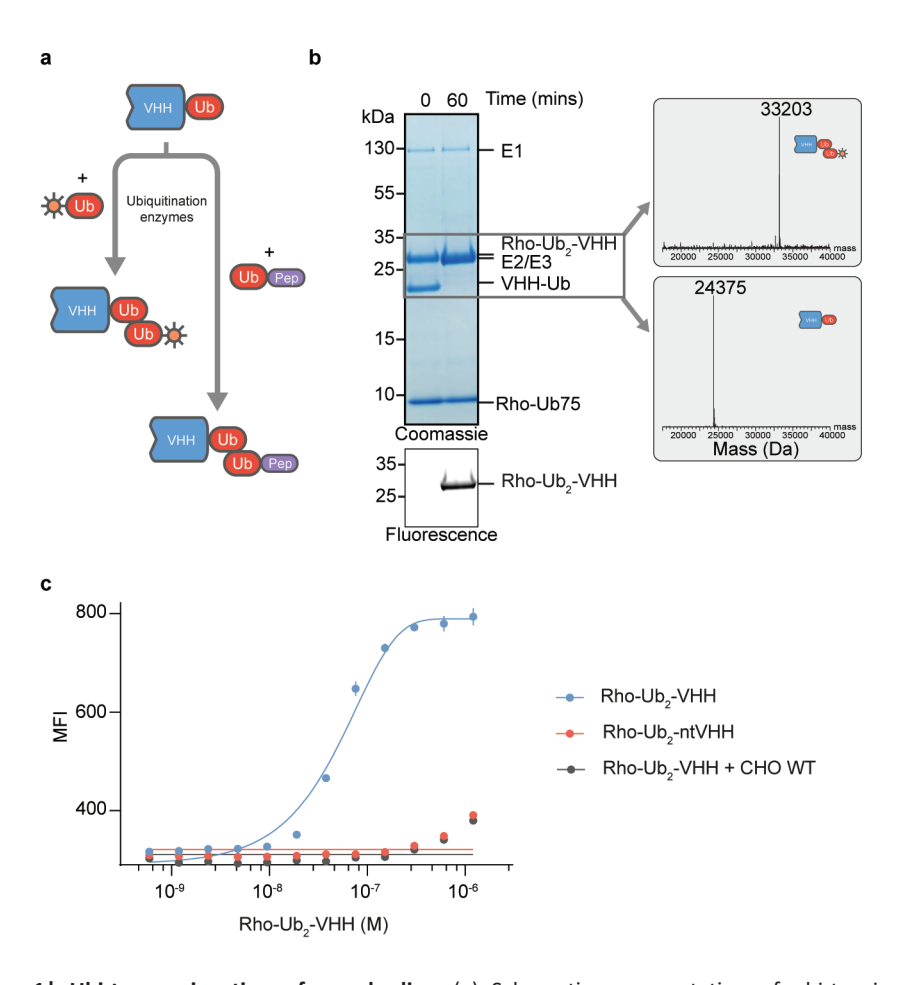


**Figure 1**| **Ubi-tag conjugation of nanobodies.** (a) Schematic representation of ubi-tagging for nanobodies. (b) Non-reducing (fluorescent) SDS-PAGE analysis and deconvoluted ESI-TOF mass spectra of formation of Rho-Ub<sub>2</sub>-VHH through ubi-tagging of VHH-Ub<sup>don</sup> and Rho-Ub<sup>acc</sup>. (c) Binding assay on DC-SIGN transfected CHO cells with DC-SIGN targeted Rho-Ub<sub>2</sub>-VHH (blue), ALFAtag targeted Rho-Ub<sub>2</sub>-ntVHH (red), and DC-SIGN targeted Rho-Ub<sub>2</sub>-VHH on WT CHO cells (black). Data are shown as MFI of Rhodamine-channel and a curve fit (Sigmoidal, 4PL, X = log(conc.)) on data points (n = 2).

In the field of targeted antigenic peptide delivery the hydrophobicity of CD8-epitopes is a prevalent problem<sup>8</sup>. We reasoned that since ubiquitin is well-known for its high solubility and stability, the fusion of a ubi-tag to hydrophobic peptides could enhance their solubility<sup>10</sup>. To demonstrate this, we generated a library of VHH-Ub<sub>2</sub>-peptide conjugates, including hydrophobic peptides known to be challenging to ligate to antibodies, nanobodies or chemokines using other techniques<sup>8,9</sup>. All tested Ub-peptide fusions were readily synthesized and conjugated to VHH-Ub(K48R)<sup>don</sup> without solubility issues (Fig. 2a and Supplementary Fig. S5).

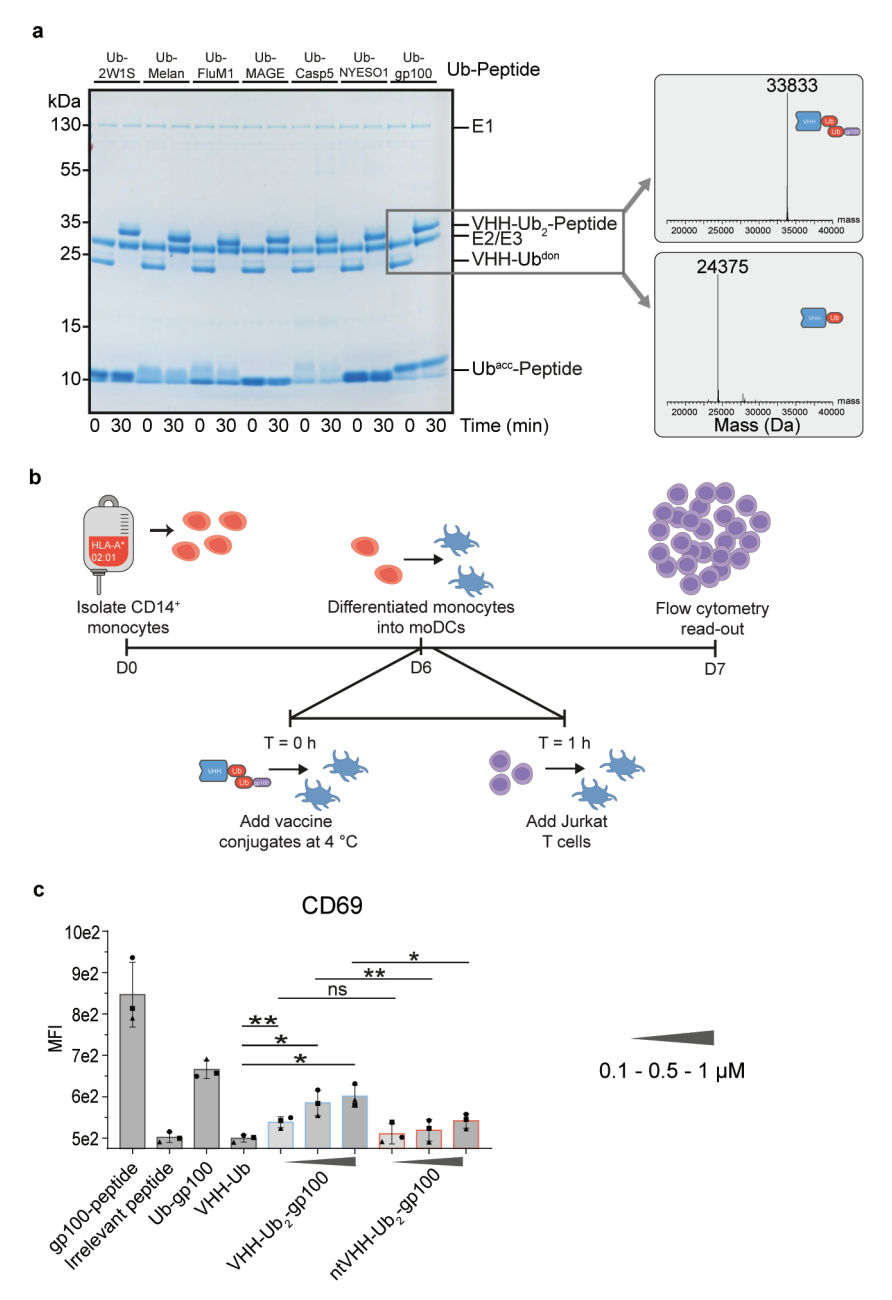


Figure 2 | Generation and validation of VHH-Ub $_2$ -antigenic peptide conjugates. (a) SDS-PAGE analysis of VHH-Ub $_2$ -antigenic peptide conjugates and deconvoluted ESI-TOF mass spectra of VHH-Ub $_2$ -gp100 $_p$ . VHH-Ub $_2$ -ontigenic peptide to respectively Ub $_2$ -EAWGALANWAVDSA (2W1S), Ub $_2$ -ELAGIGILTV (Melan), Ub $_2$ -GILGFVFTL (FluM1), Ub $_2$ -CKVLEYVIKV (MAGE), Ub $_2$ -FLIIWQNTM (Casp5), Ub $_2$ -SLLMWITQV (NYESO1) and Ub $_2$ -CYLEPGPVTA (gp100). (b) Schematic illustration of reporter Jurkat T cell activation assay. In short, moDCs were generated, pulsed (1 h., 4 °C) with vaccine conjugate (VHH-Ub $_2$ -gp100p) or non-targeting control (ntVHH-Ub $_2$ -gp100p), and washed. Subsequently, reporter Jurkat T

cells were added in 1:5 ratio and incubated overnight followed by flow cytometry analysis. (c) Flow cytometry analysis of CD69 expression. Data (N=3) are shown as mean ±SD, paired T tests, \*\*P<0.01, \*P<0.05, ns P>0.05.

Glycoprotein 100 (gp100) is considered a melanoma tumor-associated antigen of which gp100 $_{280\text{-}288}$  (gp100 $_{p}$ ) has been identified as an HLA-A\*0201 binding epitope<sup>13</sup>. We therefore proceeded to examine the functionality of the human DC targeted anti-DC-SIGN VHH-Ub $_{2}$ -gp100 $_{p}$  by pulsing moDCs and subsequent incubation with reporter Jurkat T cells recognizing the MHC I-gp100 $_{p}$  epitope complex<sup>14</sup>. Activation of the Jurkat T cells was assessed by CD69 expression the next day and indicated that the VHH-Ub $_{2}$ -gp100 $_{p}$  led to antigen presentation of the gp100 epitope by moDCs in a dose-dependent fashion (Fig. 2b,c). Significant differences were observed between the DC-SIGN targeted VHH-Ub $_{2}$ -gp100 $_{p}$  and non-targeted variant, which demonstrates the potentiating effect of receptor-mediated antigen uptake<sup>15</sup>.

In a more physiologically relevant setting, we transfected primary CD8<sup>+</sup> T cells from HLA-A\*02:01<sup>+</sup> donors with a gp100 $_p$  specific T cell receptor (TCR) (Supplementary Fig. S3) to assess the efficacy of the VHH-Ub $_2$ -gp100 $_p$  to induce HLA-A\*02:01<sup>+</sup> moDC-mediated activation of primary human T cells (Fig. 3a)<sup>15</sup>. Proliferation (Fig. 3b), activation (Fig. 3c,d) and cytokine secretion (Fig. 3e) of the T cells were assessed and showed a more potent dose-dependent increase in the conditions where moDCs were pulsed with anti-DC-SIGN VHH-Ub $_2$ -gp100 $_p$  compared to the non-targeted conjugate, indicating the potential of nanobody-peptide epitope conjugates for the development of DC-targeting vaccines in a human setting.

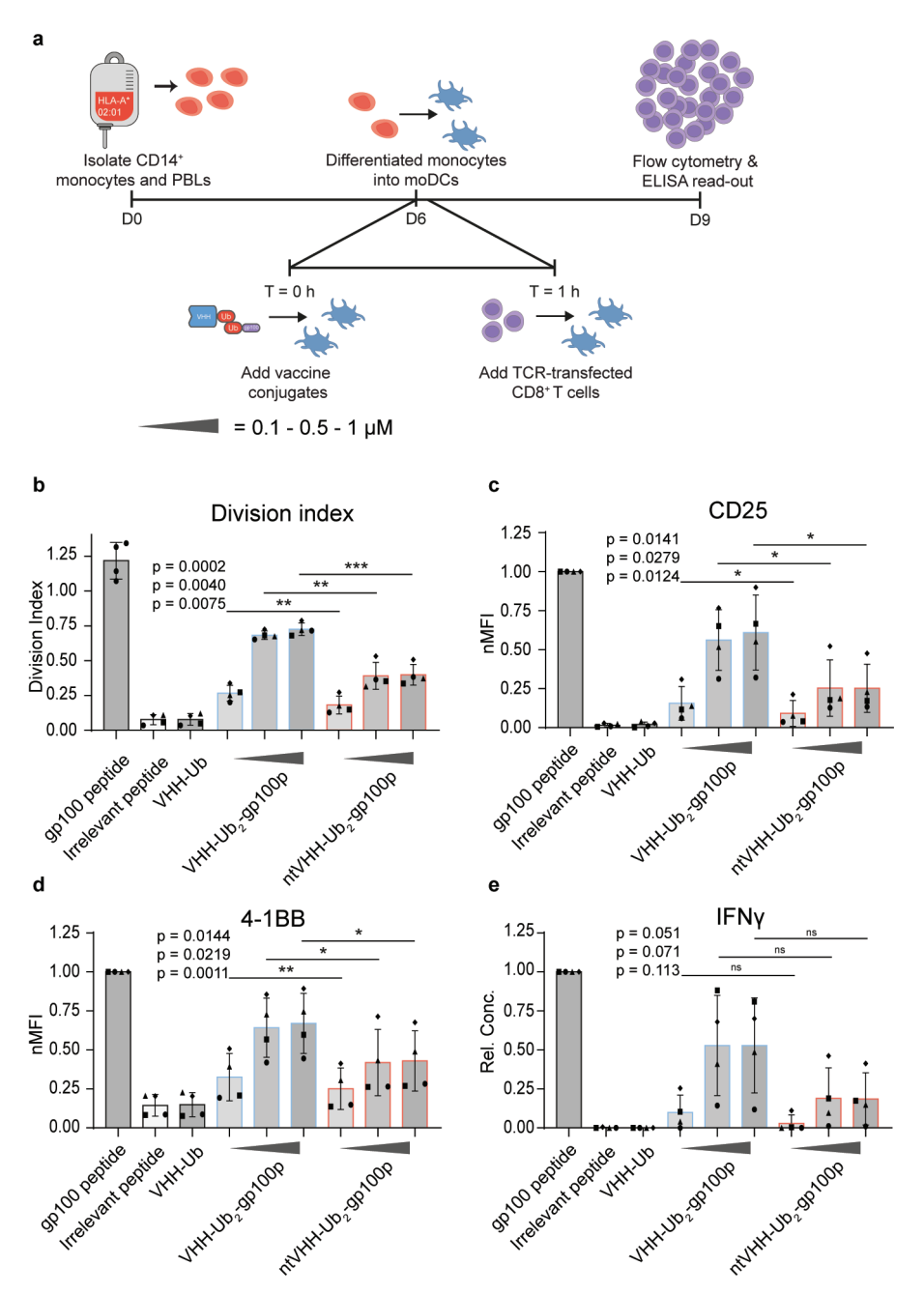


Figure 3 | Primary TCR-transfected CD8+ T cell activation assay for the validation of VHH-Ub<sub>2</sub>-gp100<sub>p</sub>. (a) Schematic representation of primary TCR-transfected CD8+ T cell activation assay. HLA-A\*02:01+ moDCs were generated and pulsed with 0.1-0.5-1  $\mu$ M vaccine conjugate or 1  $\mu$ M control condition for 1 h. at 37 °C. TCR transfected CD8+ T cells were added in 1:5 ratio and after 3 days, supernatant and cells were harvested for analysis. Transfection efficiency is shown in Supplementary Fig. S3. (b-d) flow cytometry analysis of CD8+ T cells. Division index was calculated for different conditions based on

CTV signal (b). Data (n = 4) are shown as mean  $\pm$ SD normalized to positive control (gp100 peptide) for CD25 (c), and 4-1BB (d). Paired T tests, \*\*\*P<0.001, \*\*P<0.01, \*P<0.05, ns P>0.05. (e) ELISA analysis (n = 4) for IFN $\gamma$ . Data are shown as mean  $\pm$ SD normalized to positive control. Paired T tests, p-values are noted in figure.

#### **Discussion**

In this work, we broadened the scope of ubi-tagging towards nanobody (VHH)conjugates for human DC-targeted antigen delivery. First, we showed that although ubi-tag conjugation would significantly add to the molecular weight of the conjugate, considering the size of a VHH of 15 kDa and the di-ubiquitin formed during ubi-tag conjugation around 16 kDa, it does not hinder the binding of VHH towards its target. This could be of additional benefit in therapeutic or diagnostic applications, as the increase in molecular weight will contribute to an extended half-life of the VHH and thereby enhance their efficacy<sup>16</sup>. Next, we proceeded to demonstrate that ubi-tagging improves the solubility of nanobody-antigen conjugates for a library of notoriously insoluble epitopes<sup>8,9</sup>. Ubiquitin is one of the most stable and soluble proteins in eukaryotes. Owing to these exceptional physicochemical properties, it is often used as a solubility tag to enhance the solubility and expression yield of fused proteins in bacterial expression systems by chaperoning for correct folding and reducing the chances of protein aggregation during expression<sup>10</sup>. With this in mind, we successfully attempted to enhance the solubility of antigenic epitopes known for their extremely poor solubility by chemically synthesizing these peptides fused to the C-terminus of an acceptor ubi-tag. After successfully synthesizing and purifying these ubi-tag fused peptides, we proceeded to conjugated them to a ubi-tagged VHH with a high reaction efficiency, approaching completion in 30 minutes. Next, we validated the functionality of the generated anti-DC-SIGN VHH-Ub<sub>2</sub>-gp100<sub>0</sub> as a human DC-targeting vaccine in a reporter Jurkat T cell activation assay and a primary TCR-transfected CD8+ T cell activation assay. In both assays, significant differences were observed in the results of the DC SIGN targeted VHH-Ub<sub>2</sub>-gp100<sub>n</sub> compared to the non-targeted variant, and a potent dose-dependent T cell activation was observed. The results obtained indicate that ubi-tagging enhances the solubility of hydrophobic epitopes, and demonstrate that it is feasible on nanobodies and that ubi-tagged nanobody-peptide epitope conjugates are of interest to be further examined as DC-targeted vaccine vehicles in a human setting.

#### Methods

#### General cell culture conditions

Jurkat T cells were cultured in T75 flasks in RPMI 1640 medium (ThermoFischer) supplemented with heat inactivated fetal bovine serum (10%, Greiner Bio-One), L-glutamine (4 mM, Gibco), non-essential amino acids (NEM) (1 mM, Gibco) and

Antibiotic-Antimycotic (1%, Gibco). Cells were maintained at 37  $^{\circ}$ C and 5% CO $_{2}$ , routinely examined by morphology analysis and tested for mycoplasma.

Solid-phase peptide synthesis

Solid-phase peptide synthesis (SPPS) of Rho-Ub and Ub-peptides was performed on a Syro II Multisyntech Automated Peptide synthesizer (SYRO robot; Part Nr: S002PS002; MultiSyntech GmbH, Germany) on a 25  $\mu$ mol scale using standard 9-fluorenylmethoxycarbonyl (Fmoc) based solid phase peptide chemistry. Both Ub variants were synthesized based on the procedure described by El Oualid *et al.*<sup>17</sup> using a fourfold excess of amino acids relative to pre-loaded Fmoc amino acid trityl resin (between 0.17 and 0.20 mmol/g, Rapp Polymere, Germany). Ub-peptides were prepared as a linear synthesis, where the peptides listed below were synthesized attached to the C-terminus of Ub. To prepare Rho-Ub, 5-carboxyrhodamine110 (Rho) was coupled to the N-terminus of Ub following SPPS as described by Geurink *et al*<sup>18</sup>. All synthetic products were purified by RP-HPLC on a Waters preparative RP-HPLC system equipped with a Waters C18-Xbridge 5  $\mu$ m OBD (10 x 150 mm) column. The purified products were lyophilized and assayed for purity by high resolution mass spectrometry on a Waters Acquity H-class UPLC with XEVO-G2 XS Q-TOF mass spectrometer and by SDS-PAGE analysis.

Peptide	Peptide sequence
2W1S	EAWGALANWAVDSA
Melan-A <sub>26–35,A27L</sub>	ELAGIGILTV
FluM <sub>158-66</sub>	GILGFVFTL
MAGE-A1 <sub>278-286</sub>	KVLEYVIKV
Caspase <sub>567-75</sub>	FLIIWQNTM
NY-ESO-1 <sub>157-165</sub> , C165Abu	SLLMWITQAbu
gp100 <sub>280-288</sub>	YLEPGPVTA

# Mass spectrometry

Mass spectrometry analysis was carried out on Waters ACQUITY UPLC-MS system equipped with a Waters ACQUITY Quaternary Solvent Manager (QSM), Waters ACQUITY FTN AutoSampler, Waters ACQUITY UPLC Protein BEH C4 Column (300 Å,  $1.7 \mu m$ ,  $2.1 \times 50 \text{ mm}$ ) and XEVO-G2 XS QTOF Mass Spectrometer (m/z = 200-2500) in ES+ mode. Sample were run using 2 mobile phases: A = 1% MeCN, 0.1% formic acid in water and B = 1% water and 0.1% formic acid in MeCN with a runtime of 14 minutes. In the first 4 minutes, salts and buffer components were flushed from LC column using 98% A and 2% B. In the next 7.5 minutes, a gradient of 2-100% B was used, followed by 0.5 minutes of 100% B and subsequent reduction to 2% B and 98% A in 2 minutes. Data processing

was performed using Waters MassLynx Mass Spectrometry Software 4.1, where the mass was obtained by deconvolution with the MaxEnt1 function.

#### Protein expression and purification

The E1 ubiquitin-activating enzyme UBE1 carrying an N-terminal His-tag was expressed from a pET3a vector in E. coli BL21(DE3) in autoinduction media for 2-3 hours at 37 °C, after which the bacteria were allowed to grow overnight at 18 °C. Next, bacteria were harvested and lysed by sonication, followed by His-affinity purification using Talon metal affinity resin (Clontech Inc., Palo Alto, CA, USA). Subsequently, the protein was further purified by anion exchange using a Resource Q column (GE Healthcare), followed by size exclusion using a Superdex 200 column (GE Healthcare).

The E2/E3 enzyme chimera plasmid was obtained as a gift from dr. Vincent Chau (Penn State, USA). The expression plasmid consists of the RING domain of the E3 ubiquitin ligating enzyme gp78 fused to the N-terminus of the E2 ubiquitin-conjugating enzyme Ube2g2 in a PET28a-TEV vector.

The E2/E3 enzyme chimera was expressed and purified as described<sup>19</sup>. In brief, the fusion protein was expressed in E. coli BL21(DE3) cells grown in LB at 37°C until OD<sub>600</sub> = 0.4-0.6 and induced with 0.4 mM IPTG for 4 hours at 30 °C. The harvested cells were lysed with Bugbuster protein extraction reagent (Millipore) according to manufacturer's protocol. The fusion protein was purified on Ni-NTA resin followed by size exclusion using a Superdex 200 column (GE Healthcare). Next, TEV protease cleavage was carried out overnight, and the cleaved fusion protein was further purified using a Resource Q column (GE Healthcare).

Sequences for the different VHH-ubiquitin fusions were cloned in the Pet30b vector and expressed in Rosetta-gami™ 2 (DE3) grown in LB medium at 37 °C until an OD<sub>600</sub> of 0.5 was reached and induced with 1 mM IPTG for 18 hours at 20 °C. Next, the bacteria were harvested and lysed by sonication followed by Ni-NTA purification. Subsequently, TEV protease cleavage was carried out to cleave the N-terminal his-tag and the cleaved VHH-Ub was further purified by size exclusion chromatography using a Superdex 200 column (GE Healthcare).

#### **Ubi-tag conjugation reaction**

Ubi-tag conjugation reactions were carried out in the presence of 0.25  $\mu$ M E1 enzyme, 20  $\mu$ M E2/E3 hybrid enzyme, 10 mM MgCl<sub>2</sub>, and 5 mM ATP in PBS. For analysis of the reaction efficiency by SDS-PAGE, an initial reaction sample was taken from the reaction mixture prior to the addition of ATP. After the addition of ATP, the reaction was incubated at 37°C for 30 minutes while shaking. Conjugation reaction samples were analyzed by quenching 2-5  $\mu$ L of the reaction mixture in sample buffer supplemented with  $\beta$ -mercaptoethanol, boiled for 15 minutes at 95°C and run on 12% Bis-Tris gels (Invitrogen) by SDS-PAGE with MOPS as running buffer. Gels were stained using InstantBlue Coomassie Protein

Stain (abcam) and imaged using Amersham600. Fluorescently labeled proteins were visualized by in-gel fluorescence using Typhoon FLA 9500 imaging system (GE Life Sciences) prior to staining with Coomassie. Small-scale reactions were carried out on a scale corresponding to 2.5  $\mu$ g VHH-Ub while large-scale reactions were carried out on a 200  $\mu$ g to 1 mg scale. For the purification of ubi-tagged VHH conjugates from the reaction mixture, 100  $\mu$ L HisPur<sup>TM</sup> Ni-NTA Resin was added to the completed reaction mixture and incubated for 15 mins at 4 °C to capture the his-tagged E1 and E2/E3 enzyme, followed by centrifugation. The supernatant containing the Ubi-tagged VHH conjugates was further purified using size exclusion chromatography using a Superdex 200 column (GE Healthcare).

# Binding study VHH-Ub,-Rho

CHO cells transfected with DC-SIGN, WT CHO cells or day 6 moDCs (GM-CSF, IL-4) were harvested and plated at 30,000 cells per well. VHH-Ub<sub>2</sub>-Rho was added in a dilution series to the cells and the cells were incubated (30 min., 4 °C). Cells were washed and fluorescence on alive cells was measured using a FACSVerse<sup>TM</sup> (BD Biosciences).

#### **Jurkat T cell activation assay**

moDCs from HLA-A\*02:01 donors prepared as described below were harvested and plated at 10,000 cells per condition. moDCs were pulsed (0.5 h., 4 °C) with vaccine conjugates at 0.1, 0.5 or 1  $\mu$ M. After the incubation, Jurkat T cells<sup>20</sup> (50,000, 1:5 ration) were added and the co-culture was incubated (1 d., 37 °C). The cells were spun down (1700 rpm., 2 min., 4 °C) and the cells were analyzed using a FACSVerse<sup>TM</sup> (BD Biosciences).

# Primary TCR-transfected T cell activation assay

Donor-matched PBLs were thawed and CD8<sup>+</sup>T cells were isolated using magnetic-assisted cell sorting according to manufacturer's protocol (CD8<sup>+</sup> T cell Isolation Kit, human, Miltenyi Biotec). T cells were mRNA-transfected by electroporation with a TCR recognizing the gp100<sub>280-288</sub> epitope (YLEPGPVTA)<sup>21</sup>. Afterwards, cells were recovered in X-VIVO, phenol free (Lonza) supplemented with 5% human serum. In tandem, moDCs from HLA-A\*02:01 donors prepared as described below were harvested and plated at 10,000 cells per condition. moDCs were pulsed (1 h., 37 °C) with vaccine conjugates at 0.1, 0.5 or 1 μM. In tandem, transfected CD8<sup>+</sup> T cells were stained with CellTrace<sup>TM</sup> Violet (ThermoFischer) for 20 min. at 37 °C and recovered in X-VIVO supplemented with 2% human serum. Then, moDCs were washed and transfected CD8<sup>+</sup> T cells (50,000) were added. The moDC-CD8 T cell coculture was incubated (3 d., 37 °C). The cells were spun down (1700 rpm., 2 min., 4 °C), supernatant was stored for ELISA analysis, and the cells were analyzed using a FACSVerse<sup>TM</sup> (BD Biosciences).

#### moDCs generation

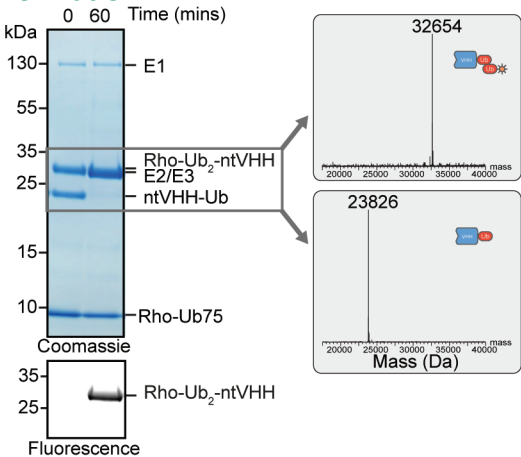
Buffy coats were obtained from Sanquin (Nijmegen, The Netherlands) and diluted to 200 mL with PBS supplemented with 2 mM EDTA. The suspension was divided over conical 5 x 50 mL tubes and 10 mL of Lymphoprep (07851, Stemcell) was added below. Cells were spun (20 min., rt, 2100 rpm., brake (3,1)). Afterwards, PBMCs were collected and washed with wash buffer (1% human serum, 2 mM EDTA in PBS) until supernatant was clear. Then ACK lysis was performed by adding 5 mL ACK buffer (150 mM NH<sub>4</sub>Cl, 10 mM KHCO<sub>3</sub>, 0.1 mM EDTA, pH=7.4) for 5 min. at room temperature. Afterwards cells were washed with PBS and CD14<sup>+</sup> monocytes were isolated using magnetic-assisted cell sorting according to manufacturer's protocol (CD14 MicroBeads UltraPure, human, Miltenyi Biotec). Flowthrough PBLs were stored, while CD14<sup>+</sup> monocytes were seeded at 8-12e6 cells per T75 flask in 10 mL X-VIVO (Lonza) supplemented with 2% human serum, 300 U/mL IL-4, and 450 U/mL GM-CSF. At day 3, medium was refreshed. At day 6, moDCs were harvested and used in experiments.

#### **ELISA**

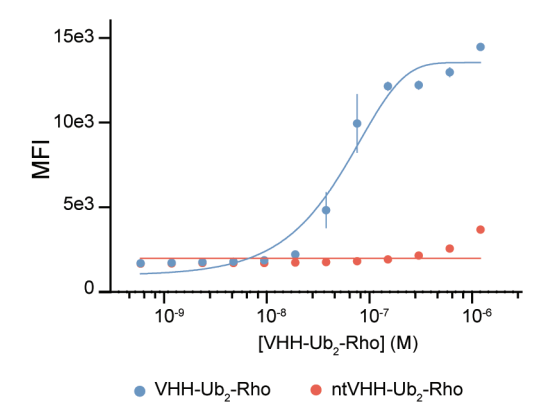
Supernatant was stored at -20  $^{\circ}$ C and thawed for ELISA analysis. Manufacturer's protocol was followed for hIFN $\gamma$  (IFN gamma Uncoated ELISA kit, Invitrogen). Flow cytometry and antibodies

For FACS analysis, cells were washed with PBS, followed by life/death staining (20 min., rt) in 50 μL eBioscience™ Fixable Viability Dye eFluor™ 780 (1:2000, ThermoFischer). Cells were washed once with PBA and antibody mixes were added (30 min., 4 °C). Cells were washed twice with PBA, taken up in 100 μL PBA and FACS analyses were performed on a FACSLyric™ (BD Biosciences) or a FACSVerse™ (BD Biosciences). The following antibodies were used for staining: hCD8 (1:20 dil., APC, clone RPA-T8, BD Biosciences), hCD25 (1:50 dil., PE/Cy7, clone BC96, BioLegend), hCD69 (1:20 dil., PerCP, clone L78, BD Biosciences), h4-1BB (1:20 dil., PE, clone 4B4-1, BD Pharmingen).



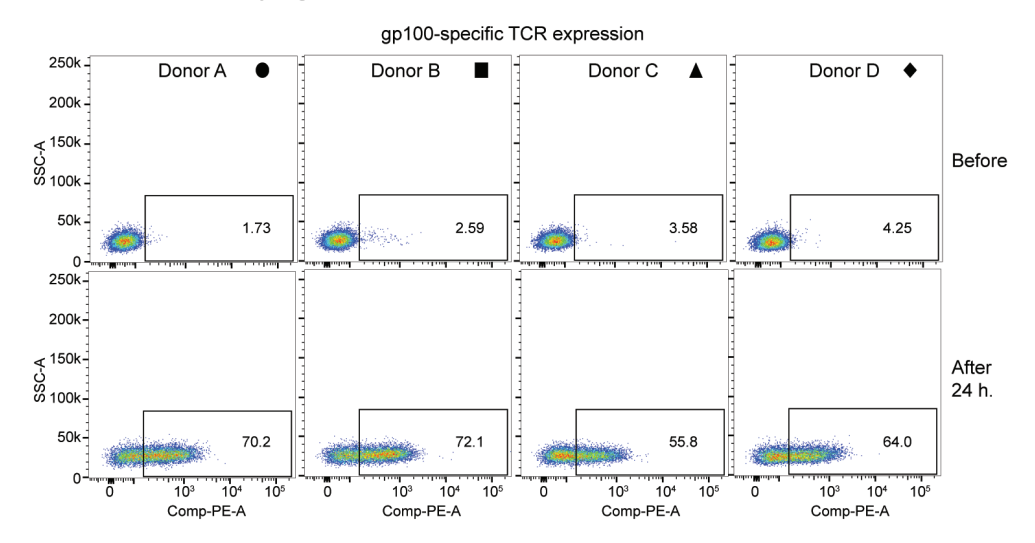


**S1 Conjugation of ntVHH-Ub**<sup>don</sup> **to or Rho-Ub**<sup>acc</sup>. SDS-PAGE analysis visualized by Coomassie Blue staining. The generated Rho-Ub<sub>2</sub>-ntVHH was isolated from the reaction mixture and its purity assessed using ESI-TOF mass spectrometry.

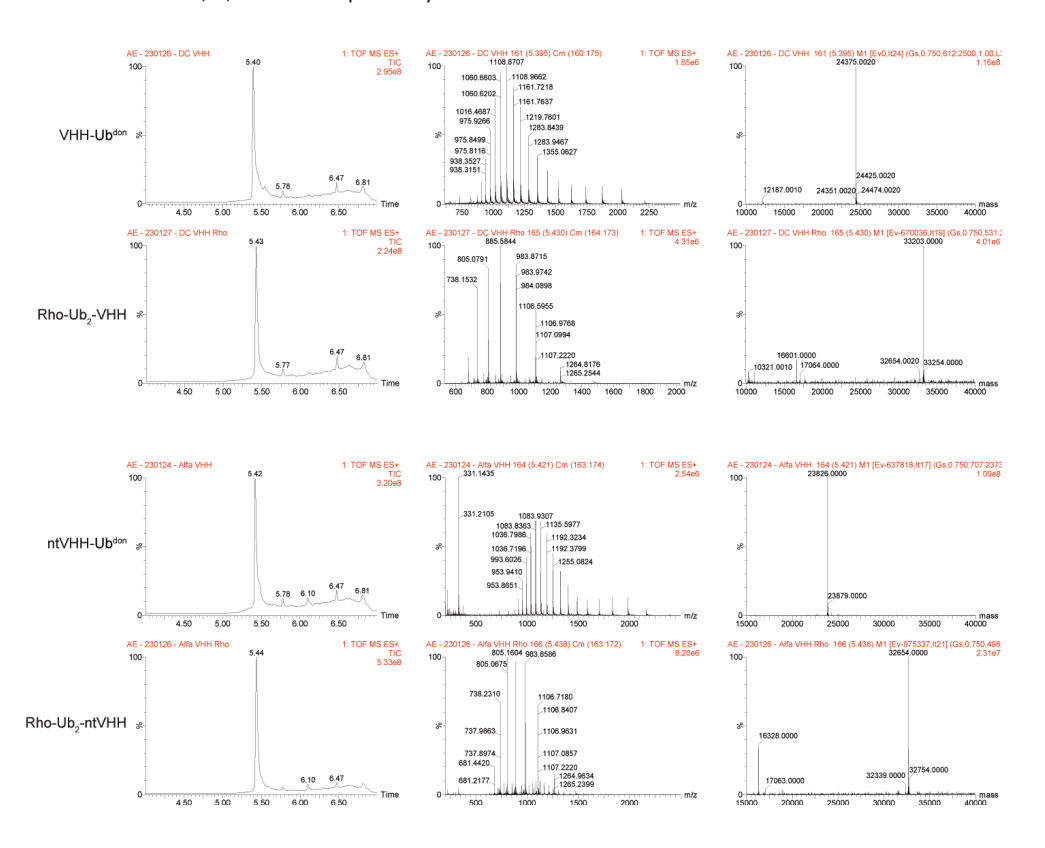


**S2 Binding assay of VHH-Ub<sub>2</sub>-Rho on moDCs.** moDCs were incubated (30 min., 4 °C) with rhodamine-labed anti-DC-SIGN VHH (VHH-Ub<sub>2</sub>-Rho) or anti-ALFAtag VHH (ntVHH-Ub<sub>2</sub>-Rho). Fluorescence was assessed using flow cytometry. Data (N=3) are shown as mean  $\pm$ SD with a curve fit (Sigmoidal, 4PL, X = log(conc.)).

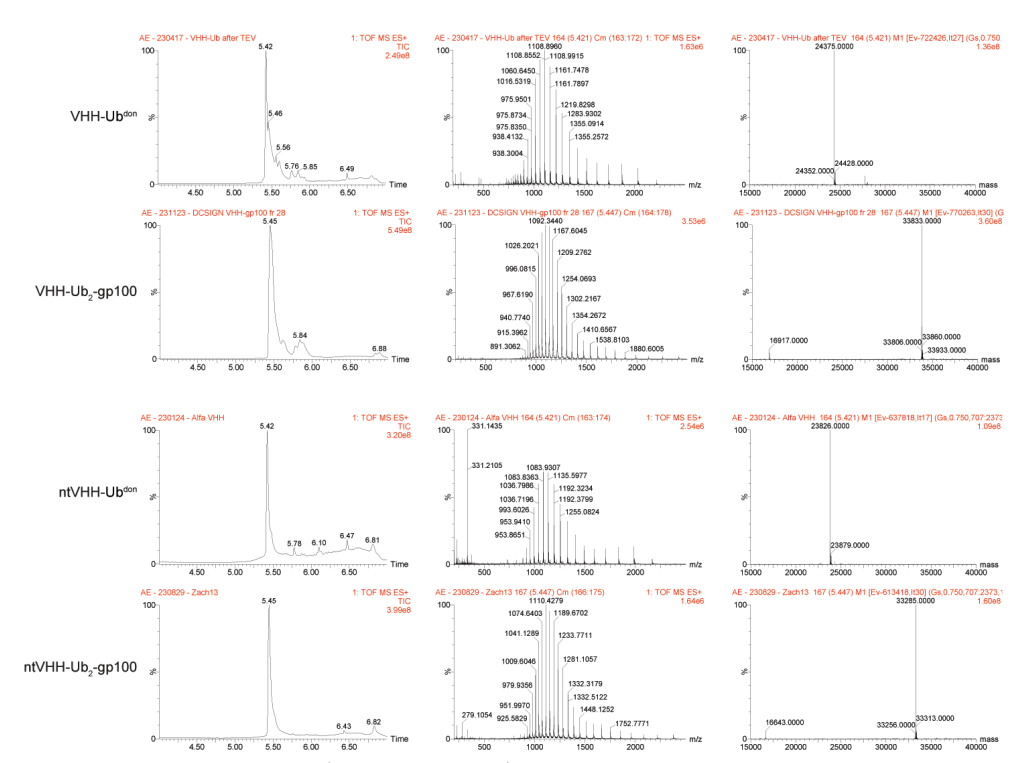
# Transfection efficiency Fig 3a



**S3** Transfection efficiency of TCR on primary CD8<sup>+</sup> T cells after 24 h. Transfection efficiency of TCR was analyzed by dextramer staining. After 24 h. transfection effeciencies were 68.5%, 69.5%, 52.2% and 59.8% for donor A, B, C and D respectively.



**S4** LC-MS analysis of VHH-Ub<sup>don</sup> and ntVHH-Ub<sup>don</sup> conjugation to Rho-Ub<sup>acc</sup> forming Rho-Ub<sub>2</sub>-VHH and Rho-Ub<sub>2</sub>-ntVHH, respectively. Total ion chromatograms (left), ESI-TOF spectra (middle) and deconvoluted ESI-TOF mass spectra (right).



**S5** LC-MS analysis of VHH-Ub $^{don}$  and ntVHH-Ub $^{don}$  conjugation to Ub $^{acc}$ -gp100p forming VHH-Ub $_2$ -gp100p and ntVHH-Ub $_2$ -gp100p, respectively. Total ion chromatograms (left), ESI-TOF spectra (middle) and deconvoluted ESI-TOF mass spectra (right).

**Table S1 VHH-Ub**<sup>don</sup> **sequences.** Table displays protein sequences of VHH-Ub<sup>don</sup> used. The N-terminal His-tag can be removed by TEV-protease to obtain the VHH-linker-ubiquitin construct. The sequence for the anti-DC-SIGN VHH was obtained in house, whereas the sequence for the anti-ALFAtag VHH was obtained from literature.

	Sequence
His-tag + TEV	MGSSHHHHHHHHHSSGENLYFQG
anti-DC-SIGN-VHH	MQVQLVESGGGLVQAGGSLRLSCVVSGRTFNLYPMGWFRQTPGKEREFVAA LSQDGLSKDYADSNGLSKDYADPVKGRFTISGDNAKHTLYLHMNSLEPDDTAV YYCASGSLLRPVSRSRTDYGYWGQGTQVTVSS
Linker-Ub <sup>don</sup>	GGGGSGGGGGGGSMQIFVKTLTGKTITLEVEPSDTIENVKAKIQDKEGIPP DQQRLIFAGRQLEDGRTLSDYNIQKESTLHLVLRLRGG*
His-tag + TEV	MGSSHHHHHHHHHSSGENLYFQG

anti-ALFAtag-VHH	MGSGDASDSEVQLQESGGGLVQPGGSLRLSCTASGVTISALNAMAMGW YRQAPGERRVMVAAVSERGNAMYRESVQGRFTVTRDFTNKMVSLQMD NLKPEDTAVYYCHVLEDRVDSFHDYWGQGTQVTVSS
Linker-Ub <sup>don</sup>	GGGGSGGGGGGGSMQIFVKTLTGKTITLEVEPSDTIENVKAKIQDKEGI PPDQQRLIFAGRQLEDGRTLSDYNIQKESTLHLVLRLRGG*

#### References

- 1. Verhaar, E. R., Woodham, A. W. & Ploegh, H. L. Nanobodies in cancer. *Semin Immunol* **52**, (2021).
- 2. Fang, T. *et al.* Targeted antigen delivery by an anti-class II MHC VHH elicits focused αMUC1(Tn) immunity. *Chem Sci* **8**, 5591–5597 (2017).
- 3. Pishesha, N. *et al.* Induction of antigen-specific tolerance by nanobody—antigen adducts that target class-II major histocompatibility complexes. *Nature Biomedical Engineering 2021 5:11* **5**, 1389–1401 (2021).
- 4. Duarte, J. N. *et al.* Generation of Immunity against Pathogens via Single-Domain Antibody-Antigen Constructs. *J Immunol* **197**, 4838–4847 (2016).
- 5. Woodham, A. W. *et al.* Nanobody-Antigen Conjugates Elicit HPV-Specific Antitumor Immune Responses. *Cancer Immunol Res* **6**, 870–880 (2018).
- 6. Cauwels, A. *et al.* Delivering type i interferon to dendritic cells empowers tumor eradication and immune combination treatments. *Cancer Res* **78**, 463–474 (2018).
- 7. Cauwels, A. *et al.* Targeting interferon activity to dendritic cells enables in vivo tolerization and protection against EAE in mice. *J Autoimmun* **97**, 70–76 (2019).
- 8. Chowell, D. *et al.* TCR contact residue hydrophobicity is a hallmark of immunogenic CD8+ T cell epitopes. *Proc Natl Acad Sci U S A* **112**, E1754–E1762 (2015).
- 9. Le Gall, C. *et al.* Efficient targeting of NY-ESO-1 tumor antigen to human cDC1s by lymphotactin results in cross-presentation and antigen-specific T cell expansion. *J Immunother Cancer* **10**, (2022).
- 10. Roscoe, B. P., Thayer, K. M., Zeldovich, K. B., Fushman, D. & Bolon, D. N. A. Analyses of the effects of all ubiquitin point mutants on yeast growth rate. *J Mol Biol* **425**, 1363–1377 (2013).
- 11. Geijtenbeek, T. B. H. *et al.* Identification of DC-SIGN, a novel dendritic cell-specific ICAM-3 receptor that supports primary immune responses. *Cell* **100**, 575–585 (2000).
- 12. Götzke, H. *et al.* The ALFA-tag is a highly versatile tool for nanobody-based bioscience applications. *Nat Commun* **10**, (2019).
- 13. Cox, A. L. *et al.* Identification of a peptide recognized by five melanoma-specific human cytotoxic T cell lines. *Science* **264**, 716–719 (1994).

- 14. Schaft, N., Lankiewicz, B., Gratama, J. W., Bolhuis, R. L. H. & Debets, R. Flexible and sensitive method to functionally validate tumor-specific receptors via activation of NFAT. *J Immunol Methods* **280**, 13–24 (2003).
- 15. Wijfjes, Z., van Dalen, F. J., Le Gall, C. M. & Verdoes, M. Controlling Antigen Fate in Therapeutic Cancer Vaccines by Targeting Dendritic Cell Receptors. *Mol Pharm* **20**, 4826–4847 (2023).
- 16. van Faassen, H. *et al.* Serum albumin-binding VHHs with variable pH sensitivities enable tailored half-life extension of biologics. *The FASEB Journal* **34**, 8155–8171 (2020).
- 17. el Oualid, F. *et al.* Chemical synthesis of ubiquitin, ubiquitin-based probes, and diubiquitin. *Angewandte Chemie International Edition* **49**, 10149–10153 (2010).
- 18. Geurink, P. P. *et al.* Development of Diubiquitin-Based FRET Probes To Quantify Ubiquitin Linkage Specificity of Deubiquitinating Enzymes. *ChemBioChem* **17**, 816–820 (2016).
- 19. Blythe, E. E., Olson, K. C., Chau, V. & Deshaies, R. J. Ubiquitin- A nd ATP-dependent unfoldase activity of P97/VCP•NPLOC4•UFD1L is enhanced by a mutation that causes multisystem proteinopathy. *Proc Natl Acad Sci U S A* **114**, E4380–E4388 (2017).
- 20. Schaft, N., Lankiewicz, B., Gratama, J. W., Bolhuis, R. L. H. & Debets, R. Flexible and sensitive method to functionally validate tumor-specific receptors via activation of NFAT. *J Immunol Methods* **280**, 13–24 (2003).
- 21. Schaft, N. *et al.* Peptide Fine Specificity of Anti-Glycoprotein 100 CTL Is Preserved Following Transfer of Engineered TCR $\alpha\beta$  Genes Into Primary Human T Lymphocytes. *The Journal of Immunology* **170**, 2186–2194 (2003).



# Total Chemical Synthesis of a Functionalized GFP Nanobody

5

Published in:

A.F. Elhebieshy\*, Y. Huppelschoten\*, et al. Total Chemical Synthesis of a Functionalized GFP Nanobody. ChemBioChem 23, e202200304 (2022).



# **Total Chemical Synthesis of a Functionalized GFP Nanobody**

Angela F. Elhebieshy, Yara Huppelschoten, Dharjath S. Hameed, Aysegul Sapmaz, Jens Buchardt, Thomas E. Nielsen, Huib Ovaa and Gerbrand J. van der Heden van Noort.

# **Abstract**

Chemical protein synthesis has proven to be a powerful tool to obtain homogenously modified proteins. The chemical synthesis of nanobodies (Nbs) would open up opportunities to design tailored Nbs with an array of chemical modifications such as tags, reporter groups, and small molecules. In this study, we describe the total chemical synthesis of a 123 amino-acid Nb targeting GFP. We applied a native chemical ligation—desulfurization strategy to successfully synthesize this GFP Nb, modified with a propargyl (PA) moiety for on-demand functionalization. Biophysical characterization indicated that the synthetic GFP Nb-PA was correctly folded after internal disulfide bond formation. Subsequently, we functionalized the synthetic Nb with either a biotin or a sulfo-Cyanine5 dye by copper(I)-catalyzed azide-alkyne cycloaddition (CuAAC) chemistry, resulting in two distinct probes. We used these probes for functional *in vitro* validation of the synthetic Nb in pull-down and confocal microscopy applications.

#### Introduction

Camelid species produce unique heavy-chain IgG antibodies consisting of a single antigen-binding variable heavy-chain domain (V,H) only, also referred to as nanobodies (Nbs).<sup>1,2</sup> These Nbs have unique properties such as their small size (~15 kD), robustness, high solubility, and monomeric nature, making them ideal for structural, cell, and developmental biology research tools.<sup>3–8</sup> Moreover, their high affinity (nM range) for targets, easy tissue penetration, and low immunogenicity make them promising candidates for new therapeutics. 9,10 Accordingly, much interest has been raised in functionalizing Nbs for various applications such as diagnostic tools, Nb-drug conjugates, and bivalent Nb conjugates. 11 Traditionally, Nbs are produced via recombinant protein expression, which easily provides functional Nbs but limits modification possibilities that are often based on using NHS- or maleimide chemistry, resulting in unselective chemical labeling that could drastically compromise the affinity of the Nb towards its target. We imagined that the chemical synthesis of a Nb would accelerate the process of generating homogeneous Nb-conjugates, considering that the chemical synthesis of proteins offers greater freedom of modification with both natural and unnatural amino acids. 12 Many functional groups suitable for chemoselective labeling could be thus easily introduced at defined, non-interfering regions of the Nb through a synthetic approach. Furthermore, since the structure of Nbs is highly conserved, it is an attractive protein for generic chemical synthesis that could pave the way for a modular synthetic approach that, with minor customization, could be broadly applied to a multitude of nanobodies. The general Nb structure comprises nine  $\beta$ -strands organized in a four- and a five-stranded  $\beta$ -sheet forming the conserved framework regions (FRs), connected via the complementarity determining region (CDR) loops and a conserved disulfide bond (Fig. 1). <sup>13,14</sup> The specificity for its target is obtained through the three CDRs at the ends of the variable domains. The long CDR3 loop contributes the most significantly to the specificity and affinity of the Nb. As a proof-of-concept, we selected a nanobody against GFP (referred to hereafter as GFP Nb), aiming to validate a synthetic approach that could prove useful within multiple applications. <sup>15</sup>

Considering the importance of the N-terminal clustering of the CDR loops in the affinity of Nbs towards their targets (Fig. 1), we envisioned that incorporating a propargyl moiety at the C-terminus would be ideal for later modifications using copper-mediated azide-alkyne cycloaddition (CuAAC) chemistry which uses mild, near physiological reaction conditions. <sup>16</sup> In this study, we present a native chemical ligation-based synthesis for the generation of a functionalizable GFP Nb. The on-demand conjugation of the synthetic Nb results in easy access to Nb-conjugates in a versatile manner. We applied this for the conjugation of either an affinity tag or a fluorescent moiety, which we used for pull-down and confocal microscopy experiments, respectively.

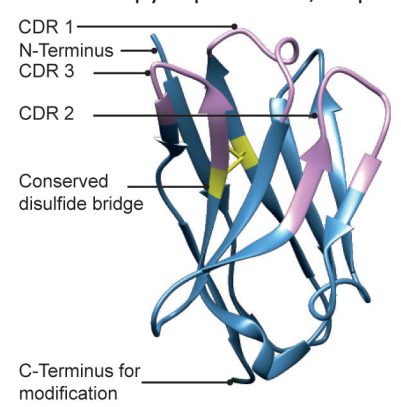


**Figure 1**| Structure of GFP Nb (PDB: 30GO). Indicated are the CDR domains in purple, the conserved disulfide bridge in yellow, and the C-terminus as a point of modification.

#### Results and discussion

#### Total chemical synthesis of GFP-Nb

Although the GFP Nb is relatively small, containing 123 amino acids, the  $\beta$ -sheet-rich structure is known to increase the likelihood of aggregation, on-resin and in-solution, during Fmoc-based solid-phase peptide synthesis (SPPS). Initial investigations proved that a three-segment NCL approach was necessary for the synthesis of the GFP Nb. The GFP Nb contains two native Cys residues, of which only one, however, is located at an appropriate potential ligation position (Cys<sub>97</sub>)(Fig. 2A). Therefore, NCL-desulfurization chemistry was chosen to assemble the Nb as an Ala-to-Cys mutation could facilitate a

NCL position that could be converted back to the native Ala using radical desulfurization post NCL. Accordingly, we envisioned using the acetamidomethyl (Acm) group to protect the other native Cys and prevent unwanted thioesterification or desulfurization during the construction of the GFP Nb. Our strategy for the synthesis of GFP Nb is outlined in Figure 2B, where we divided the polypeptide sequence into three fragments. Thioester fragment GFP Nb<sub>1-49</sub> (1), hydrazide fragment Cys-GFP Nb<sub>50-96</sub> (2), and Cys-GFP Nb<sub>97-123</sub> (4) were all prepared according to Fmoc-SPPS strategy on hydrazide or 2-chlorotrityl resins.  $^{19}$ 

Peptide **1** and **2A** were prepared as hydrazides for subsequent (*in-situ*) activation and thiolysis. Peptide **1** was synthesized with a final yield of 9 % (Fig. S1). For the synthesis and purification of peptide **2**, four pseudo-proline building blocks were incorporated during SPPS (underscored in Fig. 2A and Table S2), and the Fmoc was retained at the N-terminus of the peptide to enhance purification efficiency, resulting in 13% yield for **2A** (Fig. S2). Peptide **4** was synthesized with a GT iso-acyl dipeptide (underscored in Fig. 2A) incorporated to increase the solubility and improve the purification process, resulting in pure peptide (7% yield)(Fig. S3).

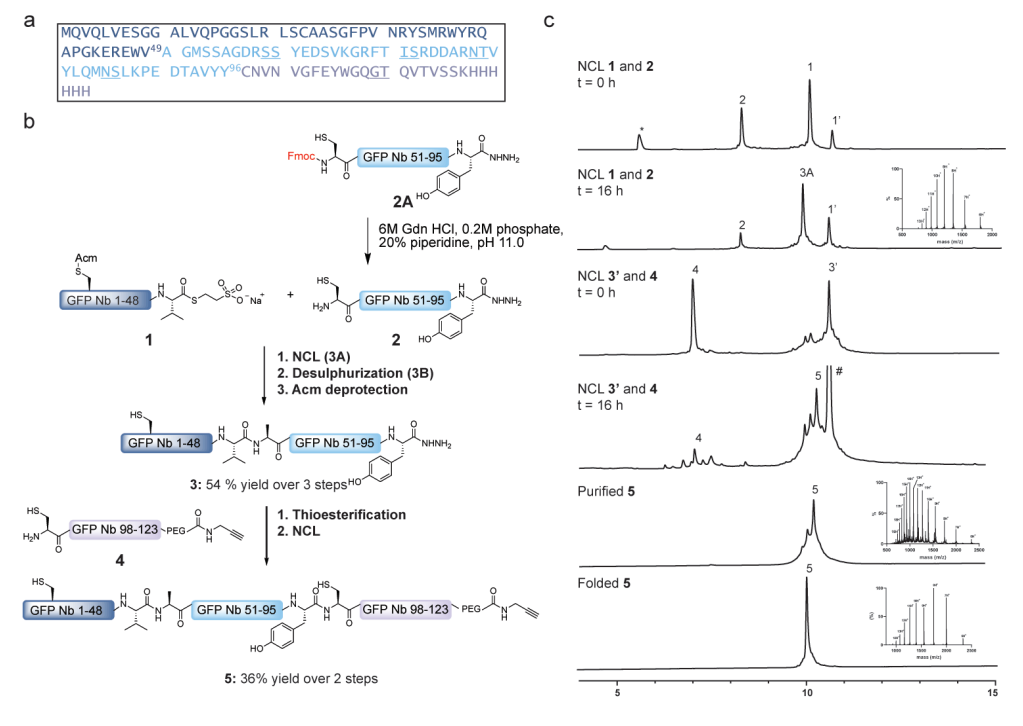


**Figure 2** (a) Sequence of GFP Nb, with underlined pseudo-proline dipeptides and iso-acyl dipeptides used in SPPS. (b) Synthetic strategy for obtaining GFP Nb. The complete synthetic approach is shown in Scheme S1-5 in the supplementary information. (c) UPLC analysis of the NCL of 1 and 2, the NCL of 3 and 4, purification of 5 and folding of 5. 'indicated MPAA thioesters, \* indicates dibenzofulvene adduct, # indicates MPAA disulfide adduct.

For the NCL of peptide **1** with peptide **2**, we used a one-pot Fmoc deprotection and NCL strategy described by Kar et al.<sup>20</sup> via *in-situ* preparation of **2** from **2A** (Fig. 2C, S4 and S5). After NCL between **1** and **2**, the Cys residue in the resulting conjugate was desulfurized to yield the native Ala residue, followed by an Acm deprotection step to liberate the N-terminal Cys leading to **3**. The one-pot thioesterification of **3** and ligation to **4**, yielded final GFP Nb product **5** that was obtained in 36% yield after HPLC purification (Fig. 2C, Fig.S8-9).

#### Chemically synthesized GFP Nbs show comparable folding to expressed GFP Nbs

With the full-length GFP  $Nb_{1-123}$ -linker-PA in hand, we continued to the folding step, including disulfide bond formation. The folding was carried out by stepwise dialysis in phosphate buffered saline (PBS). Spontaneous disulfide formation did not occur within 48 hours in PBS, so 2,2'-Dithio-dipyridin (DTP) $^{21,22}$ , a known disulfide bond formation accelerator, was added. Indeed, after the addition of 1 mM DTP to the folding buffer, initiation of disulfide bond formation was observed after 1 hour and completed within 16 hours, as observed in the high-resolution mass spectrum by the loss of 2 Da (Fig 3A, 3B and S10). To confirm the proper folding of the chemically synthesized and folded GFP Nb (5), we conducted circular dichroism (CD) experiments. The synthetic GFP Nb exhibited absorptions of  $\beta$ -sheet structures similar to the recombinantly expressed GFP Nb<sup>15</sup>, indicating that their folding is comparable (Fig. 3C).

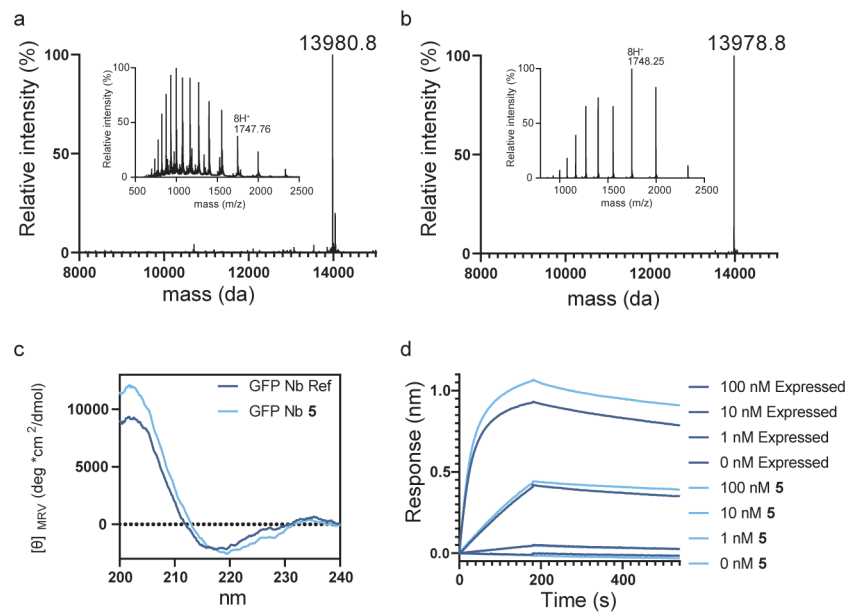


**Figure 3** (a) Deconvoluted mass spectrum and ESI Mass spectrum (inset) of unfolded 5. (b) Deconvoluted mass spectrum and ESI Mass spectrum (inset) of folded 5. (c) Circular dichroism spectra comparing recombinant and synthetic GFP Nb. (d) Bio Layer Interferometry analysis of folded 5 in comparison to expressed GFP Nb.

# Chemically synthesized GFP Nbs retain antigen-binding affinity

To determine the affinity of the synthetic GFP Nb **5** to its target protein GFP and compare it to that of the recombinantly expressed GFP Nb, biolayer interferometry (BLI) experiments were performed. The C-terminal His-tag on both the expressed and synthetic Nb was used to immobilize the Nbs on Ni-NTA biosensor tips, and untagged GFP was used as the analyte at concentrations ranging from 1 nM to 100 nM. With this setup, the expressed and synthetic GFP Nb showed similar binding profiles (Fig 3D) and affinities of 1.12 and 1.11 nM, respectively. These values are in agreement with previously reported data in literature (1.4 nM).<sup>15</sup>

#### On-demand functionalization of GFP Nb-PA

Next, we wanted to show the adaptability of the fully synthetic Nb as a chemical tool by modifying the C-terminal propargyl moiety using a bio-orthogonal labeling strategy. Accordingly, we used copper(I)-catalyzed alkyne-azide cycloaddition (CuAAC) chemistry to functionalize the synthetic Nb with an azide-functionalized biotin molecule for the purpose of pull-down experiments (Fig. 4A). Unfolded, purified 5 was reacted with biotin-azide using mild reaction conditions (3 mM CuSO,, 10 mM sodium ascorbate, and 2 mM tris-(hydroxypropyltriazolylmethyl)amine (THPTA)) to form the GFP Nb-biotin conjugate (6) (Fig. S11). After the CuAAC, the synthetic Nb was folded as described previously for compound 5, removing all additives from the CuAAC reaction during the dialysis step. In addition, we envisioned that modification of 5 with sulfo-Cyanine5azide (Cy5) would lead to the opportunity to validate the proper functioning and target binding of our Nb by co-localization of the Nb with GFP-tagged proteins in cells using confocal microscopy. Hence, we used the same procedure to synthesize a GFP Nb-Cy5 conjugate (7)(Fig. S12). Next, we measured CD to warrant the correct folding of the functionalized Nbs (Fig. 4B, S13) and continued with CD denaturing experiments to investigate the stability of the synthetic Nb-conjugates carrying two different payloads compared to the expressed GFP Nb. Both Nb-conjugates showed a similar denaturing pattern as the expressed GFP Nb, indicating that the introduction of C-terminal cargo onto the Nb did not alter its biophysical properties (Fig. S14-S16).

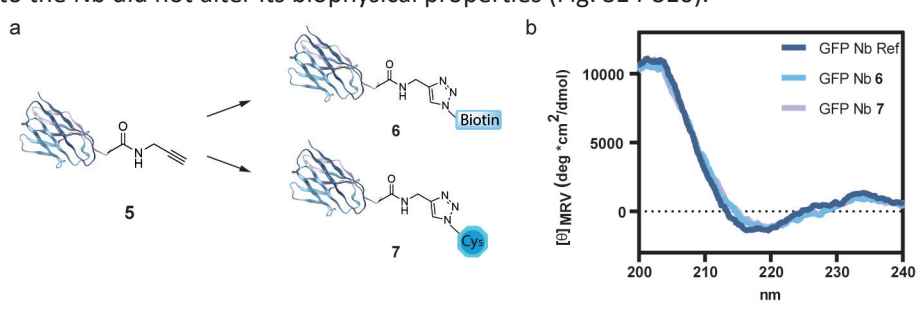


**Figure 4** (a) Functionalization of synthetic Nb 5. Nanobody structure PDB:3OGO17 (b) Circular Dichroism of expressed GFP Nb, synthetic GFP Nb conjugates 6 and 7.

# Synthetic GFP Nb is functional as an in vitro research tool

Next, we wanted to assess the functionality of Nb conjugates **6** and **7** as research tools in *in vitro* assays for the recognition of GFP-labeled proteins. First, we set out to validate the binding of the synthetic GFP Nb to GFP-fusion proteins in a complex protein mixture by performing a pull-down assay. For this purpose, we decided to use the MelJuSo cell line established in our lab<sup>23</sup> that stably expresses GFP-tagged small GTPase Rab7, a central regulator of membrane trafficking in multiple directions.<sup>24</sup> Hence, we incubated the GFP Nb-biotin conjugate (**6**) with cell lysate of MelJuSo cells expressing GFP-Rab7 to perform a pull-down assay. To ensure GFP-specific binding, we used WT MelJuSo cells that did not express GFP-Rab7 as a negative control. After two hours of incubating conjugate **6** with the cell lysates of both GFP-Rab7 MelJuSo or WT MelJuSo, we were able to selectively pull down the GFP-Rab7 protein from the cell lysate showing a signal around 55 kDa, equal to the molecular weight of GFP-Rab7 (Fig. 5A). Negligible background signal confirms the selectivity of the synthetic GFP Nb for GFP over other proteins present in the cell lysate (Fig. S18).

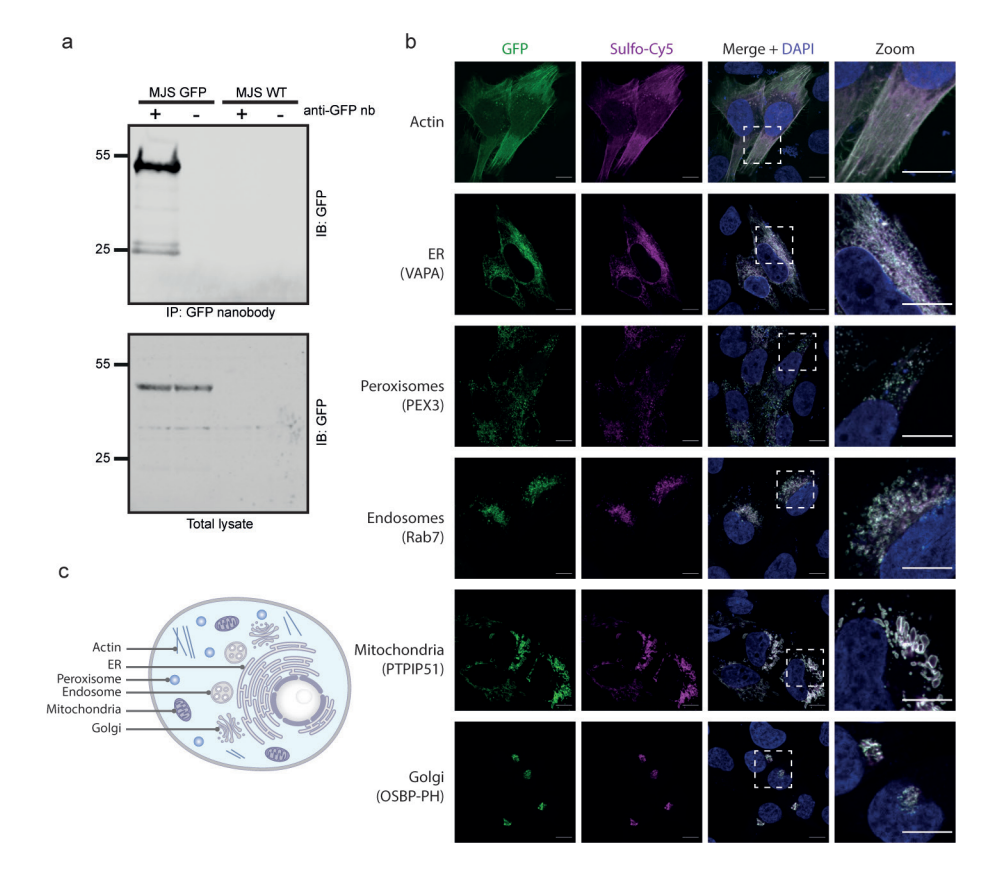


**Figure 5** (a) Western blot analysis of the pull-down of GFP-Rab7 from cell lysate using GFP Nb-biotin conjugate 6. The signal around 25 kDa is GFP as a result of protein degradation. (b) Confocal images of MelJuSo cells expressing GFP-Rab7 in the presence of GFP Nb-Cy5 7. (c) Illustration of a cell highlighting the cellular compartments visualized in B.

We also tested the synthetic GFP Nb in a confocal microscopy setting, where we used GFP Nb-Cy5 conjugate **7** to examine co-localization with GFP-tagged proteins located in different cellular compartments (cytoskeleton, endoplasmic reticulum (ER), peroxisomes, endosomes, mitochondria, and golgi). For this, MelJuSo cells were transfected with six different plasmids encoding for GFP tagged Actin, VAMP-Associated Protein A (VAPA), Peroxisomal biogenesis factor 3 (PEX3), Rab7, Protein tyrosine phosphatase interacting protein 51 (PTPIP51) and Oxysterol binding protein (OSBP-PH) proteins (Fig. 5B and C). The cells were fixed, and the membranes were permeabilized before incubation with the conjugate **7** for 1 hour. The incubation of the transfected MelJuSo cells with **7** resulted in a complete overlap between the GFP signal and the Cy5 signal, indicating the colocalization of the synthetic Cy5-Nb with the GFP tagged proteins (Fig. 5B). The staining with conjugate **7** resulted in a strong signal in each of the tested cell compartments with minimal background, indicating full target engagement of our synthetic Nb (Fig. 5B). The ability to visualize GFP fusion proteins at various cellular locations further efficiently showcases the broad applicability of the synthetic Nb.

#### Conclusion

In conclusion, we have developed a practical native chemical ligation-based synthetic approach for the generation of a synthetic GFP Nb ready for on-demand functionalization. With this method, we can obtain homogenous batches of labeled Nb by selectively labeling the Nb using CuAAC without altering the properties of the Nb, such as folding or thermo-stability. This technology was successfully applied to modify the GFP-Nb with either a biotin or a fluorophore, which were used in pull-down and confocal microscopy experiments, respectively. The Nb labeling is performed without compromising the antigen-binding site, making this method also applicable for Nbs containing a Cys residue in their CDR domains, that could be jeopardized during conventional maleimide based modification strategies. In addition, easy modification of the CDR3 domain can be obtained because it is introduced in one of the final synthesis steps in our native chemical ligation based synthesis scheme. We envision that with this protocol in hand, Nbs against other targets can be synthesized using a similar strategy due to the high sequence and structure similarities between Nbs. This methodology could potentially also be applied to the streamlined preparation of Nb drug-conjugates or (heterogeneous) Nb multimers. Moreover, unnatural amino acids can be easily introduced through the SPPS protocol, e.g. to confer stability of the Nb against degradation in vivo and broaden the applicability of this protein scaffold. 25,26

# **Methods**

#### **General procedures**

# **Materials and solvents**

Reagents were obtained from Sigma-Aldrich of the highest available grade and used without further purification. Standard Fmoc-protected amino acid derivatives were used and purchased from Gyros Protein Technologies unless mentioned otherwise. Fmoc-Cys(Acm)-OH and resins for SPPS were obtained from Novabiochem (Merck Millipore), Apigenex and PCAS Biomatrix. Pseudo-proline dipeptides were obtained from Corden Pharma or Bachem. Iso-acyl dipeptides were obtained from AAPPTec. Solvents for SPPS were obtained from Biosolve. VA-044 was procured from Wako Pure Chemical Corporation. Oxyma Pure® was purchased from Gyros Protein Technologies. HPLC grade acetonitrile was obtained from Merck.

#### **Analytical methods**

#### LC-MS conditions

LC-MS measurements were performed on a Waters Acquity UPLC H Class system, Waters Xevo G2-XS QTof with a Waters Acquity BEH 300 Å, C4, 1.7  $\mu$ m, 2.1 mm x 50 mm (0.4 mL/min). Samples were run at 60 °C using 3 mobile phases: A = 0.1 % formic acid in MilliQ water, B = 0.1 % formic acid in acetonitrile and C = 0.01 % TFA in MilliQ water with a gradient of 5 to 25% B over 1 min, 25 to 65 % B over 6 min followed by 65 to 95 % B over 0.5 min maintaining a composition of 5% C throughout. Data processing was performed using Waters MassLynx Mass Spectrometry Software V4.2 (deconvolution with MaxEnt I function).

# **Analytical UPLC conditions**

UPLC measurements were performed on a Waters Acquity UPLC H Class system with a Waters Acquity BEH 300 Å, C4, 1.7  $\mu$ m, 2.1 mm x 100 mm (0.4 mL/min). Samples were run at 40 °C using 2 mobile phases: A = 0.05 % TFA in MilliQ water and B = 0.05 % TFA in acetonitrile with a gradient of 5 to 50 % B over 20 min followed 50 to 95% B over 0.5 min. Data processing was performed using Empower software.

#### Quantification

# **Charged Aerosol Detection (CAD)**

Purified samples were quantified using a Thermo Scientific Vanquish, Corona Veo CAD. Samples were run on a Acquity BEH 300 Å, C4, 1.7  $\mu$ m, 2.1 mm x 50 mm at 40 °C using 2 mobile phases: A = 0.1 % TFA in MilliQ water and B = 0.1 % TFA in acetonitrile with a gradient of 0 to 80 % B over 7 min.

# Solid Phase Peptide Synthesis (SPPS) Preloading 2-chlorotrityl resin

2-Chlorotrityl resin (0.57 mmol/gram) was swollen in dry DCM for 30 minutes. A solution of Fmoc-AA-OH (1 equiv.) in dry DCM and DIPEA (4 equiv.) was added, and the resin was shaken for 30 minutes. The resin was washed with DCM twice before capping the remaining trityl groups with methanol/DIPEA/DCM 17:2:1, v/v/v. The resin was dried *in vacuo* prior to the determination of the estimated loading of the first amino acid.

#### **Automated Fmoc SPPS**

SPPS was performed on a Symphony X (Gyros Protein Technologies) automated peptide synthesizer using standard 9-fluorenylmethoxycarbonyl (Fmoc) based SPPS. Fmoc deprotection was achieved with 2 x 10 min. treatment of 20 vol. % piperidine, 0.1 % Oxyma Pure® in DMF. Peptide couplings were performed using DIC/Oxyma. Amino acid/Oxyma solutions (0.3 M/0.3 M in DMF) were added to the resin at 4-6-fold excess together with equal equivalents of DIC (1.5 M in DMF). The coupling time was 2 hours unless specified otherwise. All dipeptide building blocks were coupled for 4 hours. The residual free amino groups after the coupling reaction were capped by the addition of collidine (3.3 equiv., 1.5 M in DMF) and acetic anhydride (11 equiv., 1.0 M in DMF) and were reacted for 20 minutes. After the final Fmoc deprotection the resin was washed with DMF and DCM.

#### Global deprotection from the resin and side chain deprotection

Polypeptide sequences containing a cysteine residue were detached from the resin and deprotected by treatment with Reagent K (TFA/phenol/H<sub>2</sub>O/thioanisole/EDT, 82.5:5:5:5:2.5 v/v/v/v/v) for 2-3 hours followed by precipitation in ice cold diethylether and collection by centrifugation. Polypeptide sequences containing methionine residues were detached from the resin and deprotected by treatment with TFA/TIPS/H<sub>2</sub>O/DCM/NH<sub>4</sub>I/DTT, 87:5:2.5:2.5:0.5:2.5, v/v/v/v/v for 2-3 hours followed by precipitation in ice cold diethylether and collection by centrifugation. The pellet was resuspended in diethylether before being collected by centrifugation again. The pellet was dissolved and lyophilized from H<sub>3</sub>O/CH<sub>3</sub>CN/AcOH, 65:25:10, v/v/v before purification.

# **Preparative HPLC purification**

Preparative purification was performed on a Gilson HPLC system using a reversed phase HPLC column as specified in the experimental section. Elution was performed using 2 mobile phases: A =  $0.1\,\%$  TFA in MilliQ water and B = 0.1% TFA in acetonitrile using a linear gradient. Fractions were collected using a Gilson fraction collector. Relevant fractions were assessed by LC-MS and pure peptide was pooled and lyophilized.

# Nanobody characterization

The construct for GFP Nb was obtained from addgene (49172) and expressed as described previously by Kubala et al.<sup>15</sup> In brief, protein expression was conducted in E. coli strain BL21(DE3) in a flask containing LB medium and grown to an OD<sub>600</sub> of 0.5 at 37°C, and then, protein expression was induced using 0.5 mM IPTG. Further fermentation was carried out at 20°C for 20 h. Resultant cell mass was harvested by centrifugation, disrupted by sonication, and subjected to centrifugation to remove cell debris. The cleared cell lysate was subjected to HisTrap affinity purification followed by size-exclusion fractionation (Superdex 75) using an Akta Purifier FPLC system (GE Healthcare).

# Cell culture and pull-down of overexpressed GFP-Rab7

MelJuSo (human melanomas) cell lines stably expressing GFP-Rab7 were kindly gifted by A. Sapmaz (LUMC, Leiden) and WT MelJuSo cells, kindly provided by Prof. G. Riethmuller (LMU, Munich).  $^{23}$  The cells were lysed in lysis buffer (0.8 % NP40, 150 mM NaCl, 50 mM Tris-HCl pH 8.0, 0.05 mM MgCl $_{\rm 2}$  + protease inhibitor) followed by brief sonication. Cell debris was removed by centrifugation. Next, 5 µg of biotin tagged synthetic GFP Nb was added to cell lysates of both GFP-Rab7 expressing cells and WT cells and incubated by rotating for 2 hours at 4 °C. Thereafter, high capacity neutravidin beads (Thermo Scientific, Cat# 29202) were added and incubated by rotating for 1 hour at 4 °C. The beads were extensively washed with lysis buffer and after completely removing the washing buffer, SDS sample buffer supplemented with 2-mercaptoethanol was added to the beads and boiled at 95°C. The proteins were separated by SDS-PAGE followed by western blotting and detection by ponceau s followed by antibody staining using rabbit anti-GFP antibody  $^{27}$  followed by IRDye 800CW goat anti-rabbit IgG (H + L) (Li-COR, Cat# 926-32211). The signal was detected using direct imaging by the Odyssey Classic imager (LI-COR).

#### Confocal microscopy

MelJuso cells were seeded into 24-well plates containing glass coverslips to achieve 40-50% confluency the following day. Cells were transfected with the DNA plasmids in table 1 using X-tremeGENE HP (Roche Cat# XTGHP-RO) according to manufacturer's instruction and cultured for 18-24 hours. Next, the cells were fixed in 3.7% formaldehyde in PBS for 20 min and subsequently permeabilized using 0.1% Triton X-100 in PBS for 10 min. After permeabilization, cells were blocked using 5% (w/v) skim milk powder in PBS for 30 min and incubated with 1  $\mu$ g Cy5-labelled synthetic Nb (7) in blocking buffer for 1 hour at RT. Next, cells were washed and mounted using ProLong Gold antifade Mounting medium with DAPI (Life Technologies, Cat# P36941). Samples were imaged using Leica SP5 or SP8 microscopes equipped with appropriate solid-state lasers, HCX

PL 63x magnification oil emersion objectives and HyD detectors. Image processing and co-localization analyses were performed using the Fiji software.

Table 1. DNA plasmids used for transfection with the corresponding protein.

Protein	Cell compart- ment	Plasmid	Reference and cloning
RAB7A	Endosomes	GFP-RAB7A	28
VAMP-Associated Protein A (VAPA)	ER	GFP-VAPA	29
Peroxisomal biogenesis factor 3 (PEX3)	Peroxisomes	PEX3*-SBP-GFP	PEX3*-SBP-GFP was a gift from Juan Bonifacino  (Addgene plasmid # 120174).30
Protein tyrosine phosphatase interacting protein 51 (PTPIP51)	Mitochondria	PTPIP51-GFP	PTPIP51 ORF was cloned into GFP-C1 vector from PTPIP51-RFP using HindIII and BamHI restriction enzymes. <sup>29</sup>
Oxysterol binding protein (OSBP-PH)	Golgi	EGFP-OSBP-PH	EGFP-OSBP-PH was a gift from Marci Scidmore (Ad- dgene plasmid # 49571). <sup>31</sup>
LifeAct	Actin filaments	Lifeact-EGFP	Addgene Plasmid # 58470

# **Bio Layer Interferometry-measurements**

BLI measurements were performed on an OctetRed system (ForteBio). 100 nM of the expressed GFP Nb or the synthetic GFP Nb were loaded on Ni-biosensors for 2 minutes and washed in binding buffer (phosphate-buffered saline (PBS), 0.05 % Tween-20, 0.01 % BSA, pH 7.4). Thereafter, the sensors were transferred into solutions containing varying concentrations of GFP (100 - 1 nM) to measure the association of the analyte for 3 minutes. Subsequently, the dissociation of the complex was measured in binding buffer for 6 minutes. Dissociation constants (Kd) were calculated using the ForteBio Data Analysis software by co-fitting all concentrations simultaneously.

# **Acknowledgments**

We would like to thank Dr. Birol Cabukusta at the LUMC for plasmids used for confocal microscopy experiments. YH acknowledges funding from the European Union's Horizon 2020 research and innovation programme under the Marie Skłodowska-Curie grant agreement No 765445 (ITN UbiCODE), AFE acknowledges funding by ICI (grant No ICI00013) and GJvdHvN acknowledges funding by NWO (VIDI grant VI.192.011).

# **Supplementary information**

# **Synthesis strategy**

**Scheme S1.** Complete synthetic approach towards synthetic GFP Nb using NCL-desulfurization chemistry.

# Sequences GFP Nanobody:

- 1 MQVQLVESGG ALVQPGGSLR LSCAASGFPV NRYSMRWYRQ
- 41 APGKEREWVA GMSSAGDRSS YEDSVKGRFT ISRDDARNTV
- 81 YLQMNSLKPE DTAVYYCNVN VGFEYWGQGT QVTVSSKHHH HHH

**Table S2.** Amino acid sequences of the Nb fragments, psuedoprolines are underscored and iso-acyl dipeptides in bold.

Segment ID	SPPS sequence
GFP 1-48	$\label{eq:h-mqvqlvesggalvqpggslrlsc} \mbox{H-mqvqlvesggalvqpggslrlsc(acm)} \mbox{Aasgfpvnrysmrwyrqapg-} \\ \mbox{Kerewv-nhnh}_{\mbox{\scriptsize 1}} $
Fmoc-GFP 49-96	H-CGMSSAGDR <u>SS</u> YEDSVKGRFT <u>IS</u> RDDAR <u>NT</u> VYLQM <u>NS</u> LKPEDTAVYY-NHNH <sub>2</sub>
GFP 98-123 OEG	H-CNVN <u>VG</u> FEYWGQ <b>GT</b> QVTVSSKHHHHHHHX-OH

X was incorporated as a Fmoc-Peg2-OH. Underlined dipeptide sequences were coupled as the respective pseudoproline dipeptides or DMB dipeptides. Italic dipeptides were coupled as the respective iso-acyl dipeptides.

# Preparation of peptide fragments Synthesis of GFP 1-48 thioester 1

The synthesis was performed following general procedures using 2-chlorotrityl hydrazine resin (1.0 gram, 0.32 mmol/gram). The peptide was cleaved from the resin according to the general procedures and purified by preparative HPLC using a Phenomenex, Luna 100 Å, C8(2), 10  $\mu$ m, 30 mm x 250 mm column (25 to 35%B over 20 min, 30mL/min). Peptide 1 was dissolved in 45 mL of 6 M Gdn.HCl pH 3.0 and 1 M NaNO $_2$  in MilliQ (3.2 mL, 3.2 mmol, 10 equiv.) was added and stirred for 15 min at 0 °C. The reaction was warmed to room temperature and MESNa (5.1 gram, 32 mmol, 100 equiv.) in 6 M Gdn.HCl, 0.2 M phosphate pH 7.0 was added. The pH was adjusted to pH 7.0 and the solution was stirred for 60 min. before purification by preparative RP-HPLC using Phenomenex, Luna 100 Å, C8(2), 10  $\mu$ m, 30 mm x 250 mm (22 to 32 % B over 45 min, 30mL/min) followed by lyophilization afforded peptide 1 as a white solid (171.6 mg, 9.3 % yield).

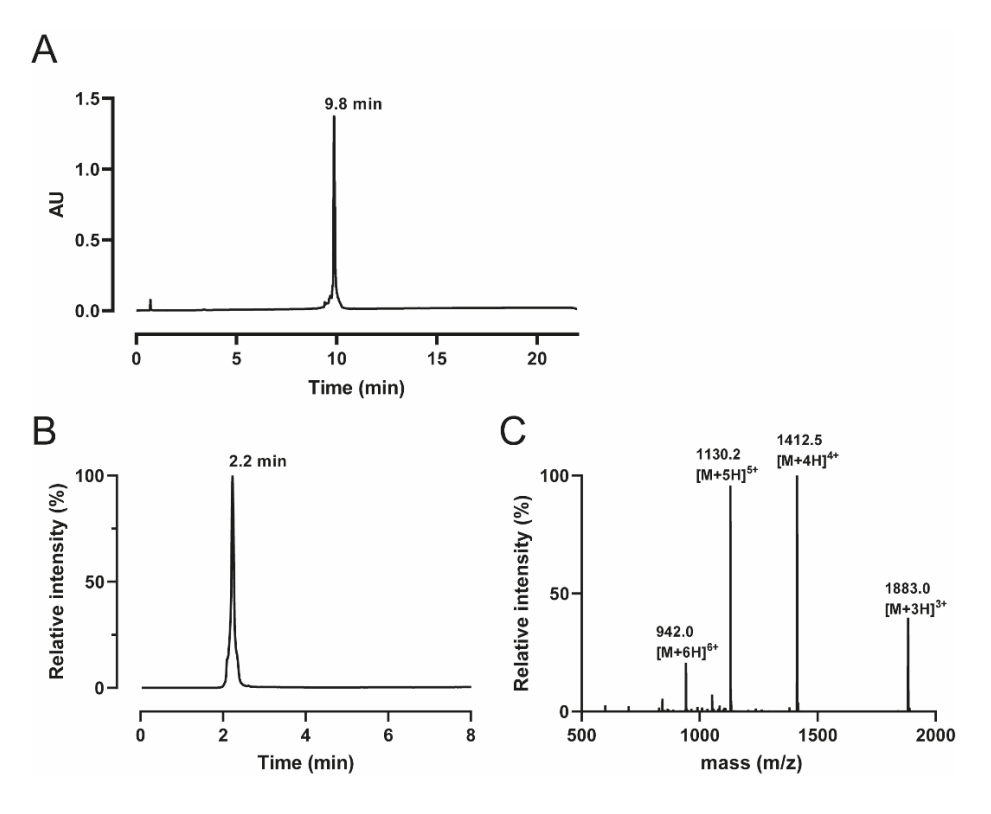


**Figure S1.** (A) UPLC UV chromatogram of purified 1, Rt 9.86 min. (B) Total ion chromatogram (LC-MS method C4) of purified 1, Rt 2.23 min. (C) Observed ESI spectrum of purified 1. Calculated Mass (average isotope composition): 5645.74; Observed:  $[M + 3H]^{3+}$ : 1882.9,  $[M + 4H]^{4+}$ : 1412.4,  $[M + 5H]^{5+}$ : 1130.1,  $[M + 6H]^{6+}$ : 941.9.

# Synthesis of Fmoc-GFP 49-96 hydrazide 2A

The synthesis was performed following general procedures using 2-chlorotrityl hydrazine resin (1.27 gram, 0.32 mmol/gram). The peptide was cleaved from the resin according to the general procedures and purified by preparative RP-HPLC using a Phenomenex, Luna 100 Å, C8(2), 10  $\mu$ m, 30 mm x 250 mm column (26 to 33 % B over 40 min, 30 mL/min) followed by lyophilization afforded peptide **2A** as a white solid (296.6 mg, 13.2% yield).

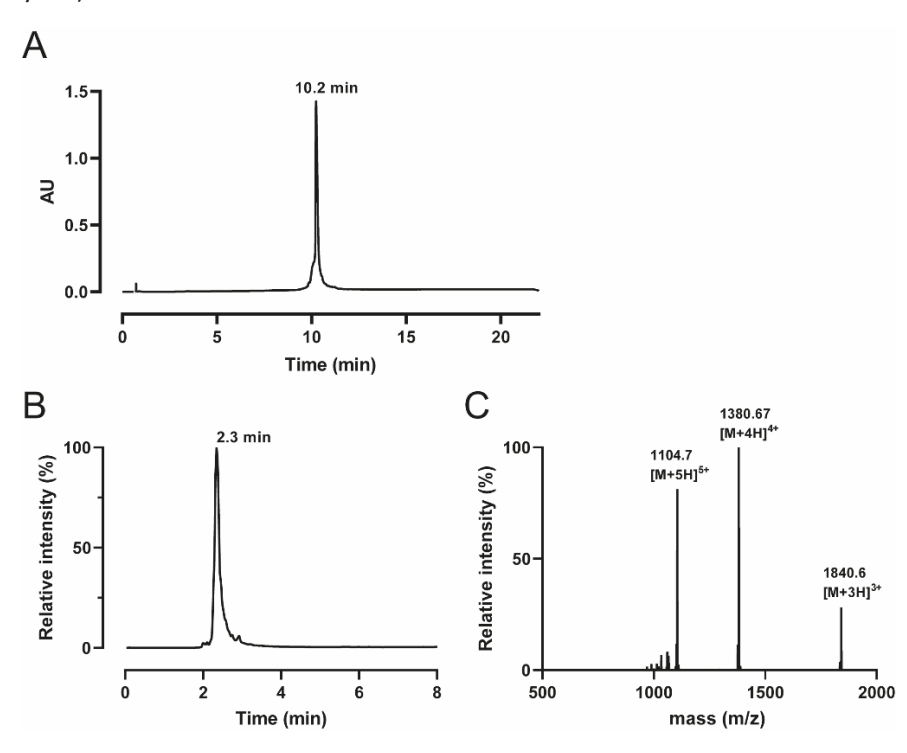


**Figure S2.** (A) UPLC UV chromatogram of purified 2A, Rt 10.23 min. (B) Total ion chromatogram (LC-MS method C4) of purified 2A, Rt 2.35 min. (C) ESI spectrum of purified 2A. Calculated Mass (average isotope composition): 5518.53; Observed: [M + 3H]<sup>3+</sup>: 1840.51, [M + 4H]<sup>4+</sup>: 1380.63, [M + 5H]<sup>5+</sup>: 1104.71.

# Synthesis of GFP 98-123 propargyl amide 4A

The synthesis was performed following general procedures using Fmoc-OEG preloaded CTC resin (1.45 gram, 0.2 mmol/gram). The amino acids colored in red were coupled using single 6 hours coupling. For the underlined amino acids in the sequence an isoacyl dipeptide Boc-Thr(Fmoc-Gly)-OH was coupled following the general procedures. The iso-acyl dipeptide was incorporated to increase solubility of the peptide during purification.

#### **CNVNV**GFEYWGQGTQVTVSSKHHHHHH

The protected polypeptide was cleaved from the resin by treatment with 3 x 15 mL of DCM/HFIP 7:3 v/v for 15 min and filtered. The combined filtrates were concentrated *in vacuo* and co-evaporated with DCM 3x and dried under high vacuum. The protected peptide (1 equiv.) was dissolved in DCM (10 mL) and propargylamine (75  $\mu$ L, 1.16 mmol, 4 equiv.) was coupled using PyBOP (597 mg, 1.16 mmol, 4 equiv.) and DIPEA (396  $\mu$ L, 2.32 mmol, 8 equiv.) for 16 hours. Thereafter, the solvents were removed *in vacuo* and the protecting groups was cleaved according to the general procedures. The crude peptide was purified by RP-HPLC using Phenomenex, Gemini® 110 Å, C18, 5  $\mu$ m, 30 mm x 250 mm column (15-35 % B over 20 min, flow 30 mL/min) and lyophilized to afford the desired peptide (65.07 mg, 6.7 % yield).

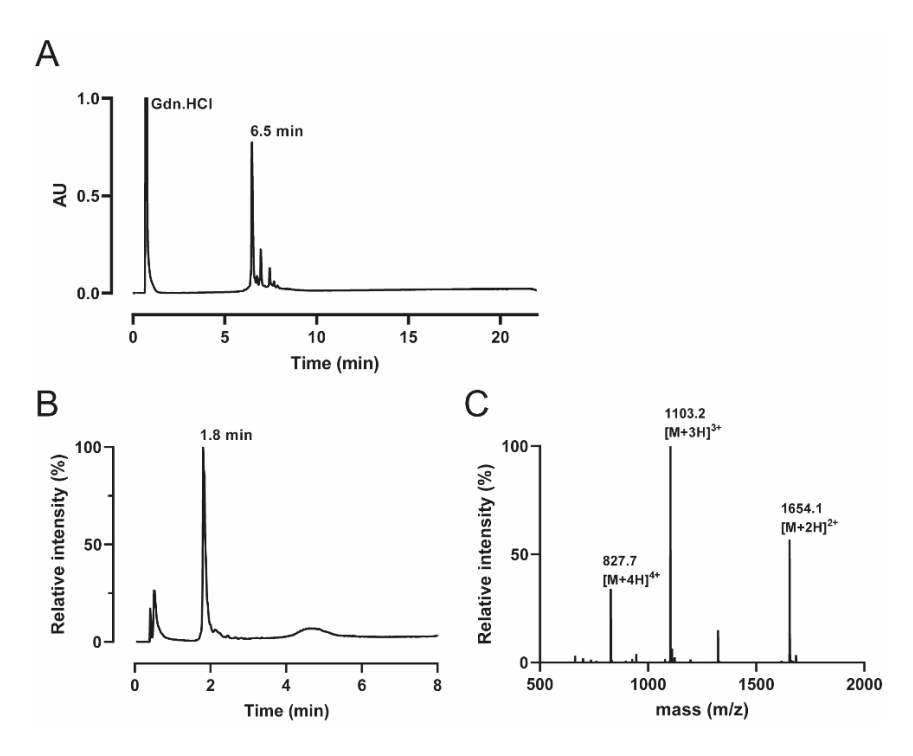


**Figure S3.** (A) UPLC UV chromatogram of purified 4, Rt 6.53 (B) Total ion chromatogram (LC-MS method C4) of purified 4, Rt 1.8 min. (C) ESI spectrum of purified 4. Calculated Mass (average isotope composition): 3306.52; Observed: [M + 2H]<sup>2+</sup>: 1654.26, [M + 3H]<sup>3+</sup>: 1103.17, [M + 4H]<sup>4+</sup>: 827.63

# Assembly of GFP Nb

# One-pot Fmoc deprotection and ligation for the assembly of 3

Scheme S2. Fmoc deprotection of 2A.

A solution of **2A** (73.56 mg, 13.3 µmol) was prepared in 6 M Gdn.HCl, 0.2 M phosphate pH = 7.0 (5 mL), then 406 µL of conc. HCl was added and finally 1375 µL of piperidine, final pH of 10.7. The reaction mixture was shaken (350 rpm) for 10 min before the pH was adjusted to pH 7.0. The reaction progress was assessed by analyzing a small sample by LC-MS. Analysis revealed complete Fmoc deprotection within 10 min. to afford compound **2** in solution.

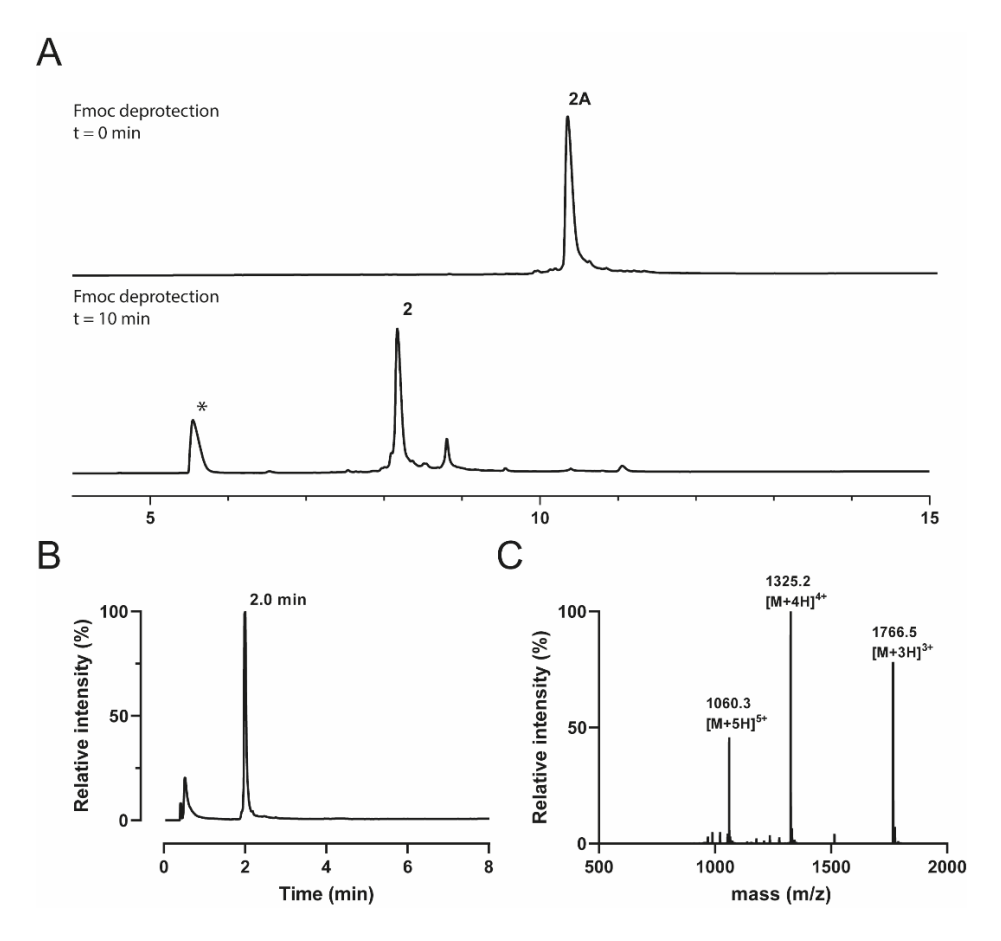
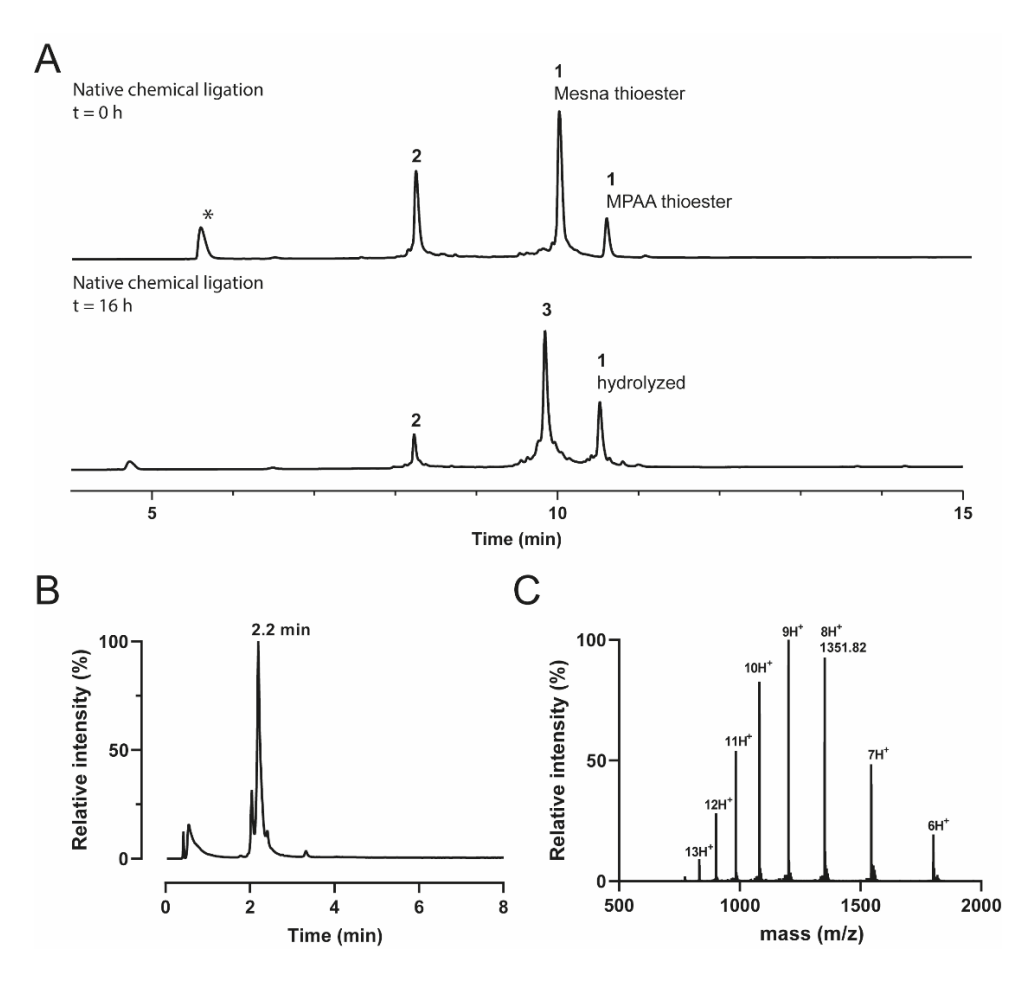


Figure S4. (A) UPLC UV chromatogram of the Fmoc deprotection of 2At = 0 min. (top chromatogram) and t = 10 min. (bottom chromatogram). \*dibenzofulvene-piperidine adduct (B) Total ion chromatogram (LC-MS method C4) of 2, Rt 2.0 min. (C) ESI spectrum of 2. Calculated Mass (average isotope composition): 5296.46; Observed:  $[M + 3H]^{3+}$ : 1766.48,  $[M + 4H]^{4+}$ : 1325.11,  $[M + 5H]^{5+}$ : 1060.29.

Scheme S3. Ligation of peptides 1 and 2 followed by desulfurization and Acm deprotection to assemble peptide 3.

Next peptide 1 (60.51 mg, 0.01286 mmol) was added as a solid to the reaction mixture containing 2. MPAA (186.4 mg, 1.1 mmol, 100 equiv.) was dissolved in 400 µL of 4 M NaOH and added to the reaction mixture and TCEP was added to a final concentration of 25 mM. The final pH was adjusted to 7.0 and the reaction was shaken for 16 hours at 37 °C upon which LCMS analysis showed that the reaction was complete. The MPAA was removed using a 3 kDa cut-off spin filter until LCMS no longer showed presence of MPAA. To the 6 M Gdn.HCl, 0.2 M phosphate pH = 7.0 solution (3 mL), 0.5 M TCEP in water (3 mL) was added and the solution was degassed with argon. To this solution glutathione (101.5 mg, 50 mM) and VA-044 (57 mg, 25 mM) were added and the reaction mixture was shaken at 40 °C for 18 hours at final pH 6.5. To afford peptide 3 in 101.6 mg with a 88 % yield over 2 steps. The buffer was exchanged again using a 3 kDa cut-off spin filter to 6 M Gdn.HCl, 0.2 M phosphate pH 7.0. Next PdCl<sub>3</sub> (29.6 mg, 20 equiv.) was added, and the reaction was shaken at 40 °C for 1 hour. To quench the reaction DTT (137.3 mg, 100 equiv.) was added and the solution was centrifuged. The supernatant was purified on an Äkta system using a HiLoad 26/600 Superdex 75 pg column (flow: 1 mL/min) to obtain GFP 1-96 in a solution of 6 M Gdn.HCl, 0.2 M phosphate, pH 7.0 (9.6 mg/mL, 62.2 mg, 61.7 % yield over 4 steps).

All concentrations/amounts were determined using CAD as described in the general protocols.



**Figure S5.** (A) UPLC UV chromatogram of the NCL of 1 and 2, t = 0 h (top chromatogram) and t = 16 h (bottom chromatogram). \*dibenzofulvene-piperidine adduct (B) Total ion chromatogram (LC-MS method C4) of 3, Rt 2.2 min. (C) ESI spectrum of 3. Calculated Mass (average isotope composition): 10800.22; [M + 6H]<sup>6+</sup>: 1801.04, [M + 7H]<sup>7+</sup>: 1543.89, [M + 8H]<sup>8+</sup>: 1351.03, [M + 9H]<sup>9+</sup>: 1201.02, [M + 10H]<sup>10+</sup>: 1081.02, [M + 11H]<sup>11+</sup>: 1081.02, [M + 11H]<sup>11+</sup>:

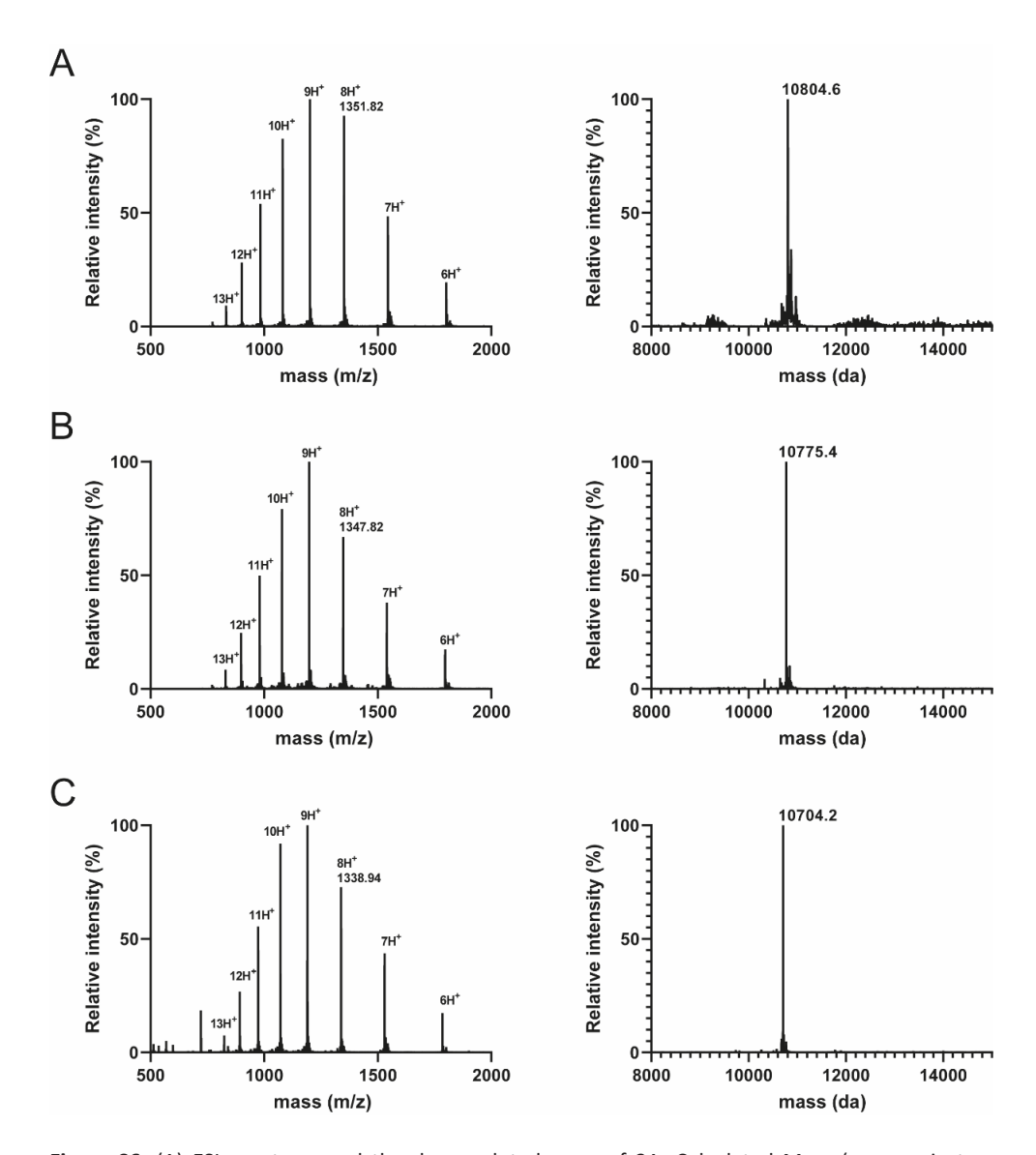


**Figure S6.** (A) ESI spectrum and the deconvoluted mass of 3A. Calculated Mass (average isotope composition):10800.22, Observed: 10801.52. Deconvoluted mass calculated: 10807.0, Observed: 10804.6 (B) ESI spectrum and the deconvoluted mass of 3B. Calculated Mass (average isotope composition): 10768.25, Observed: 10769.52. Deconvolute mas calculated: 10774.9, Observed: 10775.4. (C) ESI spectrum and the deconvoluted mass of 3 Calculated Mass (average isotope composition): 10697.21, Observed: 10698.4. Deconvolute mass calculated: 10703.9, Observed: 10704.2.

# **Iso-acyl shift of 4A**

As described in the synthesis section of peptide **4A**, an iso-acyl dipeptide was incorporated to increase solubility during purification. The ester bond is not stable during NCL and therefore has to undergo an  $O \rightarrow N$  acyl shift to form the stable native peptide (Scheme S4).

Scheme S4. Shift of the iso-acyl dipeptide.

The peptide **4A** (9.4 mg, 2.8  $\mu$ mol) was dissolved in 400  $\mu$ L 6 M Gdn.HCl, 0.2 M phosphate, pH 7.4. After 10 minutes an UPLC sample was measured and the retention time of the peptide shifted from 6.47 to 6.96 minutes (UPLC method 2), indicating that the iso-acyl had shifted successfully (Fig. S7).

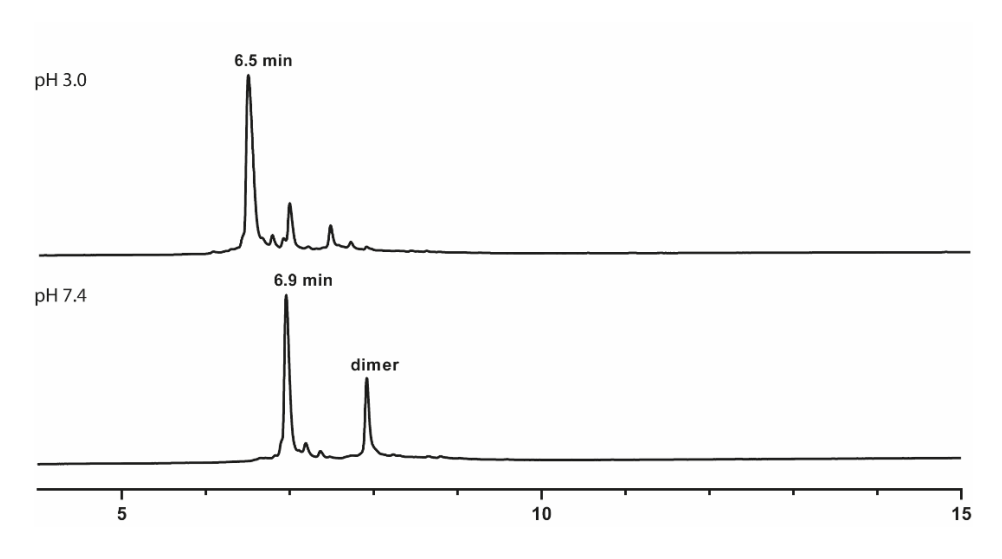


Figure S7. UPLC UV chromatogram of 4A at pH 3.0 (top chromatogram) and 4 at pH 7.4 (bottom chromatogram).

# One-pot thioesterification and ligation to GFP 1-123-PA

Scheme S5. One-pot thioesterification and NCL of 3 and 4 to obtain the final product 5.

A solution of **3** (28.8 mg, 2.69  $\mu$ mol) in 3 mL of 6 M Gdn.HCl, 0.2 M phosphate, pH 3.0 was cooled to 0 °C before adding 27  $\mu$ L of 1 M NaNO<sub>2</sub> in MilliQ. After 15 minutes the solution was warmed to room temperature and MPAA (51 mg, 303  $\mu$ mol, 100 equiv.) in 4 M NaOH (50  $\mu$ L), and **4** (9.4 mg, 2.8  $\mu$ mol) were added, and the pH was adjusted to pH 7.13. The mixture was shaken over night at room temperature to reach completion

before purification on a Äkta system using a HiLoad\* 26/600 Superdex\* 75 pg column (flow: 1 mL/min) to obtain in a solution of 6 M Gdn.HCl, 0.2 M phosphate, pH 7.0 (9.13 mg/mL, 13.71 mg, 36.4 % yield based on recovered starting material).

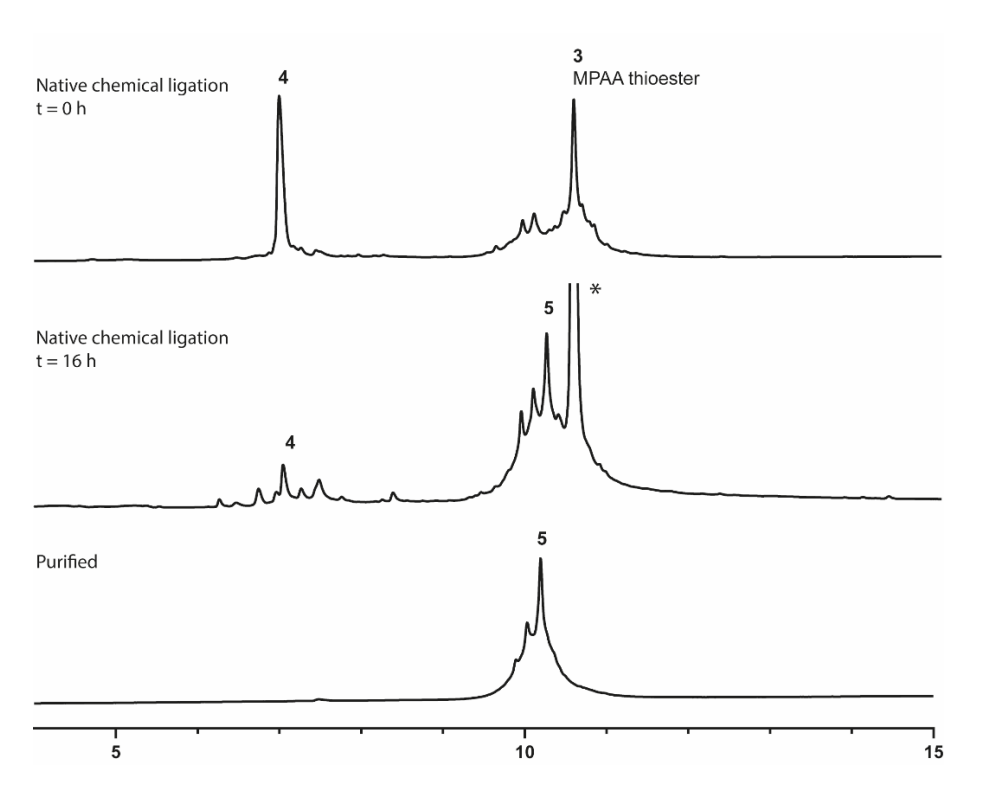


Figure S8. UPLC UV chromatogram of NCL between 4 and 3 t = 0 h (top chromatogram), t = 16 h (middle chromatogram), and purified 5 (bottom chromatogram)

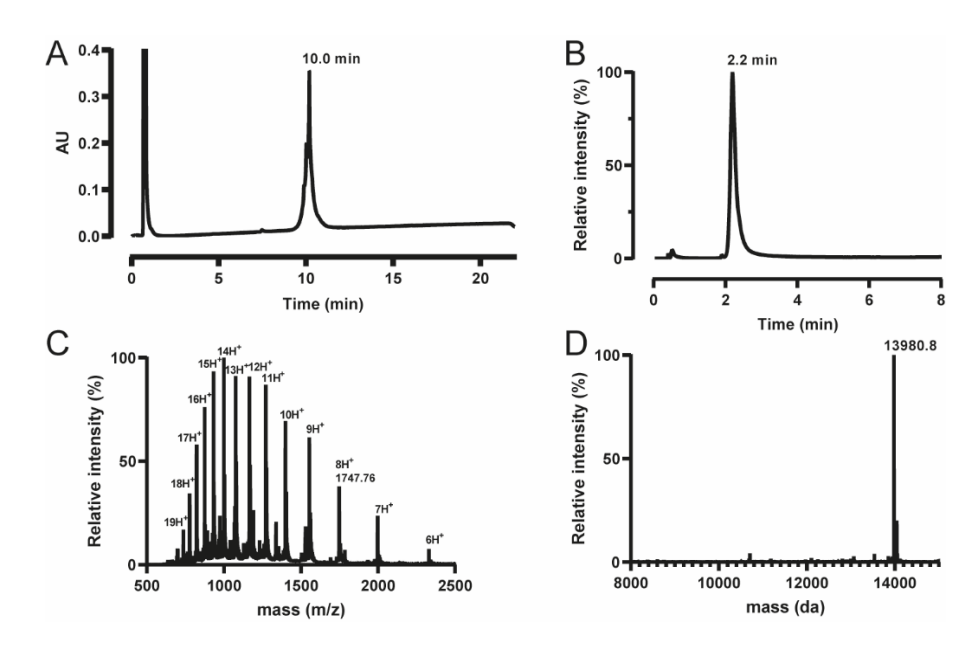


Figure S9. (A) UPLC UV chromatogram of 5, Rt 13.9 min. (B) Total ion chromatogram (LC-MS method C4) of 5, Rt 2.2 min. (C) ESI spectrum of 5. Calculated Mass (average isotope composition): 13971.70;  $[M+6H]^{6+}$ : 2329.62,  $[M+7H]^{7+}$ : 1996.95,  $[M+8H]^{8+}$ : 1747.46,  $[M+9H]^{9+}$ : 1553.41,  $[M+10H]^{10+}$ : 1398.17,  $[M+11H]^{11+}$ : 1271.16,  $[M+12H]^{12+}$ : 1165.31,  $[M+13H]^{13+}$ : 1075.75,  $[M+14H]^{14+}$ : 998.97. Observed: ;  $[M+6H]^{6+}$ : 2329.81,  $[M+7H]^{7+}$ : 1997.14,  $[M+8H]^{8+}$ : 1747.62,  $[M+9H]^{9+}$ : 1553.45,  $[M+10H]^{10+}$ : 1398.30,  $[M+11H]^{11+}$ : 1271.18,  $[M+12H]^{12+}$ : 1165.33,  $[M+13H]^{13+}$ : 1075.78,  $[M+14H]^{14+}$ : 999.00. (D) Deconvoluted mass of 5, calculated: 13980.4, observed: 13980.8.

#### Folding of 5

PBS buffer, pH 7.4 was freshly prepared from Gibco PBS tablets and sterilized with a bottle top vacuum filter, 0.22  $\mu$ m (Corning). A solution of crude unfolded **5** (0.65 mM, 1.5 mL) in 6 M Gdn.HCl, 0.2 M phosphate, pH 7.0 was added to a prewashed Slide-A-Lyzer<sup>TM</sup> MINI Dialysis Devices (3.5 kDa cut-off) containing 3 M Gdn.HCl 0.2 M phosphate, pH 7.0. After 2 hours the buffer was exchanged to PBS, pH 7.4 and the mixture was shaken gently over night at 10 °C. The mixture was analyzed by LC-MS revealing the correct MW corresponding to a loss of 2 Da. The mixture was concentrated using a prewashed centrifugal 3 kDa molecular weight cut-off device and concentrated to ~ 400  $\mu$ L.

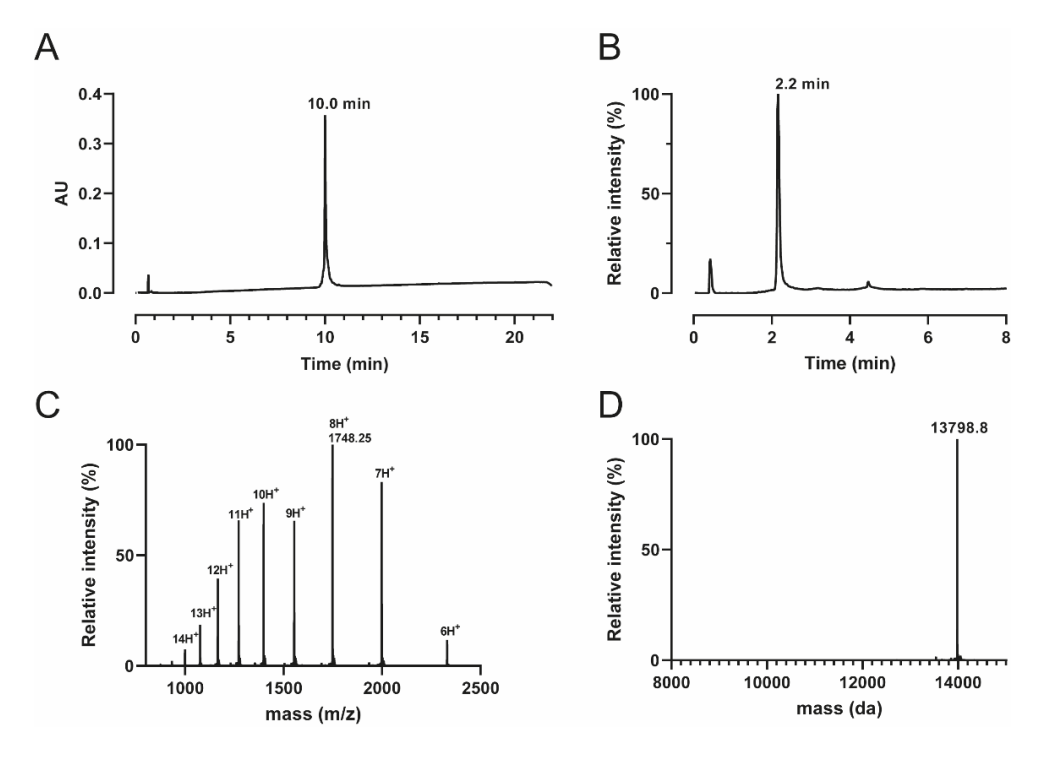
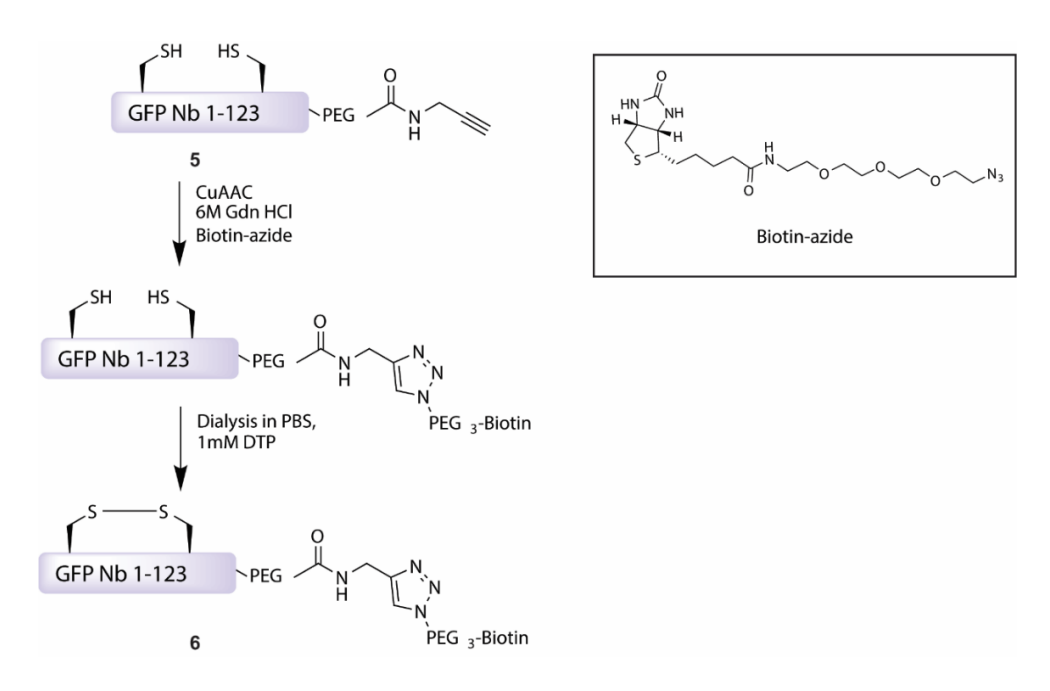


Figure S10. (A) UPLC UV chromatogram (method 1) of folded 5, Rt 10.0 min. (B) Total ion chromatogram (LC-MS method C4) of folded 5, Rt 2.2 min (C) ESI spectrum of folded 5. Calculated Mass (average isotope composition): 13978.4;  $[M+6H]^{6+}$ : 2329.28,  $[M+7H]^{7+}$ : 1996.70,  $[M+8H]^{8+}$ : 1747.21,  $[M+9H]^{9+}$ : 1553.19,  $[M+10H]^{10+}$ : 1398.97,  $[M+11H]^{11+}$ : 1270.97,  $[M+12H]^{12+}$ : 1165.14,  $[M+13H]^{13+}$ : 1075.59,  $[M+14H]^{14+}$ : 998.83. Observed: 13978.8;  $[M+6H]^{6+}$ : 2329.83,  $[M+7H]^{7+}$ : 1997.14,  $[M+8H]^{8+}$ : 1748.25,  $[M+9H]^{9+}$ : 1553.45,  $[M+10H]^{10+}$ : 1398.30,  $[M+11H]^{11+}$ : 1271.18,  $[M+12H]^{12+}$ : 1165.33,  $[M+13H]^{13+}$ : 1075.78,  $[M+14H]^{14+}$ : 999.00. (D) Deconvoluted mass of folded 5, calculated: 13978.4, Observed: 13798.8.

## **CuAAC** chemistry on 5



Scheme S6. Click chemistry on purified 5 followed by disulfide bond formation of 6.

To purified **5** (3.65 mg, 0.26  $\mu$ mol, 1.0 equiv.) in 400  $\mu$ L 6 M Gdn.HCl, 0.2 M phosphate pH 7.2, 25  $\mu$ L of freshly prepared click-mixture (1:1:1  $\nu/\nu/\nu$ , CuSO<sub>4</sub>·5H<sub>2</sub>0 (40.7 mg/mL in water): sodium ascorbate (120 mg/mL in water): THPTA ligand (42.5 mg/mL in water)) was added before adding 65  $\mu$ L of Biotin-PEG-azide (CAS Number: 875770-34-6)(10 mM in DMSO, 0.65  $\mu$ mol, 2.5 equiv.). The reaction was shaken for 60 minutes at room temperature when LC-MS showed full conversion to **6**. The reaction mixture was quenched with 5  $\mu$ L EDTA (0.5 M in MilliQ water) before purification by Äkta, Superdex\* 200 Increase 10/300 GL (flow: 0.5 mL/min) to obtain **6** (2.48 mg, 66 % yield). Thereafter, **6** was folded as previously described for **5**, resulting in folded **6** (Fig S11).

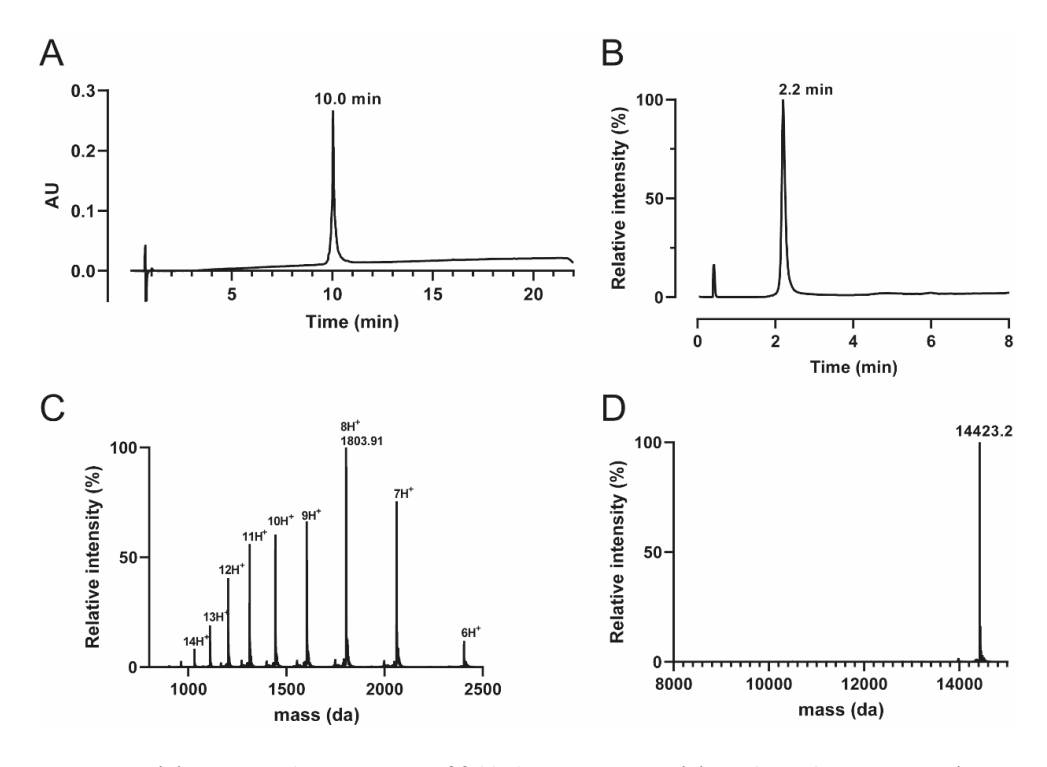
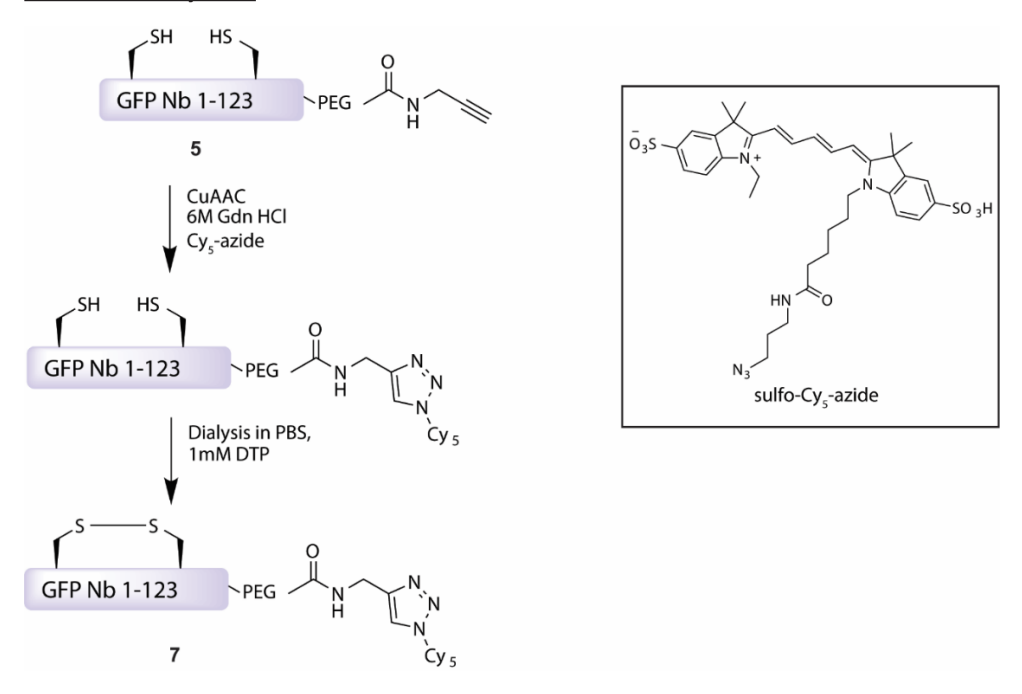


**Figure S11.** (A) UPLC UV chromatogram of folded 6, Rt 10.0 min. (B) Total ion chromatogram (LC-MS method C4) of folded 6, Rt 2.2 min (C) ESI spectrum of folded 6. Calculated Mass (average isotope composition): 14422.9;  $[M+6H]^{6+}$ : 2403.32,  $[M+7H]^{7+}$ : 2060.13,  $[M+8H]^{8+}$ : 1802.74,  $[M+9H]^{9+}$ : 1602.54,  $[M+10H]^{10+}$ : 1442.39,  $[M+11H]^{11+}$ : 1311.35,  $[M+12H]^{12+}$ : 1202.16,  $[M+13H]^{13+}$ : 1109.76,  $[M+14H]^{14+}$ : 1030.56,  $[M+15H]^{15+}$ : 961.93. Observed: Calculated Mass (average isotope composition): 14423.2.4;  $[M+6H]^{6+}$ : 2403.67,  $[M+7H]^{7+}$ : 2060.46,  $[M+8H]^{8+}$ : 1803.16,  $[M+9H]^{9+}$ : 1602.80,  $[M+10H]^{10+}$ : 1442.63,  $[M+11H]^{11+}$ : 1311.56,  $[M+12H]^{12+}$ : 1202.35,  $[M+13H]^{13+}$ : 1109.95,  $[M+14H]^{14+}$ : 1030.73. (D) Deconvoluted mass of folded 6, calculated: 14422.8, observed: 14423.2.

#### Click chemistry on 5



Scheme S7. Click chemistry on purified 5 followed by disulfide bond formation of 7.

To purified **5** (3.65 mg, 0.26  $\mu$ mol, 1.0 equiv.) in 400  $\mu$ L 6 M Gdn.HCl, 0.2 M phosphate pH 7.2, 25  $\mu$ L of freshly prepared click-mixture (1:1:1 v/v/v, CuSO<sub>4</sub>·5H<sub>2</sub>0 (40.7 mg/mL in water): sodium ascorbate (120 mg/mL in water): THPTA ligand (42.5 mg/mL in water)) was added before adding 65  $\mu$ L of sulfo-Cy5-azide (CAS Number. : 1621101-43-6) (10 mM in DMSO, 0.65  $\mu$ mol, 2.5 equiv.). The reaction was shaken for 60 minutes at room temperature when LC-MS showed full conversion of the **7**. The reaction mixture was quenched with 5  $\mu$ L EDTA (0.5M in MilliQ water) before purification by Äkta, Superdex\* 200 Increase 10/300 GL (flow: 0.5 mL/min) to obtain **7** (1.58 mg, 41 % yield). Thereafter, **7** was folded as previously described for **5**, resulting in folded **7** (Fig. S12).

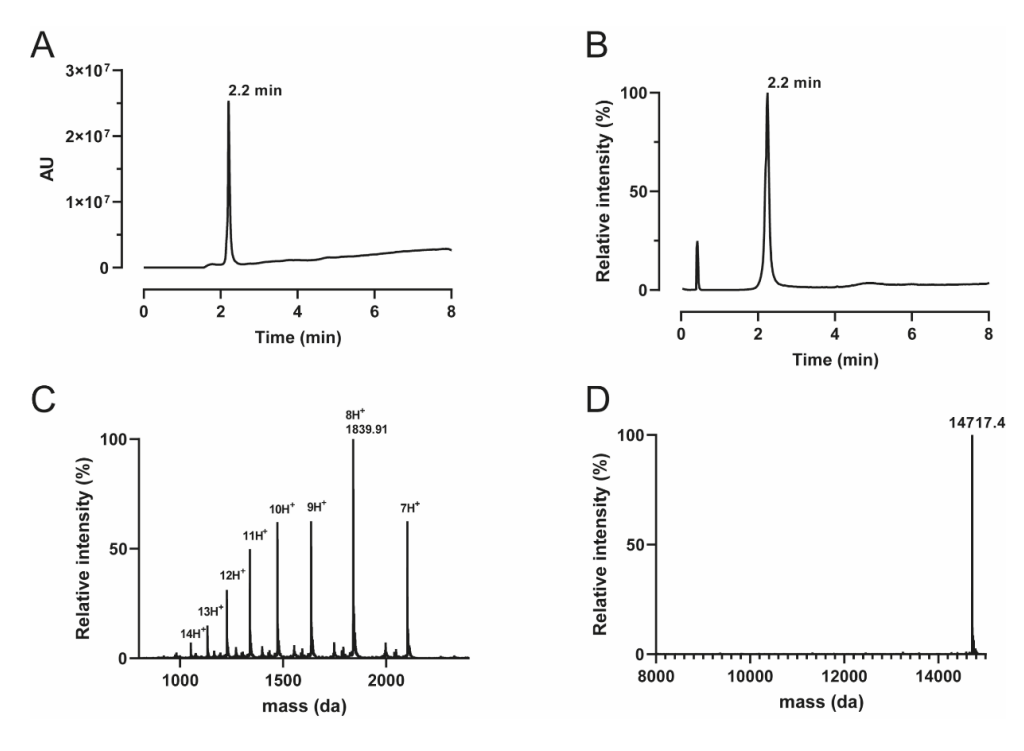


**Figure S12.** (A) UPLC UV chromatogram of folded 7, Rt 10.0 min. (B) Total ion chromatogram (LC-MS method C4) of folded 7, Rt 2.2 min (C) ESI spectrum of folded 7. Calculated Mass (average isotope composition): 14717.3; [M + 6H]<sup>6+</sup>: 2452.33, [M + 7H]<sup>7+</sup>: 2102.14, [M + 8H]<sup>8+</sup>: 1839.50, [M + 9H]<sup>9+</sup>: 1635.22, [M + 10H]<sup>10+</sup>: 1471.80, [M + 11H]<sup>11+</sup>: 1338.09, [M + 12H]<sup>12+</sup>: 1226.66, [M + 13H]<sup>13+</sup>: 1132.38, [M + 14H]<sup>14+</sup>: 1051.56. Observed: Calculated Mass (average isotope composition): 14717.4; [M + 6H]<sup>6+</sup>: 2452.86, [M + 7H]<sup>7+</sup>: 2102.62, [M + 8H]<sup>8+</sup>: 1839.78, [M + 9H]<sup>9+</sup>: 1635.59, [M + 10H]<sup>10+</sup>: 1472.04, [M + 11H]<sup>11+</sup>: 1338.31, [M + 12H]<sup>12+</sup>: 1226.87, [M + 13H]<sup>13+</sup>: 1132.57, [M + 14H]<sup>14+</sup>: 1051.83. (D) Deconvuluted mass of folded 7, calculated: 14717.3 Observed: 14717.4.

#### Circular dichroism

CD measurements were performed using a Jasco 1500 spectropolarimeter at concentrations of 0.1 mg/mL in PBS, pH 7.4, concentrations were measured using a NanoDrop spectrophotometer at A280 (calculated extinction coefficient of 26930 cm<sup>-1</sup>M<sup>-1</sup>). Measurements between 250 and 190 nm were taken using a quartz cuvette with a path length of 0.02 cm. In total, 8 cumulative measurements were made and the average was calculated and plotted using Graphpad PRISM.

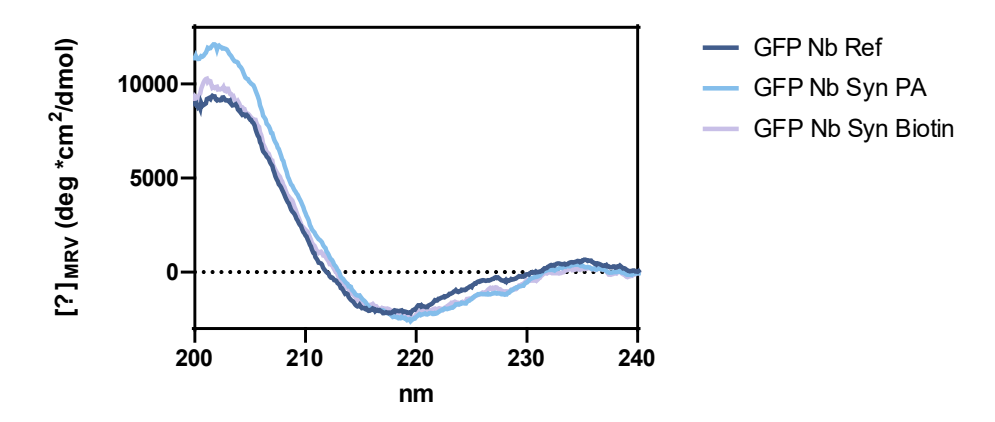


Figure S13. CD chromatogram of the expressed Nb, 5 and 6.

Unfolding CD measurements were performed with a 1 °C/min increase, with a measurement containing 8 scans every 10 °C from 20 °C to 90 °C.

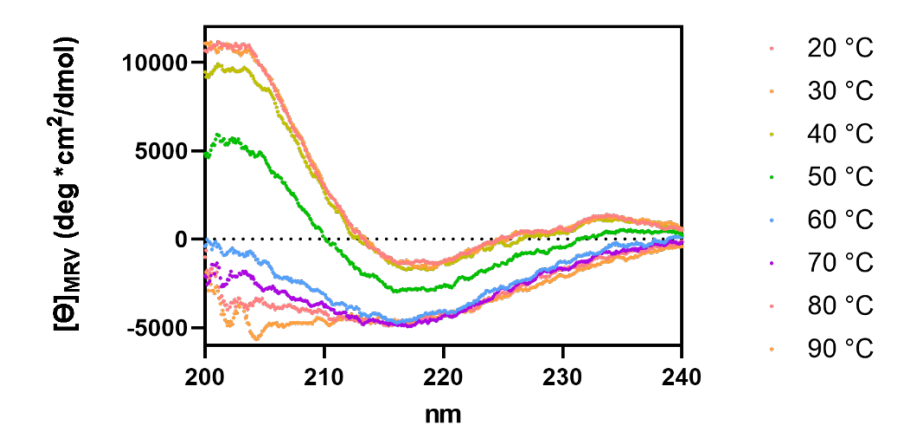


Figure S14. CD spectra of expressed GFP Nb with heating.

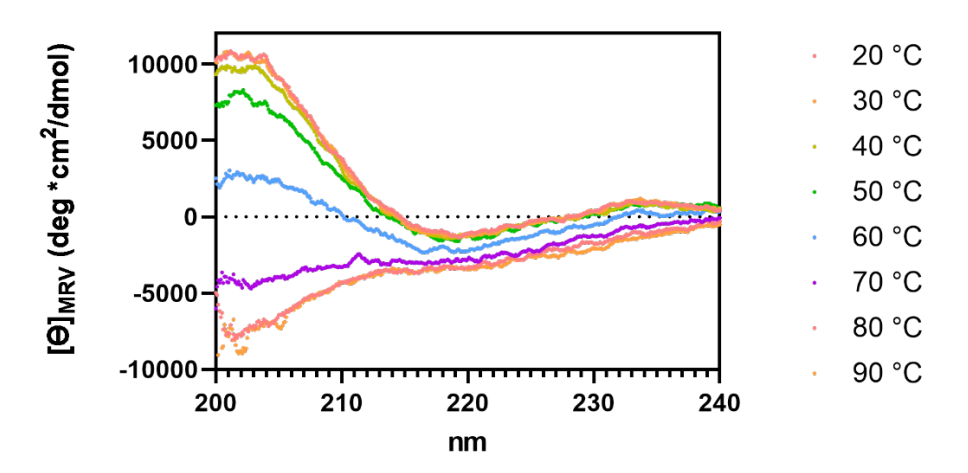


Figure S15. CD spectra of 6 with heating.

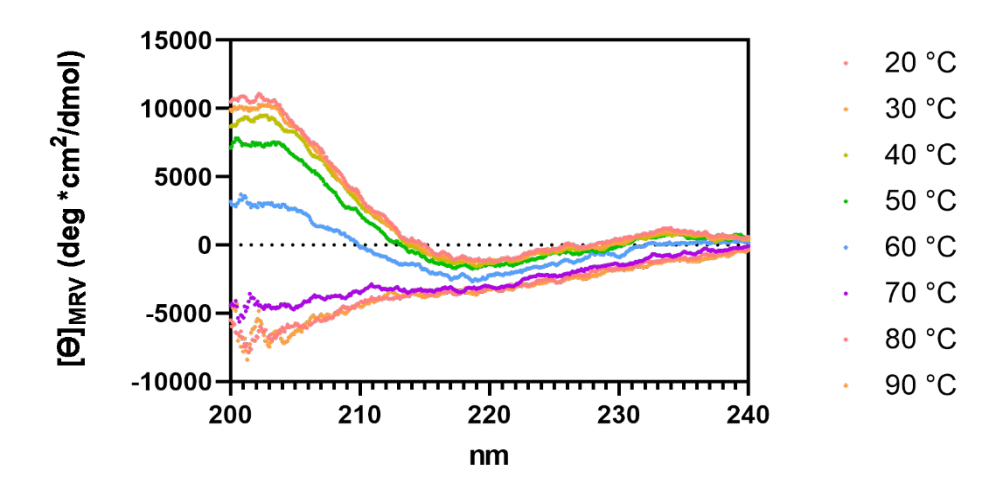


Figure S16. CD spectra of 7 with heating.

### **Bio Layer Interferometry**

Bio Layer Interferometry (BLI) analyses of binding experiments. Graphs show concentrations in nM and fitted curves as dotted lines. The data was fitted using the Octet96 software.

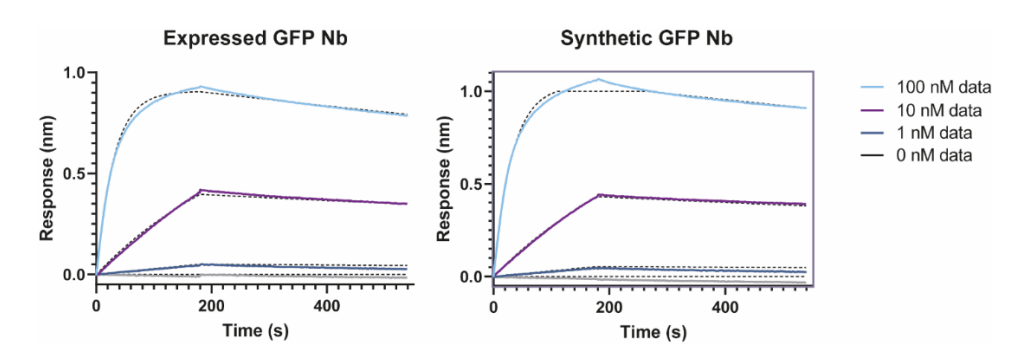


Figure S17. BLI data for binding of the expressed GFP Nb to GFP and the synthetic GFP Nb to GFP.

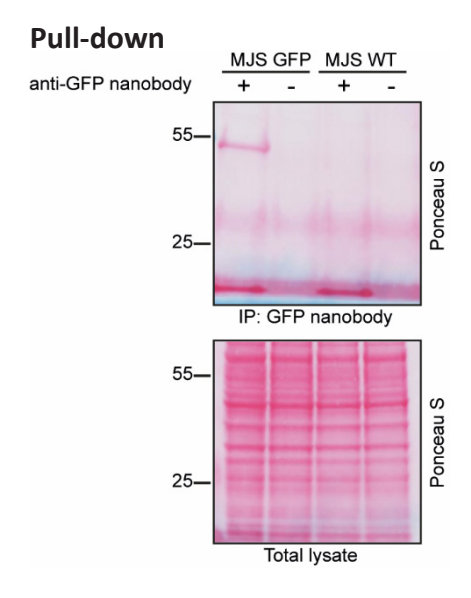


Figure S18. Ponceau S staining of the GFP-Rab7 pull-down. Signal above the 25 kDa marker is streptavidin which is released from the streptavidin beads.

#### References

- 1. Harmsen, M. M. & De Haard, H. J. Properties, production, and applications of cameld single-domain antibody fragments. *Appl Microbiol Biotechnol* **77**, 13–22 (2007).
- 2. Dumoulin, M. *et al.* Single-domain antibody fragments with high conformational stability. *Protein Science* **11**, 500–515 (2009).
- 3. Herce, H. D. *et al.* Cell-permeable nanobodies for targeted immunolabelling and antigen manipulation in living cells. *Nat Chem* **9**, 762–771 (2017).
- 4. Manglik, A., Kobilka, B. K. & Steyaert, J. Nanobodies to Study G Protein-Coupled Receptor Structure and Function. *Annu Rev Pharmacol Toxicol* **57**, 19–37 (2017).
- 5. Cheloha, R. W., Harmand, T. J., Wijne, C., Schwartz, T. U. & Ploegh, H. L. Exploring cellular biochemistry with nanobodies. *Journal of Biological Chemistry* **295**, 15307–15327 (2020).
- 6. Bao, G., Tang, M., Zhao, J. & Zhu, X. Nanobody: a promising toolkit for molecular imaging and disease therapy. *EJNMMI Res* **11**, (2021).
- 7. Wesolowski, J. *et al.* Single domain antibodies: Promising experimental and therapeutic tools in infection and immunity. *Med Microbiol Immunol* **198**, 157–174 (2009).
- 8. Zhang, H. *et al.* Covalently Engineered Nanobody Chimeras for Targeted Membrane Protein Degradation. *J Am Chem Soc* **143**, 16377–16382 (2021).
- 9. Ackaert, C. *et al.* Immunogenicity Risk Profile of Nanobodies. *Front Immunol* **12**, (2021).
- 10. Vincke, C. *et al.* General strategy to humanize a camelid single-domain antibody and identification of a universal humanized nanobody scaffold. *Journal of Biological Chemistry* **284**, 3273–3284 (2009).
- 11. Yang, E. Y. & Shah, K. Nanobodies: Next Generation of Cancer Diagnostics and Therapeutics. *Front Oncol* **10**, (2020).
- Tan, Y., Wu, H., Wei, T. & Li, X. Chemical Protein Synthesis: Advances, Challenges, and Outlooks. *J. Am. Chem. Soc.* 20288–20298 (2020) doi:10.1021/jacs.0c09664.
- 13. Muyldermans, S. Nanobodies: Natural single-domain antibodies. *Annu Rev Biochem* **82**, 775–797 (2013).
- 14. Mitchell, L. S. & Colwell, L. J. Comparative analysis of nanobody sequence and structure data. *Proteins: Structure, Function and Bioinformatics* **86**, 697–706 (2018).
- 15. Kubala, M. H., Kovtun, O., Alexandrov, K. & Collins, B. M. Structural and thermodynamic analysis of the GFP:GFP-nanobody complex. *Protein Science* **19**, 2389–2401 (2010).
- 16. Tornøe, C. W., Christensen, C. & Meldal, M. Peptidotriazoles on solid phase:

- [1,2,3]-Triazoles by regiospecific copper(I)-catalyzed 1,3-dipolar cycloadditions of terminal alkynes to azides. *Journal of Organic Chemistry* **67**, 3057–3064 (2002).
- 17. Paradís-Bas, M., Tulla-Puche, J. & Albericio, F. The road to the synthesis of 'difficult peptides'. *Chem Soc Rev* **45**, 631–654 (2016).
- 18. Hartmann, L. *et al.* VHH characterization. Comparison of recombinant with chemically synthesized anti-HER2 VHH. *Protein Science* **28**, 1865–1879 (2019).
- 19. Fang, G. M. *et al.* Protein chemical synthesis by ligation of peptide hydrazides. *Angewandte Chemie International Edition* **50**, 7645–7649 (2011).
- 20. Kar, A. *et al.* Efficient Chemical Protein Synthesis using Fmoc-Masked N-Terminal Cysteine in Peptide Thioester Segments. *Angewandte Chemie International Edition* **59**, 14796–14801 (2020).
- 21. Giribaldi, J. *et al.* Synthesis, structure and biological activity of CIA and CIB, two  $\alpha$ -conotoxins from the predation-evoked venom of Conus catus. *Toxins (Basel)* **10**, (2018).
- 22. Maruyama, K., Nagasawa, H. & Suzuki, A. 2,2'-Bispyridyl disulfide rapidly induces intramolecular disulfide bonds in peptides. *Peptides (N.Y.)* **20**, 881–884 (1999).
- 23. Sapmaz, A. *et al.* USP32 regulates late endosomal transport and recycling through deubiquitylation of Rab7. *Nat Commun* **10**, 1–18 (2019).
- 24. Guerra, F. & Bucci, C. Multiple roles of the small GTPase Rab7. *Cells* **5**, (2016).
- 25. De Filippis, V., De Antoni, F., Frigo, M., De Laureto, P. P. & Fontana, A. Enhanced protein thermostability by Ala  $\rightarrow$  Aib replacement. *Biochemistry* **37**, 1686–1696 (1998).
- 26. Cabri, W. *et al.* Therapeutic Peptides Targeting PPI in Clinical Development: Overview, Mechanism of Action and Perspectives. *Front Mol Biosci* **8**, 1–21 (2021).
- 27. Rocha, N. *et al.* Cholesterol sensor ORP1L contacts the ER protein VAP to control Rab7-RILP-p150Glued and late endosome positioning. *Journal of Cell Biology* **185**, 1209–1225 (2009).
- 28. Jongsma, M. L. *et al.* SKIP HOPS recruits TBC 1D15 for a Rab7-to-Arl8b identity switch to control late endosome transport . *EMBO J* **39**, 1–25 (2020).
- 29. Cabukusta, B. *et al.* Human VAPome Analysis Reveals MOSPD1 and MOSPD3 as Membrane Contact Site Proteins Interacting with FFAT-Related FFNT Motifs. *Cell Rep* **33**, 108475 (2020).
- 30. Guardia, C. M. *et al.* Reversible association with motor proteins (RAMP): A streptavidin-based method to manipulate organelle positioning. *PLoS Biol* **17**, 1–27 (2019).
- 31. Moorhead, A. M., Jung, J. Y., Smirnov, A., Kaufer, S. & Scidmore, M. A. Multiple host proteins that function in phosphatidylinositol-4-phosphate metabolism are

recruited to the chlamydial inclusion. Infect Immun 78, 1990–2007 (2010).

- 32. Carpino, L. A. *et al.* Synthesis of 'difficult' peptide sequences: application of a depsipeptide technique to the Jung–Redemann 10- and 26-mers and the amyloid peptide A $\beta$ (1–42). *Tetrahedron Lett* **45**, 7519–7523 (2004).
- 33. Mutter, M. *et al.* Switch Peptides In Statu Nascendi: Induction of Conformational Transitions Relevant to Degenerative Diseases. *Angewandte Chemie International Edition* **43**, 4172–4178 (2004).
- 34. Yoshiya, T., Kawashima, H., Sohma, Y., Kimura, T. & Kiso, Y. O-acyl isopeptide method: efficient synthesis of isopeptide segment and application to racemization-free segment condensation. *Org Biomol Chem* **7**, 2894–2904 (2009).



# Summary and future prospects

6



#### **Summary**

Antibody conjugation techniques have revolutionized the development of multifunctional antibody-based therapeutics and diagnostics. Despite the advancements in antibody conjugation technologies, several challenges remain. Achieving site-specific conjugation while preserving antibody functionality is crucial, though often challenging. Developing improved conjugation strategies is vital to broaden the applications and effectiveness of antibody-based therapies, diagnostics, and research.

**Chapter 1** provides an overview of approaches for the generation of multi-specific antibodies and antibody conjugation strategies for the generation of various antibody formats. In particular, antibody-antigen conjugates are discussed in the context of targeted antigen delivery to DCs. In addition, ubiquitin is discussed, touching upon the enzymes involved in ubiquitination and different ubiquitin chains. The chemical synthesis of ubiquitin-based tools is highlighted to emphasize the versatility of the chemical synthesis of ubiquitin.

In Chapter 2, we introduce ubi-tagging, a ubiquitin-based modular antibody conjugation platform, establish its feasibility, and explore the potential of this conjugation method for the generation of antibody conjugates and complexes of various formats. This conjugation method exploits the site specificity of the enzymatic process of ubiquitination to covalently attach antibodies to payload or to other antibodies through ubiquitin chain formation. By fusing ubiquitin to an antibody or antibody fragment, it can be used as a conjugation tag. To ensure the controlled conjugation of one ubi-tag to another, it is essential to use ubiquitin as a tag in two complementary forms, which we named the donor ubi-tag and acceptor ubi-tag. In the Donor ubi-tag, the C-terminal glycine residue is free and available for conjugation to another ubitag, whereas the lysine residue specific for the E2 and E3 pair used in the reaction is mutated. In contrast, the acceptor ubi-tag has this specific lysine residue available for conjugation, while its C-terminal glycine is either lacking or blocked by the presence of a fused short peptide. Thus, during the ubiquitination reaction using the corresponding E2 and E3, the C-terminus of a donor-ubitag can only covalently attach to the lysine residue of an acceptor ubitag and no other conjugate can be formed. In this chapter, we first generated Fab-ubitag fusion proteins and used them to establish the feasibility of this conjugation method for the generation of fluorescently labelled Fab fragments, Fab-multimers, and a Fab heterodimer that can be site-specifically elongated for fluorescent labeling or trimer formation. We also demonstrated the recognition and processing of the formed conjugates by deubiquitinating enzymes (DUBs). We then demonstrated that ubi-tagging can also be applied to the conjugation of mAbs, where each mAb carries two ubi-tags, one fused to each heavy chain. We used ubi-tagging to generate fluorescently labelled monoclonal antibodies (mAbs) and a bivalent bispecific antibody conjugate.

Ubi-tagging is further expanded in **Chapter 3**, where it is applied for the generation of ubi-tagged antibody-peptide conjugates for dendritic cell (DC)-targeted antigen delivery. We conjugated anti-mDCE205 to the ovalbumin antigenic peptide SIINFEKL by both ubi-tagging and the current state-of-the-art sortagging. When tested in vitro, the ubi-tagged conjugates induced significantly higher T cell activation and cytokine secretion compared to the sortagged conjugates. Building on these results, we assessed the *in vivo* efficacy of both conjugates where the mice treated with the ubi-tagged conjugates exhibited robust OT-I cell proliferation, whereas the sortagged conjugates induced minimal proliferation at the same concentration. Biodistribution studies revealed preferential uptake of ubi-tagged conjugates by CD11c+ dendritic cells, suggesting that this increased uptake underlies the enhanced T cell activation.

In **chapter 4**, we translate ubi-tagged DC-targeting vaccines to human applications. Here, we use ubi-tagged VHHs for the generation of VHH-peptide conjugates for the targeted antigen delivery to human DCs. Considering the relatively large size of ubi-tag conjugation with regard to the molecular weight of VHHs, we first demonstrate that ubi-tag conjugation does not interfere with the antigen-binding capacity of VHHs. We then proceed to successfully conjugate ubi-tagged VHHs to a library of notoriously insoluble epitopes, showing that the presence of the ubi-tag fused to these hydrophobic epitopes enhanced their solubility. We demonstrated the functionality of the generated anti-DC-SIGN VHH-Ub<sub>2</sub>-gp100<sub>a</sub> in vitro, showing dose-dependent T cell activation.

In **chapter 5** we move from an enzymatic approach of antibody conjugation to a synthetic approach using native chemical ligation (NCL) to generate a synthetic GFP nanobody (Nb) primed for on-demand functionalization. We successfully modified the GFP-Nb using CuAAC to selectively attach either a biotin or a fluorophore, and used them in pull-down and confocal microscopy experiments, respectively. We demonstrate that the labelling process does not compromise the antigen-binding site, enabling its application for nanobodies with a cysteine residue in the CDR regions, which can be disrupted by conventional maleimide-based modification.

## **Discussion and future prospects**

In this thesis, we present new broadly applicable approaches for the generation of antibody conjugates. We successfully applied both (chemo)enzymatic and chemical approaches for the efficient generation of chemically defined, site-specifically modified, homogenous antibody conjugates in various formats (Fig. 1).

For the ubi-tagging antibody conjugation technique presented in chapters 2, 3, and 4, we use the E2-E3 pair gp78RING-Ube2g2, which is specific for K48, and the donor ubi-tags used were K48R mutants. We used a gp78RING-Ube2g2 chimera, in which the c-terminus of the RING domain of gp78 was engineered to be fused to the N-terminus of Ube2g2 separated by linker<sup>1</sup>. This fusion results in a much higher enzyme activity of the pair compared to when used as separate proteins (Fig. 2). This enhanced activity

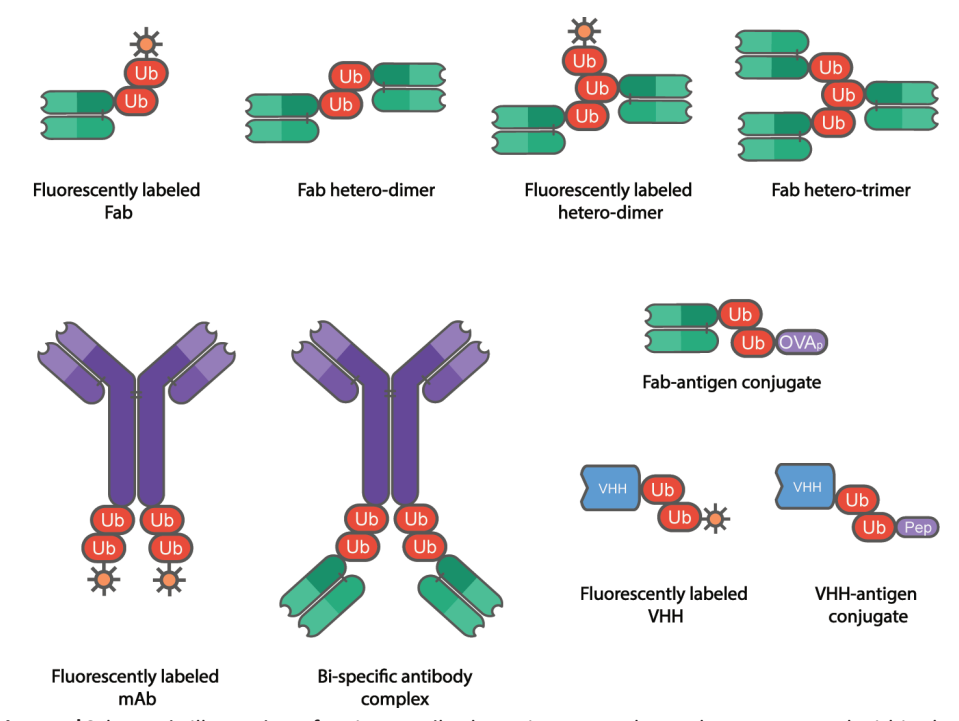


**Figure 1**|Schematic illustration of various antibody conjugates and complexes generated within the scope of this thesis.

largely contributed to the efficiency of the ubi-tag reactions in this thesis (Fig. 3). Although this E2/E3 pair is K48 specific, ubi-tagging is not restricted to this linkage type. Considering the variety of linkage-specific ubiquitination enzymes and the resulting ubiquitin chains, it would be interesting to further explore ubi-tagging using different ubiquitin linkage types. In particular, because differently linked ubiquitin chains are known to have very different conformations, which in the context of ubi-tagging could be exploited to gain control over the spatial orientation of the antibodies or proteins to be conjugated to each other. Another level of flexibility provided by ubi-tagging as an antibody conjugation technique, is its reversibility by DUBs. Although very lightly touched upon in this study, it was established that the ubi-tagged conjugates are recognized and processed by DUBs such as UCHL3 and OTUB1. This could be interesting for further exploration in applications where the conditional cleavage for the disassembly of the conjugate is desired.

Another aspect that adds to the versatility of this platform is the plethora of chemical modifications that can be synthetically incorporated in ubiquitin as its full chemical synthesis is well established and the ubiquitin toolbox is continuously expanding.<sup>2</sup> One of the synthetic ubiquitin variants that might be interesting to in the context of ubi-tagging is DOTA-Ub.<sup>3</sup> Conjugating it to an antibody or antibody fragment could

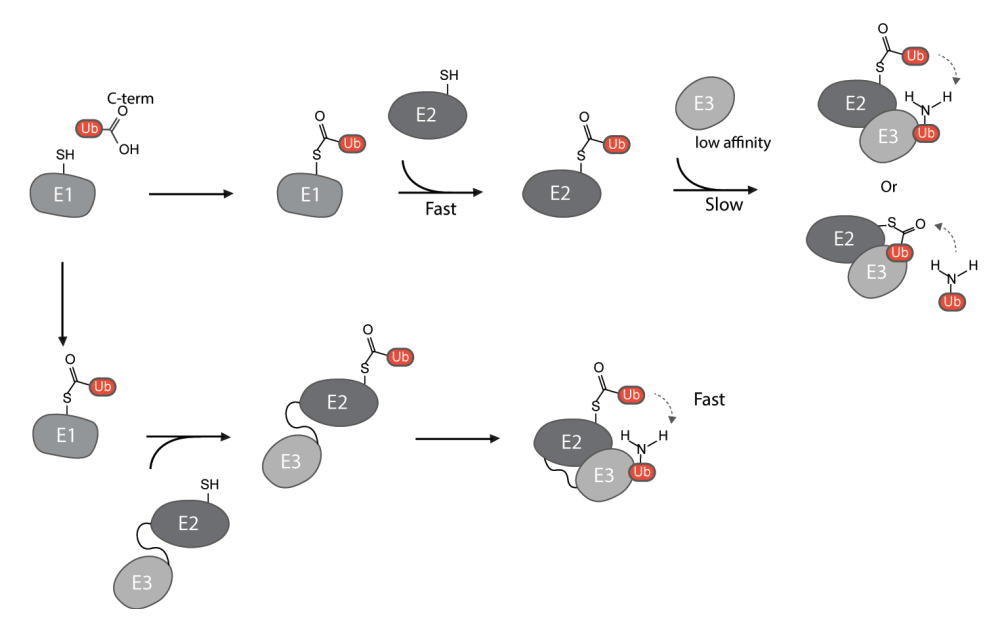


Figure 2|Schematic illustration showing the mechanism of the enhanced activity of the fusion of the E2/E3 pair gp78RING-Ube2g2 compared to the reaction in which the enzymes are not fused.

result in an antibody-DOTA conjugate that can be used as a lanthanide-based contrast agent in diagnostic applications. It is also interesting to explore the attachment of multiple chemical handles to ubiquitin with the idea of generating a scaffold that can be functionalized on demand with multiple payloads, such as multiple cytotoxic drug moieties, for the generation of ubi-tag-based antibody-drug conjugates. Such a scaffold could also be used to attach multiple fluorophores in research and diagnostic applications, where a high detection sensitivity is required. Additionally, since we showed that the ubi-tag enhanced the solubility of antigenic peptides in the context of targeted antigen delivery to DCs, it would be interesting to generate chemically synthesized libraries of ubiquitin fused to antigenic peptides that can be readily conjugated to antibodies for the generation of DC-targeted vaccines.

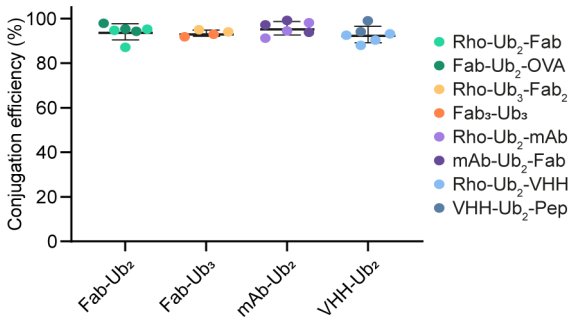


Figure 3|The Efficiency of ubi-tag conjugation reactions conducted in this thesis. Conjugation reactions involving ubi-tagged Fab fragments forming di-ubiquitin chains showed an average reaction

efficiency of 94.2%, whereas conjugation reactions involving ubi-tagged Fabs forming tri-ubiquitin chains showed an average efficiency of 93.4%. Conjugation of ubi-tagged mAbs showed an average reaction efficiency of 95.7%, whereas ubi-tagged VHHs reacted with an average efficiency of 92.8% within 60 mins.

Combining ubi-tagging with other approaches to generate multimeric antibody complexes may also be worth exploring. For instance, combining Fab-arm exchange<sup>4</sup> with ubi-tagging could be an approach to generate a trispecific antibody complex where only one Fab-arm would carry a ubi-tag or even a tetraspecific antibody complex where the both Fab-arms are ubi-tagged and separately conjugated to two different ubi-tagged Fabs before mixing for exchange.

Future prospect of synthetic nanobodies: Synthetic antibody fragments, such as fully synthetic nanobodies, offer exciting prospects for preclinical research. Their completely synthetic nature allows for precise design and rapid development, enabling highly targeted drug delivery, diagnostics, and therapeutic applications. These synthetic constructs can be easily modified for use in sensitive immunoassays, diagnostic platforms, and imaging techniques, without the limitations of traditional antibodies. With the ability to reduce immunogenicity, improve tissue penetration, and facilitate high-throughput screening, synthetic antibody fragments are poised to revolutionize drug discovery, diagnostic tools, and targeted therapies in preclinical settings.

Collectively, in this thesis a novel modular ubiquitin-based antibody conjugation method is presented. While we successfully applied this method for the generation of a range of antibody conjugates, limitless other antibody formats and conjugates can be generated using this method. We also present the chemical synthesis of a nanobody that can be functionalized on-demand. The implementation of the work presented here empowers researchers with new strategies for the generation of antibody -based tools and therapeutics.

#### References

- 1. Blythe, E. E., Olson, K. C., Chau, V. & Deshaies, R. J. Ubiquitin- A nd ATP-dependent unfoldase activity of P97/VCP•NPLOC4•UFD1L is enhanced by a mutation that causes multisystem proteinopathy. *Proc Natl Acad Sci U S A* **114**, E4380–E4388 (2017).
- 2. Huppelschoten, Y. & van der Heden van Noort, G. J. State of the art in (semi-) synthesis of Ubiquitin- and Ubiquitin-like tools. *Semin Cell Dev Biol* (2021) doi:10.1016/J. SEMCDB.2021.11.025.
- 3. El Oualid, F. *et al.* Chemical synthesis of ubiquitin, ubiquitin-based probes, and diubiquitin. *Angewandte Chemie International Edition* **49**, 10149–10153 (2010).
- 4. Labrijn, A. F. *et al.* Controlled Fab-arm exchange for the generation of stable bispecific IgG1. *Nature Protocols 2014 9:10* **9**, 2450–2463 (2014).



Nederlandse samenvatting
Curriculum Vitae
Publications
Portfolio
Acknowledgements

A



#### **Nederlandse samenvatting**

Dit proefschrift richt zich op de ontwikkeling en verbetering van antilichaam-conjugatie technologieën.

Antilichaam-conjugatie technologieën zijn essentieel voor het maken van antilichaam-gebaseerde diagnostische en onderzoeks gereedschap en voor het maken van antilichaam conjugaten voor therapeutische toepassingen. Deze technologieën omvatten een reeks van fluorescent gelabelde antilichamen voor beeldvorming tot bispecifieke antilichamen voor dubbele antigeendoelwitten en antilichaamdrug conjugaten (ADC's) voor de gerichte aflevering van cytotoxische middelen. De huidige strategieën voor antilichaamconjugatie kampen echter met uitdagingen zoals inefficiëntie en heterogeniteit, die de stabiliteit, farmacokinetiek, toxiciteitsprofielen en batchconsistentie aanzienlijk kunnen beïnvloeden. Ook gezien de toenemende belangstelling voor multispecifieke antilichaam complexen, is er een dringende behoefte aan verbeteringen in conjugatietechnieken. Dit proefschrift heeft tot doel covalente, site-specifieke conjugatietechnologieën te ontwikkelen en te optimaliseren om de efficiëntie, reproduceerbaarheid en functionele prestaties van antilichaamconjugaten te verbeteren. Het onderzoek verkent bovendien de toepassing van synthetische peptidechemie om de huidige beperkingen te overwinnen, wat leidt tot een betere controle over conjugatieplaatsen, verbeterde reproduceerbaarheid en verbeterde functionele prestaties.

**Hoofdstuk 2** introduceert 'ubi-tagging', een innovatief platform dat de site-specifieke en efficiënte enzymatische processen van ubiquitinatie gebruikt. Deze techniek maakt gebruik van ubiquitine als een conjugatietag, die is gefuseerd aan antilichamen of antilichaamfragmenten om fluorescente labels aan antilichamen te hechten of voor het multimeriseren van antilichamen. De veelzijdigheid van deze methode en de rol van ubiquitine in cellulaire signaalroutes voor proteasome-gemedieerde degradatie benadrukken de potentieel revolutionaire toepassingen van deze techniek.

**Hoofdstuk 3** bouwt voort op de ubi-tagging technologie door deze toe te passen op het genereren van antilichaam-gebaseerde DC-gerichte vaccijns. Deze benadering gebruikt ubi-tagging voor het conjugeren van chemisch gesynthetiseerde Ub-OTI peptides aan DC-targeting anti-DEC205 Fab-Ub, en demonstreert de superieure effectiviteit van ubi-tag gebaseerde conjugaten vergeleken met traditionele sortaggingtechnieken in zowel in vitro als in vivo toepassingen.

**Hoofdstuk** 4 test de toepasbaarheid van ubi-tagging op kleinere antilichaamfragmenten zoals nanobodies, en demonstreert hun functionaliteit in de context van gerichte vaccinatie aan menselijke DC's in vitro. Dit hoofdstuk toont ook de verbeterde oplosbaarheid en stabiliteit van ubi-tag gefuseerde eiwitten aan, wat suggereert dat ubi-tagging de oplosbaarheid van hydrofobe antigenen kan verbeteren.

Hoofdstuk 5 presenteert de totale chemische synthese van een 123 aminozuren

tellend nanobody dat GFP herkent. Dit nanobody, gemodificeerd met een propargyl functionaliteit voor on-demand functionalisatie, toont de homogeniteit en gedefinieerde kwaliteit die de voorbereiding van nanobody-drug conjugaat en multimeren kan vergemakkelijken.

De innovaties gepresenteerd in dit proefschrift benadrukken het belang van geavanceerde conjugatietechnologieën binnen de biomedische wetenschappen. De nieuwe methoden, zoals ubi-tagging, bieden substantiële vooruitgang in de precisie en efficiëntie waarmee antilichaamconjugaten geproduceerd kunnen worden. Deze technologieën beloven aanzienlijke verbeteringen voor zowel fundamenteel onderzoek als klinische toepassingen en openen nieuwe deuren naar de ontwikkeling van multispecifieke en multifunctionele antilichaamconjugaten.



#### **Curriculum Vitae**

Angela el Hebieshy was born on the 21st of February 1989 in Hulst, the Netherlands. From a young age, she harbored a strong interest in biomedical sciences and biotechnology and in 2012, she obtained her Bachelor's degree in Clinical Pharmacy from the Suez Canal University in Ismailia, Egypt. Eager to pursue her research interests, she moved back to the Netherlands to study the Drug Discovery and Safety Master's program at the VU Amsterdam from 2012 to 2015, specializing in Molecular Pharmacology. During her Master's, Angela joined Huib Ovaa's research group for an internship, a decision that profoundly shaped her career. It was soon clear to her that this was the research group where she found the scientific freedom and encouragement to thrive as a scientist. And hence, following her internship she transitioned to a full-time role, initially as a technician for one year after which she started her PhD trajectory under his supervision. During her PhD, she developed Ubi-tagging, a modular site specific antibody conjugation technology that provides a new method for the development of antibody-based vaccines, antibody-based research and diagnostic tools, and multispecific antibody complexes. What started as a side project, quickly grew into multiple big projects with great potential. Filing the patent application for the Ubi-tagging technology, sparked her interest in entrepreneurship and that was the moment when she decided that the next step in her career will be towards the life sciences industry. Currently, she is working as a Project and Grant Manager at FFUND, a life sciences consultancy company, where she manages projects and portfolios of multiple grants and loans that run through research departments and innovative companies.

#### **Publications**

#### Journal articles

#### Site-directed multivalent conjugation of antibodies to ubiquitinated payloads

Angela F. el Hebieshy\*, Zacharias Wijfjes\*, Camille M. Le Gall, Jim Middelburg, Kim E. de Roode, Felix L. Fennemann, Marjolein Sluijter, Thorbald van Hall, Douwe J. Dijkstra, Leendert A. Trouw, Floris J. van Dalen, Andrea Rodgers Furones, Johan M.S. van der Schoot, Ian Derksen, Hans de Haard, Bas van der Woning, Cami M.P. Talavera Ormeño, Bjorn R. van Doodewaerd, Carl G. Figdor, Gerbrand J. van der Heden van Noort, Paul W.H.I. Parren, Sandra Heskamp, Huib Ovaa, Martijn Verdoes, Ferenc A. Scheeren. Accepted for publication: Nature Biomedical Engineering.

#### Total Chemical Synthesis of a Functionalized GFP Nanobody.

<u>Angela F. el Hebieshy</u>\*, Yara Huppelschoten\*, Dharjath S. Hameed, Aysegul Sapmaz, Jens Buchardt, Thomas E. Nielsen, Huib Ovaa, Gerbrand J. van der Heden van Noort. ChemBioChem, vol. 23, no. 19, p. e202200304, Oct. 2022, doi: 10.1002/CBIC.202200304.

# Thermal-exchange HLA-E multimers reveal specificity in HLA-E and NKG2A/CD94 complex interactions.

Paula Ruibal, Ian Derksen, Marjolein van Wolfswinkel, Linda Voogd, Kees L.M.C. Franken, <u>Angela F. el Hebieshy</u>, Thorbald van Hall, Tom A.W. Schoufour, Ruud H. Wijdeven, Tom H.M. Ottenhoff, Ferenc A. Scheeren, Simone A. Joosten. Immunology. 2023 Mar;168(3):526-537. doi:10.1111/imm.13591.

# Malaria parasite evades mosquito immunity by glutaminyl cyclase-mediated posttranslational protein modification.

Surendra Kumar Kolli, Alvaro Molina-Cruz, Tamasa Araki, Fiona J.A. Geurten, Jai Ramesar, Severine Chevalley-Maurel, Hans J. Kroeze, Sascha Bezemer, Clarize de Korne, Roxanne Withers, Nadia Raytselis, <u>Angela F. el Hebieshy</u>, Robbert Q. Kim, Matthew A. Child, Soichiro Kakuta, Hajime Hisaeda, Hirotaka Kobayashi, Takeshi Annoura, Paul J. Hensbergen, Blandine M. Franke-Fayard, Carolina Barillas-Mury, Ferenc A. Scheeren, Chris J. Janse. Proc Natl Acad Sci U S A. 2022 Aug 30;119(35):e2209729119. doi: 10.1073/pnas.2209729119. Epub 2022 Aug 22.

# Temperature-based MHC class-I multimer peptide exchange for human HLA-A, B and C

Cilia R. Pothast, Ian Derksen, Anneloes van der Plas-van Duijn, <u>Angela F. el Hebieshy</u>, Wesley Huisman, Kees L.M.C. Franken, Jacques Neefjes, Jolien J. Luimstra, Marieke Griffioen, Michel Kester, Maarten H. Vermeer, Mirjam H.M. Heemskerk, Ferenc A. Scheeren. bioRxiv 2024.12.23.630039; doi: https://doi.org/10.1101/2024.12.23.630039

#### Synthetic and semi-synthetic strategies to study ubiquitin signaling.

Gabriëlle B.A. van Tilburg, <u>Angela F. el Hebieshy</u>, and Huib Ovaa. Curr Opin Struct Biol, vol. 38, pp. 92–101, Jun. 2016, doi: 10.1016/J.SBI.2016.05.022.

#### **Patents**

#### Polypeptide conjugates.

Ferenc A. Scheeren, Huib Ovaa and Angela F. el Hebieshy. WO2020101498A1. 22 May, 2020.



#### **Portfolio**

PhD student: AF el Hebieshy F

Primary thesis advisor: prof.dr. JJC Neefjes

Other thesis advisor(s): dr. FA Scheeren

dr. GJ van der Heden van Noort

Research programme: 40801 Chemical Immunology

Title of Thesis: Repurposing ubiquitination for innovative antibody conjugation

## **PhD** training

	Year	Hours
Mandatory courses		
- Leiden University Onboarding Programme Inform & Connect (2 activities) (exempted)		5
- Responsible Research (2 activities) (exempted)		42
- Basic Methods and Reasoning in Biostatistics (exempted)		42
Generic/disciplinary courses		
- Confocal Microscopy training LUMC	2016	3
- Flowcytometry training LUMC	2017	3
- BioLegend/Excyte Flow Cytometry training	2019	15
- Biobusiness winter school	2021	24
- Presentation skills for PhDs	2018	16
- Time and project management (ICI)	2017	16
- Communication in Science (ICI)	2016	16
- Personal leadership (ICI)	2017	16
- Experimental Oncology (NKI)	2016	40
Attended lectures, LUMC presentations, participation in meetings		
- Literature meeting	2017	8
- Literature meeting	2018	8
- Literature meeting	2019	8

- CCB Meeting	2018	8
- CCB Meeting	2020	8
- CCB Meeting	2021	8
Congress attendance and poster or oral presentations		
- ICI PhD day	2017	8
- CHAINS	2018	24
- CHAINS	2021	16
- CHAINS	2022	16
- Next generation Antibodies and Protein analysis (Gent)	2017	16
Teaching activities		
Lecturing, lab assistance, student supervision		
- FOS Course student supervision	2017	40
- FOS Course student supervision	2018	40
- Supervision of Intern Ian Derksen	2019	200
TOTAL number of hours		646

#### **Publications**

Publications in peer reviewed journals (article, review, editorial, letter to editor)

Year

- Synthetic and semi-synthetic strategies to study ubiquitin signaling; van Tilburg Gabrielle B. A., Elhebieshy Angela F., Ovaa Huib; 2016; Journal article
- Malaria parasite evades mosquito immunity by glutaminyl cyclase-mediated posttranslational protein modification; Kolli, S.K.; Molina-Cruz, A.; Araki, et al.; 2022; Journal article 2022
- Thermal-exchange HLA-E multimers reveal specificity in HLA-E and NKG2A/CD94 complex interactions; Ruibal P, Derksen I, van Wolfswinkel M, et al.; 2022; Journal article 2022
- Total chemical synthesis of a functionalized GFP nanobody; Huppelschoten Y, Elhebieshy AF, Hameed DS, et al.; 2022; Journal article 2022
- Polypeptide Conjugates; 2020; Scheeren FA, Ovaa H and El Hebieshy AF. 2020



#### **Acknowledgements**

I am profoundly grateful to my late promotor, Huib Ovaa, whose support and guidance during the first half of my PhD trajectory have been pivotal in my pursuit of the work I am passionate about. His belief in my capabilities and his mentorship have significantly shaped my growth as a scientist and as a person, for which I am eternally thankful. I would also like to express my sincere appreciation to my promotor Jacques Neefjes, who graciously stepped in and provided stability and guidance following Huib's passing. I also wish to extend my thanks to my co-promotor Ferenc Scheeren, for his unwavering support and belief in my potential throughout my PhD. His presence and guidance at every step have been a source of strength and inspiration. I am equally thankful to Gerbrand van der Heden van Noort, for his readiness and efficiency in providing guidance and support when it was most needed, which has been invaluable and greatly appreciated. Additionally, I must acknowledge the crucial contributions of my collaborators, whose efforts have been fundamental to the success of this work and my colleagues for their unwavering support and for the fun and friendly working environment that greatly enriched my experience.



